PROBING THE BIOPHYSICAL MECHANISMS OF GENE DELIVERY BY SYNTHETIC EVOLUTION OF COMBINATORIAL POLYMERIC VECTOR LIBRARIES

A Dissertation

Presented to the Faculty of the Graduate School

of Cornell University

in Partial Fulfillment of the Requirements for the Degree of

Doctor of Philosophy

by

Sharon Yan Wong

August 2008

PROBING THE BIOPHYSICAL MECHANISMS OF GENE DELIVERY BY SYNTHETIC EVOLUTION OF COMBINATORIAL POLYMERIC VECTOR LIBRARIES

Sharon Yan Wong, Ph.D.

Cornell University 2008

The prospect of treating debilitating and even fatal diseases by way of genetic-based interventions has been the long-standing goal of gene therapy. However, its widespread clinical use has been severely limited due to a dearth of effective gene delivery systems. Further stalling the development of viable vectors is the lack of clear mechanistic understanding of the barriers that vectors must overcome for successful transfection.

The goal of this research is to better understand the structure-function relationships that govern polymer-mediated transfection to serve as guiding principles for the rational design of safer and more efficient polymeric vectors. To achieve this goal, we developed a simple and robust synthetic protocol to synthesize combinatorial libraries of polymeric gene vector candidates. We evaluated three combinatorial libraries of polymeric vectors formulated from single and serially-incremented binary combinations of seven cationic, pH-sensitive, and hydrophobic pendant groups at three different molecular weights (10kDa, 30kDa, 50kDa). High levels of transfection correlated with increasing molecular weights and were achieved by polymers co-functionalized with primary amino and imidazole groups. These high-transfecting polymers appeared to harness the superior charge neutralizing and size condensing capacity of primary amino groups while benefiting from imidazole's polyplex-stabilizing ability. Imidazole groups were found to effectively bind with DNA via

non-electrostatic interactions, resulting in polyplexes that were more resistant to premature polyplex dissociation, which ultimately led to more efficient delivery to cells.

The effects on transfection of the polydispersity index (PDI) of polymeric vectors were also evaluated by comparing two identically-formulated libraries, each representing a different PDI (1.3 and 2.0). Within the higher PDI library, we identified several polymer formulations that achieved transfection levels superior to branched-PEI (25kDa), while maintaining superb cell viability. Biophysical characterization of these high-performing polymers revealed a greater degree of polyplex stability compared to their lower PDI, low-transfecting counterparts.

The results from this research have provided a deeper understanding of how several widely used polymeric structures influence gene delivery. The polymeric system and the approach presented herein serves as the foundation upon which future nucleic acid-based therapies (e.g., RNAi therapy) may be based in the move towards safer and more efficient delivery systems.

BIOGRAPHICAL SKETCH

Born in San Francisco, CA, Sharon Wong graduated from California Polytechnic State University, San Luis Obispo in 1999 with a B.S. in Materials Engineering. She then worked as a Research and Development Engineer for three years at Guidant Corporation designing guidewires and stent delivery systems for angioplasty procedures. She began her Ph.D. studies in Biomedical Engineering at Cornell University in 2002 and earned her doctorate in May of 2008.

To my parents,
my number one cheerleaders and my role models

ACKNOWLEDGMENTS

I had the great privilege of training under the guidance of three remarkable and accomplished advisors – Dave Putnam, Mike Shuler, and Volker Vogt. I am grateful to Dave for continual funding throughout my graduate career, careful editing of all my manuscripts, and an open door policy for round the clock research and career advice. His enthusiasm as a scientist and an advisor often challenged me beyond my limits, but it was this intensity that sharpened my scientific thinking and developed me into the scientist I am today. Prof. Shuler provided helpful insight and critique of my research and has been an invaluable engineering influence in my graduate training. I also wish to express my gratitude to Volker for his guidance and mentorship in both career and research matters. His sincerity as a mentor, precision as a scientist, and humility as a scholar serves as the standard to which I strive as a person and a budding scientist.

I would like to offer a special acknowledgment to the Putnam group for all the salad days shared in the office where no information was too personal to publicize. I thank Dave Chen for six years of stimulating scientific discussions, delirious moments of Monte Carlo simulations, and entertaining renditions of Rihanna songs. I thank Peter for providing the comic relief to the office and the lab. His infectious laugh and uncanny ability to relate all situations to a Simpsons episode always made the tough days easier. Sara was my source for all questions and matters pertaining to fashion and online shopping. Without her critical eye for fashion, I am afraid to consider how far I would have let myself go. I thank Jeisa for teaching me the value of assuming 'Jeisa-mode' and for providing warm meals and a warm apartment on many cold winter nights.

I was extremely fortunate to have worked with two outstanding undergraduate researchers, Theresa Chan and Nimil Sood. Aside from their invaluable contributions to my research, it has been extremely rewarding to see both mature into capable scientists and conscientious thinkers during the course of their time in our group.

I extend my deepest gratitude to my family for affording me the space to find and be myself, whether that was traveling around the world, moving to New York City to be a hostess, or doing all the non-conventional things that I do. A heartfelt thanks is also due to the Hurwitz/Wessler family for their support, encouragement, and generosity. Without them, I could never have considered the east coast my new home. A special thanks to Matt, who has endured with me the emotional and psychological rollercoaster that is graduate school. His healthy perspective, unconditional support, and most of all, his witty sense of humor have been a source of comfort and stability that has kept me sane through it all.

Funding for this research was provided through a Biomedical Research Grant from the Whitaker Foundation.

TABLE OF CONTENTS

LIST OF FIGURES

CHAPTER 2

CHAPTER 3

CHAPTER 4

CHAPTER 5

CHAPTER 6

CHAPTER 7

LIST OF TABLES

CHAPTER 2

CHAPTER 3

CHAPTER 4

CHAPTER 5

CHAPTER 6

CHAPTER 7

CHAPTER 1

INTRODUCTION

The lack of safe and efficient gene delivery systems represents the single biggest challenge facing gene therapy today. Despite innovative strategies that have created more effective delivery systems, the current technology has fallen short in transforming gene therapy into a clinical reality. Perhaps one of the most active areas of vector research is the design of polymer-based delivery systems. By virtue of their synthetic versatility and amenability to diverse chemical modification, polymers offer an attractive platform upon which sophisticated delivery systems can be based. However, polymer vector research currently suffers from an opaque understanding of the structure-function relationships that govern polymer-mediated gene delivery. Without a clear understanding of how polymeric structures and features influence the transfection capacity of polymeric vectors, rationally designing safer and more effective vectors will continue to be an extremely challenging task.

This thesis aims to address this gap in knowledge through the iterative synthesis of combinatorial libraries of polymeric gene vector candidates. Chapter 2 provides a review of the prolific research into polymer-based delivery systems, and the wealth of knowledge that has been generated over the past two decades, with a focus on recent developments within the past three years. Chapter 3 details the synthetic approach that was developed to streamline the synthesis of large and diverse polymer libraries. Chapter 4 discusses the evaluation of three combinatorial libraries of cationic and hydrophobic polymers and the structure-function relationships deduced from this library. In Chapter 5, we evaluated the polydispersity of polymeric vectors and its effects on gene delivery.

The final two chapters discuss two additional methods that were formulated to support the synthesis of combinatorial libraries for future structure-function studies. In Chapter 5 we devised a high throughput equilibrium dialysis system designed to purify and isolate polymeric compounds from 96 well plates. Finally, Chapter 6 details a stochastic Monte Carlo (MC) model that was developed to facilitate the design and iterative redesign of richer and more focused combinatorial libraries. The utility of MC methods for library design was established based on an experimental data set of over five thousand combinatorially-assembled buffer formulations for refolding denatured protein into its functional conformation. The protein refolding experimental platform may initially seem unrelated from the polymeric vector research. However, the combinatorial nature of the polymeric vector library in the gene vector study is akin to the buffer formulation library and is therefore amenable to the use of MC methods that were demonstrated on the combinatorial library in the MC study.

CHAPTER 2

POLYMER SYSTEMS FOR GENE DELIVERY – PAST, PRESENT, AND FUTURE [1]

2.1. ABSTRACT

Gene therapy has long sought to treat disease by delivering therapeutic genes to diseased cells. However, its widespread clinical use has faltered in the face of several challenges, most notably in the area of delivery. Efforts to understand the biological barriers that prevent the effective delivery of therapeutic genes to targeted tissues, and developing safe and efficient vectors that can overcome the barriers, stand at the heart of current gene delivery research. The first part of this review provides a comprehensive discussion of the current understanding of these biological barriers and the rich collection of polymers and design strategies that have accumulated from nearly two decades of research aimed at overcoming these hurdles. The second part highlights the challenges that remain and several innovative approaches and methods that have recently been developed representing, in part, the future directions of gene delivery research.

2.2. INTRODUCTION

Long heralded by some as the next revolution in modern medicine, gene therapy has the potential to profoundly shift the way human disease is managed and treated [1]. The concept is simple - deliver exogenous, therapeutic genes to the body to treat genetic-based diseases. The results could be substantial - diseases once

[1] Reproduced with permission from Wong, S., Pelet, J., Putnam, D., Polymer systems for gene delivery-past, present, and future, *Progress in Polymer Science*, 32, 8-9, 799-837 (2007). Copyright [2007] Elsevier.

considered incurable may be treated or even prevented, for instance, with DNA vaccines that inoculate against infectious diseases [2]. Thanks to advances in molecular biology and genomic research, numerous diseases (e.g., sickle cell anemia, HIV, Parkinson's disease, Huntington's disease, Alzheimer's disease) have been given a genetic identity for which gene therapy may be a possible prescription [3-6].

However, the promise of gene therapy has yet to be fulfilled due to challenges associated with cell targeting specificity, gene transfer efficiency, gene expression regulation, and vector safety. Engineered viruses were the first delivery agents employed to meet these challenges. Using viruses that were either genetically rendered to be replication defective or gutted of their genetic material and replaced with therapeutic genes, some of the earliest clinical trials produced promising results leading many to believe that viral vectors were poised to achieve the goal of gene therapy [7-10]. It was not long after these initial reports of successful clinical implementation, however, that the severe side effects possible with viral-based gene therapy were made strikingly evident. The concern that viral vectors could induce cancer via insertional mutagenesis – random transgenic insertion into the host chromosome disrupting the normal expression of a critical gene that ordinarily regulates cell growth and division – was realized when three clinical trial participants developed leukemia-like complications post retroviral-based gene therapy [11-13]. Moreover, the viral vectors themselves can initiate an immunogenic response which, in at least one reported incident, has led to a fatal outcome [14].

Although these safety issues do not necessarily preclude the use of viruses as gene vectors, they have motivated the exploration for safer, less pathogenic and immunogenic gene delivery alternatives including lipid-based vectors, chemically modified viruses, inorganic materials, and polymer-based gene delivery systems. In addition to the potential safety benefits, such non-viral systems offer greater structural

and chemical versatility for manipulating physicochemical properties, vector stability upon storage and reconstitution, and a larger gene capacity compared to their viral counterparts. Lipid-based vectors, chemically modified viruses, and inorganic materials are the subject of several reviews to which the reader is referred [7, 15, 16]. The scope of this review aims to highlight the progress that has been made toward developing polymer-based gene delivery systems with an emphasis on recent progress reported within the past three years.

The first part of this review discusses the current understanding of the various biological barriers that face efficient gene delivery (Figure 2-1) and the rich collection of polymers and design strategies that have accumulated from nearly two decades of intense and prolific research aimed at overcoming these barriers. The second part of this report highlights the challenges that remain and several innovative approaches and methods that have been recently developed representing, in part, the future directions of gene delivery research.

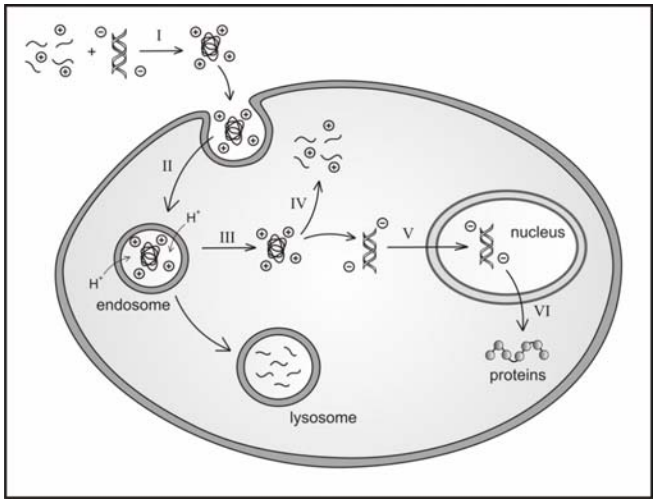

Figure 2-1. Barriers to Gene Delivery - Design requirements for gene delivery systems include the ability to **I)** package therapeutic genes; **II)** gain entry into cells; **III)** escape the endo-lysosomal pathway; **IV)** effect DNA/vector release; **V)** traffic through the cytoplasm and into the nucleus; **VI)** enable gene expression; and **VII)** remain biocompatible.

2.3. GENE PACKAGING

The fundamental design criteria for any synthetic gene delivery system includes the ability to 1) neutralize the negatively charged phosphate backbone of DNA to prevent charge repulsion against the anionic cell surface; 2) condense the bulky structure of DNA to appropriate length scales for cellular internalization (i.e., nanometers for receptor-mediated endocytosis; micrometers for macropinocytosis or phagocytosis); and 3) to protect the DNA from both extracellar and intracellular nuclease degradation [17-19]. To meet these requirements, researchers have relied on three main packaging strategies: electrostatic interaction, encapsulation, and adsorption (Figure 2-2).

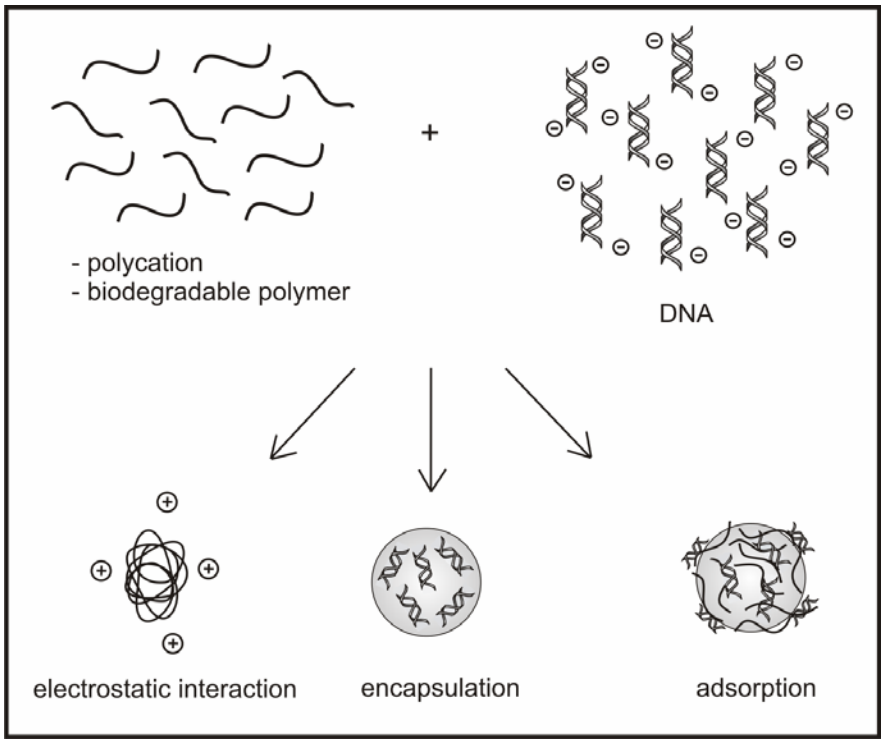

Figure 2-2. Gene Packaging – The three main strategies employed to package DNA are via 1) electrostatic interaction, 2) encapsulation within or 3) adsorption onto biodegradable nano- or microspheres.

2.3.1. Electrostatic interaction

Many of the polymeric vectors developed to date have exploited the anionic nature of DNA to drive complexation via electrostatic interaction. Table 2-1 identifies several commonly used polycations that have been used in such a capacity. All of these polymers possess amino groups, at least a portion of which are protonated at neutral pH, to enable electrostatically-driven self assembly with DNA. At a sufficient nitrogen to phosphate (N:P) charge ratio, the polymer can condense DNA to sizes compatible with cellular uptake while providing steric protection from nuclease degradation [20].

Although the presence of the positive-charge carrying moieties forms the basis for this method of DNA packaging, it is the cationic charge that appears to correlate with the high degree of cytotoxicity typically associated with polycations. Moreover, a strong electrostatic charge, though conducive for DNA packaging and protection, may lead to difficulties of DNA release once the polyplex arrives at the site of action. For these reasons, researchers have developed biodegradable polycations as well as alternative methods of DNA packaging, namely via encapsulation and adsorption.

2.3.2. Encapsulation

An alternative to electrostatic condensation of DNA is its encapsulation within biodegradable spherical structures. The vast majority of biodegradable polymers that have been used for nano- or microspherical encapsulation are shown in Table 2-1. Owing to the ester linkages along their backbones, all of these polymers (i.e., polyesters) can be hydrolytically degraded to shorter oligomeric and monomeric components that are more readily cleared from the body. Furthermore, degradation kinetics can be modulated by various factors including polymer properties and composition thereby enabling control over DNA release [21-23]. Similar to their

polycation counterparts, these DNA-encapsulating agents protect the incorporated genes from enzymatic degradation. The size of the DNA-encapsulated complex, however, is determined by the method of particle formulation, which can be tailored to range from the nanometer to micrometer length scale [24]. The current methods available for encapsulation represent one of the main limitations of this packaging method, as it often involves high shear stresses and exposure to organic solvents and extreme temperatures that can degrade the genetic cargo [25]. Other limitations include low encapsulation efficiency, potential DNA degradation due to a low pH microenvironment within the hydrolyzing polyester, and low DNA bioavailability due to incomplete release from the polymer [26-28].

2.3.3. Adsorption

In response to the limitations posed by current encapsulation methods, adsorption techniques were developed as a DNA packaging alternative. DNA adsorption represents a marriage of the two above-mentioned approaches in that it involves adsorbing or conjugating cationic moieties (e.g., cationic surfactants, PDMAEMA, PEI) to the surface of biodegradable particles to which DNA can electrostatically bind [59, 81-83]. This approach offers the benefit of enhancing the amount of DNA available for immediate release while reducing its exposure to harsh encapsulation conditions. However, surface presentation of the nucleic acids can render them susceptible to enzymatic degradation although this may be mitigated by the type of polycation employed and the resultant degree of electrostatic interaction with the adsorbed DNA [59, 64].

Table 2-1. Structures of some widely used gene-packaging polymers.

Polycations
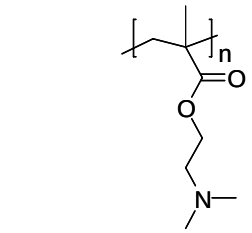 poly(2-(dimethylamino)ethyl methacrylate) (PDMAEMA)
branched poly(ethylenimine) (b-PEI) 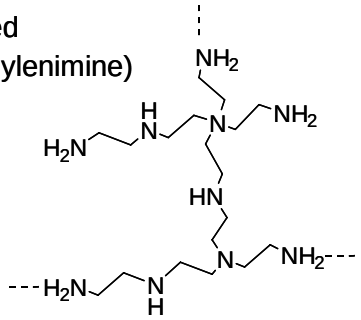
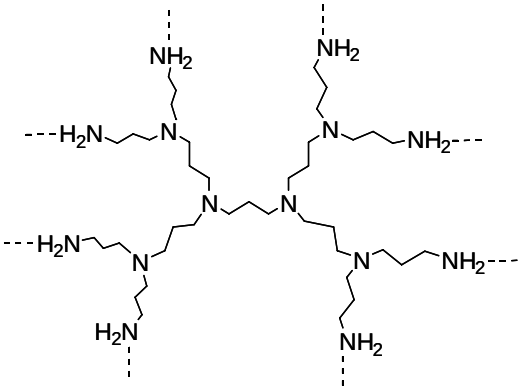 poly(propylenimine) (PPI)
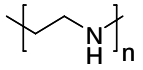 linear poly(ethylenimine) (L-PEI)
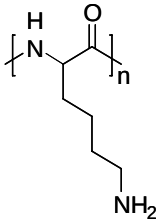 poly(lysine) (PLL)
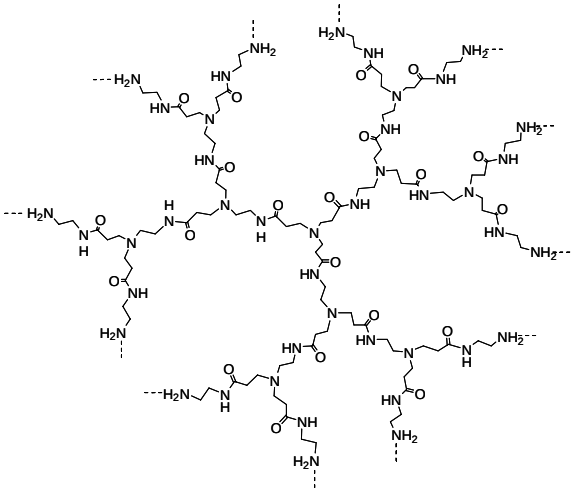 poly(amidoamine) (PAMAM)

Table 2-1. *(continued)*

Polycations *(continued)*

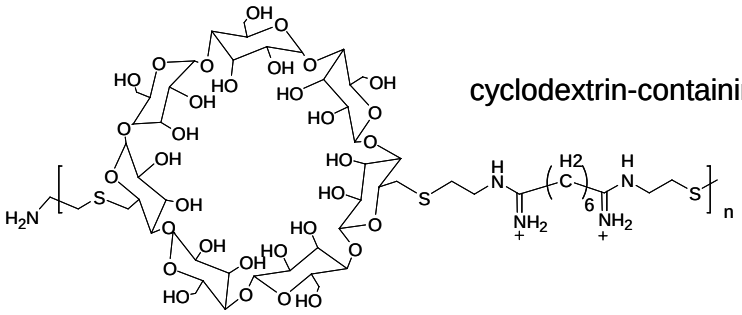

cyclodextrin-containing polycations

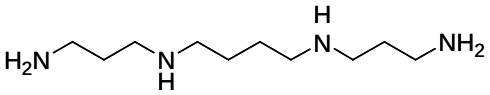

spermine

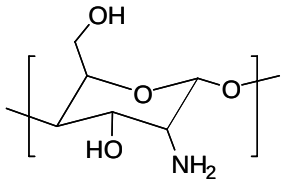

chitosan

Biodegradable polymers

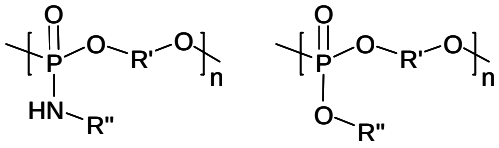

poly(phosphoester)

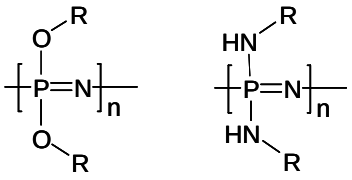

poly(phosphazene)

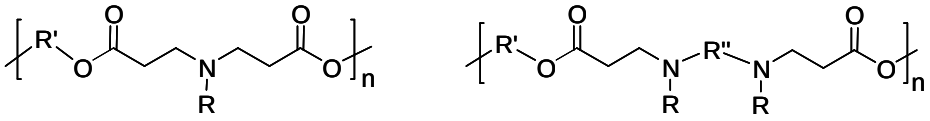

poly(β-amino ester)

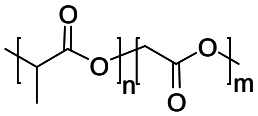

poly(lactide-*co*-glycolide)
(PLGA)

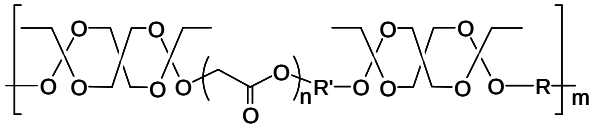

poly(orthoester)

Table 2-1. *(continued)*

Biodegradable polymers *(continued)*

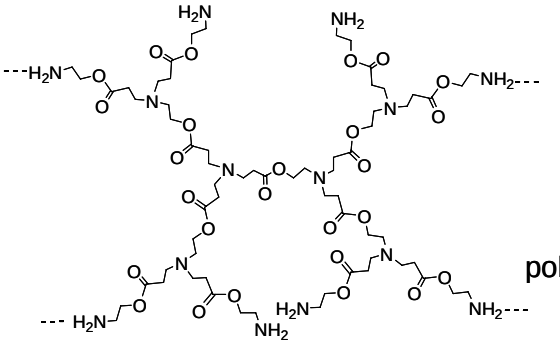

hyperbranched poly(amino ester)

(h-PAE)

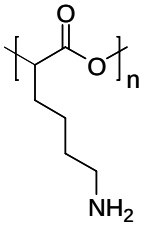

poly(α-[4-aminobutyl]-1-glycolic acid)

(PAGA)

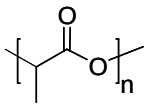

poly(lactic acid)

(PLA)

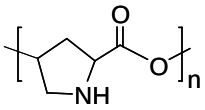

poly(4-hydroxy-1-proline ester)

(PHP-ester)

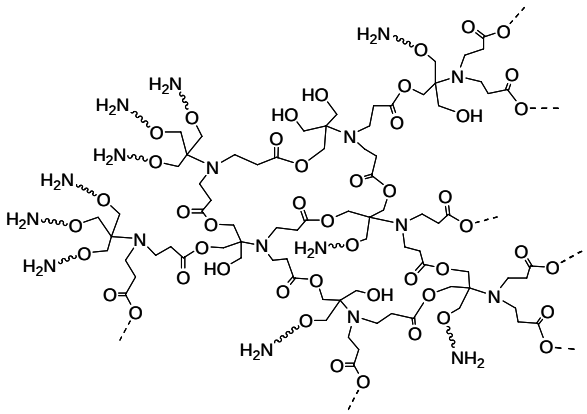

networked poly(amino ester)

(n-PAE)

References: L-PEI and b-PEI [29, 30]; PDMAEMA [31-35]; PAMAM [20, 36-38]; PPI [39, 40]; PLL [41-45]; chitosan [46-50]; spermine [51-53]; cyclodextrin-containing polycations [54]; poly(phoshphoester) [55, 56]; poly(phosphazene) [57, 58]; PLA [59, 60]; PLGA [61-64]; poly(orthoester) [65, 66]; poly(β-amino ester) [67-70]; h-PAE [71, 72]; n-PAE [73, 74]; PAGA [75-77]; PHP-ester [78-80]

The polymers highlighted in Table 2-1 represent various molecular backbones and delivery platforms upon which synthetic vector designs are based. The versatility of polymer chemistry allows these polymers to be functionalized, copolymerized, or structurally modified (e.g., into various architectures) to impart physicochemical properties upon the vector to overcome the barriers of gene delivery. Using both traditional and more recently developed polymers and synthetic techniques, researchers have created an extensive collection of polymer tools that can be drawn upon for subsequent vector designs. The following discussion highlights the diverse assortment of polymer tools and strategies that have been developed to overcome the barriers to safe and efficient gene delivery.

2.4. CELLULAR ENTRY

On a cellular level, the first obstacle encountered by the polymer/DNA complex, or "polyplex", is the plasma membrane. To gain entry into the cell, passive diffusion is typically not afforded to polyplexes due to size restrictions of transmembrane pores and channels and low partition coefficients into lipid bilayers. Many of the strategies developed to surmount this physical barrier have taken advantage of the process by which cells naturally use to internalize macromolecules (e.g., nutrients, bacteria) from the extracellular space, namely endocytosis. As with most physiological processes responsible for sustaining the livelihood of the cell, cellular entry must be tightly regulated lest the uptake of undesirable or unnecessary particles and macromolecules should occur. As such, endocytic uptake occurs by at least five known pathways to afford a diverse, yet regulated mechanism of controlling cellular entry – phagocytosis, macropinocytosis, clathrin-mediated endocytosis, caveolae-mediated endocytosis, and clathrin- and caveolae-independent endocytosis [84]. In terms of polymer-mediated gene delivery, all share a common uptake mode

of enclosing the internalized polyplexes within transport vesicles derived from the plasma membrane. Differences arise, however, in the subsequent intracellular processing and routing of internalized polyplexes, which consequently affects the extent to which the polyplexes can deliver their genetic cargo efficiently. The factors that determine the pathway though which polyplexes will be internalized remain unclear and are briefly discussed in the next section. Discussed below are several of the strategies that have been developed to induce endocytosis, referred to generally in this section unless distinguished otherwise, of polymer-based gene delivery systems (Figure 2-3).

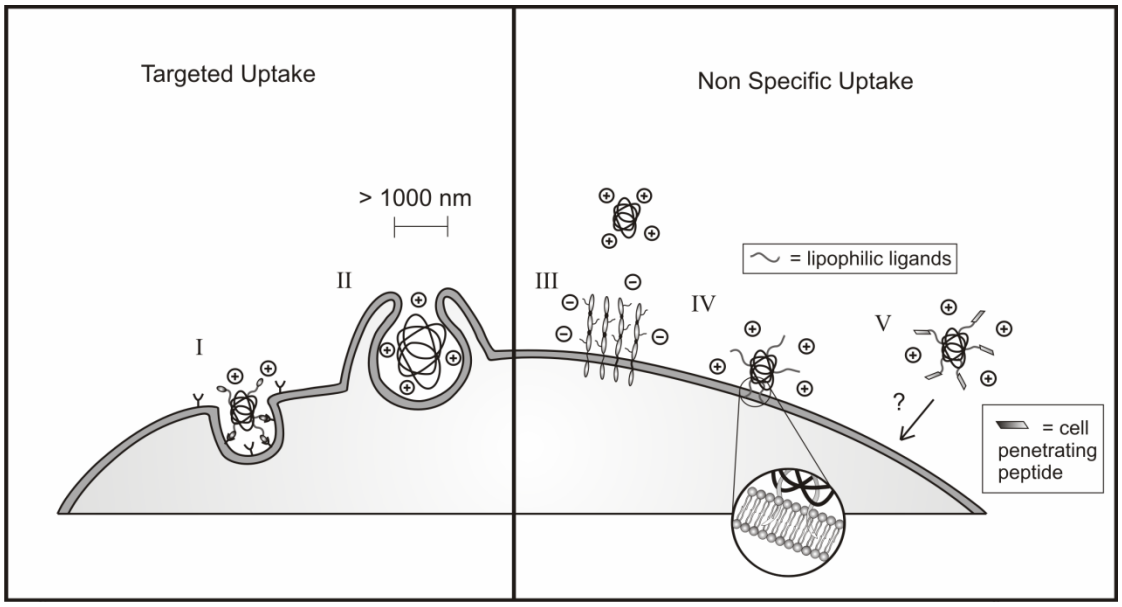

Figure 2-3. Cellular Entry – Polyplexes may gain entry into cells through **I)** receptor-mediated endocytosis; **II)** phagocytosis via size exclusion; **III)** non-specific ionic interactions with membrane-bound proteoglycans; **IV)** non-specific lipophilic interactions with phospholipid components of the cell membrane; or **V)** cell penetrating peptide (CPP)-mediated uptake, the mechanism of which remains unclear.

2.4.1. Targeted uptake

2.4.1.1. *Receptor – mediated targeting and endocytosis*

Numerous polyplexes have been designed to gain cellular entry via receptor-mediated endocytosis. Vectors that bear targeting ligands, which induce endocytosis upon binding to their cognate surface receptors, have been used to mediate internalization in a cell-specific manner. Indeed, for most diseased conditions where the therapeutic genes must be delivered to a certain cell type, targeting receptors that are present only on certain cell populations has provided a useful tool in gene delivery.

A panoply of targeting ligands have been investigated including proteins, carbohydrates, peptide sequences, biomolecules, and antibodies. Table 2-2 lists several examples of the most commonly used ligands that have provided selective targeting to various cell types displaying the appropriate receptor protein.

Table 2-2. Ligands used to promote cellular uptake

	Ref.
Endogenous Ligands	
Transferrin	[86-89]
TGF-α	[90]
Folate	[91, 92]
FGF	[87, 93]
EGF	[94, 95]
VEGF	[87]
Asialoorosomucoid	[96, 97]
RGD peptide	[98-101]
Carbohydrates	
Galactose	[102, 103]
Mannose	[104-106]
Lactose	[105, 107]
Antibodies	
antiCD3	[88, 108]
antiEGF	[109]
antiHER2	[110, 111]
antiIgR	[112]
antiJL-1	[113]
Cell penetrating peptides	
HIV Tat	[101, 114, 115]
Penetratin	[116, 117]
Transportan	[117, 118]
Polyarginine	[119]

Selection of the appropriate targeting ligand can be influenced by a myriad of factors. Endogenous ligands, such as folate and transferrin, are the most widely used class of targeting moieties based on their biocompatibility and fairly well studied receptor distribution [85]. However, their inherent circulation in the body can also lead to competitive interference with those attached as targeting moieties. In contrast, exogenous ligands, such as the peptide- and antibody-based targeting agents may avoid these problems although their foreign nature renders them susceptible to an immune response, which could limit their utility [85].

2.4.1.2. *Size exclusion and phagocytosis*

Targeting and subsequent cellular uptake can also be mediated via size exclusion. It has been shown that DNA-encapsulated microspheres with diameters between 1-10 μm are preferentially internalized by phagocytic cells such as antigen-presenting cells (APCs) of the immune system [120]. As such, this strategy has been widely adopted for DNA vaccine applications where APCs are the target cells [66, 82].

2.4.2. Non-specific uptake

2.4.2.1. *Ionic interactions with membrane – bound proteoglycans and endocytosis*

Cellular entry can also be gained in the absence of targeting strategies. A number of polyplexes have been able to induce cellular uptake through charge-mediated interactions with proteoglycans that are present on the cell surface [121]. Proteoglycans are composed of a membrane-associated core protein from which a chain of sulfated or carboxylated glycosaminoglycans (GAGs) extends into the extracellular space [122]. These highly anionic GAG units determine much of the interactions between the cell surface and extracellular macromolecules and are responsible for the overall negative charge of the plasma membrane [123]. Although

the exact mechanism by which these membrane-bound molecules mediate cellular internalization remains unclear, they are believed to play a central role in the endocytic uptake of many non-targeted, positively-charged gene delivery systems [121, 124]. It is important to consider, however, that differences in proteoglycan distribution between cell types can lead to varying degrees of internalization from one cell type to another. Additionally, the non-specificity of this mode of interaction can lead to indiscriminate uptake and undesirable gene expression by unanticipiated cell populations.

2.4.2.2. *Lipophilic interaction with phospholipid membrane and endocytosis*

An alternative opportunity for cellular uptake relies on the interaction between vector-bound lipophilic residues and the phospholipid layers that comprise the cellular membrane [125]. Through a series of rationally incremented chemical modifications to branched PEI, Thomas and Klibanov demonstrated the potential ability of long, lipophilic alkyl chains (i.e., dodecane, hexadecane) to induce endocytosis through interactions with the cell membrane resulting in increased transfection efficiencies [126]. Moreover, their results revealed that the position of lipophilic substitution (i.e., primary vs. tertiary amines of PEI) can have profound effects on the extent of this interaction and thus transfection efficiencies [126].

2.4.2.3. *Cell penetrating peptide – mediated uptake*

More recently, cell penetrating peptides (CPP) have been extensively investigated for their ability to facilitate membrane translocation (Table 2-2). Originally derived from viral proteins, these peptides are typically 5-40 amino acids in length, positively charged, and amphipathic in nature. By virtue of their net positive charge, some CPPs have served as both the DNA-binding and the cell penetrating component [114, 115,

127]. Although the mechanism by which CPPs facilitate cellular uptake remains controversial, the prevailing hypotheses of CPP-mediated uptake include 1) formation of peptide-lined pores within the membrane; 2) direct penetration through the membrane and into the cytoplasm; 3) transient uptake into a membrane-bound micellar structure that inverts to release the CPP and its genetic cargo inside the cytosol; and 4) the induction of endocytosis [128] (Figure 2-4). As with any peptide or protein-based component, incorporation into vector designs should not be pursued without caution due to potential immunogenicity concerns. Furthermore, it is believed that peptide conformation may play a critical role in membrane penetration and therefore the method of incorporation must be careful not to disrupt peptide activity.

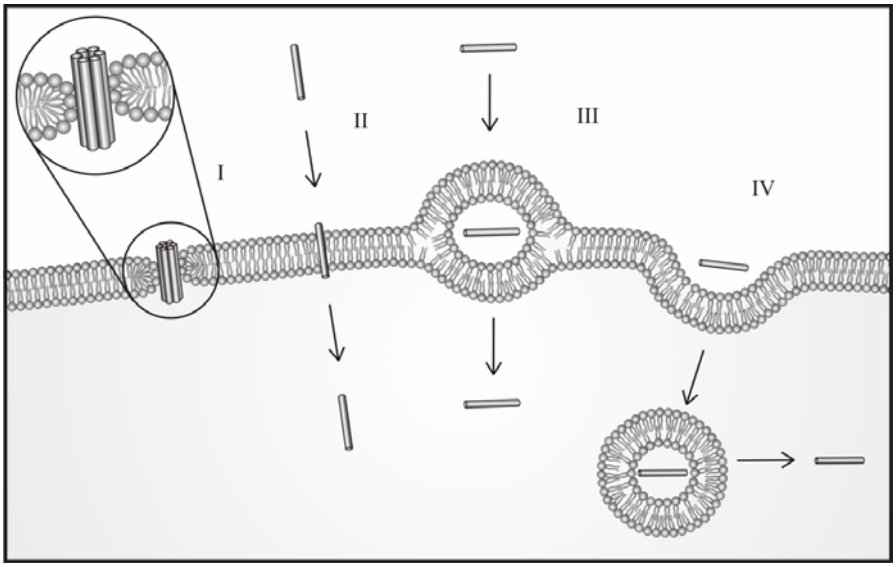

Figure 2-4. Cell Penetrating Peptide (CPP)-Mediated Uptake – Hypothesized mechanisms of CPP-mediated entry include **I)** formation of peptide-lined pores within the cell membrane; **II)** direct penetration through the membrane and into the cytoplasm; **III)** transient uptake into a membrane-bound micellar structure that inverts to release the CPP and its genetic cargo inside the cytosol; and **IV)** induction of endocytosis. (Adapted from [128, 129])

2.5. ENDO-LYSOSOMAL ESCAPE

If cellular entry is gained by endocytosis, subsequent intracellular routing of vesicle-bound polyplexes can include recycling back to the cell surface, sorting to acidic, degradative vesicles (e.g., lysosome, phagosome), or delivery to an intracellular organelle (e.g., Golgi apparatus, endoplasmic reticulum) [130]. The intracellular itinerary that the endocytic vesicles follow depends upon the pathway by which they were internalized (i.e., phagocytosis, macropinocytosis, clathrin-mediated endocytosis, caveolae-mediated endocytosis, and clathrin- and caveolae-independent endocytosis). Currently, clathrin-mediated endocytosis is the most characterized pathway and has served as the route for which synthetic gene delivery systems have been designed. It is important to consider, however, the emerging evidence suggesting that the uptake pathway, and thus intracellular routing and consequently transfection efficiency, is dependent upon a number of factors including cell line, polyplex type, and the conditions under which the polyplex is formulated [131, 132]. Thus, elucidating the mechanistic details of the other internalization routes will be important for the design of more optimized synthetic vectors.

Within the clathrin-mediated endocytic pathway, polyplexes can be sequestered within endosomal vesicles and shuttled through the endo-lysosomal pathway. Release from these vesicles is paramount to avoiding enzymatic degradation within the lysosomal compartment (Figure 2-5). Because these vesicles acidify (pH decreases from ~6 to ~5) as they mature from endosomes to lysosomes, escape mechanisms have attempted to harness the influx of protons through the use of pH-responsive moieties (Table 2-3).

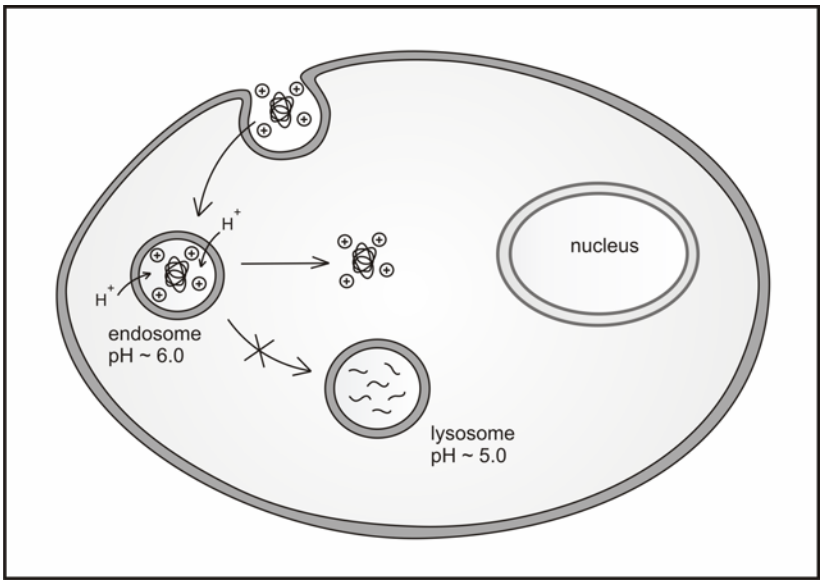

Figure 2-5. Endo-lysosomal Escape – Polyplexes that are internalized via endocytosis can be sequestered within endosomal vesicles and trafficked to the lysosome to be enzymatically degraded. Vesicles acidify (pH reduces from ~6 to ~5), through the action of vesicle-bound proton pumps, as they mature along the endo-lysosomal pathway. Strategies to escape lysosomal degradation have exploited the influx of protons by incorporating pH-sensitive moieties into vector designs.

2.5.1. Protonable amines

The most commonly used pH-sensitive excipients are protonatable amino groups with $5 < pK_a < 7$ (e.g., 2° and 3° amines, imidazole). As the vesicle acidifies, these amino groups are thought to become protonated thus preventing the vesicle from attaining the desired pH. As a result of this endosome buffering activity, commonly referred to as the "proton sponge" effect, the endo-lysosomal vesicle osmotically swells, ruptures, and releases its contents into the cytosol [133, 134].

Table 2-3. Ligands used to promote endo-lysosomal escape

	Ref.
Protonable amines	
Imadazole groups	[44, 140-144]
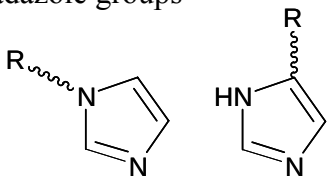	
L-PEI	[29, 30]
b-PEI	[29, 30]
PDMAEMA	[31-35]
PAMAM	[20, 36-38]
Endosomal release peptides	
Viral derived	
Melittin	[145]
Influenze virus hemalgglutinin HA-2	[146, 147]
Diptheria toxin	[148]
Synthetic peptides	
GALA	[37]
KALA	[149, 150]
JTS-1	[151]
Alyklated carboxylic acids	
	[46, 139]
poly (propylacrylic acid) poly (ethylacrylic acid) poly (ethylacrylate-co-acrylic acid)	
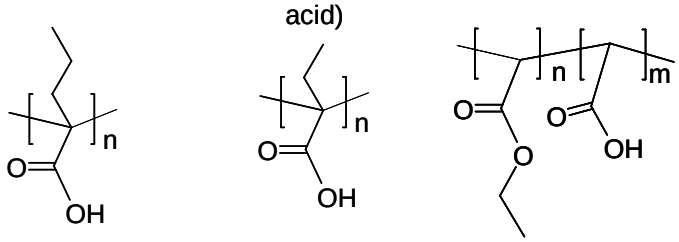	

2.5.2. Endosomal release peptides

Endosomal release peptides have also been used to promote translocation through the endosomal membrane. These peptides differ slightly from CPPs in that they undergo a structural transformation from a random coil at neutral pH to an α-helical conformation at lower pH environments. Triggering of the α-helical conformation is believed to induce membrane interaction and disruption leading to subsequent release of the endosomal contents into the cytosol [135].

2.5.3. Alkylated carboxylic acid

Inspired by the membrane-disruptive abilities of the endosomal release peptides, but concerned with their potential immunogenicity and high manufacturing costs, an alternative class of synthetic, pH-sensitive polymers was developed. These polymers were designed to contain the same functional groups, namely alkyl and carboxyl groups, that are presumably responsible for the membrane-disruptive properties of the α-helical endosomal release peptides [136]. The carboxyl component functions as the protonatable species while the hydrophobic alkyl groups interact with the endosomal membrane to collectively enhance vesicle escape. Through a series of structure-function experiments, it was determined that pH-induced membrane lytic ability can be modulated by the carboxylic acid to alkyl group ratio with poly(propylacrylic acid) exhibiting the most promising utility in gene vector design [136-139].

2.6. CYTOSOLIC TRANSPORT AND NUCLEAR IMPORT

Polyplexes that enter the cytosol, either directly upon cellular internalization or upon escaping the endo-lysosomal pathway, are immediately faced with a physically and metabolically hostile environment (Figure 2-6).

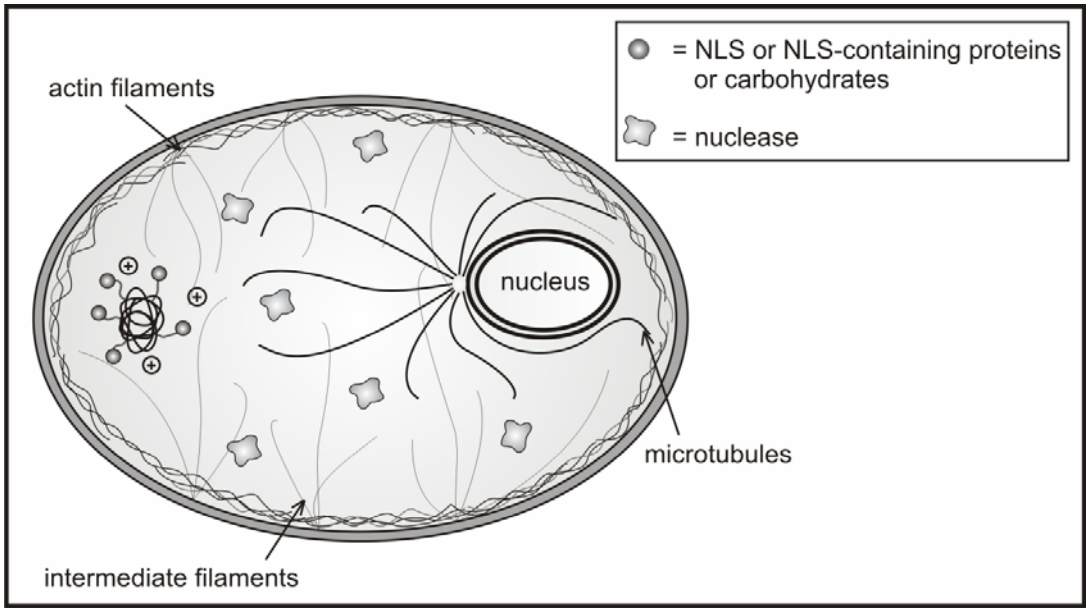

Figure 2-6. Cytosolic Transport and Nuclear Import –Polyplexes entering into the cytosol are faced with nucleolytic enzymes interspersed amongst the filamentous network of the cytoskeleton. Strategies to minimize residence time within the cytosol and promote transport toward and into the nucleus include incorporating nuclear localization signals (NLS), NLS-containing proteins, and carbohydrates into vector designs.

Within the cytosolic milieu, nucleolytic enzymes ready to degrade unprotected nucleic acids are interspersed amongst microtubules, intermediate filaments, and microfilaments that are organized into a dense network to form the cytoskeleton [152]. These filaments provide an internal structure to the cell and function in cell motility and intracellular transport of vesicles, chromosomes, and macromolecules. It has been shown that the mesh-like structure of the cytoskeleton, and more specifically cross-linked actin filaments, can severely impede the diffusion of naked DNA greater than 250 bp in size with an extended linear length of approximately 85 nm [153, 154]. Thus, free diffusion of polyplexes that are typically on the order of 150-200 nm is not likely to be the main mode of cytosolic transport.

In order to minimize residence time within the cytosol and promote transport toward and into the nucleus, researchers have recruited natural endogenous cytosolic factors and their associated cellular pathways to facilitate the shuttling of either polyplexes or DNA itself (Table 2-4).

Table 2-4. Ligands used to promote cytosolic transport and nuclear import.

	Ref.
Nuclear localization signals (NLS)	
Human T cell leukemia virus type 1 (HTLV)	[155]
M9	[156]
HIV Type – 1 viral protein R (Vpr)	[157, 158]
SV40 Large T antigen	[155, 159, 160]
NLS – containing proteins	
Protamine	[161, 162]
Histone	[89, 163]
High mobility group proteins	[164, 165]
Carbohydrates	
Lactose	[166]
Mannose	[167]
N – acetylglucosamine	[168]

2.6.1. Nuclear localization signal (NLS)

The nuclear import machinery, naturally utilized by cells to transport large proteins into the nucleus, has motivated the application of nuclear localization signals (NLS) in gene vector design. Proteins less than 40 kDa in MW or 9 nm in diameter can passively diffuse through channels, known as nuclear pore complexes (NPC), that perforate the nuclear envelope [169]. Proteins greater in size, however, require the assistance of import proteins (e.g., importins) to actively shuttle them through the NPCs. Cytosolic proteins destined for the nucleus contain a distinct amino acid

sequence, known as the NLS, that are recognized by import proteins which direct their subsequent transport into the nucleus.

Significant effort has been devoted to exploit this highly sophisticated and efficient trafficking pathway to mediate intracellular transport of both exogenous and vectorized DNA [170]. Since most NLSs are short, cationic peptide sequences, they can be used to electrostatically interact and condense DNA thus abrogating the need for a distinct polycation condensing agent [157]. Alternatively, NLSs can be attached to a polymer vector that is subsequently complexed with its genetic cargo [160, 171]. Despite their promising fitness for gene delivery, the extent to which NLSs can enhance cytosolic trafficking and nuclear uptake may be limited by the size and type of DNA used (i.e., linear, plasmid), the method of NLS incorporation (i.e., covalent conjugation to DNA, electrostatic complexation with DNA, or conjugation to a polymer vector), type of NLS peptide employed, the number of NLSs incorporated, and the type of polymer vector used (e.g., liposomes, PEI) [155, 172].

2.6.2. NLS – containing proteins

In addition to using NLS sequences for nuclear targeting, researchers have also explored the possibility of using various natural or recombinant nuclear proteins from which NLS sequences were derived. The large majority of nuclear proteins examined for gene delivery applications fall into two broad categories – histones and non-histone proteins. Histones are a subset of nuclear proteins involved with DNA binding and condensation as well as regulating transcription and cell cycle progression [173, 174]. Non-histone proteins, such as the high mobility group proteins, function similarly and support various DNA-related activities including transcription, replication, and recombination [174]. Both groups of nuclear proteins typically carry

a net positive charge and contain natural NLS sequences thus making them readily amenable to participate in both a DNA-packaging and nuclear targeting capacity.

Recently, greater resolution of the NLS-mediated trafficking pathway has been reported. By binding the NLS-bearing nuclear protein, p50, to plasmid DNA and microinjecting the complex into the cytoplasm, Mesika *et al*. demonstrated that importins can recognize and bind to the p50-bound DNA, subsequently migrating along microtubules driven by dynein motor proteins. The importin and its conjoined cargo travel toward the microtubule organizing center located adjacent to the nucleus. Upon arrival near the nucleus, the importins dock onto the NPC and shuttle the p50-bound DNA into the nucleus [175].

These results and other recent reports have shed light on the potential role of microtubules in the cytosolic trafficking of both NLS-bearing plasmids and endosomally-enclosed polyplexes [176, 177]. Coupled with the possibility that dynein motor proteins are the drivers of such transport, an exciting opportunity exists in exploiting these cellular entities directly (i.e., in the absence of NLSs and import proteins) to facilitate cytosolic transport and ultimately improve transfection efficiencies.

2.6.3. Carbohydrates

Carbohydrate-binding receptors, known as lectins, that reside intracellularly have offered researchers an opportunity to use sugars to direct the cytonuclear transport of synthetic gene delivery systems [178, 179]. Although carbohydrate-mediated transport shares some common features with NLS-based transport – both are energy- and signal-dependent processes that import their cargo into the nucleus through nuclear pores- the former appears to translocate through the nuclear pores

along a distinct pathway that does not require the presence of cytosolic factors to facilitate import [180, 181].

The identification of specific carbohydrates and their respective intracellular lectins that can be used in this capacity remains an active area of research. It appears that certain carbohydrates used to target cell surface lectins to facilitate cellular targeting and uptake may not necessarily facilitate subsequent intracellular trafficking due to a difference in carbohydrate specificity by intracellular lectins [178, 182]. There have also been conflicting reports about the involvement of certain sugars in mediating cytonuclear transport of polyplexes that will require further scrutiny to resolve [166, 183, 184]. Nevertheless, the relative ease of synthesis, inherent biocompatibility, and reduced immunogenic concerns associated with carbohydrate-based moieties have contributed to its advantageous utility in gene vector design.

2.6.4. Cell mitosis

If dividing cells are targeted, polyplexes may also gain nuclear entry upon nuclear reformation during mitosis. It has been shown that reporter gene expression may be considerably enhanced if transfection occurs shortly before cell division presumably due to the temporary breakdown of the nuclear envelope which allows inclusion of DNA within the nuclear space [185]. However, this behavior appears to be vector type-dependent and may be clinically limited as most cells in the body are postmitotic [185].

2.7. GENE EXPRESSION

Upon arrival into the nucleus, exogenous genes must recruit methods to express their encoded therapeutic proteins (Figure 2-7).

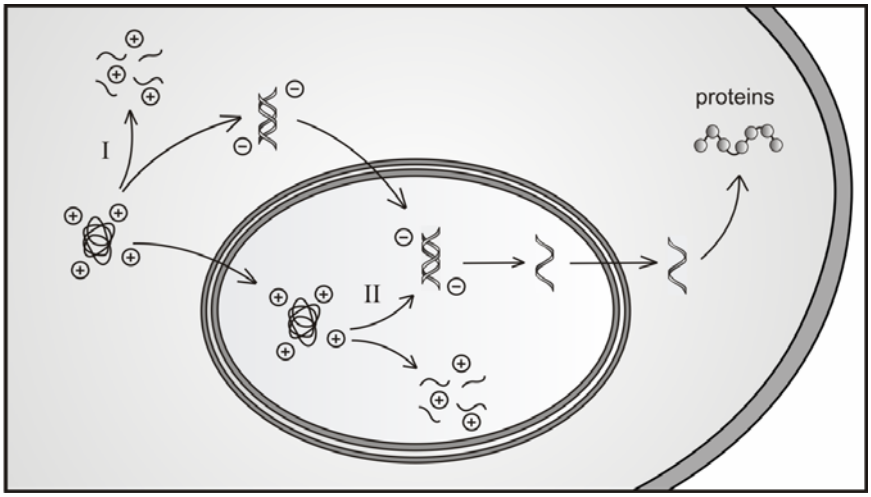

Figure 2-7. Gene Expression – Subsequent to DNA/vector dissociation in the I) cytosol or II) nucleus, released genes must be transcribed and translated into the prescribed therapeutic proteins.

Stable, long term expression is generally achieved through transgenic insertion into the host genome whereas transient, short term expression results from episomal transgene retention. Attempts to direct genome insertion have primarily relied on incorporating DNA transposons within the delivery system. Transposons are naturally occurring DNA sequences capable of enzymatically excising themselves, through the activity of a self-encoded transposase component, out of one chromosomal locus and re-inserting themselves into another locus [186] (Figure 2-8a). By incorporating the transposon sequence either on the same plasmid as the transgene or on a separate plasmid and co-delivering it with the transgenic plasmid, chromosomal insertion may be induced resulting in longer transgene expression [187-192] (Figure 2-8b). The *Sleeping Beauty* (*SB*) transposon is the most widely studied system for gene therapy applications. Table 2-5 provides several other transposon systems that are receiving increasing attention.

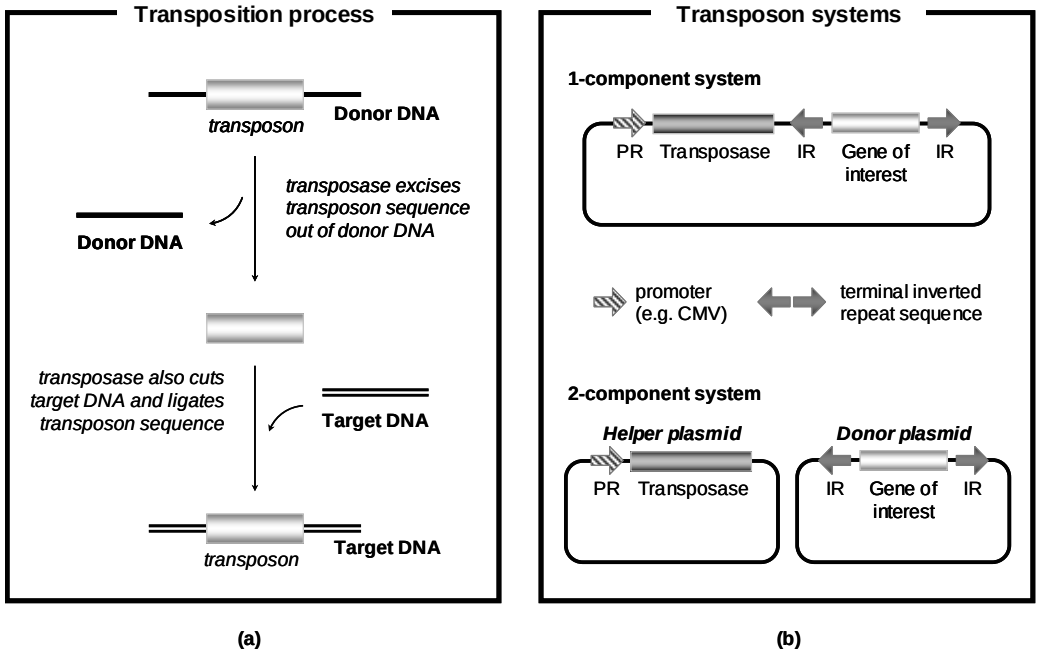

Figure 2-8. Schematic illustration of **a)** *the transposition process* – transposons partially encode for a transposase component that excises and subsequently ligates the transposon into target DNA (Adapted from [193]); **b)** *transposon systems used in gene delivery* - 1-component systems comprise the transposase and therapeutic gene sequences delivered on the same plasmid; 2-component systems comprise a transposase-encoding helper plasmid that is co-delivered with the plasmid containing the therapeutic gene of interest. (Adapted from [187, 194])

Table 2-5. DNA elements used to direct gene expression.

	Ref.
Transposons	
Sleeping beauty	[187, 189, 190, 195]
Tol2	[188]
Piggybac	[192]
Himar 1	[191]
Site – specific elements	
ΦC31	[196, 197]
Gal4 DNA binding domain	[192, 198, 199]
Zinc finger DNA binding domain	[200]
Transcription – regulating promoters	
Mammalian and viral promoters	[201]
Stimuli – inducible promoters	
Tetracycline – induced	[202]
Rapamycin – induced	[203]
Hypoxia – induced	[204]
Glucose – starvation	[205]

An important limitation of transposon-mediated genome integration is the random insertion into the host genome that can lead to inadvertent gene disruption and consequently unwanted side effects such as disruption of essential or tumor-suppressor genes and oncogene activation. Thus targeted, site-specific integration capabilities have been explored with the use of integrase enzymes derived from bacteriophages (e.g., ϕC31 integrase) and the creation of engineered hybrid systems comprised of a transposable element and a DNA sequence recognition element (e.g. DNA binding domain). Both systems provide a certain degree of site specificity through their ability to recognize and dock the transgenic plasmid to a known genome locus after which transgene insertion occurs. However, both systems are not without their respective limitations. A recent study showed that ϕC31-mediated gene insertion may be

accompanied by small chromosomal deletions thus compromising the fidelity of transgenic integration.[206] In the case of the hybrid systems, the methods involved in chimerically fusing a transposable element to a sequence recognition element can potentially disrupt the activity of one or both. Indeed, Wu *et al*. recently probed such concerns by fusing the Gal4 DNA binding domain (DBD) to four different transposons, namely *SB11* (a hyperactive version of *SB*), *Tol2*, *piggybac*, and *Mos1* [192]. The results from their evaluation in four different mammalian cell lines revealed that Gal4 DBD fusion essentially abolished the ability of the *SB11*- and *Tol2*-based systems to mediate chromosomal integration thereby highlighting the potential detriments of these molecularly engineered systems [192].

An additional layer of control currently under investigation is the ability to regulate transcription by introducing or withholding a stimulus. Efforts in this direction have primarily focused on including stimuli-responsive promoter sequences upstream of the therapeutic gene sequence. Both chemical and physical stimuli have been explored and are listed in Table 2-5.

2.8. DNA/VECTOR DISSOCIATION

It has been posited that DNA dissociation from its vector is necessary in order for efficient gene expression to occur [207, 208]. Moreover, expression can be further enhanced if dissociation occurs within the nucleus so as to minimize the residence time of unprotected DNA within the nuclease-rich cytosol [209] (Figure 2-7). Toward this goal, researchers have devised several strategies to effect the intracellular release of DNA, namely by incorporating thermoresponsive properties or hydrolytically degradable or reducible linkages within the polymeric vector (Table 2-6).

Table 2-6. Strategies used to promote DNA/vector dissociation.

	Ref.
Thermoresponsive polymers	
Poly(N-isopropylacrylamide) 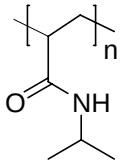	[210-212]
Disulfide bonds	[44, 70, 213, 214]
Ester bonds	[215-217]

2.8.1. Thermoresponsive polymers

Recent investigations of thermoresponsive polymers for gene delivery applications have attempted to regulate the degree of DNA condensation via temperature cues. This class of polymers undergoes a reversible coil-to-globule phase transition in response to changes in temperature [218]. The coil phase is characterized by a relaxed, hydrophilic, extended-chain conformation whereas the globule phase represents a collapsed, hydrophobic, tightly coiled conformation [218]. The transition temperature, above which the globule phase exists and below which the coil phase exists, is often referred to as the Lower Critical Solution Temperature (LCST) [218]. Poly(*N*-isopropylacrylamide) (NIPAM) is one of the most studied thermoresponsive polymers in gene vector design. Its LCST of 32°C can be increased or decreased by copolymerization with hydrophilic or hydrophobic monomers, respectively, thus offering a modification method through which other functionalities may be incorporated while strategically tuning its thermoresponsive behavior [219].

In principle, thermoresponsive polymers with LCSTs below body temperature can be used to deliver tightly condensed DNA complexes to cells. Once inside the

cells, an externally applied temperature reduction to below the LCST induces the relaxed, extended-chain conformation to result in DNA release [211, 219] (Figure 2-9).

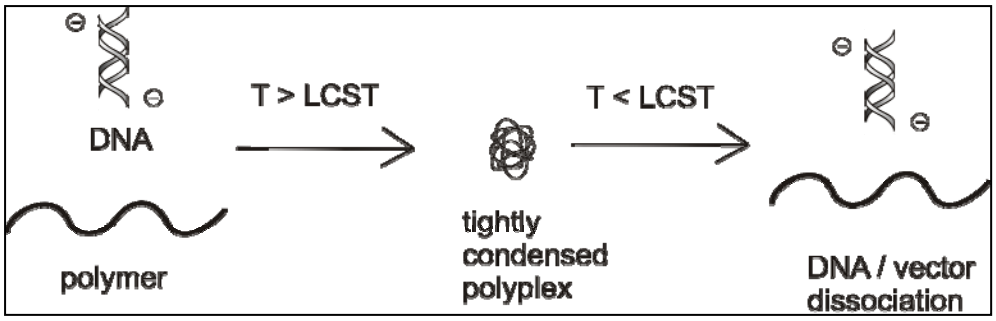

Figure 2-9. Schematic illustration of thermoresponsive polymers as gene vectors. Polymers with a lower critical solution temperature (LCST) below body temperature assume a collapsed conformation at T>LCST to form tightly condensed polyplexes, which promotes cellular uptake. Upon reducing the temperature to T<LCST (e.g., from an externally applied source), the polymer assumes a relaxed, linear conformation to enable DNA/vector dissociation.

Indeed, several groups have demonstrated the ability to enhance transfection efficiency in a temperature-dependent manner with the use of NIPAM-based vectors [210-212]. However, the evidence provided thus far has only indicated a modest level of transfection enhancement. The extent to which thermoresponsive polymers can enhance transfection will depend on optimizing several important parameters including the time and temperature protocol for effective intracellular release, the balance of other functionalities to complement the thermoresponsive properties (e.g., cationic character, hydrophobicity, endosomal escape capabilities), and the LCST range to be suitable for in vivo applications. The use of such polymers for gene delivery applications represents a nascent area of research with a potential that remains to be seen.

2.8.2. Disulfide bonds

An alternative method of effecting DNA release makes use of the redox differential between the oxidizing extracellular space and the reducing intracellular compartment. Upon entry into the cytosol, polymers containing disulfide bonds can be reduced and cleaved to two thiol groups (-SH) through the action of glutathione, one of the most abundant cytosolic peptides in mammalian cells [220].

Disulfide-bonds can be incorporated into gene delivery systems in a variety of ways. Cationic ligands can be bound to a polymer backbone via a disulfide linkage to afford electrostatically-mediated DNA packaging extracellularly with the intention of bond cleavage and subsequent DNA release upon exposure to disulfide-reducing agents in the cytosol [70, 221, 222] (Figure 2-10a). Alternatively, thiol-containing pendent groups can be attached to linear polycations such that DNA packaging results from both electrostatic interaction with cationic ligands and encagement as thiol groups crosslink with other thiol-containing chains [223] (Figure 2-10b). Disulfide bonds can also be introduced along the backbone of a polymer, for instance, by integrating cysteine residues within the polymer chain [44, 213] (Figure 2-10c). In this system, reduction of the backbone to its smaller molecular weight components aims to promote not only DNA release, but reduced cytotoxicity that is typically associated with lower MW polymers [44, 213, 214, 224].

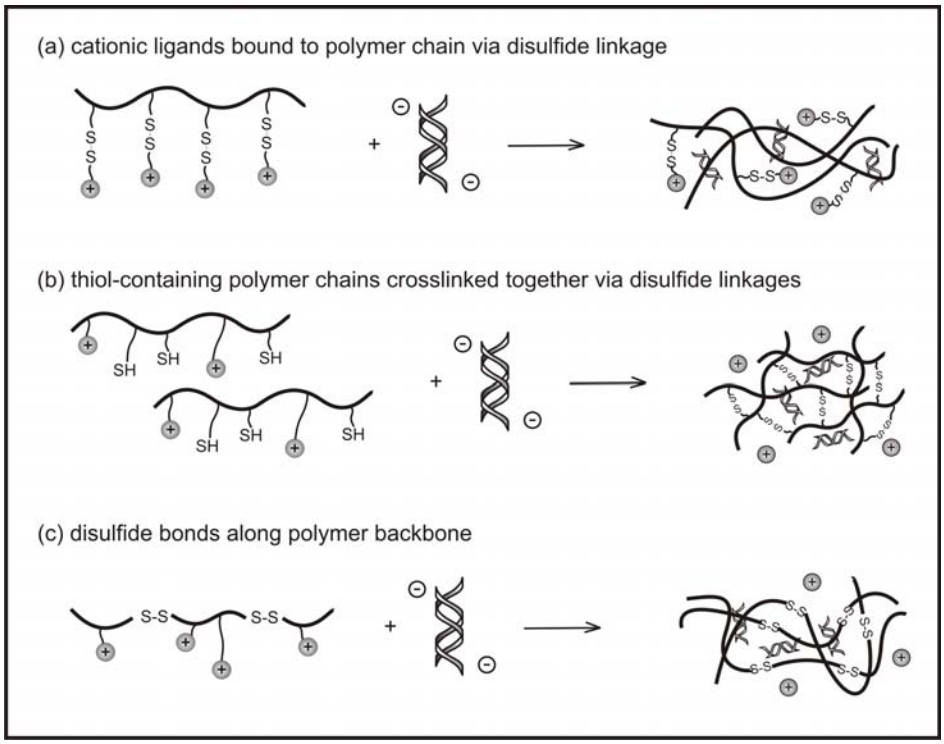

Figure 2-10. Schematic illustration of disulfide bonds incorporated into polymer vectors to afford DNA/vector dissociation upon exposure to a reducing environment (e.g., cytosol). Methods include **a)** binding cationic ligands to the polymer backbone via disulfide linkages; **b)** conjugating thiol-containing pendant groups to linear polycations that can crosslink with other thiol-containing chains; and **c)** introducing disulfide bonds along the polymer backbone.

It is important to consider, however, the presence of other disulfide reducing agents extracellularly and within other intracellular compartments (e.g., endosome, lysosome) that can result in premature release of disulfide-bound ligands [220]. Regardless, the inherent reversibility of disulfide linkages and their relative stability in plasma have provided an attractive tool for conjugating a variety of ligands (e.g., targeting, endosomal release peptides, CPPs) that need to be released in the cytosol.

2.8.3. Ester bonds

Hydrolytically-sensitive ester bonds can also be used to bring about DNA release in a temporally controlled manner. Like disulfide bonds, ester bonds have been used as labile crosslinkers for higher ordered structures (e.g., branched, network), as linkages for cationic pendent groups to a polymer backbone, as well as along the backbone (e.g., biodegradable nano- and microspheres) so as to afford low MW degraded by-products [78, 215-217, 225]. In contrast to their disulfide counterparts, water molecules are the cleaving agents and as such, hydrolysis can occur upon first exposure to physiological environments. Several studies have explored the parameters (e.g., MW, crosslinking density, cationic charge density) that potentially mediate degradation kinetics and thus DNA release; however the structural and chemical requirements for the controlled and sustained release have yet to be fully defined [78, 226].

2.8.4. Charge reduction or modification

A more passive approach for effecting DNA release has been pursued by either reducing or modifying the cationic charge of the vector such that polymer/DNA interactions are weakened and DNA can dissociate more readily in the presence of anionic biological macromolecules (e.g., mRNA, heparin, proteoglycans). Erbacher *et al*. and Gabrielson *et al*. partially substituted the cationic primary amines of PLL and PEI with gluconyl and acetyl groups, respectively, in order to reduce the cationic charge [227, 228]. Kimura *et al*. evaluated the effects of both reducing and modifying the cationic charge by chemically modifying poly(lysine) with hydroxyl and quarternary ammonium groups, respectively [229] (Figure 2-11). All three groups demonstrated the ability of charge reduction and/or modification to weaken the

DNA/polymer interaction and attribute the resultant enhancement in transfection, at least partially, to the easier dissociation of DNA from its vector.

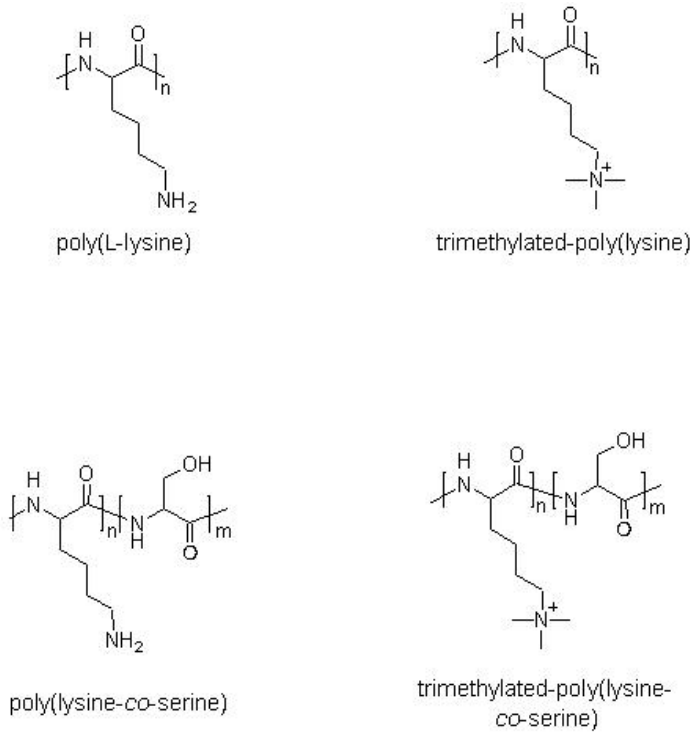

Figure 2-11. Structures of poly(L-lysine) (PLL) derivatives prepared by Kimura *et al*. to evaluate the effects of charge reduction and/or modification on DNA/vector dissociation behavior [229].

2.9. BIOCOMPATABILITY

One of the biggest challenges facing synthetic gene delivery systems, second to subtherapeutic transfection efficiencies, is the issue of biocompatibility. The current biocompatibility design criteria for gene delivery systems require both systemic stability within the bloodstream as well as minimal induction of toxic effects at the cellular level.

2.9.1. Systemic stability in the bloodstream

The clinical viability of any gene delivery system requires the unimpeded systemic delivery through the bloodstream and oftentimes to disseminated regions of the body. It has been shown that cationic polyplexes can 1) interact with blood components (e.g., serum proteins, blood cells) to form large, aggregated, embolytic entities; 2) aggregate with other individual polyplexes due to exposure in varying physiological salt conditions; 3) activate the complement system; or 4) become recognized and cleared by the reticuloendothelial system [230, 231]. The induction of any one of these events can lead to premature elimination of the polyplex preventing delivery of the genetic cargo to its final destination [230, 231]. By designing for sufficient serum stability to account for these clearance mechanisms, polyplexes may experience extended circulation times, in turn improving the chance for extravasation into the targeted tissue and increasing the opportunity for polyplex-cell interactions.

The incorporation of poly(*N*-(2-hydroxypropyl)methacrylamide) (pHPMA), poly(ethylene glycol) (PEG), and various oligosaccharides into vector designs represents the most widely used strategy for improving stability within the bloodstream (Table 2-7). By virtue of their hydrophilic, non-ionic nature, these materials have been shown to increase polyplex solubility and reduce the interactions between individual polyplexes as well as with serum components resulting in prolonged circulation times [232, 233].

Table 2-7. Ligands used to stabilize polyplexes in bloodstream.

	Ref.
Non – ionic hydrophilic polymers	[234-236]
Poly(ethylene glycol) (PEG) 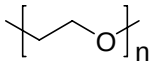	
Poly(N-(2-hydroxypropyl)methacrylamide) (pHPMA) 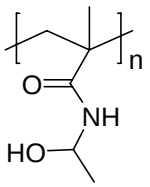	[61, 237]
Oligosaccharides	
Alginate	[238]
Dextran	[239-241]
Hyaluronic acid	[242]
Trehalose	[243]
Cyclodextrin	[54]

PEG and pHPMA are thought to stabilize the polyplex by creating a hydrophilic shell that effectively masks its serum-destabilizing properties (e.g., ionic, hydrophobic residues). It is becoming clear that in order for the hydrophilic shell to provide steric stability (i.e., prevention of serum-induced aggregation) without compromising transfection efficiency, it must also provide lateral stability (i.e., it must not contribute to or allow disruption of the electrostatic interaction between the polycation and DNA) [244]. It has been shown that PEG or pHPMA moieties, when grafted to or copolymerized with the polycation, can indeed stabilize the polyplex in a serum-rich environment; yet, at the same time, it may interfere with DNA complexation resulting in poorly condensed polyplexes and reduced transfection efficiencies [239, 245]. To alleviate this problem, several methods of PEG or pHPMA

incorporation have been developed to create an effective hydrophilic coat that 1) does not interfere with DNA/polycation complexation; 2) protects against penetration from competing anionic biomolecules that can disrupt polymer/DNA interaction; and 3) surrounds the polyplex to provide steric stability. These methods include coating the surface of preformed polyplexes with monovalent or multivalent PEG or pHPMA chains that can bind to amino groups extending from the polyplex [233, 246-248] (Figurea 2-12a and 2-12b). Multivalent chains have the ability to cooperatively bind with multiple amino groups per hydrophilic chain forming a covalently crosslinked coating that offers both steric and lateral stability [246-248] (Figure 2-12b).

Additional gene transfer-enhancing functionalities (e.g., targeting) can also be incorporated with heterobifunctional PEG or multivalent HPMA chains that bind to extended amino groups of the polyplex at one reactive site and additional functional groups at other reactive sites along the same chain [87, 94, 95, 234] (Figure 2-12c). Alternatively, serum-stabilizing chains can be bound to the vector via degradable bonds (e.g., acid-labile hydrazone or acetal bonds, reducible disulfide bonds) that can be cleaved upon exposure to the appropriate intracellular environment thereby shedding the hydrophilic coating to reveal its underlying functionalities (e.g., endosomal escape) [61, 249, 250] (Figure 2-12d).

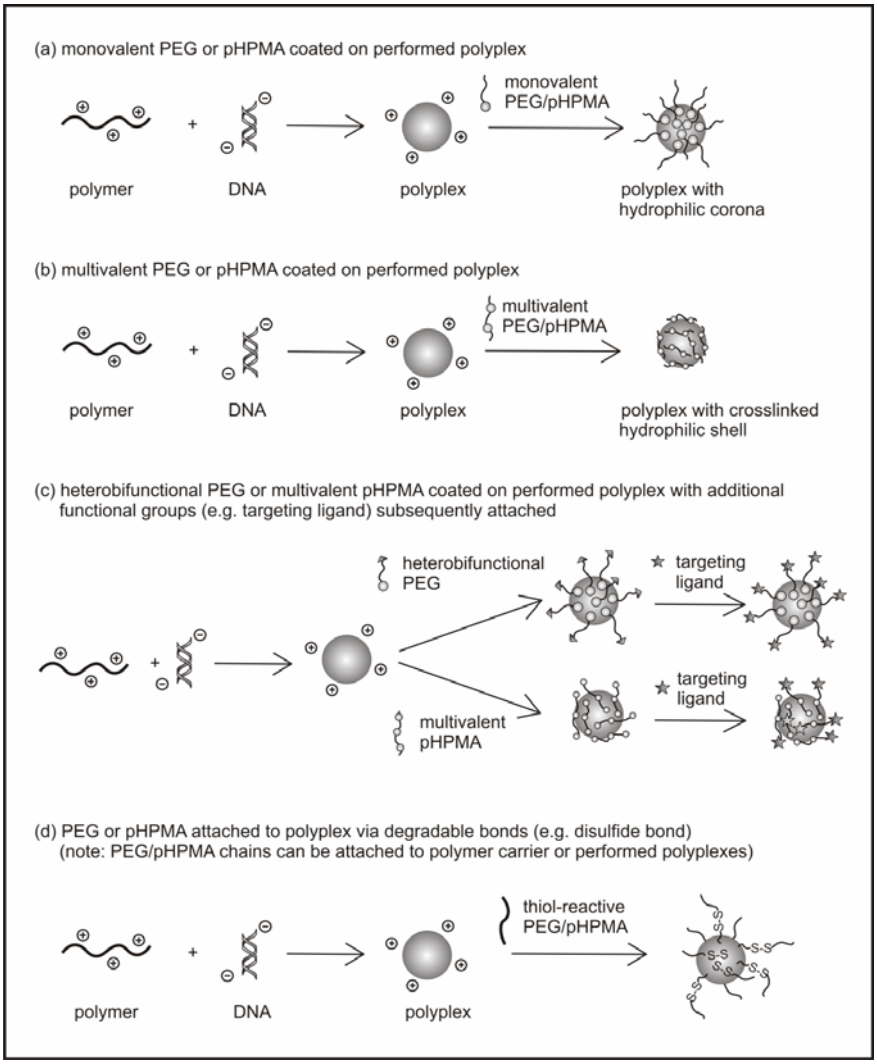

Figure 2-12. Schematic illustration of poly(ethylene glycol) (PEG) and poly(*N*-(2-hydroxypropyl)methacrylamide) (pHPMA) attachment to polymeric gene delivery systems to improve polyplex stability in the bloodstream. Methods include **a)** coating preformed polyplexes with monovalent PEG/pHPMA chains; **b)** coating preformed polyplexes with multivalent PEG/pHPMA chains to form a crosslinked hydrophilic shell; **c)** coating preformed polyplexes with heterobifunctional PEG or multivalent pHPMA chains that can attach additional functional groups at remaining reactive sites; and **d)** binding PEG/pHPMA chains via disulfide bonds to effect subsequent cytosolic release of the hydrophilic coat.

Due to their inherent solubility, biocompatibility, biodegradability, and potential targeting capacity, oligosaccharides have also been considered as an attractive alternative to synthetic stabilizers. Table 2-7 lists a few such compounds that have been employed in a serum-stabilizing capacity. Of the oligosaccharides shown, cyclodextrin (CD) is distinct in its ability to accommodate hydrophobic molecules within the hydrophobic interior of its cup-shaped structure while remaining readily soluble by virtue of the hydrophilic shell that surrounds its exterior. As a result of its functional flexibility, CDs have been incorporated in gene vector designs in various creative capacities [251, 252].

The aforementioned serum-stabilizing agents have all demonstrated the ability for hydrophilic, non-ionic polymers to reduce polyplex aggregation, increase solubility, reduce surface charge, and prolong circulation in the bloodstream. The extent to which these hydrophilic moieties are able to stabilize the polyplex, however, is dependent on a number of factors including the chain length of the hydrophilic moiety or the polycation vector, polycation type, grafting density, and identity and density of co-functionalized ligands and should be appropriately considered for the specific gene delivery application [253, 254].

2.9.2. Cytotoxicity

For gene therapy to be successful, the cells that are targeted must remain viable to sustain transcription and translation to the prescribed proteins. In this regard, the cytotoxic effects of both the polyplex and the free vector, derived from any uncomplexed vector remaining after polyplex formation or upon intracellular release of the DNA, must be considered [255, 256]. Although the mechanisms that govern the cytotoxic effects of certain polyplex and vector properties remain uncertain, the prevailing hypothesis suggests that cytotoxicity is mediated by ionic interactions

between anionic domains on the cell surface and cationic moieties present on the vector [257]. The ionic interaction is thought to result in polyplex aggregation and accumulation at the cell surface which can severely impair membrane function and ultimately lead to cell death [258]. Moreover, structural parameters that might promote such interactions can further exacerbate the cytotoxic effect. Such parameters include the following vector and polyplex properties - MW, structure (e.g., linear, branched), degree of branching, cationic charge density, type of cationic functionality, polyplex size, polyplex surface charge, three-dimensional conformation, and polyplex flexibility [259-261].

Of these properties, MW has been shown in numerous studies to be directly proportional to both cell toxicity and transfection efficiency. This apparent dichotomy poses a challenge to gene vector design, since low cytotoxicity and high transfection efficiency are two fundamental design criteria for all gene delivery systems, and has inspired investigators to seek creative approaches to overcome the challenge. Most of the strategies employed have attempted to exploit both the low cytotoxic effects typically correlated with lower MW (≤ 2 kDa) vectors and the enhanced transfection efficiencies typically associated with high MW (≥ 25 kDa) vectors. Such efforts coincide with the strategies used to facilitate DNA release where low MW polymers are crosslinked or linearly linked together by degradable linkages (e.g., disulfide bonds, ester bonds) to form a high MW polymer that can eventually degrade to its lower MW components [78, 213, 214, 262-265]. These lower MW components can then be cleared either via renal elimination for MWs less than 30 kDa (e.g., 1.8 kDa PEI) or through natural metabolic pathways for low MW polymers that are endogenous metabolites (e.g., poly(4-hydroxyl-L-proline ester)) [78, 79, 142].

2.10. STRUCTURAL AND PROCESSING CONSIDERATIONS

The synthetic versatility that is afforded by polymer chemistry has enabled the creation of a diverse array of polymers ranging in size, architecture, and chemical composition. Polymers spanning in MW from 10^2 to 10^6 Da in a linear, branched, crosslinked, or dendritic structure with various physicochemical properties have been developed as potential gene vector candidates. In contrast to the chemical entities that have been developed to fulfill specific vector criteria (e.g., pHPMA for serum stability, polycations for DNA packaging), the role that structural features (e.g., MW, architecture, side chain distribution) play in gene transfer is less straightforward. They appear to play a more supporting role that act synergistically with chemical entities to modulate their gene transfer functionality.

Numerous studies have shown that structural features such as MW, architecture, side chain termini composition, side chain density, and side chain length can greatly influence the transfection potential of a gene vector [43, 266-269]. Even minor structural differences such as the stereochemistry of a single side chain group can significantly affect transfection [270, 271].

Adding to the growing list of chemical and structural properties that impact transfection are the experimental conditions under which polyplexes are formulated and evaluated. Parameters such as polymer compound purity, the ionic environment in which polyplexes are formed, the presence of free polycations in solution during transfection, DNA concentration, N:P ratio, cell seeding densities, and incubation times can affect a vector's ability to successfully mediate gene delivery [30, 39, 255, 256, 272].

These parameters, from chemical properties to structural dimensions to experimental parameters, have been highlighted to serve as points of consideration in

both the design of safe and efficient vectors as well as the interpretation of transfection results.

2.11. CHALLENGES AND FUTURE DIRECTION

Although research has produced a robust arsenal of polymer tools and design strategies to date, the challenge still remains in creatively integrating the different functionalities into a single multifaceted vector. Several strategies have emerged to offer new and interesting perspectives on meeting this challenge. One approach seeks to develop alternative gene delivery platforms through the use of higher ordered macromolecular structures such as interlocked, multi-component supramolecules or 2-D and 3-D scaffolds. Another approach seeks to enhance existing vector platforms (i.e., covalent functionalization of polymer chains) by adopting combinatorial strategies and high throughput technology as a way to systematically evaluate the vast parameter space of vector design and accelerate vector discovery.

Gene delivery research will also see the development of more sophisticated analytical methods to quantify the various aspects of gene delivery. Methods that can more accurately characterize the physicochemical characteristics of multifaceted vectors, evalulate the specific delivery-enhancing effects of various physicochemical vector features, and quantify the behavior of polyplexes within the cellular environment will offer researchers invaluable tools for probing the mechanisms that govern gene transfer.

Another important area of gene delivery research is the continued effort toward resolving the biological landscape through which gene delivery systems must traverse. Several groups have recently identified the involvement of previously unsuspected intracellular entities and pathways in gene delivery, underscoring the complexity of

the cellular environment that still remains obscure. Resolving the biological landscape and its implication in gene delivery will be critical toward improving vector designs.

2.11.1. Multi – component supramolecules

2.11.1.1. *Polyrotaxanes*

Polyrotaxanes are a specialized class of supramolecular structures composed of one or more ring-like molecules that are non-covalently threaded over a linear polymer chain with bulky end groups capping each chain termini to prevent dethreading of the ring molecules [273]. Recently, Ooya *et al*. demonstrated the utility of such polymers in gene delivery applications by threading cationically-rendered α-cyclodextrin (α-CD) molecules over a PEG chain (M_n=4 kDa) and capping both ends with benzyloxycarbonyl tyrosine groups via disulfide bonds [251] (Figure 2-13).

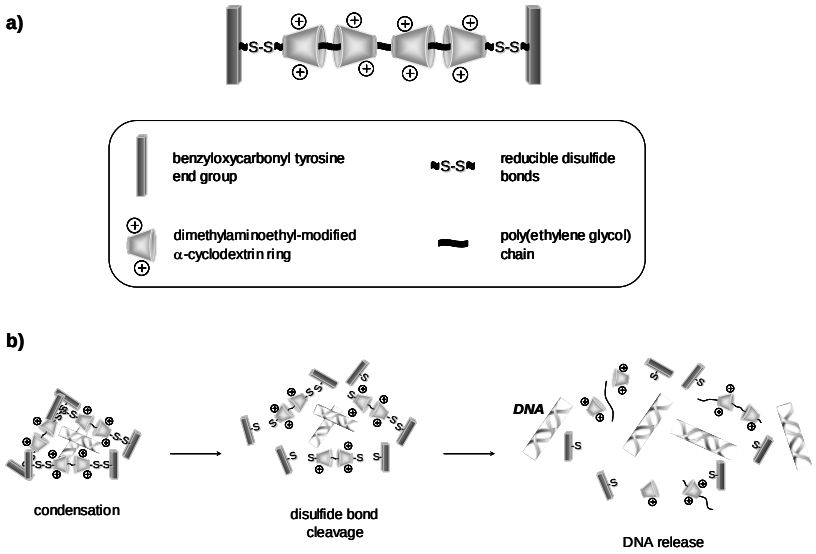

Figure 2-13. a) Schematic representation of biocleavable polyrotaxane-based vector designed by Ooya *et al*. Polyrotaxanes are composed of one or more ring-like molecules that are non-covalently threaded over a linear polymer chain. Bulky end groups cap each chain termini to prevent dethreading of the ring molecules. **b)** DNA can be condensed to <200 nm polyplexes and subsequently released upon disulfide bond cleavage (Adapted from [251]).

The assemblage of dimethylaminoethyl (DMAE)-modified α-CDs imparted upon each polyrotaxane unit a cationic charge capable of condensing DNA to <200 nm-sized polyplexes and neutralizing its negative charge at N:P ratios of 0.5. The DMAE functional groups also appeared to mediate endo-lysosomal escape by acting presumably in a buffering capacity resulting in greater nuclear accumulation of the liberated polyplexes compared to PEI-based polyplexes. Moreover, disulfide bond cleavage facilitated both the release of DNA in the presence of competing polyanions and the breakdown of the supramolecular vector to its non-toxic, lower MW components as evidenced by the >90% cell viability at N:P ratios up to 10.

In comparison to linear PEI (22 kDa), a commercially available polymer often considered to be the gold standard for polymer-based vectors, polyplexes formed at an N:P of 0.5 were unable to form tightly packed polyplexes and possessed a negatively charged surface. At higher N:P ratios, where PEI was able to form tightly condensed polyplexes with DNA, transfection efficiencies and cell viability profiles were comparable for both polyrotaxane-and PEI-based polyplexes at N:P=2. As N:P ratios were increased to 5 and 10, however, polyrotaxane-mediated transfection efficiencies remained the same with no apparent reduction in cell viability; whereas, PEI-based polyplexes mediated greater transfection efficiencies, but with an accompanying increase in cytotoxicity. These preliminary data suggest such multi-functional supramolecules to be viable gene delivery platforms and warrants further investigation to optimize their transfection potential. Indeed, there have been several polymers relevant to gene delivery systems that have already been incorporated into polyrotaxane structures including PEI, PLL, polyesters, and poly(lactic acids) [274]. Of the handful of ring-like molecules explored to date, CDs have been the most extensively studied and lend themselves readily to polyrotaxane-based gene delivery

systems based on the substantial precedents within the literature of their utility in vector design [54, 275-277].

2.11.1.2. *Substrate-mediated delivery*

The past several years have seen a steady growth in interest in releasing naked DNA or polyplexes from surface-erodible substrates or biodegradable 2-D and 3-D scaffolds. Such substrate-mediated delivery typically requires implantation of the DNA-loaded substrate or scaffold proximate to target cells as a means of overcoming serum instability and clearance from the bloodstream that is often associated with in vivo systemic injection [278]. Localized substrate placement exposes targeted cell populations to a microenvironment with higher transgene concentrations compared to a systemically delivered bolus injection, which can become diluted upon circulation. As a result, gene delivery via implantable substrates requires less DNA or polyplex loading, and therefore a lower risk of cytotoxic side effects, to achieve comparable transfection levels as systemic delivery [279]. Moreover, DNA or polyplex release profiles can be regulated by the degradation kinetics of the engineered systems to afford a controlled and sustained release rate and ultimately prolonged gene expression.

2.11.1.3. *DNA – eluting films*

Substrate-mediated gene delivery has seen significant progress recently with the development of layer-by-layer (LBL) film deposition technology. LBL fabrication entails the alternating, stepwise adsorption of multivalent layers to produce finely structured, dimensionally controlled, self-organized films that conform readily to topologically complex surfaces, in a variety of patterns, and for a range of materials (e.g., polymers, metals) [280-282]. Owing to its ease and versatility, LBL methods

have been used to fabricate submicron-thick polyelectrolyte films loaded with DNA onto planar substrates that can mediate gene transfer to an overlaid monolayer of cultured cells [283-285].

Recently Jessel *et al*. demonstrated the ability to further control the sequence of release of multiple DNA constructs to three different model cell types [286]. By embedding two distinct DNA constructs at different levels within a poly(L-lysine) (PLL) and poly(L-glutamic acid) (PGA) multilayered film, they showed that the onset of protein expression was dependent upon the depth at which the DNA was embedded within the film. Furthermore, they showed that transfection required the assistance of a cationic chaperone (pyridyl-β-cyclodextrin) and speculated that enzymatic degradation of the PLL and PGA matrix, as opposed to the passive diffusion of DNA out of the matrix, was likely the mechanism by which cells obtained access to the embedded DNA.

In another study, Jewell *et al*. demonstrated the conformability of LBL-fabricated films to complex surface topologies by depositing a homogenous, 120 nm thick, physically robust multilayered film on stainless steel intravascular stents [281]. The film, composed of a hydrolytically degradable polyamine interdigitated with DNA, was able to erode in an aqueous environment to effect the release of the embedded DNA and transfect cells in serum-containing media. Furthermore, the integrity of the film remained largely intact upon exposing the coated stent to mechanical stresses representative of those experienced during stent delivery and deployment.

2.11.1.4. *2 – D and 3 – D scaffolds*

Another form of substrate-mediated delivery seeds or adsorbs naked DNA or polyplexes within or onto the surface of porous, biodegradable matrices that encourage both cell ingrowth within the scaffold and temporally controlled release of

the embedded DNA or polyplexes. Such systems have been used primarily in tissue engineering applications where the scaffold serves as both a physical support for cell adhesion and subsequent tissue formation as well as a depot from which naked or condensed DNA are eluted. The majority of scaffolds that serve in this capacity are fabricated from synthetic polyesters such as poly(lactide-*co*-glycolide) (PLGA) and poly(lactic acid) or natural polymers such as collagen, hyaluronan, and alginate.

DNA-loaded scaffolds can be constructed from nanofibers interlocked together to form a mesh-like network that mimics the natural fibrillar architecture of the extracellular matrix. Using specialized polymer processing techniques (e.g., electrospinning, interfacial complexation fiber drawing), several groups have demonstrated the ability to incorporate DNA or polyplexes into the structural unit of each fiber without compromising the transfection competence of the impregnated DNA upon release from the fibers [287-289]. Such scaffolds have been shown to support cell adhesion and growth while eluting DNA or polyplexes to adhered cells for up to three weeks.

Scaffolds can also be fabricated into porous, sponge-like plugs that provide the same tissue-inductive guidance as fibrous scaffolds. DNA and polyplexes have been incorporated into such scaffolds through a variety of techniques including non-specific surface adsorption, specific surface interactions (e.g., biotin-avidin interaction), covalent attachment, and encapsulation within the matrix [279, 290-292]. Mooney and co-workers and Shea and co-workers have demonstrated the in vivo efficacy of such 3-D matrices to sustain DNA or polyplex release on the order of months to cells located within and around the implanted scaffold [291, 293, 294]. Interestingly, Mooney and co-workers showed that polyplexes incorporated into PLGA scaffolds afforded longer and greater levels of gene expression compared to both bolus injection of polyplexes and scaffolds embedded with uncondensed DNA. These comparisons

underscore the systemic advantage of localized, implant-mediated delivery as well as the benefits of DNA condensation, presumably for overcoming intracellular barriers, to result in greater transfection efficiencies [291].

Efforts to further guide the spatial delivery of DNA have included orienting the adhesion of and subsequent delivery to cells along topographical features that are patterned into the scaffold [292]. The opportunity for even finer spatial resolution and architectural complexity may be achieved with nanofabrication techniques, an application that could make significant contributions to substrate-mediated gene delivery.

2.11.2. Combinatorial strategies

2.11.2.1. *Combinatorial libraries and high throughput screening*

Optimal transfection hinges upon a critical balance between the various structural and chemical properties endowed upon a vector. Properties designed to overcome one barrier can directly hinder the ability to overcome other barriers. For example, polyplexes with a positive surface charge may interact favorably with cell surface proteoglycans while excess positive charge may result in serum instability or cytotoxicity. Moreover, some features require a minimum threshold be met to exert their intended transfection functionality. For instance, it has been shown that certain sugars used as targeting moieties may require a minimum number of sugar residues represented on the polyplex to achieve sufficient avidity with their cell surface lectin to induce binding and subsequent uptake [178]. Unfortunately, rationally designing synthetic vectors with optimally balanced physicochemical properties remains extremely difficult since the biological barriers that must be overcome are still mechanistically ill-defined.

Within the last decade, combinatorial chemistry has emerged as a promising, complementary tool to overcome the challenges that limit the rational design of polymeric vectors. In principle, combinatorial chemistry entails the parallel synthesis of compounds that share common properties (e.g., molecular backbone, molecular weight) in addition to other structural features (e.g., functional groups) that are incrementally varied over an appropriate and relevant range [295]. The incremental variation of features offers a systematic approach to ascertain the critical balance required between different physicochemical properties. Upon screening each compound, one can identify both hits - specific compounds that possess desirable properties - and trends that demonstrate how an incrementally varied feature affects the measured output. In the context of polymeric vector design, hits are desired because they identify polymers that possess the desired biophysical and chemical properties (e.g., high transfection efficiency, low cytotoxicity). Equally important are the trends that are observed between polymers that share an incrementally varied feature. These trends may provide information about the functional effects of a particular structural feature (i.e., structure-function relationship) and ultimately shed light on the underlying biochemical and physical landscape and mechanisms that govern these structure-function relationships and, in turn, gene transfer [295].

Combinatorial libraries that span a large and diverse property range enable exploration of a broad chemical and structural parameter space. Furthermore, the information gleaned from screening these libraries can guide subsequent syntheses of more focused libraries allowing investigators to probe the depth of this parameter space for a more optimized vector design.

Anderson *et al*. recently demonstrated the feasibility of such an approach in vector design by employing automated fluid-handling systems to facilitate the one-step synthesis and cell-based screening of over two thousand unique gene vector

candidates [296]. The synthesis of all pairwise combinations of 94 amino monomers and 25 diacrylate monomers at an equimolar ratio yielded 2,350 compositionally unique yet related polymers. Subsequent screening of each compound revealed 46 hits, that is, polymers with greater transfection efficiencies than the control vector, PEI. Additionally, the authors were able to identify common features with possible transfection-enhancing effects amongst the top performing polymers, namely a hydrophobic component, mono- or dialcohol side groups, and linear, bis(secondary amines).

With these results, the authors subsequently created a more focused library of polymers, using 18 of the amino and 12 of the acrylate monomers from the initial library [67]. To optimize vector design, amino to acrylate monomer ratios were varied (from 0.6-1.4) for each pairwise combination as a way to introduce two additional features to the combinatorial library - 1) chain end group composition (amine or acrylate) and 2) MW (1000 to 61,000 Da) [297]. To probe the underlying structure-function relationships, all polymers were initially screened for transfection efficiency at various N:P ratios and top performing polymers were subsequently evaluated for particle size and surface charge to explore their roles in gene transfer. The results of this second-generation study identified a different set of polymers that brought about greater transfection efficiencies than the top performing polymers from the initial library. The three most effective polymers contained hydrophobic and alcohol groups thus confirming the compositional trends observed previously. These polymers were also all greater than 10 kDa in MW and able to condense DNA into polyplexes of less than 100 nm in diameter with a surface charge greater than 10 mV. Interestingly, as the amine to acrylate monomer ratio was increased, maximum transfection efficiency occurred at intermediate ratios. This result further highlights the benefits of utilizing combinatorial approaches to probe the effects of incremental variations in vector

properties in order to discover polymers that possess an optimal balance in their physicochemical properties. Attempts have been made to further optimize vector performance, based on monomers from the second-generation library, by adding cell targeting sequences and disulfide linkages to promote cytosolic DNA release and have recently been reported [70].

The benefits of combinatorial strategies cannot be fully realized unless the technical hurdles associated with high volume compound synthesis, characterization, and screening are sufficiently resolved: synthetic schemes should ideally be simple with a minimal number of steps required from chemical reaction to compound purification and isolation; characterization techniques must be accurate to derive true structure-function relationships; and screening assays should be amenable for rapid and high throughput platforms to facilitate evaluation of extensive libraries of compounds.

2.11.2.2. *Computational methods*

Recent advances in high throughput technology have made possible the ability to rapidly polymerize, characterize (e.g., gel permeation chromatography, MALDI-TOF mass spectrometry) and screen (e.g., transfection assay) libraries of compounds using high-speed instrumentation and automated fluid-handling systems [296, 298]. Additionally, computational modeling techniques can be used to facilitate library design and compound discovery. This idea is predicated on the notion that computational methods can be used to model and predict the biological response of each compound in a combinatorial library thereby abrogating the need to exhaustively synthesize and evaluate every compound.

Smith *et al*. demonstrated this concept by using an artificial neural network (ANN) model to predict the extent to which individual polymers, each belonging to a

combinatorial library of related biomaterials, promote fibrinogen adsorption [299, 300]. The model was configured based on the fibrinogen adsorption data of a pre-existing combinatorial library of 112 polymeric biomaterials [295]. A randomly selected half of the experimental data set was used to "train" the ANN model. The remaining half of the data set was used to validate its prediction accuracy by comparing the experimentally-determined versus predicted values. A critical aspect of model development is the identification of common polymer parameters that can accurately represent the extent to which each polymer can support fibrinogen adsorption. These molecular descriptors (MD), as they are called, may be experimentally measured (e.g. glass transition temperature, air-water contact angle) or mathematically derived (e.g., log of the octanol/water partition coefficient, total flexibility index). Each polymer is quantitatively represented by a set of such MDs to be used as input variables into the ANN model for adsorption prediction. Smith *et al.* identified three out of 106 MDs that were computationally determined to be the most highly correlative with fibrinogen adsorption – glass transition temperature, number of hydrogen atoms in the molecule, and log of the octanol/water partition coefficient calculated from a linear atom type model.

The results from their study demonstrated the ability of their semi-empirical model to predict 70% of the data to within experimental error, which the authors propose to be a sufficient level of accuracy for materials evaluation [299, 300]. The model was also able to distinguish between the highest and lowest fibrinogen adsorbing polymers which, upon closer analysis, identified distinct structural differences between the two as well as exclusive similarities within each group. Moreover, sorting out each compound based on the degree of fibrinogen adsorption can then be used to guide the actual laboratory synthesis of only the most promising candidate polymers. Interestingly, the outcome of their study bears striking

resemblance to Anderson *et al.*'s results with one salient difference being the time and cost savings associated with virtual synthesis versus actual laboratory synthesis.

It is important to consider that the degree to which the model can accurately predict the biological response relies heavily on both the quantity and quality of molecular descriptors selected to represent each compound. If the MDs chosen are experimentally measured (e.g., glass transition temperature), each compound must still be synthesized in order to measure its MD value. Although costly and arduous in vitro assays (e.g., fibrinogen adsorption) can be avoided, a model that can predict the biological response of a compound entirely in silico without the need to synthesize it may be more desirable. Therefore, Smith *et al*. modified their original model so as to predict fibrinogen adsorption affinity based solely on mathematically-derived structural MDs – molecular density, number of hydrogen atoms in the molecule, and log of the octanol/water partition coefficient calculated from a linear atom type model. The redesigned model was able to predict adsorption affinity as accurately as their original model without the use of experimentally measured MDs [301].

To our knowledge, computational models developed to facilitate the design of polymeric vector libraries have yet to be reported. In light of the similarities between Smith *et al*.'s biomaterials library and Anderson *et al*.'s vector libraries, with regard to the polymeric constitution of the combinatorial library, the biological nature of the measured output, and the subsequent data analyses, the above-mentioned computational approach appears particularly well suited and readily amenable for the design and screening of vector libraries. As combinatorial strategies gain a greater presence in vector development, the parameter space in which investigators desire to explore will inevitably expand. Computational modeling will become increasingly relevant and perhaps an imperative approach to building, screening, and mining

through vast combinatorial libraries that may otherwise be too large to exhaustively explore.

2.11.3. Analytical methods

Along with innovative approaches for integrating the diverse collection of polymer tools and technologies, the future of gene delivery research rests on the continual development of robust analytical methods that can 1) accurately characterize the physicochemical characteristics of multifaceted vectors; 2) elucidate the mechanisms by which certain physicochemical features facilitate gene transfer; and 3) quantify the behavior of polyplexes within the cellular environment in order to gain mechanistic understanding of the intracellular barriers and rate-limiting steps that impede efficient gene delivery. The creation of such methods will enable more accurate assessments of how polymers mediate gene delivery and in turn, better design principles can be established to guide the design of improved gene delivery systems.

Hennink and colleagues recently reported a more reliable, aqueous-based, size exclusion chromatography (SEC) protocol for determining the absolute molar mass and distribution of various polycations commonly employed in gene vector design [302]. The protocol was developed to address the limitations associated with sub-optimized SEC conditions that are typically used to determine such parameters. Conditions including an inappropriate ionic strength of the eluent and the anionic charge of the column packing can interact unfavorably with polycationic samples leading to inaccurate molar mass and distribution characterization. Such inaccuracies, in turn, can result in false structure-function relationships and erroneous conclusions.

A number of analytical techniques have also emerged as a result of efforts aimed at unraveling the mechanisms by which various structural features enhance the ability for a polymer vector to overcome specific barriers of the gene delivery pathway.

One such structure-function relationship that has been extensively probed is the putative endo-lysosomal escape functionality of protonatable amino groups present on several commonly used polymer vectors (e.g., PEI, poly(β-amino ester), PAMAM) [133, 303-305]. The prevailing mechanistic hypothesis behind this relationship, referred to as the "proton sponge" effect, asserts that such protonatable groups sequester protons upon endosomal acidification resulting in an influx of chloride ions to maintain electroneutrality, subsequent osmotic swelling, and finally rupture of the endosomal vesicle. Release of the polyplexes from the endosome prevents trafficking to the enzymatically degradative lysosomal compartment thereby increasing the chance for nuclear delivery and ultimately greater transfection efficiency [133]. Although the hypothesis dates back to over a decade ago, evidence supporting it has been largely qualitative [37, 134, 306, 307]. Assays developed to validate the hypothesis in a more quantitative manner have employed the combined use of pH-sensitive and pH-insensitive fluorescent probes to double-label either the polymer vector or the DNA itself [133, 303-305]. Using flow cytometry to sort and quantify the ratio of fluorescence intensities, the local pH environment of the fluorescently-labeled entity can be determined and thus intracellular location (e.g., endosome, lysosome, cytosol) may be deduced. Similarly, chlorine ion-sensitive and –insensitive fluorescent probes can be used to quantify the concentration of endosomal chloride ions and probes conjugated at self-quenching and low concentrations have been shown to enable estimations of endosome volume at various time points [308]. Collectively, the results from these assays have provided not only quantitative evidence in support of the proton sponge hypothesis, but also a set of methods by which the endo-lysosomal trafficking fate of polymeric vectors can be quantifiably assessed.

For the purpose of understanding the interactions that polyplexes potentially face as they confront the cellular membrane, Dubruel *et al.* developed a simple,

quantitative assay using surface plasmon resonance spectroscopy to study the ionic interactions between positively charged polyplexes and anionic components of the plasma membrane [309]. The authors evaluated hyaluronic acid (HA), a major glycosaminoglycan component of membrane-bound proteoglycans (See Section 2.4.2.1), against PEI- and PDMAEMA-based polyplexes as a model system. The results from their investigation revealed a greater degree of interaction presumably between the positive charge carriers of PEI and the anionic carboxyl groups of HA compared to those of PDMAEMA and HA. Moreover, the interaction was intensified as the N:P ratio was increased for both types of polyplexes, providing quantitative evidence to support the hypothesis that ionic interactions may facilitate the non-specific uptake of positively charged polyplexes in a polymer-dependent manner.

Considerable effort has also been devoted toward characterizing the global intracellular transport dynamics of polyplexes using microscopy techniques adapted for monitoring polyplexes within live cells in real time. Hanes and co-workers demonstrated the use of multiple particle tracking to examine the transport rate, mode, trajectory, and directionality of individual polyplexes within the intracellular environment [177, 310]. Kulkarni *et al.* employed spatial-temporal image correlation spectroscopy, an ensemble-averaged technique used to determine aggregate transport behavior, to monitor intracellular polyplex trafficking [176]. Both groups observed a saltatory (i.e., stop and go) motion of the internalized polyplexes, which was interpreted to be indicative of motor protein-mediated active transport along microtubules. Hanes and colleagues further distinguished transport into three major modes: 1) subdiffusive – to characterize polyplexes that are possibly encaged within quasi-stationary endosomes or trapped within the molecularly congested cytosolic space; 2) diffusive – to describe the cytosolic transport of polyplexes that have either escaped from endosomes or remained in endosomes that have detached from

microtubules and begun to diffuse randomly; and 3) active – to describe motor protein-driven transport of either the polyplexes themselves or within intracellular vesicles (e.g. endosomes). Additionally, Kulkarni *et al.* observed a demarcation of polyplex transport into two temporal regimes. At short time intervals lasting up to 10 seconds, polyplexes appeared to be transported in a non-random, directed linear fashion with the assistance of motor proteins. However, at longer time intervals (~60 seconds), transport appeared to be stochastic and non-directional. The mechanism rationalizing the two temporal regimes attributes non-random transport at short time intervals to be the activity of one group of motor proteins propelling the cargo in a directed motion. At longer time intervals, the polyplexes themselves or within endosomes may be transferred to a different set of motor proteins or possibly redirected along other microtubule tracks resulting in a non-directional, stochastic motion. Only after hours of motion did most of the polyplexes arrive in the perinuclear region, standing in stark contrast to the observation by Hanes and co-workers where they detected ~40% of polyplexes accumulated in the perinuclear region within 30 minutes and remaining at ~40% at all time points afterwards. It is unclear whether the discrepancy in the kinetics of perinuclear accumulation is due to an artifact of the different monitoring techniques employed by each group, difference in cell types (COS-7 versus HeLa), N:P ratio (6 versus 5), or some other unknown factor. Nevertheless, both groups have introduced powerful tools for studying the complex dynamics of intracellular trafficking and have brought gene delivery research one step closer toward quantitatively understanding how synthetic gene vectors are transported inside cells.

Adopting a different approach, Mitragotri and colleagues recently reported a computational framework for exploring the characteristics of intracellular polyplex transport phenomena [311]. Using experimentally-determined data, they developed a

detailed mathematical model to simulate the gene delivery pathway. The model, designed to calculate the probability that an internalized polyplex successfully delivers DNA to the nucleus, was used to determine and optimize the parameters that most greatly influenced delivery efficiency. The results of their study revealed that the spatio-temporal distribution of internalized polyplexes, and hence the systems and polyplex parameters that determine their distribution, are critical determinants of delivery efficiency. Further, the optimal values for these parameters are significantly influenced by the morphology of the cell, a factor often overlooked in gene delivery research. Cell morphology, described as the circularity of the cell and its size (quantified to be the average distance between the plasma and the nuclear membrane), was predicted to have almost an order of magnitude effect on delivery efficiency based on its influence on the spatio-temporal positioning of internalized polyplexes. For instance, small (i.e., cells with a relatively short average distance between the plasma and nuclear membrane), elongated cells have a larger fraction of the cell area nearer to the nucleus, providing internalized polyplexes greater access to the nucleus and hence higher delivery efficiency compared to larger, more circular cells. The implications of this finding are relevant from both a therapeutic applications and experimental standpoint. With regard to the former, since human cells exist in a broad range of morphologies, different vector design strategies may be required to deliver genes to flat and elongated cells (e.g., muscle cells) compared to round, stellate cells (e.g., dermal fibroblasts). From an experimental standpoint, because most synthetic gene delivery systems are evaluated and optimized in in vitro assays, assumptions that performance in vitro will be the same under in vivo conditions may be inaccurate or perhaps even invalid.

The authors also demonstrated the ability of their model to estimate the extent to which the delivery efficiency of synthetic vectors can be improved using PEI/DNA

(25 kDa) as a model polyplex system. The simulation predicted that optimal parametric configurations could afford a 20 to 100-fold increase in delivery efficiency. However, even under such conditions, for both in vitro and in vivo simulations, maximum efficiency was less than 3%, compared to the typical 10-100% efficiency of viral vectors. The authors posit that the limited efficiency of PEI-based polyplexes is primarily due to the inability of such vectors to protect the DNA, after endosomal escape, against enzymatic degradation through the cytosol until nuclear entry. Efficiency may therefore be enhanced if synthetic vectors could recruit motor proteins to direct transport toward the nucleus, similar to their viral counterparts. Even so, the maximum delivery efficiency achieved was still inferior to viral efficiencies, a prediction worth considering when assessing the relative merits of viral and non-viral vectors.

2.11.4. Resolving the biological landscape

Research has recently shed light on previously unsuspected intracellular entities and pathways and their involvement in vector-mediated gene delivery. One such intracellular organelle is the proteasome, a multicomponent protein complex that selectively degrades intracellular proteins that are marked for destruction [312]. Rice and co-workers conjectured that these cytosolic complexes may play a role in limiting the transfection efficiency of peptide-based gene delivery systems by metabolizing the peptide carriers and causing naked DNA to be released into the cytosol where it is susceptible to nuclease degradation [313]. Indeed, peptide-mediated gene expression was enhanced in the presence of proteasome inhibitors in a dose-dependent manner whereas delivery mediated by nonpeptide-based vectors (i.e., PEI, Lipofectamine) was not, further substantiating the peptide specificity of proteasome degradation.

Two additional intracellular pathways, namely potocytosis and cellular exit,

have also been implicated in having a potentially significant impact on polycation-based gene delivery [314]. Potocytosis is a cavealoe-mediated uptake mechanism that leads to the transport of internalized molecules to various intracellular locations (e.g., the cytoplasm, endoplasmic reticulum (ER), other organelles) [315]. Fajac and collaborators observed that polyplexes ≤ 100 nm in diameter were internalized primarily via potocytosis and subsequently trafficked to the ER after which their fate remains unclear. Further, polyplexes of all sizes were seen exiting the cell, an interesting observation considering that the airway epithelial cells used in the transfection studies are non-secretory in nature. Taken together, the potential role in gene delivery of the proteasome, potocytosis, and cellular exiting pathways represent not only additional hurdles that gene delivery systems must overcome, but perhaps more importantly, they represent potential opportunities that can be exploited to enhance the transfection capabilities of these systems.

2.12. CONCLUDING REMARKS

It is encouraging to recognize the tremendous progress that has been made toward developing multifaceted polymeric systems for gene delivery. From the perspective of functional polymers research, a wealth of sophisticated and innovative technology has been brought forth. From the perspective of cell biology, considerable insight has been gained into the physical and biochemical intricacies of the cellular landscape. From the perspective of gene therapy, however, polymer-based gene delivery systems have yet to achieve a significant presence in a clinical capacity based on the small percentage of non-viral vectors currently used in clinical trials [316]. As such, the challenge still stands before us to push beyond the boundaries of technology and probe deeper for a clearer understanding of the biological and cellular realm until

we arrive at a point where gene therapy is a safe and viable modality for disease treatment.

REFERENCES

[1] Tatum, E.L. Molecular biology, nucleic acids, and the future of medicine. *Perspect Biol Med* **10**(1): 19-32 (1966).

[2] Locher, C.P., Putnam, D., Langer, R., Witt, S.A., Ashlock, B.M., and Levy, J.A. Enhancement of a human immunodeficiency virus env DNA vaccine using a novel polycationic nanoparticle formulation. *Immunol Lett* **90**(2-3): 67-70 (2003).

[3] Pawliuk, R., Westerman, K.A., Fabry, M.E., Payen, E., Tighe, R., Bouhassira, E.E., Acharya, S.A., Ellis, J., London, I.M., Eaves, C.J., Humphries, R.K., Beuzard, Y., Nagel, R.L., and Leboulch, P. Correction of sickle cell disease in transgenic mouse models by gene therapy. *Science* **294**(5550): 2368-71 (2001).

[4] Von Laer, D., Hasselmann, S., and Hasselmann, K. Gene therapy for HIV infection: what does it need to make it work? *J Gene Med* **8**(6): 658-67 (2006).

[5] Burton, E.A., Glorioso, J.C., and Fink, D.J. Gene therapy progress and prospects: Parkinson's disease. *Gene Ther* **10**(20): 1721-7 (2003).

[6] Wong, L.F., Goodhead, L., Prat, C., Mitrophanous, K.A., Kingsman, S.M., and Mazarakis, N.D. Lentivirus-mediated gene transfer to the central nervous system: therapeutic and research applications. *Hum Gene Ther* **17**(1): 1-9 (2006).

[7] Boeckle, S. and Wagner, E. Optimizing Targeted Gene Delivery: Chemical Modification of Viral Vectors and Synthesis of Artificial Virus Vector Systems. *The AAPS Journal* **8**(4): E731-E742 (2006).

[8] Cavazzana-Calvo, M., Hacein-Bey, S., De Saint Basile, G., Gross, F., Yvon, E., Nusbaum, P., Selz, F., Hue, C., Certain, S., Casanova, J.L., Bousso, P., Deist, F.L., and Fischer, A. Gene therapy of human severe combined immunodeficiency (SCID)-X1 disease. *Science* **288**(5466): 669-72 (2000).

[9] Hacein-Bey-Abina, S., Le Deist, F., Carlier, F., Bouneaud, C., Hue, C., De Villartay, J.P., Thrasher, A.J., Wulffraat, N., Sorensen, R., Dupuis-Girod, S., Fischer, A., Davies, E.G., Kuis, W., Leiva, L., and Cavazzana-Calvo, M. Sustained correction of X-linked severe combined immunodeficiency by ex vivo gene therapy. *N Engl J Med* **346**(16): 1185-93 (2002).

[10] Kay, M.A., Manno, C.S., Ragni, M.V., Larson, P.J., Couto, L.B., Mcclelland, A., Glader, B., Chew, A.J., Tai, S.J., Herzog, R.W., Arruda, V., Johnson, F., Scallan, C., Skarsgard, E., Flake, A.W., and High, K.A. Evidence for gene transfer and expression of factor IX in haemophilia B patients treated with an AAV vector. *Nat Genet* **24**(3): 257-61 (2000).

[11] Check, E. A tragic setback. *Nature* **420**(6912): 116-8 (2002).

[12] Fischer, A., Hacein-Bey-Abina, S., Lagresle, C., Garrigue, A., and Cavazana-Calvo, M. Gene therapy of severe combined immunodeficiency disease: Proof of principle of efficiency and safety issues. Gene therapy, primary immunodeficiencies, retrovirus, lentivirus, genome. *Bulletin de l'Academie Nationale de Medecine* **189**: 779-788 (2005).

[13] Hacein-Bey-Abina, S., Von Kalle, C., Schmidt, M., Mccormack, M.P., Wulffraat, N., Leboulch, P., Lim, A., Osborne, C.S., Pawliuk, R., Morillon, E., Sorensen, R., Forster, A., Fraser, P., Cohen, J.I., De Saint Basile, G., Alexander, I., Wintergerst, U., Frebourg, T., Aurias, A., Stoppa-Lyonnet, D., Romana, S., Radford-Weiss, I., Gross, F., Valensi, F., Delabesse, E., Macintyre, E., Sigaux, F., Soulier, J., Leiva, L.E., Wissler, M., Prinz, C., Rabbitts, T.H., Le Deist, F., Fischer, A., and Cavazzana-Calvo, M. LMO2-associated clonal T cell proliferation in two patients after gene therapy for SCID-X1. *Science* **302**(5644): 415-9 (2003).

[14] Marshall, E. BIOMEDICINE:Gene Therapy on Trial. *Science* **288**(5468): 951-957 (2000).

[15] Martin, B., Sainlos, M., Aissaoui, A., Oudrhiri, N., Hauchecorne, M., Vigneron, J.P., Lehn, J.M., and Lehn, P. The design of cationic lipids for gene delivery. *Curr Pharm Des* **11**(3): 375-94 (2005).

[16] Zhi, P.X., Qing, H.Z., Gao, Q.L., and Ai, B.Y. Inorganic nanoparticles as carriers for efficient cellular delivery. *Chem. Eng. Sci.* **61**(3): 1027-1040 (2006).

[17] Abdelhady, H.G., Allen, S., Davies, M.C., Roberts, C.J., Tendler, S.J., and Williams, P.M. Direct real-time molecular scale visualisation of the degradation of condensed DNA complexes exposed to DNase I. *Nucleic Acids Res* **31**(14): 4001-5 (2003).

[18] Lechardeur, D., Sohn, K.J., Haardt, M., Joshi, P.B., Monck, M., Graham, R.W., Beatty, B., Squire, J., O'brodovich, H., and Lukacs, G.L. Metabolic instability of

plasmid DNA in the cytosol: a potential barrier to gene transfer. *Gene Ther* **6**(4): 482-97 (1999).

[19] Schaffer, D.V. and Lauffenburger, D.A. Optimization of cell surface binding enhances efficiency and specificity of molecular conjugate gene delivery. *J Biol Chem* **273**(43): 28004-9 (1998).

[20] Bielinska, A.U., Kukowska-Latallo, J.F., and Baker, J.R., Jr. The interaction of plasmid DNA with polyamidoamine dendrimers: mechanism of complex formation and analysis of alterations induced in nuclease sensitivity and transcriptional activity of the complexed DNA. *Biochim Biophys Acta* **1353**(2): 180-90 (1997).

[21] Jang, J.H. and Shea, L.D. Intramuscular delivery of DNA releasing microspheres: microsphere properties and transgene expression. *J Control Release* **112**(1): 120-8 (2006).

[22] Panyam, J. and Labhasetwar, V. Biodegradable nanoparticles for drug and gene delivery to cells and tissue. *Adv Drug Deliv Rev* **55**(3): 329-47 (2003).

[23] Santos, C.A., Freedman, B.D., Leach, K.J., Press, D.L., Scarpulla, M., and Mathiowitz, E. Poly(fumaric-co-sebacic anhydride). A degradation study as evaluated by FTIR, DSC, GPC and X-ray diffraction. *J Control Release* **60**(1): 11-22 (1999).

[24] Hedley, M., *Gene delivery using poly(lactide-co-glycolide) microspheres*, in *Polymeric gene delivery: principles and applications*, M.M. Amiji, Editor. 2005, CRC Press: Boca Raton, FL. p. 451-466.

[25] Ando, S., Putnam, D., Pack, D.W., and Langer, R. PLGA microspheres containing plasmid DNA: preservation of supercoiled DNA via cryopreparation and carbohydrate stabilization. *J Pharm Sci* **88**(1): 126-30 (1999).

[26] Fu, K., Pack, D.W., Klibanov, A.M., and Langer, R. Visual evidence of acidic environment within degrading poly(lactic-co-glycolic acid) (PLGA) microspheres. *Pharm Res* **17**(1): 100-6 (2000).

[27] Walter, E., Moelling, K., Pavlovic, J., and Merkle, H.P. Microencapsulation of DNA using poly(DL-lactide-co-glycolide): stability issues and release characteristics. *J Control Release* **61**(3): 361-74 (1999).

[28] Wang, D., Robinson, D.R., Kwon, G.S., and Samuel, J. Encapsulation of plasmid DNA in biodegradable poly(D, L-lactic-co-glycolic acid) microspheres as a novel approach for immunogene delivery. *J Control Release* **57**(1): 9-18 (1999).

[29] Neu, M., Fischer, D., and Kissel, T. Recent advances in rational gene transfer vector design based on poly(ethylene imine) and its derivatives. *J Gene Med* **7**(8): 992-1009 (2005).

[30] Wightman, L., Kircheis, R., Rossler, V., Carotta, S., Ruzicka, R., Kursa, M., and Wagner, E. Different behavior of branched and linear polyethylenimine for gene delivery in vitro and in vivo. *J Gene Med* **3**(4): 362-72 (2001).

[31] Cherng, J.Y., Van De Wetering, P., Talsma, H., Crommelin, D.J., and Hennink, W.E. Effect of size and serum proteins on transfection efficiency of poly ((2-dimethylamino)ethyl methacrylate)-plasmid nanoparticles. *Pharm Res* **13**(7): 1038-42 (1996).

[32] Dubruel, P. and Schacht, E. Vinyl polymers as non-viral gene delivery carriers: current status and prospects. *Macromol Biosci* **6**(10): 789-810 (2006).

[33] Funhoff, A.M., Van Nostrum, C.F., Lok, M.C., Kruijtzer, J.A., Crommelin, D.J., and Hennink, W.E. Cationic polymethacrylates with covalently linked membrane destabilizing peptides as gene delivery vectors. *J Control Release* **101**(1-3): 233-46 (2005).

[34] Van De Wetering, P., Cherng, J.Y., Talsma, H., Crommelin, D.J., and Hennink, W.E. 2-(Dimethylamino)ethyl methacrylate based (co)polymers as gene transfer agents. *J Control Release* **53**(1-3): 145-53 (1998).

[35] Vandewetering, P., Cherng, J., Talsma, H., and Hennink, W. Relation between transfection efficiency and cytotoxicity of poly(2-(dimethylamino)ethyl methacrylate)/plasmid complexes. *JOURNAL OF CONTROLLED RELEASE* **49**(1): 59-69 (1997).

[36] Choi, J.S., Nam, K., Park, J.Y., Kim, J.B., Lee, J.K., and Park, J.S. Enhanced transfection efficiency of PAMAM dendrimer by surface modification with L-arginine. *J Control Release* **99**(3): 445-56 (2004).

[37] Haensler, J. and Szoka, F.C., Jr. Polyamidoamine cascade polymers mediate efficient transfection of cells in culture. *Bioconjug Chem* **4**(5): 372-9 (1993).

[38] Kim, J.B., Choi, J.S., Nam, K., Lee, M., Park, J.S., and Lee, J.K. Enhanced transfection of primary cortical cultures using arginine-grafted PAMAM dendrimer, PAMAM-Arg. *J Control Release* **114**(1): 110-7 (2006).

[39] Gebhart, C.L. and Kabanov, A.V. Evaluation of polyplexes as gene transfer agents. *J Control Release* **73**(2-3): 401-16 (2001).

[40] Zinselmeyer, B.H., Mackay, S.P., Schatzlein, A.G., and Uchegbu, I.F. The lower-generation polypropylenimine dendrimers are effective gene-transfer agents. *Pharm Res* **19**(7): 960-7 (2002).

[41] Ahn, C.H., Chae, S.Y., Bae, Y.H., and Kim, S.W. Synthesis of biodegradable multi-block copolymers of poly(L-lysine) and poly(ethylene glycol) as a non-viral gene carrier. *J Control Release* **97**(3): 567-74 (2004).

[42] Nie, Y., Zhang, Z.R., and Duan, Y.R. Combined use of polycationic peptide and biodegradable macromolecular polymer as a novel gene delivery system: a preliminary study. *Drug Deliv* **13**(6): 441-6 (2006).

[43] Putnam, D., Gentry, C.A., Pack, D.W., and Langer, R. Polymer-based gene delivery with low cytotoxicity by a unique balance of side-chain termini. *Proc Natl Acad Sci U S A* **98**(3): 1200-5 (2001).

[44] Read, M.L., Singh, S., Ahmed, Z., Stevenson, M., Briggs, S.S., Oupicky, D., Barrett, L.B., Spice, R., Kendall, M., Berry, M., Preece, J.A., Logan, A., and Seymour, L.W. A versatile reducible polycation-based system for efficient delivery of a broad range of nucleic acids. *Nucleic Acids Res* **33**(9): e86 (2005).

[45] Wu, G.Y. and Wu, C.H. Receptor-mediated in vitro gene transformation by a soluble DNA carrier system. *J Biol Chem* **262**(10): 4429-32 (1987).

[46] Kiang, T., Bright, C., Cheung, C.Y., Stayton, P.S., Hoffman, A.S., and Leong, K.W. Formulation of chitosan-DNA nanoparticles with poly(propyl acrylic acid) enhances gene expression. *J Biomater Sci Polym Ed* **15**(11): 1405-21 (2004).

[47] Lee, D., Zhang, W., Shirley, S., Kong, X., Hellermann, G., Lockey, R., and Mohapatra, S. Thiolated chitosan/DNA nanocomplexes exhibit enhanced and sustained gene delivery. *Pharmaceutical Research* **24**(1): 157-167 (2007).

[48] Mao, H.Q., Roy, K., Troung-Le, V.L., Janes, K.A., Lin, K.Y., Wang, Y., August, J.T., and Leong, K.W. Chitosan-DNA nanoparticles as gene carriers: synthesis, characterization and transfection efficiency. *J Control Release* **70**(3): 399-421 (2001).

[49] Prabaharan, M. and Mano, J.F. Chitosan-based particles as controlled drug delivery systems. *Drug Deliv* **12**(1): 41-57 (2005).

[50] Wong, K., Sun, G., Zhang, X., Dai, H., Liu, Y., He, C., and Leong, K. PEI-g-chitosan, a novel gene delivery system with transfection efficiency comparable to polyethylenimine in vitro and after liver administration in vivo. *Bioconjug. Chem.* **17**(1): 152-158 (2006).

[51] Eliyahu, H., Siani, S., Azzam, T., Domb, A.J., and Barenholz, Y. Relationships between chemical composition, physical properties and transfection efficiency of polysaccharide-spermine conjugates. *Biomaterials* **27**(8): 1646-55 (2006).

[52] Hardy, J.G., Kostiainen, M.A., Smith, D.K., Gabrielson, N.P., and Pack, D.W. Dendrons with spermine surface groups as potential building blocks for nonviral vectors in gene therapy. *Bioconjug Chem* **17**(1): 172-8 (2006).

[53] Kanatani, I., Ikai, T., Okazaki, A., Jo, J.I., Yamamoto, M., Imamura, M., Kanematsu, A., Yamamoto, S., Ito, N., Ogawa, O., and Tabata, Y. Efficient gene transfer by pullulan-spermine occurs through both clathrin- and raft/caveolae-dependent mechanisms. *J Control Release* **116**(1): 75-82 (2006).

[54] Davis, M.E. and Brewster, M.E. Cyclodextrin-based pharmaceutics: past, present and future. *Nat Rev Drug Discov* **3**(12): 1023-35 (2004).

[55] Wang, J., Mao, H.Q., and Leong, K.W. A novel biodegradable gene carrier based on polyphosphoester. *J Am Chem Soc* **123**(38): 9480-1 (2001).

[56] Zhao, Z., Wang, J., Mao, H.Q., and Leong, K.W. Polyphosphoesters in drug and gene delivery. *Adv Drug Deliv Rev* **55**(4): 483-99 (2003).

[57] De Wolf, H.K., Luten, J., Snel, C.J., Oussoren, C., Hennink, W.E., and Storm, G. In vivo tumor transfection mediated by polyplexes based on biodegradable poly(DMAEA)-phosphazene. *J Control Release* **109**(1-3): 275-87 (2005).

[58] Luten, J., Van Steenis, J.H., Van Someren, R., Kemmink, J., Schuurmans-Nieuwenbroek, N.M., Koning, G.A., Crommelin, D.J., Van Nostrum, C.F., and Hennink, W.E. Water-soluble biodegradable cationic polyphosphazenes for gene delivery. *J Control Release* **89**(3): 483-97 (2003).

[59] Munier, S., Messai, I., Delair, T., Verrier, B., and Ataman-Onal, Y. Cationic PLA nanoparticles for DNA delivery: comparison of three surface polycations for DNA binding, protection and transfection properties. *Colloids Surf B Biointerfaces* **43**(3-4): 163-73 (2005).

[60] Vila, A., Sanchez, A., Perez, C., and Alonso, M. PLA-PEG nanospheres: New carriers for transmucosal delivery of proteins and plasmid DNA. *Polym. Adv. Technol.* **13**(10-12): 851-858 (2002).

[61] Carlisle, R.C., Etrych, T., Briggs, S.S., Preece, J.A., Ulbrich, K., and Seymour, L.W. Polymer-coated polyethylenimine/DNA complexes designed for triggered activation by intracellular reduction. *J Gene Med* **6**(3): 337-44 (2004).

[62] Csaba, N., Caamano, P., Sanchez, A., Dominguez, F., and Alonso, M.J. PLGA:poloxamer and PLGA:poloxamine blend nanoparticles: new carriers for gene delivery. *Biomacromolecules* **6**(1): 271-8 (2005).

[63] Csaba, N., Sanchez, A., and Alonso, M.J. PLGA:poloxamer and PLGA:poloxamine blend nanostructures as carriers for nasal gene delivery. *J Control Release* **113**(2): 164-72 (2006).

[64] Oster, C.G., Kim, N., Grode, L., Barbu-Tudoran, L., Schaper, A.K., Kaufmann, S.H., and Kissel, T. Cationic microparticles consisting of poly(lactide-co-glycolide) and polyethylenimine as carriers systems for parental DNA vaccination. *J Control Release* **104**(2): 359-77 (2005).

[65] Heller, J., Barr, J., Ng, S.Y., Abdellauoi, K.S., and Gurny, R. Poly(ortho esters): synthesis, characterization, properties and uses. *Adv Drug Deliv Rev* **54**(7): 1015-39 (2002).

[66] Wang, C., Ge, Q., Ting, D., Nguyen, D., Shen, H.R., Chen, J., Eisen, H.N., Heller, J., Langer, R., and Putnam, D. Molecularly engineered poly(ortho ester) microspheres for enhanced delivery of DNA vaccines. *Nat Mater* **3**(3): 190-6 (2004).

[67] Anderson, D.G., Akinc, A., Hossain, N., and Langer, R. Structure/property studies of polymeric gene delivery using a library of poly(beta-amino esters). *Mol Ther* **11**(3): 426-34 (2005).

[68] Green, J.J., Shi, J., Chiu, E., Leshchiner, E.S., Langer, R., and Anderson, D.G. Biodegradable polymeric vectors for gene delivery to human endothelial cells. *Bioconjug Chem* **17**(5): 1162-9 (2006).

[69] Lynn, D. and Langer, R. Degradable poly(beta-amino esters): Synthesis, characterization, and self-assembly with plasmid DNA. *J. Am. Chem. Soc.* **122**(44): 10761-10768 (2000).

[70] Zugates, G.T., Anderson, D.G., Little, S.R., Lawhorn, I.E., and Langer, R. Synthesis of poly(beta-amino ester)s with thiol-reactive side chains for DNA delivery. *J Am Chem Soc* **128**(39): 12726-34 (2006).

[71] Lim, Y.B., Kim, S.M., Lee, Y., Lee, W.K., Yang, T.G., Lee, M.J., Suh, H., and Park, J.S. Cationic hyperbranched poly(amino ester): A novel class of DNA condensing molecule with cationic surface, biodegradable three-dimensional structure, and tertiary amine groups in the interior. *J. Am. Chem. Soc.* **123**(10): 2460-2461 (2001).

[72] Wu, D., Liu, Y., Jiang, X., He, C., Goh, S.H., and Leong, K.W. Hyperbranched poly(amino ester)s with different terminal amine groups for DNA delivery. *Biomacromolecules* **7**(6): 1879-83 (2006).

[73] Kim, H.J., Kwon, M.S., Choi, J.S., Yang, S.M., Yoon, J.K., Kim, K., and Park, J.S. Highly effective and slow-biodegradable network-type cationic gene delivery polymer: small library-like approach synthesis and characterization. *Biomaterials* **27**(10): 2292-301 (2006).

[74] Lim, Y.B., Kim, S.M., Suh, H., and Park, J.S. Biodegradable, endosome disruptive, and cationic network-type polymer as a highly efficient and nontoxic gene delivery carrier. *Bioconjug Chem* **13**(5): 952-7 (2002).

[75] Maheshwari, A., Mahato, R.I., Mcgregor, J., Han, S., Samlowski, W.E., Park, J.S., and Kim, S.W. Soluble biodegradable polymer-based cytokine gene delivery for cancer treatment. *Mol Ther* **2**(2): 121-30 (2000).

[76] Lim, Y., Kim, C., Kim, K., Kim, S., and Park, J. Development of a safe gene delivery system using biodegradable polymer, poly[alpha-(4-aminobutyl)-L-glycolic acid]. *J. Am. Chem. Soc.* **122**(27): 6524-6525 (2000).

[77] Lim, Y.B., Han, S.O., Kong, H.U., Lee, Y., Park, J.S., Jeong, B., and Kim, S.W. Biodegradable polyester, poly[alpha-(4-aminobutyl)-L-glycolic acid], as a non-toxic gene carrier. *Pharm Res* **17**(7): 811-6 (2000).

[78] Li, Z. and Huang, L. Sustained delivery and expression of plasmid DNA based on biodegradable polyester, poly(D,L-lactide-co-4-hydroxy-L-proline). *J Control Release* **98**(3): 437-46 (2004).

[79] Putnam, D. and Langer, R. Poly(4-hydroxy-L-proline ester): Low-temperature polycondensation and plasmid DNA complexation. *Macromolecules* **32**(11): 3658-3662 (1999).

[80] Lim, Y., Choi, Y., and Park, J. A self-destroying polycationic polymer: Biodegradable poly(4-hydroxy-L-proline ester). *J. Am. Chem. Soc.* **121**(24): 5633-5639 (1999).

[81] Kasturi, S.P., Sachaphibulkij, K., and Roy, K. Covalent conjugation of polyethyleneimine on biodegradable microparticles for delivery of plasmid DNA vaccines. *Biomaterials* **26**(32): 6375-85 (2005).

[82] O'hagan, D.T., Singh, M., and Ulmer, J.B. Microparticle-based technologies for vaccines. *Methods* **40**(1): 10-9 (2006).

[83] Singh, M., Briones, M., Ott, G., and O'hagan, D. Cationic microparticles: A potent delivery system for DNA vaccines. *Proc Natl Acad Sci U S A* **97**(2): 811-6 (2000).

[84] Conner, S. and Schmid, S. Regulated portals of entry into the cell. *Nature* **422**(6927): 37-44 (2003).

[85] Schatzlein, A.G. Targeting of Synthetic Gene Delivery Systems. *J Biomed Biotechnol* **2003**(2): 149-158 (2003).

[86] Cotten, M., Langle-Rouault, F., Kirlappos, H., Wagner, E., Mechtler, K., Zenke, M., Beug, H., and Birnstiel, M.L. Transferrin-polycation-mediated introduction of DNA into human leukemic cells: stimulation by agents that affect the survival of transfected DNA or modulate transferrin receptor levels. *Proc Natl Acad Sci U S A* **87**(11): 4033-7 (1990).

[87] Fisher, K.D., Ulbrich, K., Subr, V., Ward, C.M., Mautner, V., Blakey, D., and Seymour, L.W. A versatile system for receptor-mediated gene delivery permits increased entry of DNA into target cells, enhanced delivery to the nucleus and elevated rates of transgene expression. *Gene Ther* **7**(15): 1337-43 (2000).

[88] Kircheis, R., Kichler, A., Wallner, G., Kursa, M., Ogris, M., Felzmann, T., Buchberger, M., and Wagner, E. Coupling of cell-binding ligands to polyethylenimine for targeted gene delivery. *Gene Ther* **4**(5): 409-18 (1997).

[89] Wagner, E., Cotten, M., Foisner, R., and Birnstiel, M.L. Transferrin-polycation-DNA complexes: the effect of polycations on the structure of the complex and DNA delivery to cells. *Proc Natl Acad Sci U S A* **88**(10): 4255-9 (1991).

[90] Fominaya, J., Uherek, C., and Wels, W. A chimeric fusion protein containing transforming growth factor-alpha mediates gene transfer via binding to the EGF receptor. *Gene Ther* **5**(4): 521-30 (1998).

[91] Cho, K.C., Kim, S.H., Jeong, J.H., and Park, T.G. Folate receptor-mediated gene delivery using folate-poly(ethylene glycol)-poly(L-lysine) conjugate. *Macromol Biosci* **5**(6): 512-9 (2005).

[92] Mislick, K.A., Baldeschwieler, J.D., Kayyem, J.F., and Meade, T.J. Transfection of folate-polylysine DNA complexes: evidence for lysosomal delivery. *Bioconjug Chem* **6**(5): 512-5 (1995).

[93] Sosnowski, B.A., Gonzalez, A.M., Chandler, L.A., Buechler, Y.J., Pierce, G.F., and Baird, A. Targeting DNA to cells with basic fibroblast growth factor (FGF2). *J Biol Chem* **271**(52): 33647-53 (1996).

[94] Blessing, T., Kursa, M., Holzhauser, R., Kircheis, R., and Wagner, E. Different strategies for formation of pegylated EGF-conjugated PEI/DNA complexes for targeted gene delivery. *Bioconjug Chem* **12**(4): 529-37 (2001).

[95] Lee, H., Kim, T.H., and Park, T.G. A receptor-mediated gene delivery system using streptavidin and biotin-derivatized, pegylated epidermal growth factor. *J Control Release* **83**(1): 109-19 (2002).

[96] Wu, G.Y., Wilson, J.M., Shalaby, F., Grossman, M., Shafritz, D.A., and Wu, C.H. Receptor-mediated gene delivery in vivo. Partial correction of genetic analbuminemia in Nagase rats. *J Biol Chem* **266**(22): 14338-42 (1991).

[97] Wu, G.Y. and Wu, C.H. Evidence for targeted gene delivery to Hep G2 hepatoma cells in vitro. *Biochemistry* **27**(3): 887-92 (1988).

[98] Erbacher, P., Remy, J.S., and Behr, J.P. Gene transfer with synthetic virus-like particles via the integrin-mediated endocytosis pathway. *Gene Ther* **6**(1): 138-45 (1999).

[99] Harbottle, R.P., Cooper, R.G., Hart, S.L., Ladhoff, A., Mckay, T., Knight, A.M., Wagner, E., Miller, A.D., and Coutelle, C. An RGD-oligolysine peptide: a prototype construct for integrin-mediated gene delivery. *Hum Gene Ther* **9**(7): 1037-47 (1998).

[100] Kunath, K., Merdan, T., Hegener, O., Haberlein, H., and Kissel, T. Integrin targeting using RGD-PEI conjugates for in vitro gene transfer. *J Gene Med* **5**(7): 588-99 (2003).

[101] Suk, J.S., Suh, J., Choy, K., Lai, S.K., Fu, J., and Hanes, J. Gene delivery to differentiated neurotypic cells with RGD and HIV Tat peptide functionalized polymeric nanoparticles. *Biomaterials* **27**(29): 5143-50 (2006).

[102] Hashida, M., Takemura, S., Nishikawa, M., and Takakura, Y. Targeted delivery of plasmid DNA complexed with galactosylated poly(L-lysine). *J Control Release* **53**(1-3): 301-10 (1998).

[103] Perales, J.C., Ferkol, T., Beegen, H., Ratnoff, O.D., and Hanson, R.W. Gene transfer in vivo: sustained expression and regulation of genes introduced into the liver by receptor-targeted uptake. *Proc Natl Acad Sci U S A* **91**(9): 4086-90 (1994).

[104] Engering, A.J., Cella, M., Fluitsma, D.M., Hoefsmit, E.C., Lanzavecchia, A., and Pieters, J. Mannose receptor mediated antigen uptake and presentation in human dendritic cells. *Adv Exp Med Biol* **417**: 183-7 (1997).

[105] Fajac, I., Thevenot, G., Bedouet, L., Danel, C., Riquet, M., Merten, M., Figarella, C., Dall'ava-Santucci, J., Monsigny, M., and Briand, P. Uptake of plasmid/glycosylated polymer complexes and gene transfer efficiency in differentiated airway epithelial cells. *J Gene Med* **5**(1): 38-48 (2003).

[106] Ferkol, T., Perales, J.C., Mularo, F., and Hanson, R.W. Receptor-mediated gene transfer into macrophages. *Proc Natl Acad Sci U S A* **93**(1): 101-5 (1996).

[107] Klink, D., Yu, Q.C., Glick, M.C., and Scanlin, T. Lactosylated poly-L-lysine targets a potential lactose receptor in cystic fibrosis and non-cystic fibrosis airway epithelial cells. *Mol Ther* **7**(1): 73-80 (2003).

[108] Buschle, M., Cotten, M., Kirlappos, H., Mechtler, K., Schaffner, G., Zauner, W., Birnstiel, M.L., and Wagner, E. Receptor-mediated gene transfer into human T lymphocytes via binding of DNA/CD3 antibody particles to the CD3 T cell receptor complex. *Hum Gene Ther* **6**(6): 753-61 (1995).

[109] Suzuki, M., Takayanagi, A., and Shimizu, N. Targeted gene delivery using humanized single-chain antibody with negatively charged oligopeptide tail. *Cancer Sci* **95**(5): 424-9 (2004).

[110] Chiu, S.J., Ueno, N.T., and Lee, R.J. Tumor-targeted gene delivery via anti-HER2 antibody (trastuzumab, Herceptin) conjugated polyethylenimine. *J Control Release* **97**(2): 357-69 (2004).

[111] Germershaus, O., Merdan, T., Bakowsky, U., Behe, M., and Kissel, T. Trastuzumab-polyethylenimine-polyethylene glycol conjugates for targeting Her2-expressing tumors. *Bioconjug Chem* **17**(5): 1190-9 (2006).

[112] Gupta, S., Eastman, J., Silski, C., Ferkol, T., and Davis, P.B. Single chain Fv: a ligand in receptor-mediated gene delivery. *Gene Ther* **8**(8): 586-92 (2001).

[113] Suh, W., Chung, J.K., Park, S.H., and Kim, S.W. Anti-JL1 antibody-conjugated poly (L-lysine) for targeted gene delivery to leukemia T cells. *J Control Release* **72**(1-3): 171-8 (2001).

[114] Ignatovich, I.A., Dizhe, E.B., Pavlotskaya, A.V., Akifiev, B.N., Burov, S.V., Orlov, S.V., and Perevozchikov, A.P. Complexes of plasmid DNA with basic domain 47-57 of the HIV-1 Tat protein are transferred to mammalian cells by endocytosis-mediated pathways. *J Biol Chem* **278**(43): 42625-36 (2003).

[115] Rudolph, C., Plank, C., Lausier, J., Schillinger, U., Muller, R.H., and Rosenecker, J. Oligomers of the arginine-rich motif of the HIV-1 TAT protein are capable of transferring plasmid DNA into cells. *J Biol Chem* **278**(13): 11411-8 (2003).

[116] Christiaens, B., Dubruel, P., Grooten, J., Goethals, M., Vandekerckhove, J., Schacht, E., and Rosseneu, M. Enhancement of polymethacrylate-mediated gene delivery by Penetratin. *Eur J Pharm Sci* **24**(5): 525-37 (2005).

[117] Muratovska, A. and Eccles, M.R. Conjugate for efficient delivery of short interfering RNA (siRNA) into mammalian cells. *FEBS Lett* **558**(1-3): 63-8 (2004).

[118] Kilk, K., El-Andaloussi, S., Jarver, P., Meikas, A., Valkna, A., Bartfai, T., Kogerman, P., Metsis, M., and Langel, U. Evaluation of transportan 10 in PEI mediated plasmid delivery assay. *J Control Release* **103**(2): 511-23 (2005).

[119] Siprashvili, Z., Scholl, F.A., Oliver, S.F., Adams, A., Contag, C.H., Wender, P.A., and Khavari, P.A. Gene transfer via reversible plasmid condensation with cysteine-flanked, internally spaced arginine-rich peptides. *Hum Gene Ther* **14**(13): 1225-33 (2003).

[120] Tabata, Y. and Ikada, Y. Phagocytosis of Polymer Microspheres by Macrophages. *Adv. Polym. Sci.* **94**: 107-141 (1990).

[121] Mislick, K.A. and Baldeschwieler, J.D. Evidence for the role of proteoglycans in cation-mediated gene transfer. *Proc Natl Acad Sci U S A* **93**(22): 12349-54 (1996).

[122] Hardingham, T.E. and Fosang, A.J. Proteoglycans: many forms and many functions. *Faseb J* **6**(3): 861-70 (1992).

[123] Yanagishita, M. and Hascall, V.C. Cell surface heparan sulfate proteoglycans. *J Biol Chem* **267**(14): 9451-4 (1992).

[124] Kichler, A., Mason, A.J., and Bechinger, B. Cationic amphipathic histidine-rich peptides for gene delivery. *Biochim Biophys Acta* **1758**(3): 301-7 (2006).

[125] Takigawa, D.Y. and Tirrell, D.A. Disruption of phospholipid packing by branched poly(ethylenimine) derivatives. *Macromolecules* **18**(3): 338-342 (1985).

[126] Thomas, M. and Klibanov, A.M. Enhancing polyethylenimine's delivery of plasmid DNA into mammalian cells. *Proc Natl Acad Sci U S A* **99**(23): 14640-5 (2002).

[127] Rittner, K., Benavente, A., Bompard-Sorlet, A., Heitz, F., Divita, G., Brasseur, R., and Jacobs, E. New basic membrane-destabilizing peptides for plasmid-based gene delivery in vitro and in vivo. *Mol Ther* **5**(2): 104-14 (2002).

[128] El-Andaloussi, S., Holm, T., and Langel, U. Cell-penetrating peptides: mechanisms and applications. *Curr Pharm Des* **11**(28): 3597-611 (2005).

[129] Magzoub, M. and Graslund, A. Cell-penetrating peptides: [corrected] from inception to application. *Q Rev Biophys* **37**(2): 147-95 (2004).

[130] Khalil, I., Kogure, K., Akita, H., and Harashima, H. Uptake pathways and subsequent intracellular trafficking in nonviral gene delivery. *Pharmacol Rev* **58**(1): 32-45 (2006).

[131] Rejman, J., Bragonzi, A., and Conese, M. Role of clathrin- and caveolae-mediated endocytosis in gene transfer mediated by lipo- and polyplexes. *Mol Ther* **12**(3): 468-474 (2005).

[132] Von Gersdorff, K., Sanders, N., Vandenbroucke, R., De Smedt, S., Wagner, E., and Ogris, M. The internalization route resulting in successful gene expression depends on polyethylenimine both cell line and polyplex type. *Mol Ther* **14**(5): 745-753 (2006).

[133] Akinc, A., Thomas, M., Klibanov, A.M., and Langer, R. Exploring polyethylenimine-mediated DNA transfection and the proton sponge hypothesis. *J Gene Med* **7**(5): 657-63 (2005).

[134] Boussif, O., Lezoualc'h, F., Zanta, M.A., Mergny, M.D., Scherman, D., Demeneix, B., and Behr, J.P. A versatile vector for gene and oligonucleotide transfer into cells in culture and in vivo: polyethylenimine. *Proc Natl Acad Sci U S A* **92**(16): 7297-301 (1995).

[135] Li, W., Nicol, F., and Szoka, F.C., Jr. GALA: a designed synthetic pH-responsive amphipathic peptide with applications in drug and gene delivery. *Adv Drug Deliv Rev* **56**(7): 967-85 (2004).

[136] Murthy, N., Chang, I., Stayton, P., and Hoffman, A. pH-sensitive hemolysis by random copolymers of alkyl acrylates and acrylic acid. *Macromol. Symp.* **172**(1): 49-56 (2001).

[137] Cheung, C.Y., Murthy, N., Stayton, P.S., and Hoffman, A.S. A pH-Sensitive Polymer That Enhances Cationic Lipid-Mediated Gene Transfer. *Bioconjugate Chem.* **12**(6): 906-910 (2001).

[138] Kyriakides, T.R., Cheung, C.Y., Murthy, N., Bornstein, P., Stayton, P.S., and Hoffman, A.S. pH-sensitive polymers that enhance intracellular drug delivery in vivo. *J Control Release* **78**(1-3): 295-303 (2002).

[139] Murthy, N., Robichaud, J.R., Tirrell, D.A., Stayton, P.S., and Hoffman, A.S. The design and synthesis of polymers for eukaryotic membrane disruption. *J Control Release* **61**(1-2): 137-43 (1999).

[140] Asayama, S., Sekine, T., Hamaya, A., Kawakami, H., and Nagaoka, S. Poly(L-histidine) with several aminoethyl groups for a new pH-sensitive DNA carrier. *Polym. Adv. Technol.* **16**(7): 567-570 (2005).

[141] Bikram, M., Ahn, C., Chae, S., Lee, M., Yockman, J., and Kim, S. Biodegradable poly(ethylene glycol)-co-poly(L-lysine)-g-histidine multiblock copolymers for nonviral gene delivery. *Macromolecules* **37**(5): 1903-1916 (2004).

[142] Pack, D.W., Putnam, D., and Langer, R. Design of imidazole-containing endosomolytic biopolymers for gene delivery. *Biotechnol Bioeng* **67**(2): 217-23 (2000).

[143] Pichon, C., Goncalves, C., and Midoux, P. Histidine-rich peptides and polymers for nucleic acids delivery. *Adv Drug Deliv Rev* **53**(1): 75-94 (2001).

[144] Veron, L., Ganee, A., Charreyre, M.T., Pichot, C., and Delair, T. New hydrolyzable pH-responsive cationic polymers for gene delivery: a preliminary study. *Macromol Biosci* **4**(4): 431-44 (2004).

[145] Ogris, M., Carlisle, R.C., Bettinger, T., and Seymour, L.W. Melittin enables efficient vesicular escape and enhanced nuclear access of nonviral gene delivery vectors. *J Biol Chem* **276**(50): 47550-5 (2001).

[146] Plank, C., Oberhauser, B., Mechtler, K., Koch, C., and Wagner, E. The influence of endosome-disruptive peptides on gene transfer using synthetic virus-like gene transfer systems. *J Biol Chem* **269**(17): 12918-24 (1994).

[147] Wagner, E., Plank, C., Zatloukal, K., Cotten, M., and Birnstiel, M.L. Influenza virus hemagglutinin HA-2 N-terminal fusogenic peptides augment gene transfer by transferrin-polylysine-DNA complexes: toward a synthetic virus-like gene-transfer vehicle. *Proc Natl Acad Sci U S A* **89**(17): 7934-8 (1992).

[148] Fisher, K.J. and Wilson, J.M. The transmembrane domain of diphtheria toxin improves molecular conjugate gene transfer. *Biochem J* **321**: 49-58 (1997).

[149] Lee, H., Jeong, J.H., and Park, T.G. A new gene delivery formulation of polyethylenimine/DNA complexes coated with PEG conjugated fusogenic peptide. *J Control Release* **76**(1-2): 183-92 (2001).

[150] Wyman, T.B., Nicol, F., Zelphati, O., Scaria, P.V., Plank, C., and Szoka, F.C., Jr. Design, synthesis, and characterization of a cationic peptide that binds to nucleic acids and permeabilizes bilayers. *Biochemistry* **36**(10): 3008-17 (1997).

[151] Gottschalk, S., Sparrow, J.T., Hauer, J., Mims, M.P., Leland, F.E., Woo, S.L., and Smith, L.C. A novel DNA-peptide complex for efficient gene transfer and expression in mammalian cells. *Gene Ther* **3**(5): 448-57 (1996).

[152] Lechardeur, D. and Lukacs, G.L. Nucleocytoplasmic Transport of Plasmid DNA: A Perilous Journey from the Cytoplasm to the Nucleus. *Hum. Gene Ther.* **17**: 882-889 (2006).

[153] Dauty, E. and Verkman, A.S. Actin cytoskeleton as the principal determinant of size-dependent DNA mobility in cytoplasm: a new barrier for non-viral gene delivery. *J Biol Chem* **280**(9): 7823-8 (2005).

[154] Lukacs, G.L., Haggie, P., Seksek, O., Lechardeur, D., Freedman, N., and Verkman, A.S. Size-dependent DNA mobility in cytoplasm and nucleus. *J Biol Chem* **275**(3): 1625-9 (2000).

[155] Bremner, K.H., Seymour, L.W., Logan, A., and Read, M.L. Factors influencing the ability of nuclear localization sequence peptides to enhance nonviral gene delivery. *Bioconjug Chem* **15**(1): 152-61 (2004).

[156] Subramanian, A., Ranganathan, P., and Diamond, S.L. Nuclear targeting peptide scaffolds for lipofection of nondividing mammalian cells. *Nat Biotechnol* **17**(9): 873-7 (1999).

[157] Kichler, A., Pages, J.C., Leborgne, C., Druillennec, S., Lenoir, C., Coulaud, D., Delain, E., Le Cam, E., Roques, B.P., and Danos, O. Efficient DNA transfection mediated by the C-terminal domain of human immunodeficiency virus type 1 viral protein R. *J Virol* **74**(12): 5424-31 (2000).

[158] Mizoguchi, I., Ooe, Y., Hoshino, S., Shimura, M., Kasahara, T., Kano, S., Ohta, T., Takaku, F., Nakayama, Y., and Ishizaka, Y. Improved gene expression in resting macrophages using an oligopeptide derived from Vpr of human immunodeficiency virus type-1. *Biochem Biophys Res Commun* **338**(3): 1499-506 (2005).

[159] Branden, L.J., Mohamed, A.J., and Smith, C.I. A peptide nucleic acid-nuclear localization signal fusion that mediates nuclear transport of DNA. *Nat Biotechnol* **17**(8): 784-7 (1999).

[160] Moffatt, S., Wiehle, S., and Cristiano, R.J. A multifunctional PEI-based cationic polyplex for enhanced systemic p53-mediated gene therapy. *Gene Ther* **13**(21): 1512-23 (2006).

[161] Masuda, T., Akita, H., and Harashima, H. Evaluation of nuclear transfer and transcription of plasmid DNA condensed with protamine by microinjection: the use of a nuclear transfer score. *FEBS Lett* **579**(10): 2143-8 (2005).

[162] Sorgi, F.L., Bhattacharya, S., and Huang, L. Protamine sulfate enhances lipid-mediated gene transfer. *Gene Ther* **4**(9): 961-8 (1997).

[163] Chen, J., Stickles, R.J., and Daichendt, K.A. Galactosylated histone-mediated gene transfer and expression. *Hum Gene Ther* **5**(4): 429-35 (1994).

[164] Kaneda, Y., Iwai, K., and Uchida, T. Introduction and expression of the human insulin gene in adult rat liver. *J Biol Chem* **264**(21): 12126-9 (1989).

[165] Kaneda, Y., Iwai, K., and Uchida, T. Increased expression of DNA cointroduced with nuclear protein in adult rat liver. *Science* **243**(4889): 375-8 (1989).

[166] Klink, D.T., Chao, S., Glick, M.C., and Scanlin, T.F. Nuclear translocation of lactosylated poly-L-lysine/cDNA complex in cystic fibrosis airway epithelial cells. *Mol Ther* **3**(6): 831-41 (2001).

[167] Wada, K., Arima, H., Tsutsumi, T., Chihara, Y., Hattori, K., Hirayama, F., and Uekama, K. Improvement of gene delivery mediated by mannosylated dendrimer/alpha-cyclodextrin conjugates. *J Control Release* **104**(2): 397-413 (2005).

[168] Duverger, E., Roche, A.C., and Monsigny, M. N-acetylglucosamine-dependent nuclear import of neoglycoproteins. *Glycobiology* **6**(4): 381-6 (1996).

[169] Pante, N. and Kann, M. Nuclear pore complex is able to transport macromolecules with diameters of about 39 nm. *Mol Biol Cell* **13**(2): 425-34 (2002).

[170] Cartier, R. and Reszka, R. Utilization of synthetic peptides containing nuclear localization signals for nonviral gene transfer systems. *Gene Ther* **9**(3): 157-67 (2002).

[171] Talsma, S.S., Babensee, J.E., Murthy, N., and Williams, I.R. Development and in vitro validation of a targeted delivery vehicle for DNA vaccines. *J Control Release* **112**(2): 271-9 (2006).

[172] Bergen, J.M. and Pun, S.H. Peptide-enhanced nucleic acid delivery. *MRS Bulletin* **30**(9): 663-667 (2005).

[173] Haberland, A. and Bottger, M. Nuclear proteins as gene-transfer vectors. *Biotechnol Appl Biochem* **42**(Pt 2): 97-106 (2005).

[174] Kaouass, M., Beaulieu, R., and Balicki, D. Histonefection: Novel and potent non-viral gene delivery. *J Control Release* **113**(3): 245-54 (2006).

[175] Mesika, A., Kiss, V., Brumfeld, V., Ghosh, G., and Reich, Z. Enhanced intracellular mobility and nuclear accumulation of DNA plasmids associated with a karyophilic protein. *Hum Gene Ther* **16**(2): 200-8 (2005).

[176] Kulkarni, R.P., Wu, D.D., Davis, M.E., and Fraser, S.E. Quantitating intracellular transport of polyplexes by spatio-temporal image correlation spectroscopy. *Proc Natl Acad Sci U S A* **102**(21): 7523-8 (2005).

[177] Suh, J., Wirtz, D., and Hanes, J. Efficient active transport of gene nanocarriers to the cell nucleus. *Proc Natl Acad Sci U S A* **100**(7): 3878-82 (2003).

[178] Monsigny, M., Rondanino, C., Duverger, E., Fajac, I., and Roche, A.C. Glyco-dependent nuclear import of glycoproteins, glycoplexes and glycosylated plasmids. *Biochim Biophys Acta* **1673**(1-2): 94-103 (2004).

[179] Roche, A.C., Fajac, I., Grosse, S., Frison, N., Rondanino, C., Mayer, R., and Monsigny, M. Glycofection: facilitated gene transfer by cationic glycopolymers. *Cell Mol Life Sci* **60**(2): 288-97 (2003).

[180] Duverger, E., Pellerin-Mendes, C., Mayer, R., Roche, A.C., and Monsigny, M. Nuclear import of glycoconjugates is distinct from the classical NLS pathway. *J Cell Sci* **108**(4): 1325-32 (1995).

[181] Rondanino, C., Bousser, M.T., Monsigny, M., and Roche, A.C. Sugar-dependent nuclear import of glycosylated proteins in living cells. *Glycobiology* **13**(7): 509-19 (2003).

[182] Monsigny, M., Midoux, P., Mayer, R., and Roche, A.C. Glycotargeting: influence of the sugar moiety on both the uptake and the intracellular trafficking of nucleic acid carried by glycosylated polymers. *Biosci Rep* **19**(2): 125-32 (1999).

[183] Grosse, S., Thevenot, G., Monsigny, M., and Fajac, I. Which mechanism for nuclear import of plasmid DNA complexed with polyethylenimine derivatives? *J Gene Med* **8**(7): 845-51 (2006).

[184] Grosse, S., Tremeau-Bravard, A., Aron, Y., Briand, P., and Fajac, I. Intracellular rate-limiting steps of gene transfer using glycosylated polylysines in cystic fibrosis airway epithelial cells. *Gene Ther* **9**(15): 1000-7 (2002).

[185] Brunner, S., Sauer, T., Carotta, S., Cotten, M., Saltik, M., and Wagner, E. Cell cycle dependence of gene transfer by lipoplex, polyplex and recombinant adenovirus. *Gene Ther* **7**(5): 401-7 (2000).

[186] Yant, S.R., Meuse, L., Chiu, W., Ivics, Z., Izsvak, Z., and Kay, M.A. Somatic integration and long-term transgene expression in normal and haemophilic mice using a DNA transposon system. *Nat Genet* **25**(1): 35-41 (2000).

[187] Belur, L.R., Frandsen, J.L., Dupuy, A.J., Ingbar, D.H., Largaespada, D.A., Hackett, P.B., and Scott Mcivor, R. Gene insertion and long-term expression in lung mediated by the Sleeping Beauty transposon system. *Mol Ther* **8**(3): 501-7 (2003).

[188] Hamlet, M.R., Yergeau, D.A., Kuliyev, E., Takeda, M., Taira, M., Kawakami, K., and Mead, P.E. Tol2 transposon-mediated transgenesis in Xenopus tropicalis. *Genesis* **44**(9): 438-45 (2006).

[189] Huang, X., Wilber, A.C., Bao, L., Tuong, D., Tolar, J., Orchard, P.J., Levine, B.L., June, C.H., Mcivor, R.S., Blazar, B.R., and Zhou, X. Stable gene transfer and expression in human primary T cells by the Sleeping Beauty transposon system. *Blood* **107**(2): 483-91 (2006).

[190] Ohlfest, J.R., Lobitz, P.D., Perkinson, S.G., and Largaespada, D.A. Integration and long-term expression in xenografted human glioblastoma cells using a plasmid-based transposon system. *Mol Ther* **10**(2): 260-8 (2004).

[191] Keravala, A., Liu, D., Lechman, E.R., Wolfe, D., Nash, J.A., Lampe, D.J., and Robbins, P.D. Hyperactive Himar1 transposase mediates transposition in cell culture and enhances gene expression in vivo. *Hum Gene Ther* **17**(10): 1006-18 (2006).

[192] Wu, S.C., Meir, Y.J., Coates, C.J., Handler, A.M., Pelczar, P., Moisyadi, S., and Kaminski, J.M. piggyBac is a flexible and highly active transposon as compared to sleeping beauty, Tol2, and Mos1 in mammalian cells. *Proc Natl Acad Sci U S A* **103**(41): 15008-13 (2006).

[193] Lodish, H., Berk, A., Matsudaira, P., Kaiser, C., Krieger, M., Scott, M., Zipursky, S.L., and Darnell, J., *Molecular Cell Biology*. Fifth ed. 2004, New York, NY: W H Freeman and Company.

[194] Ivics, Z. and Izsvak, Z. Transposons for gene therapy! *Curr Gene Ther* **6**(5): 593-607 (2006).

[195] Izsvak, Z. and Ivics, Z. Sleeping beauty transposition: biology and applications for molecular therapy. *Mol Ther* **9**(2): 147-56 (2004).

[196] Held, P.K., Olivares, E.C., Aguilar, C.P., Finegold, M., Calos, M.P., and Grompe, M. In vivo correction of murine hereditary tyrosinemia type I by phiC31 integrase-mediated gene delivery. *Mol Ther* **11**(3): 399-408 (2005).

[197] Keravala, A., Portlock, J.L., Nash, J.A., Vitrant, D.G., Robbins, P.D., and Calos, M.P. PhiC31 integrase mediates integration in cultured synovial cells and enhances gene expression in rabbit joints. *J Gene Med* **8**(8): 1008-17 (2006).

[198] Kaminski, J.M., Huber, M.R., Summers, J.B., and Ward, M.B. Design of a nonviral vector for site-selective, efficient integration into the human genome. *FASEB J* **16**(10): 1242-7 (2002).

[199] Maragathavally, K.J., Kaminski, J.M., and Coates, C.J. Chimeric Mos1 and piggyBac transposases result in site-directed integration. *FASEB J* **20**(11): 1880-2 (2006).

[200] Wilson, M.H., Kaminski, J.M., and George, A.L., Jr. Functional zinc finger/sleeping beauty transposase chimeras exhibit attenuated overproduction inhibition. *FEBS Lett* **579**(27): 6205-9 (2005).

[201] Al-Dosari, M., Zhang, G., Knapp, J.E., and Liu, D. Evaluation of viral and mammalian promoters for driving transgene expression in mouse liver. *Biochem Biophys Res Commun* **339**(2): 673-8 (2006).

[202] Gossen, M. and Bujard, H. Tight control of gene expression in mammalian cells by tetracycline-responsive promoters. *Proc Natl Acad Sci U S A* **89**(12): 5547-51 (1992).

[203] Auricchio, A., Gao, G.P., Yu, Q.C., Raper, S., Rivera, V.M., Clackson, T., and Wilson, J.M. Constitutive and regulated expression of processed insulin following in vivo hepatic gene transfer. *Gene Ther* **9**(14): 963-71 (2002).

[204] Ido, A., Uto, H., Moriuchi, A., Nagata, K., Onaga, Y., Onaga, M., Hori, T., Hirono, S., Hayashi, K., Tamaoki, T., and Tsubouchi, H. Gene therapy targeting for hepatocellular carcinoma: selective and enhanced suicide gene expression regulated by a hypoxia-inducible enhancer linked to a human alpha-fetoprotein promoter. *Cancer Res* **61**(7): 3016-21 (2001).

[205] Gazit, G., Hung, G., Chen, X., Anderson, W.F., and Lee, A.S. Use of the glucose starvation-inducible glucose-regulated protein 78 promoter in suicide gene therapy of murine fibrosarcoma. *Cancer Res* **59**(13): 3100-6 (1999).

[206] Ehrhardt, A., Xu, H., Huang, Z., Engler, J.A., and Kay, M.A. A direct comparison of two nonviral gene therapy vectors for somatic integration: in vivo evaluation of the bacteriophage integrase phiC31 and the Sleeping Beauty transposase. *Mol Ther* **11**(5): 695-706 (2005).

[207] Honore, I., Grosse, S., Frison, N., Favatier, F., Monsigny, M., and Fajac, I. Transcription of plasmid DNA: influence of plasmid DNA/polyethylenimine complex formation. *J Control Release* **107**(3): 537-46 (2005).

[208] Schaffer, D.V., Fidelman, N.A., Dan, N., and Lauffenburger, D.A. Vector unpacking as a potential barrier for receptor-mediated polyplex gene delivery. *Biotechnol Bioeng* **67**(5): 598-606 (2000).

[209] Pollard, H., Remy, J.S., Loussouarn, G., Demolombe, S., Behr, J.P., and Escande, D. Polyethylenimine but not cationic lipids promotes transgene delivery to the nucleus in mammalian cells. *J Biol Chem* **273**(13): 7507-11 (1998).

[210] Cheng, N., Liu, W., Cao, Z., Ji, W., Liang, D., Guo, G., and Zhang, J. A study of thermoresponsive poly(N-isopropylacrylamide)/polyarginine bioconjugate non-viral transgene vectors. *Biomaterials* **27**(28): 4984-92 (2006).

[211] Kurisawa, M., Yokoyama, M., and Okano, T. Gene expression control by temperature with thermo-responsive polymeric gene carriers. *J Control Release* **69**(1): 127-37 (2000).

[212] Sun, S., Liu, W., Cheng, N., Zhang, B., Cao, Z., Yao, K., Liang, D., Zuo, A., Guo, G., and Zhang, J. A thermoresponsive chitosan-NIPAAm/vinyl laurate copolymer vector for gene transfection. *Bioconjug Chem* **16**(4): 972-80 (2005).

[213] Read, M.L., Bremner, K.H., Oupicky, D., Green, N.K., Searle, P.F., and Seymour, L.W. Vectors based on reducible polycations facilitate intracellular release of nucleic acids. *J Gene Med* **5**(3): 232-45 (2003).

[214] Wang, Y., Chen, P., and Shen, J. The development and characterization of a glutathione-sensitive cross-linked polyethylenimine gene vector. *Biomaterials* **27**(30): 5292-8 (2006).

[215] Liu, X.H., Yang, J.W., Miller, A.D., Nack, E.A., and Lynn, D.M. Charge-shifting cationic polymers that promote self-assembly and self-disassembly with DNA. *Macromolecules* **38**(19): 7907-7914 (2005).

[216] Luten, J., Akeroyd, N., Funhoff, A., Lok, M.C., Talsma, H., and Hennink, W.E. Methacrylamide polymers with hydrolysis-sensitive cationic side groups as degradable gene carriers. *Bioconjug Chem* **17**(4): 1077-84 (2006).

[217] Veron, L., Ganee, A., Ladaviere, C., and Delair, T. Hydrolyzable p(DMAPEMA) polymers for gene delivery. *Macromol Biosci* **6**(7): 540-54 (2006).

[218] Alarcon, C.D.L.H., Pennadam, S., and Alexander, C. Stimuli responsive polymers for biomedical applications. *Chem. Soc. Rev.* **34**: 276-285 (2005).

[219] Yokoyama, M. Gene delivery using temperature-responsive polymeric carriers. *Drug Discovery Today* **7**(7): 426 (2002).

[220] Saito, G., Swanson, J.A., and Lee, K.D. Drug delivery strategy utilizing conjugation via reversible disulfide linkages: role and site of cellular reducing activities. *Adv Drug Deliv Rev* **55**(2): 199-215 (2003).

[221] El-Sayed, M.E., Hoffman, A.S., and Stayton, P.S. Rational design of composition and activity correlations for pH-sensitive and glutathione-reactive polymer therapeutics. *J Control Release* **101**(1-3): 47-58 (2005).

[222] Pichon, C., Lecam, E., Guerin, B., Coulaud, D., Delain, E., and Midoux, P. Poly[Lys-(AEDTP)]: a cationic polymer that allows dissociation of pDNA/cationic polymer complexes in a reductive medium and enhances polyfection. *Bioconjug Chem* **13**(1): 76-82 (2002).

[223] Miyata, K., Kakizawa, Y., Nishiyama, N., Harada, A., Yamasaki, Y., Koyama, H., and Kataoka, K. Block catiomer polyplexes with regulated densities of charge and disulfide cross-linking directed to enhance gene expression. *J Am Chem Soc* **126**(8): 2355-61 (2004).

[224] Christensen, L.V., Chang, C.W., Kim, W.J., Kim, S.W., Zhong, Z., Lin, C., Engbersen, J.F., and Feijen, J. Reducible poly(amido ethylenimine)s designed for triggered intracellular gene delivery. *Bioconjug Chem* **17**(5): 1233-40 (2006).

[225] Zhong, Z., Song, Y., Engbersen, J.F., Lok, M.C., Hennink, W.E., and Feijen, J. A versatile family of degradable non-viral gene carriers based on hyperbranched poly(ester amine)s. *J Control Release* **109**(1-3): 317-29 (2005).

[226] Forrest, M.L., Koerber, J.T., and Pack, D.W. A degradable polyethylenimine derivative with low toxicity for highly efficient gene delivery. *Bioconjug Chem* **14**(5): 934-40 (2003).

[227] Erbacher, P., Roche, A.C., Monsigny, M., and Midoux, P. The reduction of the positive charges of polylysine by partial gluconoylation increases the transfection efficiency of polylysine/DNA complexes. *Biochim Biophys Acta* **1324**(1): 27-36 (1997).

[228] Gabrielson, N.P. and Pack, D.W. Acetylation of polyethylenimine enhances gene delivery via weakened polymer/DNA interactions. *Biomacromolecules* **7**(8): 2427-35 (2006).

[229] Kimura, T., Yamaoka, T., Iwase, R., and Murakami, A. Effect of physicochemical properties of polyplexes composed of chemically modified PL derivatives on transfection efficiency in vitro. *Macromol. Biosci.* **2**(9): 437-446 (2002).

[230] Plank, C., Mechtler, K., Szoka, F.C., Jr., and Wagner, E. Activation of the complement system by synthetic DNA complexes: a potential barrier for intravenous gene delivery. *Hum Gene Ther* **7**(12): 1437-46 (1996).

[231] Takakura, Y., Nishikawa, M., Yamashita, F., and Hashida, M. Influence of physicochemical properties on pharmacokinetics of non-viral vectors for gene delivery. *J Drug Target* **10**(2): 99-104 (2002).

[232] Elbert, D.L. and Hubbell, J.A. Surface Treatments of Polymers for Biocompatibility. *Annual Review of Materials Science* **26**(1): 365-294 (1996).

[233] Ogris, M., Brunner, S., Schuller, S., Kircheis, R., and Wagner, E. PEGylated DNA/transferrin-PEI complexes: reduced interaction with blood components, extended circulation in blood and potential for systemic gene delivery. *Gene Ther* **6**(4): 595-605 (1999).

[234] Kleemann, E., Neu, M., Jekel, N., Fink, L., Schmehl, T., Gessler, T., Seeger, W., and Kissel, T. Nano-carriers for DNA delivery to the lung based upon a TAT-derived peptide covalently coupled to PEG-PEI. *J Control Release* **109**(1-3): 299-316 (2005).

[235] Mishra, S., Webster, P., and Davis, M.E. PEGylation significantly affects cellular uptake and intracellular trafficking of non-viral gene delivery particles. *Eur J Cell Biol* **83**(3): 97-111 (2004).

[236] Woodle, M.C., Scaria, P., Ganesh, S., Subramanian, K., Titmas, R., Cheng, C., Yang, J., Pan, Y., Weng, K., Gu, C., and Torkelson, S. Sterically stabilized polyplex: ligand-mediated activity. *J Control Release* **74**(1-3): 309-11 (2001).

[237] Parker, A.L., Fisher, K.D., Oupicky, D., Read, M.L., Nicklin, S.A., Baker, A.H., and Seymour, L.W. Enhanced gene transfer activity of peptide-targeted gene-delivery vectors. *J Drug Target* **13**(1): 39-51 (2005).

[238] Patnaik, S., Aggarwal, A., Nimesh, S., Goel, A., Ganguli, M., Saini, N., Singh, Y., and Gupta, K.C. PEI-alginate nanocomposites as efficient in vitro gene transfection agents. *J Control Release* **114**(3): 398-409 (2006).

[239] Erbacher, P., Bettinger, T., Belguise-Valladier, P., Zou, S., Coll, J.L., Behr, J.P., and Remy, J.S. Transfection and physical properties of various saccharide, poly(ethylene glycol), and antibody-derivatized polyethylenimines (PEI). *J Gene Med* **1**(3): 210-22 (1999).

[240] Tseng, W.C. and Jong, C.M. Improved stability of polycationic vector by dextran-grafted branched polyethylenimine. *Biomacromolecules* **4**(5): 1277-84 (2003).

[241] Tseng, W.C., Tang, C.H., and Fang, T.Y. The role of dextran conjugation in transfection mediated by dextran-grafted polyethylenimine. *J Gene Med* **6**(8): 895-905 (2004).

[242] Ito, T., Iida-Tanaka, N., Niidome, T., Kawano, T., Kubo, K., Yoshikawa, K., Sato, T., Yang, Z., and Koyama, Y. Hyaluronic acid and its derivative as a multi-functional gene expression enhancer: protection from non-specific interactions, adhesion to targeted cells, and transcriptional activation. *J Control Release* **112**(3): 382-8 (2006).

[243] Srinivasachari, S., Liu, Y., Zhang, G., Prevette, L., and Reineke, T.M. Trehalose click polymers inhibit nanoparticle aggregation and promote pDNA delivery in serum. *J Am Chem Soc* **128**(25): 8176-84 (2006).

[244] Oupicky, D., Ogris, M., Howard, K.A., Dash, P.R., Ulbrich, K., and Seymour, L.W. Importance of lateral and steric stabilization of polyelectrolyte gene delivery vectors for extended systemic circulation. *Mol Ther* **5**(4): 463-72 (2002).

[245] Oupicky, D., Konak, C., Dash, P.R., Seymour, L.W., and Ulbrich, K. Effect of albumin and polyanion on the structure of DNA complexes with polycation containing hydrophilic nonionic block. *Bioconjug Chem* **10**(5): 764-72 (1999).

[246] Dash, P.R., Read, M.L., Fisher, K.D., Howard, K.A., Wolfert, M., Oupicky, D., Subr, V., Strohalm, J., Ulbrich, K., and Seymour, L.W. Decreased binding to proteins and cells of polymeric gene delivery vectors surface modified with a multivalent hydrophilic polymer and retargeting through attachment of transferrin. *J Biol Chem* **275**(6): 3793-802 (2000).

[247] Subr, V., Konak, C., Laga, R., and Ulbrich, K. Coating of DNA/poly(L-lysine) complexes by covalent attachment of poly[N-(2-hydroxypropyl)methacrylamide]. *Biomacromolecules* **7**(1): 122-30 (2006).

[248] Ward, C.M., Pechar, M., Oupicky, D., Ulbrich, K., and Seymour, L.W. Modification of pLL/DNA complexes with a multivalent hydrophilic polymer permits folate-mediated targeting in vitro and prolonged plasma circulation in vivo. *J Gene Med* **4**(5): 536-47 (2002).

[249] Murthy, N., Campbell, J., Fausto, N., Hoffman, A.S., and Stayton, P.S. Design and synthesis of pH-responsive polymeric carriers that target uptake and enhance the intracellular delivery of oligonucleotides. *J Control Release* **89**(3): 365-74 (2003).

[250] Walker, G.F., Fella, C., Pelisek, J., Fahrmeir, J., Boeckle, S., Ogris, M., and Wagner, E. Toward synthetic viruses: endosomal pH-triggered deshielding of targeted polyplexes greatly enhances gene transfer in vitro and in vivo. *Mol Ther* **11**(3): 418-25 (2005).

[251] Ooya, T., Choi, H.S., Yamashita, A., Yui, N., Sugaya, Y., Kano, A., Maruyama, A., Akita, H., Ito, R., Kogure, K., and Harashima, H. Biocleavable polyrotaxane-plasmid DNA polyplex for enhanced gene delivery. *J Am Chem Soc* **128**(12): 3852-3 (2006).

[252] Park, I.K., Von Recum, H.A., Jiang, S., and Pun, S.H. Supramolecular assembly of cyclodextrin-based nanoparticles on solid surfaces for gene delivery. *Langmuir* **22**(20): 8478-84 (2006).

[253] Glodde, M., Sirsi, S.R., and Lutz, G.J. Physiochemical properties of low and high molecular weight poly(ethylene glycol)-grafted poly(ethylene imine) copolymers and their complexes with oligonucleotides. *Biomacromolecules* **7**(1): 347-56 (2006).

[254] Mao, S., Neu, M., Germershaus, O., Merkel, O., Sitterberg, J., Bakowsky, U., and Kissel, T. Influence of polyethylene glycol chain length on the physicochemical and biological properties of poly(ethylene imine)-graft-poly(ethylene glycol) block copolymer/SiRNA polyplexes. *Bioconjug Chem* **17**(5): 1209-18 (2006).

[255] Boeckle, S., Von Gersdorff, K., Van Der Piepen, S., Culmsee, C., Wagner, E., and Ogris, M. Purification of polyethylenimine polyplexes highlights the role of free polycations in gene transfer. *J Gene Med* **6**(10): 1102-11 (2004).

[256] Godbey, W.T., Wu, K.K., Hirasaki, G.J., and Mikos, A.G. Improved packing of poly(ethylenimine)/DNA complexes increases transfection efficiency. *Gene Ther* **6**(8): 1380-8 (1999).

[257] Morgan, D.M., Larvin, V.L., and Pearson, J.D. Biochemical characterisation of polycation-induced cytotoxicity to human vascular endothelial cells. *J Cell Sci* **94**(3): 553-9 (1989).

[258] Fischer, D., Bieber, T., Li, Y., Elsasser, H.P., and Kissel, T. A novel non-viral vector for DNA delivery based on low molecular weight, branched polyethylenimine: effect of molecular weight on transfection efficiency and cytotoxicity. *Pharm Res* **16**(8): 1273-9 (1999).

[259] Fischer, D., Li, Y., Ahlemeyer, B., Krieglstein, J., and Kissel, T. In vitro cytotoxicity testing of polycations: influence of polymer structure on cell viability and hemolysis. *Biomaterials* **24**(7): 1121-31 (2003).

[260] Hill, I.R., Garnett, M.C., Bignotti, F., and Davis, S.S. In vitro cytotoxicity of poly(amidoamine)s: relevance to DNA delivery. *Biochim Biophys Acta* **1427**(2): 161-74 (1999).

[261] Lv, H., Zhang, S., Wang, B., Cui, S., and Yan, J. Toxicity of cationic lipids and cationic polymers in gene delivery. *J Control Release* **114**(1): 100-9 (2006).

[262] Kim, Y.H., Park, J.H., Lee, M., Kim, Y.H., Park, T.G., and Kim, S.W. Polyethylenimine with acid-labile linkages as a biodegradable gene carrier. *J Control Release* **103**(1): 209-19 (2005).

[263] Petersen, H., Merdan, T., Kunath, K., Fischer, D., and Kissel, T. Poly(ethylenimine-co-L-lactamide-co-succinamide): a biodegradable polyethylenimine derivative with an advantageous pH-dependent hydrolytic degradation for gene delivery. *Bioconjug Chem* **13**(4): 812-21 (2002).

[264] Tang, G.P., Guo, H.Y., Alexis, F., Wang, X., Zeng, S., Lim, T.M., Ding, J., Yang, Y.Y., and Wang, S. Low molecular weight polyethylenimines linked by beta-cyclodextrin for gene transfer into the nervous system. *J Gene Med* **8**(6): 736-44 (2006).

[265] Thomas, M., Ge, Q., Lu, J.J., Chen, J., and Klibanov, A.M. Cross-linked small polyethylenimines: while still nontoxic, deliver DNA efficiently to mammalian cells in vitro and in vivo. *Pharm Res* **22**(3): 373-80 (2005).

[266] Chen, D.J., Majors, B.S., Zelikin, A., and Putnam, D. Structure-function relationships of gene delivery vectors in a limited polycation library. *J Control Release* **103**(1): 273-83 (2005).

[267] Georgiou, T.K., Vamvakaki, M., Phylactou, L.A., and Patrickios, C.S. Synthesis, characterization, and evaluation as transfection reagents of double-hydrophilic star copolymers: effect of star architecture. *Biomacromolecules* **6**(6): 2990-7 (2005).

[268] Godbey, W.T., Wu, K.K., and Mikos, A.G. Size matters: molecular weight affects the efficiency of poly(ethylenimine) as a gene delivery vehicle. *J Biomed Mater Res* **45**(3): 268-75 (1999).

[269] Tang, M.X. and Szoka, F.C. The influence of polymer structure on the interactions of cationic polymers with DNA and morphology of the resulting complexes. *Gene Ther* **4**(8): 823-32 (1997).

[270] Eldred, S.E., Pancost, M.R., Otte, K.M., Rozema, D., Stahl, S.S., and Gellman, S.H. Effects of side chain configuration and backbone spacing on the gene delivery properties of lysine-derived cationic polymers. *Bioconjug Chem* **16**(3): 694-9 (2005).

[271] Liu, Y. and Reineke, T.M. Hydroxyl stereochemistry and amine number within poly(glycoamidoamine)s affect intracellular DNA delivery. *J Am Chem Soc* **127**(9): 3004-15 (2005).

[272] Thomas, M., Lu, J.J., Ge, Q., Zhang, C., Chen, J., and Klibanov, A.M. Full deacylation of polyethylenimine dramatically boosts its gene delivery efficiency and specificity to mouse lung. *Proc Natl Acad Sci U S A* **102**(16): 5679-84 (2005).

[273] Harada, A., Li, J., and Kamachi, M. The Molecular Necklace - a Rotaxane Containing Many Threaded Alpha-Cyclodextrins. *Nature* **356**(6367): 325-327 (1992).

[274] Wenz, G., Han, B.H., and Muller, A. Cyclodextrin rotaxanes and polyrotaxanes. *Chem Rev* **106**(3): 782-817 (2006).

[275] Bellocq, N.C., Pun, S.H., Jensen, G.S., and Davis, M.E. Transferrin-containing, cyclodextrin polymer-based particles for tumor-targeted gene delivery. *Bioconjug Chem* **14**(6): 1122-32 (2003).

[276] Davis, M.E., Pun, S.H., Bellocq, N.C., Reineke, T.M., Popielarski, S.R., Mishra, S., and Heidel, J.D. Self-assembling nucleic acid delivery vehicles via linear, water-soluble, cyclodextrin-containing polymers. *Curr Med Chem* **11**(2): 179-97 (2004).

[277] Pun, S.H., Bellocq, N.C., Liu, A., Jensen, G., Machemer, T., Quijano, E., Schluep, T., Wen, S., Engler, H., Heidel, J., and Davis, M.E. Cyclodextrin-modified polyethylenimine polymers for gene delivery. *Bioconjug Chem* **15**(4): 831-40 (2004).

[278] Storrie, H. and Mooney, D.J. Sustained delivery of plasmid DNA from polymeric scaffolds for tissue engineering. *Adv Drug Deliv Rev* **58**(4): 500-14 (2006).

[279] Jang, J.H., Bengali, Z., Houchin, T.L., and Shea, L.D. Surface adsorption of DNA to tissue engineering scaffolds for efficient gene delivery. *J Biomed Mater Res A* **77**(1): 50-8 (2006).

[280] Hammond, P.T. Form and function in multilayer assembly: New applications at the nanoscale. *Advanced Materials* **16**(15): 1271-1293 (2004).

[281] Jewell, C.M., Zhang, J., Fredin, N.J., Wolff, M.R., Hacker, T.A., and Lynn, D.M. Release of plasmid DNA from intravascular stents coated with ultrathin multilayered polyelectrolyte films. *Biomacromolecules* **7**(9): 2483-91 (2006).

[282] Yamauchi, F., Kato, K., and Iwata, H. Layer-by-layer assembly of poly(ethyleneimine) and plasmid DNA onto transparent indium-tin oxide electrodes for temporally and spatially specific gene transfer. *Langmuir* **21**(18): 8360-7 (2005).

[283] Jewell, C.M., Zhang, J., Fredin, N.J., and Lynn, D.M. Multilayered polyelectrolyte films promote the direct and localized delivery of DNA to cells. *J Control Release* **106**(1-2): 214-23 (2005).

[284] Meyer, F., Ball, V., Schaaf, P., Voegel, J.C., and Ogier, J. Polyplex-embedding in polyelectrolyte multilayers for gene delivery. *Biochim Biophys Acta* **1758**(3): 419-22 (2006).

[285] Zhang, J., Chua, L.S., and Lynn, D.M. Multilayered thin films that sustain the release of functional DNA under physiological conditions. *Langmuir* **20**(19): 8015-21 (2004).

[286] Jessel, N., Oulad-Abdelghani, M., Meyer, F., Lavalle, P., Haikel, Y., Schaaf, P., and Voegel, J.C. Multiple and time-scheduled in situ DNA delivery mediated by beta-cyclodextrin embedded in a polyelectrolyte multilayer. *Proc Natl Acad Sci U S A* **103**(23): 8618-21 (2006).

[287] Chu, B., Liang, D.H., Hadjiargyrou, M., and Hsiao, B.S. A new pathway for developing in vitro nanostructured non-viral gene carriers. *Journal of Physics-Condensed Matter* **18**(36): S2513-S2525 (2006).

[288] Lim, S.H., Liao, I.C., and Leong, K.W. Nonviral gene delivery from nonwoven fibrous scaffolds fabricated by interfacial complexation of polyelectrolytes. *Mol Ther* **13**(6): 1163-72 (2006).

[289] Luu, Y.K., Kim, K., Hsiao, B.S., Chu, B., and Hadjiargyrou, M. Development of a nanostructured DNA delivery scaffold via electrospinning of PLGA and PLA-PEG block copolymers. *J Control Release* **89**(2): 341-53 (2003).

[290] Bengali, Z. and Shea, L.D. Gene delivery by immobilization to cell-adhesive substrates. *MRS Bulletin* **30**(9): 659-662 (2005).

[291] Huang, Y.C., Riddle, K., Rice, K.G., and Mooney, D.J. Long-term in vivo gene expression via delivery of PEI-DNA condensates from porous polymer scaffolds. *Hum Gene Ther* **16**(5): 609-17 (2005).

[292] Segura, T., Chung, P.H., and Shea, L.D. DNA delivery from hyaluronic acid-collagen hydrogels via a substrate-mediated approach. *Biomaterials* **26**(13): 1575-84 (2005).

[293] Jang, J.H., Rives, C.B., and Shea, L.D. Plasmid delivery in vivo from porous tissue-engineering scaffolds: transgene expression and cellular transfection. *Mol Ther* **12**(3): 475-83 (2005).

[294] Shea, L.D., Smiley, E., Bonadio, J., and Mooney, D.J. DNA delivery from polymer matrices for tissue engineering. *Nat Biotechnol* **17**(6): 551-4 (1999).

[295] Brocchini, S., James, K., Tangpasuthadol, V., and Kohn, J. Structure-property correlations in a combinatorial library of degradable biomaterials. *J Biomed Mater Res* **42**(1): 66-75 (1998).

[296] Anderson, D.G., Lynn, D.M., and Langer, R. Semi-automated synthesis and screening of a large library of degradable cationic polymers for gene delivery. *Angew Chem Int Ed Engl* **42**(27): 3153-8 (2003).

[297] Akinc, A., Anderson, D.G., Lynn, D.M., and Langer, R. Synthesis of poly(beta-amino ester)s optimized for highly effective gene delivery. *Bioconjug Chem* **14**(5): 979-88 (2003).

[298] Meier, M.A.R., Hoogenboom, R., and Schubert, U.S. Combinatorial methods, automated synthesis and high-throughput screening in polymer research: The evolution continues. *Macromol. Rapid Commun.* **25**(1): 21-33 (2004).

[299] Smith, J.R., Knight, D., Kohn, J., Rasheed, K., Weber, N., Kholodovych, V., and Welsh, W.J. Using surrogate modeling in the prediction of fibrinogen adsorption onto polymer surfaces. *J Chem Inf Comput Sci* **44**(3): 1088-97 (2004).

[300] Smith, J.R., Seyda, A., Weber, N., Knight, D., Abramson, S., and Kohn, J. Integration of combinatorial synthesis, rapid screening, and computational modeling in biomaterials development. *Macromol. Rapid Commun.* **25**(1): 127-140 (2004).

[301] Smith, J.R., Kholodovych, V., Knight, D., Kohn, J., and Welsh, W.J. Predicting fibrinogen adsorption to polymeric surfaces in silico: a combined method approach. *Polymer* **46**(12): 4296-4306 (2005).

[302] Jiang, X., Van Der Horst, A., Van Steenbergen, M.J., Akeroyd, N., Van Nostrum, C.F., Schoenmakers, P.J., and Hennink, W.E. Molar-mass characterization of cationic polymers for gene delivery by aqueous size-exclusion chromatography. *Pharm Res* **23**(3): 595-603 (2006).

[303] Akinc, A. and Langer, R. Measuring the pH environment of DNA delivered using nonviral vectors: Implications for lysosomal trafficking. *Biotechnol Bioeng* **78**(5): 503-508 (2002).

[304] Forrest, M. and Pack, D. On the kinetics of polyplex endocytic trafficking: Implications for gene delivery vector design. *Mol Ther* **6**(1): 57-66 (2002).

[305] Sonawane, N., Szoka, F., and Verkman, A. Chloride accumulation and swelling in endosomes enhances DNA transfer by polyamine-DNA polyplexes. *J Biol Chem* **278**(45): 44826-44831 (2003).

[306] Behr, J. The proton sponge: A trick to enter cells the viruses did not exploit. *CHIMIA* **51**(1-2): 34-36 (1997).

[307] Bieber, T., Meissner, W., Kostin, S., Niemann, A., and Elsasser, H. Intracellular route and transcriptional competence of polyethylenimine-DNA complexes. *J Control Release* **82**(2-3): 441-454 (2002).

[308] Sonawane, N., Thiagarajah, J., and Verkman, A. Chloride concentration in endosomes measured using a ratioable fluorescent Cl- indicator - Evidence for chloride accumulation during acidification. *J Biol Chem* **277**(7): 5506-5513 (2002).

[309] Dubruel, P., Urtti, A., and Schacht, E. Surface plasmon resonance Spectroscopy as a tool to study polyplex-glycoaminoglycan interactions. *Macromol. Rapid Commun.* **26**(12): 992-997 (2005).

[310] Suh, J., Wirtz, D., and Hanes, J. Real-time intracellular transport of gene nanocarriers studied by multiple particle tracking. *Biotechnol Prog* **20**(2): 598-602 (2004).

[311] Dinh, A., Pangarkar, C., Theofanous, T., and Mitragotri, S. Understanding intracellular transport processes pertinent to synthetic gene delivery via stochastic simulations and sensitivity analyses. *Biophys J* **92**(3): 831-846 (2007).

[312] Goldberg, A.L. Functions of the proteasome: the lysis at the end of the tunnel. *Science* **268**(5210): 522-3 (1995).

[313] Kim, J., Chen, C.P., and Rice, K.G. The proteasome metabolizes peptide-mediated nonviral gene delivery systems. *Gene Therapy* **12**(21): 1581-1590 (2005).

[314] Grosse, S., Aron, Y., Thevenot, G., Francois, D., Monsigny, M., and Fajac, I. Potocytosis and cellular exit of complexes as cellular pathways for gene delivery by polycations. *J Gene Med* **7**(10): 1275-86 (2005).

[315] Mineo, C. and Anderson, R.G. Potocytosis. Robert Feulgen Lecture. *Histochem Cell Biol* **116**(2): 109-18 (2001).

[316] http://www.wiley.co.uk/genetherapy/clinical/

CHAPTER 3

SYNTHESIS AND CHARACTERIZATION OF FUNCTIONALIZED POLYMERIC GENE VECTORS[1]

3.1. ABSTRACT

Combinatorial polymer libraries have recently gained popularity for the development of novel materials for a variety of biomedical applications including non-viral gene delivery systems and biodegradable polymers for tissue engineering. To streamline the non-trivial task of library synthesis, activated ester homopolymers have been used to serve as a backbone to which primary amine-containing functional groups (NH_2-FGs) can be covalently bound at varying ratios. Poly(methacryloxysuccinimide) (poly(MAOS)) is one such homopolymer that was previously reported to be an attractive precursor for polymeric drug and gene delivery systems. The reported functionalization protocols entailed conjugating the precursor with two equivalents of the NH_2-FG at a reaction concentration of 25 mg poly(MAOS)/150μL DMSO for either 5 hours at 50 °C or 16 hours at 25 °C. More recently, both protocols were revealed to be associated with ring-opening and glutarimide-forming side reactions that compromise the utility of the homopolymer. Using 1-dimensional and 2-dimensional NMR spectroscopy techniques, we have characterized the side product distributions that result from conjugations performed at 50 °C/5 hours and 25 °C/16 hours. Moreover, by systematically altering the equivalents of the NH_2-FGs, polymer concentration, reaction time, and reaction

[1] Reproduced with permission from Wong, S., Putnam, D., Overcoming limiting side reactions associated with an NHS-activated precursor of polymethacrylamide-based polymers, *Bioconjugate Chemistry*, 18, 3, 970-982 (2007). Copyright [2007] American Chemical Society.

temperature, we have established a protocol that overcomes these side reactions. Using a final reaction protocol of five equivalents of the NH_2-FG at a reaction concentration of 25mg poly(MAOS)/600μL DMSO for 24 hours at 75 °C, we have obtained functionalized polymers with minimal side products. This protocol is applicable for polymers ranging from 5K to 50K g/mol, compatible with a variety of functional groups, and amenable to conjugating combinations of functional groups.

3.2. INTRODUCTION

With the ever-increasing demand for more sophisticated, multifaceted polymeric materials in various applications, many researchers have begun looking to combinatorial approaches to facilitate the materials discovery process. One of the first successful demonstrations of employing combinatorial strategies to develop degradable polymers for medical applications was reported almost a decade ago by Kohn and coworkers. [1, 2] Their work exemplified how combinatorial strategies can 1) offer a systematic approach to designing libraries of compounds that encompass a broad range of physicochemical properties and 2) assist in identifying structure-function relationships that correlate a polymeric structural feature to a biological response.

Building on this work, Brocchini and coworkers, Haddleton and coworkers, and others have applied the combinatorial approach towards developing water-soluble polymers for drug and gene delivery systems. [3-9] To expedite the library synthesis process, the former two groups employed the use of the activated homopolymeric precursor, poly(methacryloxysuccinimide) (poly(MAOS), **1**) to which primary amine-containing functional groups (NH_2-FGs) can be covalently bound via amidation chemistry. [10] (Figure 3-1).

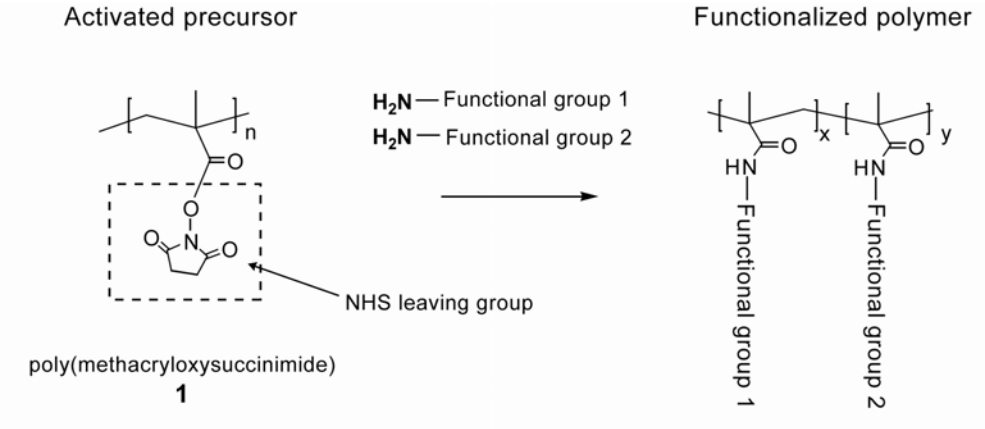

Figure 3-1. Theoretical synthetic scheme for functionalizing the N-hydroxysuccinimide (NHS)-activated precursor, poly(methacryloxysuccinimide) (poly(MAOS), 1), to form poly(methacrylamide)-based polymers.

Recently, greater resolution of the potential side reactions that can occur with the poly(MAOS) precursor was reported. [11] In our hands, we also observed similar problems upon functionalizing poly(MAOS) that resulted in at least two unexpected side reactions: 1) ring opening of the succinimide moiety and 2) glutarimide formation between presumably neighboring active esters. These side products were confirmed by ^{1}H NMR, diffusion ordered spectroscopy (DOSY), heteronuclear multi bond correlation spectroscopy (HMBC), and homonuclear correlated spectroscopy (COSY) analyses (Figure 3-2).

However, these limitations do not ultimately preclude the use of this polymeric precursor as was previously suggested. [11] In this report, we describe the protocol that we have established to overcome these side reactions allowing poly(MAOS) to serve as a viable precursor for poly(methacrylamide)-based materials. Additionally, we show that this protocol is applicable for polymers ranging from 5K to 50K g/mol, compatible with a variety of functional groups, and amenable to conjugating combinations of functional groups.

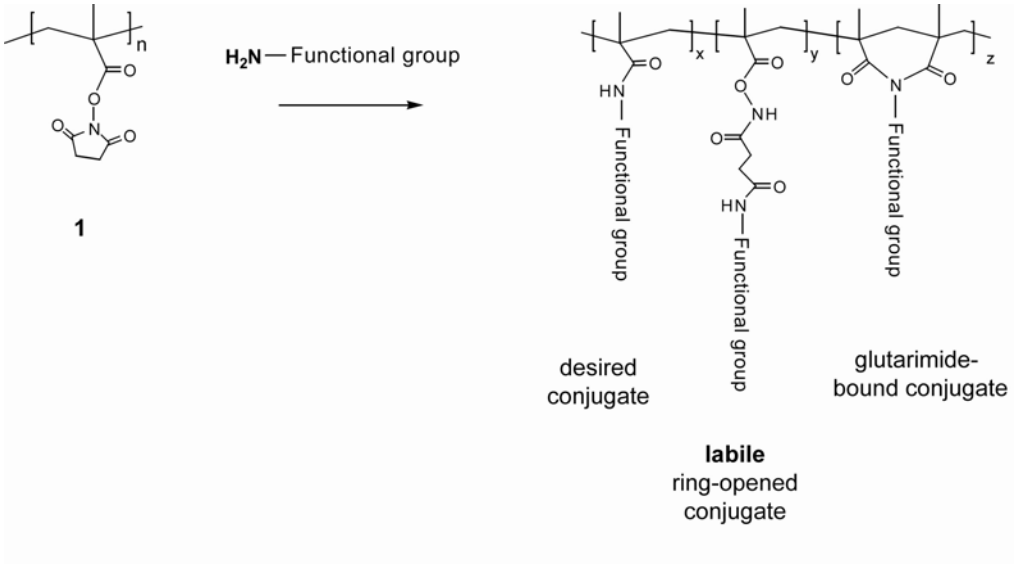

Figure 3-2. Side reactions can occur during conjugation of NH_2-FGs to 1 resulting in a functionalized polymer with three pendant groups: 1) the desired amide-bound conjugate; 2) a hydrolytically-unstable ring-opened conjugate; and 3) a glutarimide-bound conjugate.

3.3. **EXPERIMENTAL PROCEDURE**

N-methacryloxysuccinimide monomer was synthesized as previously reported. [12] Cu(I)Br (99.999%), Cu(II)Br_2 (99.999%), 2,2'-dipyridyl (≥ 99%), ethyl 2-bromoisobutyrate (98%), benzylamine (≥ 99.5%), n-butylamine (≥ 99.5%), hexylamine (≥ 99.5%), 1-amino-2-propanol (≥ 98%), N-Boc-N-methylethylenediamine (≥98.0%), N-Boc-ethylenediamine (≥ 98%), N,N-dimethylethylenediamine (≥ 98%), 2-(aminoethyl)-trimethylammonium chloride – HCl (99%), histamine (≥ 97%), anhydrous DMSO, DMSO-d_6, DMF-d_7 were all purchased from Aldrich.

3.3.1. General procedure for synthesis of poly(methacryloxysuccinimide) (poly(MAOS)

The polymer precursor was synthesized with a slight modification to a previously reported method. [5] A 5 ml pear shaped flask with flea magnetic stir bar was fitted with a rubber septum and flame dried while purging with N_2(g) until cooled to ambient temperature. N-methacryloxysuccinimide (0.5 g, 2.73 mmol), Cu(I)Br (0.0078 g, 0.055 mmol), Cu(II)Br_2 (0.0122 g, 0.055 mmol), and 2,2'-dipyridyl (0.0171 g, 0.11 mmol) were placed in the flask and placed under a nitrogen atmosphere for 10 minutes. Cu(II)Br_2 was added to the reaction as an inhibitor of chain terminations to control polydispersities. [13] Deoxygenated anhydrous DMSO (0.2 mL) was injected into the flask and the contents were stirred until dissolved. Ethyl-2-bromoisobutyrate (81 μl, 0.55 mmol) was weighed directly into a separate dram vial and dissolved in deoxygenated anhydrous DMSO (0.5 mL). Upon complete dissolution of the contents, a 1/10 aliquot (50 μL) of the ethyl 2-bromoisobutyrate solution was injected into the flask and immersed into a 100 °C thermostated oil bath. To stop the polymerization, the flask was quenched in an ice bath and the product was diluted with anhydrous DMSO (1.5 mL). The final polymer was isolated as a white powder by precipitating into stirring acetone. ^{1}H NMR (DMSO-d_6) δ: 1.44 (b,3H,CH_3), 2.41 (b,2H,CH_2), 2.78 (b,4H,CH_2CH_2).

Molecular weight and polydispersity were determined by hydrolyzing poly(MAOS) to its Na-salt. Upon dissolving poly(MAOS) (0.010 g, 0.055 mmol) in DMSO (0.080 mL), 22 μL of 5M NaOH was added dropwise to the reaction and allowed to stir for 7 hours at room temperature. The cloudy solution was redissolved with 0.8 mL of filtered deionized water and allowed to stir overnight at room temperature. The reaction was then dialyzed against deionized water using

Spectra/Por regenerated cellulose tubing (MWCO 3500 Da) for 3 days. The dialysate was subsequently lyophilized to give a white feathery powder.

3.3.2. **General procedure for functionalized poly(MAOS)**

Prior to each reaction, a 5 ml pear shaped flask with flea magnetic stir bar was fitted with a rubber septum and flame dried while purging with N_2(g) until cooled to ambient temperature. Poly(MAOS) (0.025 g, 0.14 mmol) was added to the flask and dissolved with deoxygenated anhydrous DMSO (0.6 mL). Upon dissolution of the contents, 5 equivalents of the NH_2-FG was dropwise added via a Hamilton syringe and immersed in a 75 °C thermostated oil bath. For the binary conjugations, the first amine was dropwise added via a Hamilton syringe followed immediately by dropwise addition of the second amine via a separate Hamilton syringe. The flask was removed from the oil bath after 24 hours and the septum removed. To remove excess solvent, the flask mouth was covered with Parafilm, punctured approximately seven times with a 21 gauge needle, and placed *in vacuo* for 4 hours. The final product was isolated via dropwise addition into stirring acetone and filtered through a fine fritted Buchner funnel and washed twice with acetone, twice with diethyl ether, and dried overnight *in vacuo*. N-Boc-protected functionalized polymers were isolated via dropwise addition into diethyl ether. The gummy precipitate was redissolved in methylene chloride and reprecipitated into diethyl ether as a white flaky powder. The powder was filtered through a fine fritted Buchner funnel and immediately deprotected with 20 equivalents of neat trifluoroacetic acid for 8 minutes. The final product was isolated via dropwise addition into stirring diethyl ether and filtered through a fine fritted Buchner funnel. Polymers functionalized with water solubilizing FGs, including all binary conjugations, were redissolved in, and dialyzed against, 0.1N HCl in Spectra/Por

regenerated cellulose tubing (MWCO 3500 Da) for 4 days. The dialysate was subsequently lyophilized to give a flaky solid.

3.3.2.1. *Characterization*

Benzylamine-functionalized poly(MAOS): ^{1}H NMR (DMSO-d_6) δ:0.89 (b,3H,CH_3), 1.89 (b,2H,CH_2), 7.86 (b,1H,NH), 4.11 (b,2H,CH_2), 7.26 (b,5H,C_6H_5), 4.68 (b,2H,glutarimide-CH_2); butylamine-functionalized poly(MAOS): ^{1}H NMR (DMSO-d_6) δ:0.89 (b,3H,CH_3), 1.89 (b,2H,CH_2), 7.29 (b,1H,NH), 2.93 (b,2H,CH_2), 1.25 (b,4H,CH_2CH_2), 0.86 (b,3H,CH_3); hexylamine-functionalized poly(MAOS): ^{1}H NMR (DMSO-d_6) δ:0.89 (b,3H,CH_3), 1.89 (b,2H,CH_2), 7.29 (b,1H,NH), 2.93 (b,2H,CH_2), 1.24 (b,8H,$(CH_2)_4$), 0.86 (b,3H,CH_3); ethylenediamine-functionalized poly(MAOS): ^{1}H NMR (D_2O) δ:1.14 (b,3H,CH_3), 1.84 (b,2H,CH_2), 3.43 (b,2H,CH_2), 3.13 (b,2H,CH_2); N-methylethylenediamine-functionalized poly(MAOS): ^{1}H NMR (D_2O) δ:1.14 (b,3H,CH_3), 1.84 (b,2H,CH_2), 3.44 (b,2H,CH_2), 3.17 (b,2H,CH_2), 2.76 (b,3H,CH_3); N,N-dimethylethylenediamine-functionalized poly(MAOS): ^{1}H NMR (D_2O) δ:1.14 (b,3H,CH_3), 1.84 (b,2H,CH_2), 3.52 (b,2H,CH_2), 3.28 (b,2H,CH_2), 2.94 (b,6H,CH_3CH_3), 4.05 (b,2H,glutarimide-CH_2); 2-(aminoethyl)-trimethylammonium-functionalized poly(MAOS): ^{1}H NMR (D_2O) δ:1.14 (b,3H,CH_3), 1.84 (b,2H,CH_2), 3.61 (b,2H,CH_2), 3.44 (b,2H,CH_2), 3.20 (b,6H,$(CH_3)_3$), 4.15 (b,2H,glutarimide-CH_2); 1-amino-2-propanol-functionalized poly(MAOS): ^{1}H NMR (D_2O) δ:1.14 (b,3H,CH_3), 1.84 (b,2H,CH_2), 3.14 (b,2H,CH_2), 3.91 (b,1H,CH), 1.17 (b,3H,CH_3); histamine-functionalized poly(MAOS): ^{1}H NMR (D_2O) δ:1.14 (b,3H,CH_3), 1.84 (b,2H,CH_2), 3.43 (b,2H,CH_2), 2.93 (b,2H,CH_2), 7.29 (b,1H,CH), 8.61 (b,1H,CH), 3.97 (b,2H,glutarimide-CH_2).

3.3.3. Determination of relative percent conjugation

For mono-functionalized conjugations, a sample calculation of the relative percent conjugation of each pendant group is demonstrated with benzylamine-conjugated poly(MAOS) as determined from the ^{1}H NMR spectra using the following equations:

$$\%Z = \frac{I_{4.68}}{2} \times 100$$

$$\%Y = \frac{I_{2.4}}{4} \times 100$$

$$\%X = 100 - \%Y - \%Z$$

where Z=glutarimide-bound conjugate, Y=ring-opened conjugate, X=desired amide-bound conjugate, $I_{4.68}$ = signal intensity of the two glutarimide methylene protons, and $I_{2.4}$ = signal intensity of the four ring-opened methylene protons. I_δ = signal intensity at δ ppm when $I_{7.26}$ = 5.0.

For binary conjugations, the relative percent conjugation of each functional group is demonstrated with the N,N-dimethylethylenediamine(3N)/benzylamine conjugation as determined from the ^{1}H NMR spectra using the following equations:

$$\%\ \text{Benzylamine} = \frac{\frac{I_{7.26}}{5}}{1 + \frac{I_{7.26}}{5}} \times 100$$

$$\%\ 3N = 100 - \%\ \text{Benzylamine}$$

where $I_{7.26}$= peak intensity of the five benzyl protons at 7.26 ppm when $I_{2.94}$= 6.0. $I_{2.94}$= peak intensity of the six methyl protons of 3N.

3.3.4. **Molecular weight characterization**

Gel permeation chromatography was carried out using Waters Ultrahydrogel 250 and 500 columns in series coupled to UV (Waters 2487) and RI (Waters 2414) detectors. The mobile phase was phosphate buffered saline (pH=7.4) at a flow rate of 0.8 mL/min at 30 °C. Calibration was performed using PMAA-Na standards (Polysciences, Inc. and Polymer Standards Service-USA, Inc.) in the range of 1.6 kg mol^{-1} to 110 kg-mol^{-1}.

3.3.5. NMR spectroscopy

All NMR analyses were performed with 7 mg of sample dissolved in 1 mL of deuterated solvent and all spectra were processed using standard Varian software. One-dimensional ^{1}H NMR analyses were performed at room temperature on an Inova 600 MHz spectrometer with a proton observation frequency of 599.8 MHz. Chemical shifts were referenced relative to tetramethylsilane (0.0 ppm) when possible or the residual solvent signal - D_2O (4.8 ppm), DMSO-d_6 (2.5 ppm) or DMF-d_7 (2.75 ppm). Spectra were acquired with a 5.6 μs pulse width corresponding to a 45° flip angle, 3 s acquisition time, 4.8 kHz spectral width, 16 transients, and a 1 s recycle delay. An exponential multiplication of approximately 0.3 Hz was applied prior to Fourier transformation.

Proton homonuclear correlated spectroscopy (^{1}H-^{1}H COSY) was performed at 120 °C on an Inova 500 MHz spectrometer with a proton observation frequency of 499.9 MHz. Spectra were obtained using the gCOSY pulse program in the VnmrJ

software with 1,024 (t_2) × 512 (t_1) data points collected at 2 scans per t1 increment. Spectral widths of 6.4 kHz in F2 and F1 were used along with a 0.1608 s acquisition time and a 1 s recycle delay time. Fourier transformation was done on a 2K x 2K data matrix with sine bell window function applied to F1 and F2.

The long-range ^{1}H–^{13}C correlation spectroscopy (HMBC) was performed at room temperature on an Inova 600 MHz spectrometer with a proton frequency of 599.8 MHz. Spectra were obtained using the gHMBC pulse program in the VnmrJ software with 1,024 (t_2) × 400 (t_1) data points collected at 28 scans per t1 increment. Spectral widths of 7 kHz in F2 and 36.2 kHz in F1 were used along with a 0.1608 s acquisition time and a 1 s recycle delay. Fourier transformation was done on a 1K (F2) x 4K (F1) data matrix with Gaussian processing applied to F2 only.

3.3.6. Diffusion – ordered NMR spectroscopy

^{1}H detected DOSY experiments were performed at 22 °C on an Inova 600 MHz spectrometer equipped with a triple resonance probe head capable of producing gradients in the z direction with strength of up to 70 G cm^{-1}. DOSY experiments were performed using a bipolar pulse pair double stimulated echo experiment. The gradient strength was logarithmically incremented in 16 steps from 2.3 up to 60 G cm^{-1}. Diffusion times and gradient pulse durations were optimized for each experiment in order to achieve a 90% decrease in the resonance intensity at the largest gradient amplitude. Diffusion times varied between 600 and 900 ms, and bipolar rectangular gradient pulses of 2 ms were employed. Data was analyzed using the VnmrJ software package.

3.4. RESULTS AND DISCUSSION

Our initial attempts to conjugate benzylamine to poly(MAOS) following two independent protocols resulted in two unexpected side reactions that accompanied the desired conjugation: 1) ring opening of the succinimide moiety and 2) glutarimide formation between presumably neighboring active esters. These side reactions were thoughtfully characterized and recently reported by Devenish et al. and shown again in Figure 3-3 and Figure 3-4 for ease of reference. [11]

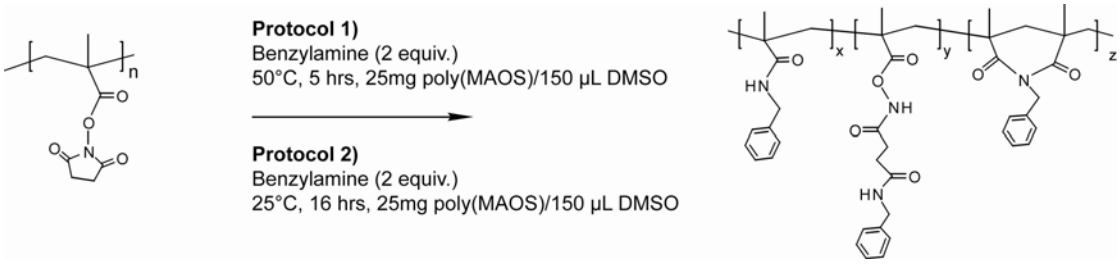

Figure 3-3. Resultant functionalized polymer produced from previously reported protocols. Two unexpected side reaction products accompany the desired conjugation: 1) a labile ring-opened conjugate and 2) a glutarimide-bound conjugate. (Protocol 1-Ref 7; Protocol 2-Ref 8).

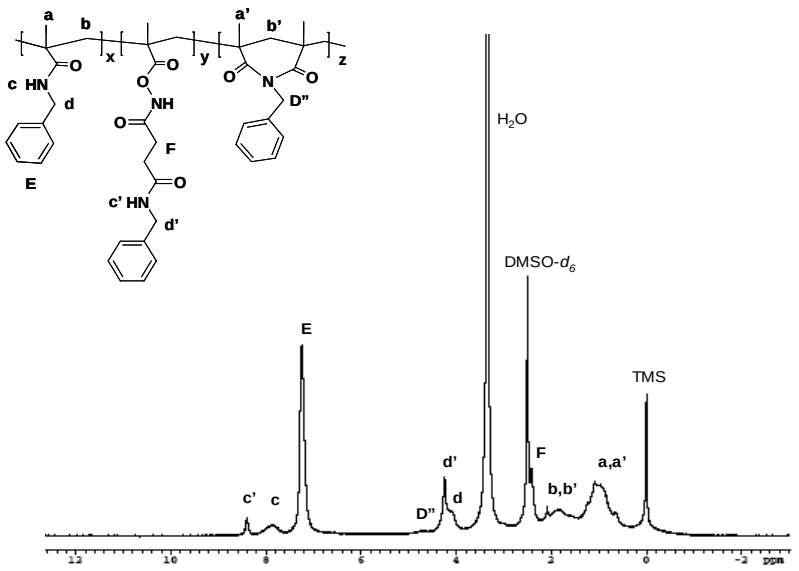

(a)

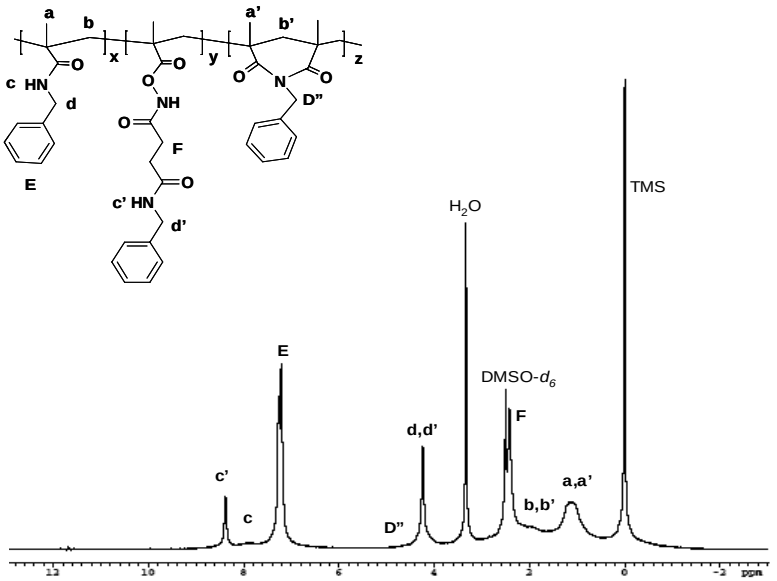

(b)

Figure 3-4. Representative ^{1}H NMR spectra of resultant functionalized polymer produced from **(a)** Protocol 1- 2 equivalents benzylamine, 50 °C, 5 hrs, 25mg poly(MAOS)/150μL DMSO and **(b)** Protocol 2 - 2 equivalents benzylamine, 25 °C, 16 hrs, 25mg poly(MAOS)/150μL DMSO. Both spectra provide evidence of a ring-opened side product (indicated by peaks F, d', and c') and glutarimide-bound side product (indicated by peak D"). Peaks labeled in capital letters were used for quantification via signal integration of the respective pendant groups. Note: These spectra were obtained during our analysis but are consistent with the results of Devenish et al. and are shown here to clarify the method of quantification.

To further verify that the ^{1}H NMR peak corresponding to the methylene protons of the ring-opened pendant group (peak F in Figure 3-4) was not just residual low molecular weight by-product, we performed DOSY experiments to provide evidence of covalent linkage to the backbone. [14] This pulsed field gradient NMR experiment yields a 2D spectrum with NMR chemical shifts on the horizontal axis and relative diffusion coefficients on the vertical axis. DOSY has been used for the analysis of polymer mixtures to determine the molecular weight (MW) of individual components. [15] In this paper, DOSY was utilized to confirm that the ring-opened side reaction product was diffusing at a similar rate as the polymer and thus covalently bound to the polymer as evidenced in Figure 3-5. Additionally, HMBC experiments were performed to identify long-range (2-3 bonds) correlations between protons and neighboring carbons. Figure 3-6 reveals that the ring-opened methylene protons (peak f) are correlated to carbonyl carbons (carbons 4 and 5). Taken together, these data provide strong evidence that the ring-opened pendant group is indeed covalently bound to the polymer.

Using signal integration of the ^{1}H NMR spectra (Figure 3-4) to quantify the relative degree of conjugation of each pendant group, we observed a marked disparity in pendant distribution between the two protocols which essentially differ only by time and temperature. Protocol 1 produces approximately 75% of the desired conjugation (x), 20% ring-opened side product (y), and 5% glutarimide-bound conjugate (z). Protocol 2 generates conjugations estimated to be about 30%, 70%, and 0%, respectively.

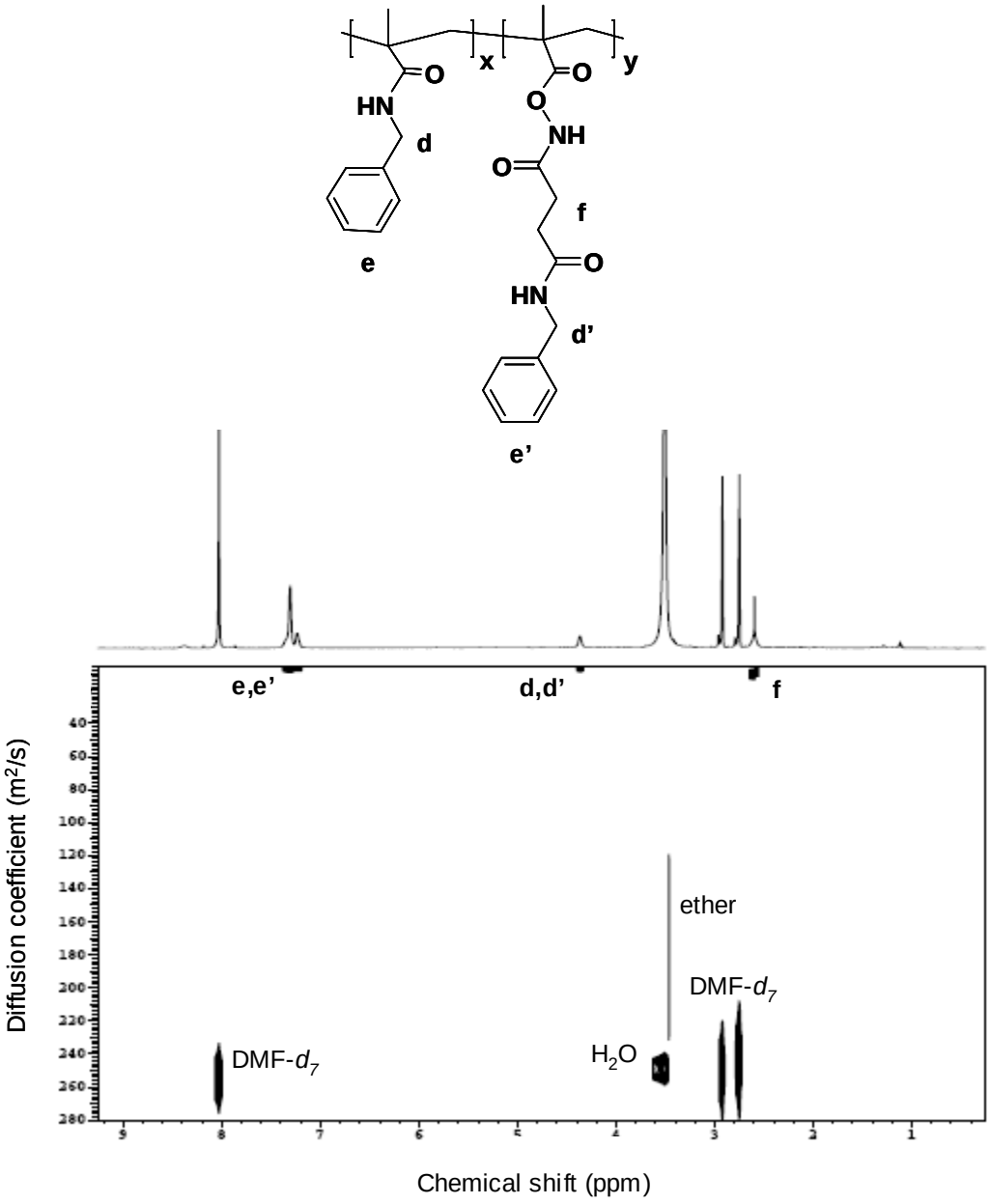

Figure 3-5. ^{1}H-detected DOSY spectrum of poly(MAOS) functionalized with benzylamine following protocol 2 - 2 equivalents benzylamine, 25 °C, 16 hrs, 25mg poly(MAOS)/150μL DMSO. Peak f, corresponding to the methylene protons of the ring-opened side product, has a similar diffusion coefficient as the rest of the polymer providing evidence that the side reaction product is covalently bound to the polymer. Peaks corresponding to low molecular weight solvents are shown to diffuse faster as expected.

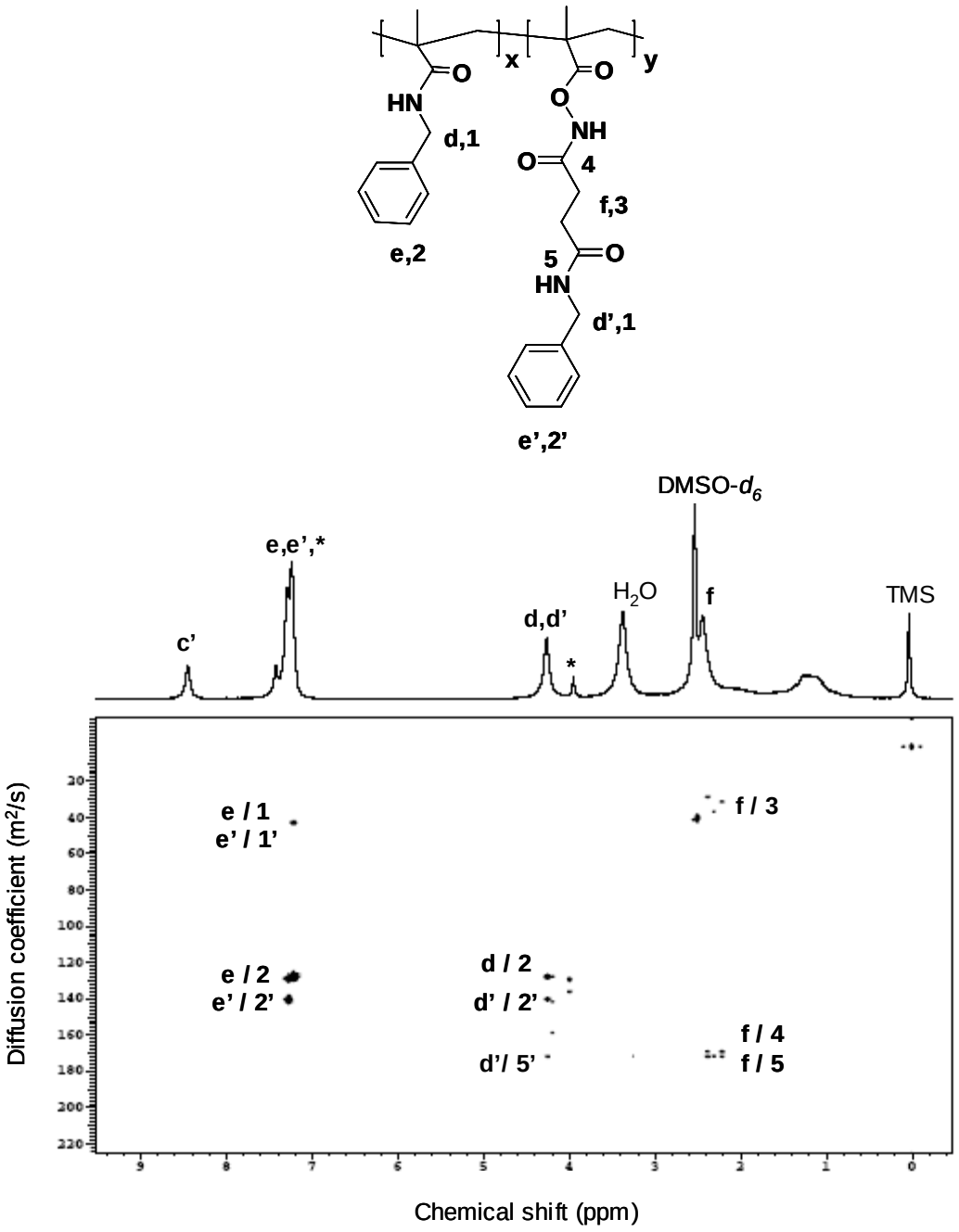

Figure 3-6. ^{1}H-^{13}C HMBC spectrum of poly(MAOS) functionalized with benzylamine following protocol 2 - 2 equivalents benzylamine, 25 °C, 16 hrs, 25mg poly(MAOS)/150μL DMSO. Peak f, corresponding to the ring-opened side product, is shown to correlate with carbonyl carbons thus providing further evidence of the presence and identity of the ring-opened side product (Correlations f/4 and f/5). Peaks labeled with letters correspond to protons and numbers correspond to carbons. (* = excess benzylamine)

Incidentally, the benzylamine-conjugated polymer synthesized by Monge and Haddleton employed a low MW polymer precursor (~3K g/mol). To examine whether MW might play a role in the resultant conjugation profile, we evaluated Protocol 1 at three different MWs- 5K, 30K, and 50K g/mol. We also explored the effects of several other reaction parameters, namely poly(MAOS) concentration, reaction time, and reaction temperature, on the resultant conjugation profile. The data shown in Figures 3-7 to 3-9 suggest that the pendant distribution is independent of MW, precursor concentration, and reaction time, yet greatly dependent upon reaction temperature where an increase in temperature leads to a greater proportion of the desired and glutarimide-bound conjugates and less of the ring-opened conjugate. In contrast to the time dependency of the resultant conjugation profile reported by Devenish et al., our examination did not reveal any appreciable reduction in the ring-opened side product at either temperature evaluated (25°C and 50°C). However, the reaction time range of 5 to 16 hours evaluated in our study contrasts sharply with that of Devenish et al.'s 5 hours to 7 days. As such, our time range may have been too narrow to produce any noticeable effects on conjugation profile and does not necessarily contradict the findings by Devenish et al.

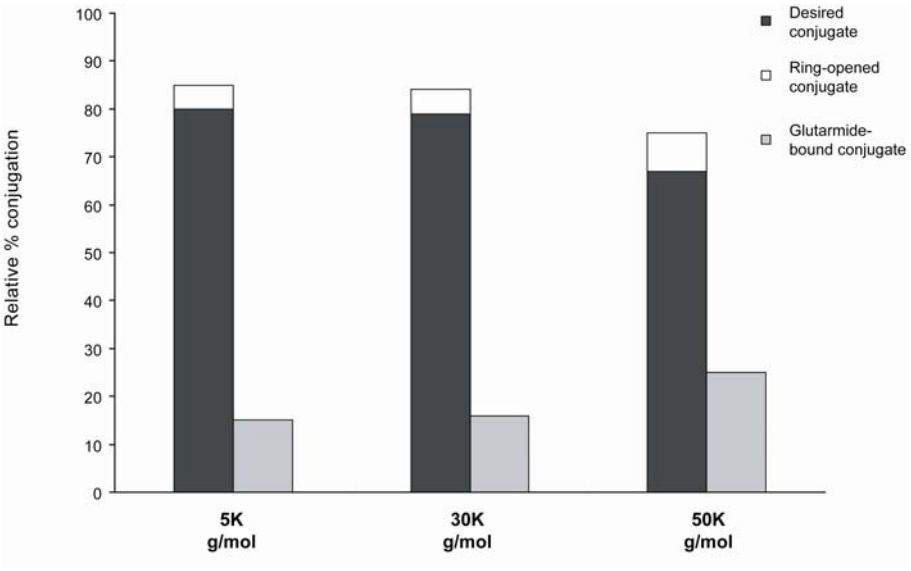

Figure 3-7. The effect of molecular weight on conjugation profile following protocol 1- 2 equivalents benzylamine, 50 °C, 5 hrs, 25mg poly(MAOS)/150µL. Pendant distribution remained similar for all three molecular weights evaluated.

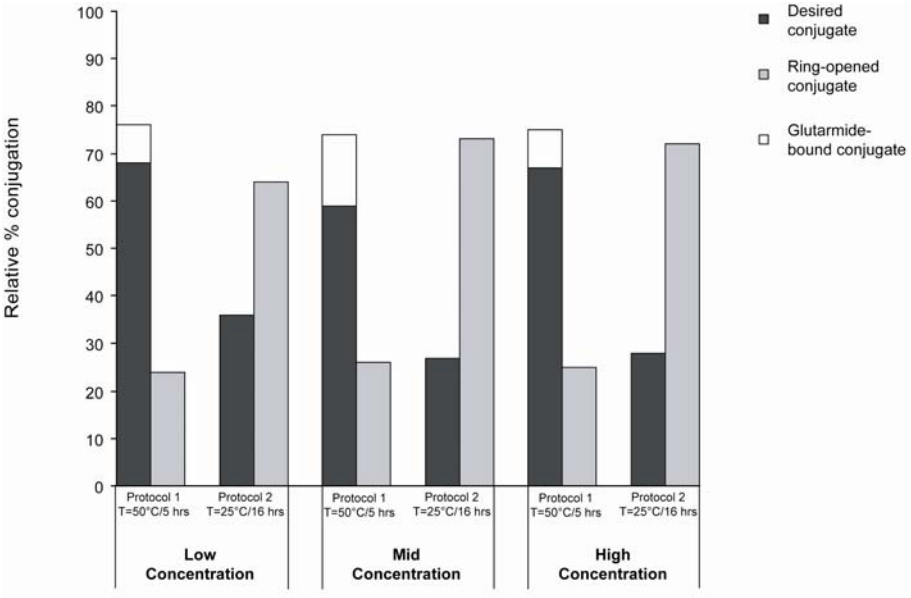

Figure 3-8. The effect of poly(MAOS) concentration on conjugation profile following two reported protocols. Each protocol results in similar pendant distributions regardless of precursor concentration. Low conc. = 25mg poly(MAOS)/1mL DMSO; Mid Conc. = 25 mg poly(MAOS)/600µL DMSO; High Conc. = 25 mg poly(MAOS)/150µL DMSO. 30K g/mol poly(MAOS) was used for all reactions. Reactions performed at low and mid concentrations included an additional 4 hours *in vacuo* concentration of the reaction mixture prior to precipitation.

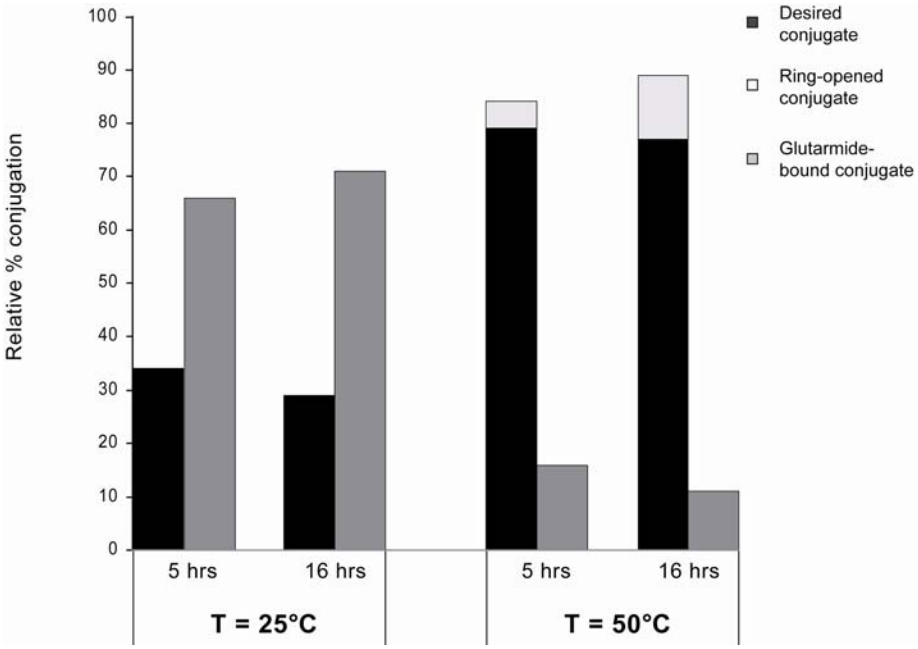

Figure 3-9. The effect of reaction time and temperature on conjugation profile. Increasing temperature leads to a greater proportion of the desired and glutarimide-bound conjugates and less of the ring-opened conjugate. 2 equivalents benzylamine, 25mg poly(MAOS)/150μL DMSO, 30K g/mol poly(MAOS) was used for all reactions.

Guided by the apparent time and temperature dependency of poly(MAOS) conjugation, we modified the previously reported protocols by increasing time, temperature, and equivalents of NH_2-FG while decreasing the precursor concentration. This revised protocol minimizes both labile ring-opened side products (as indicated by the disappearance of the 2.4, 4.3, and 8.4 ppm peaks) with a minimal amount of the glutarimide-bound conjugate (~7%) remaining (Figures 3-10 and 3-11). Because the glutarimide linkage is stable, its minimal presence is acceptable for polymer library synthesis. The revised protocol was further verified to be independent of MWs ranging from 5K – 50K g/mol and reaction concentrations ranging from 25mg poly(MAOS)/600μL DMSO to 25mg poly(MAOS)/mL DMSO (data not shown).

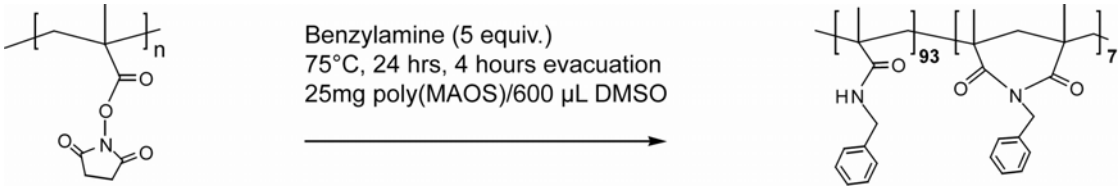

Figure 3-10. Preparation of functionalized poly(MAOS) free of ring-opened side product.

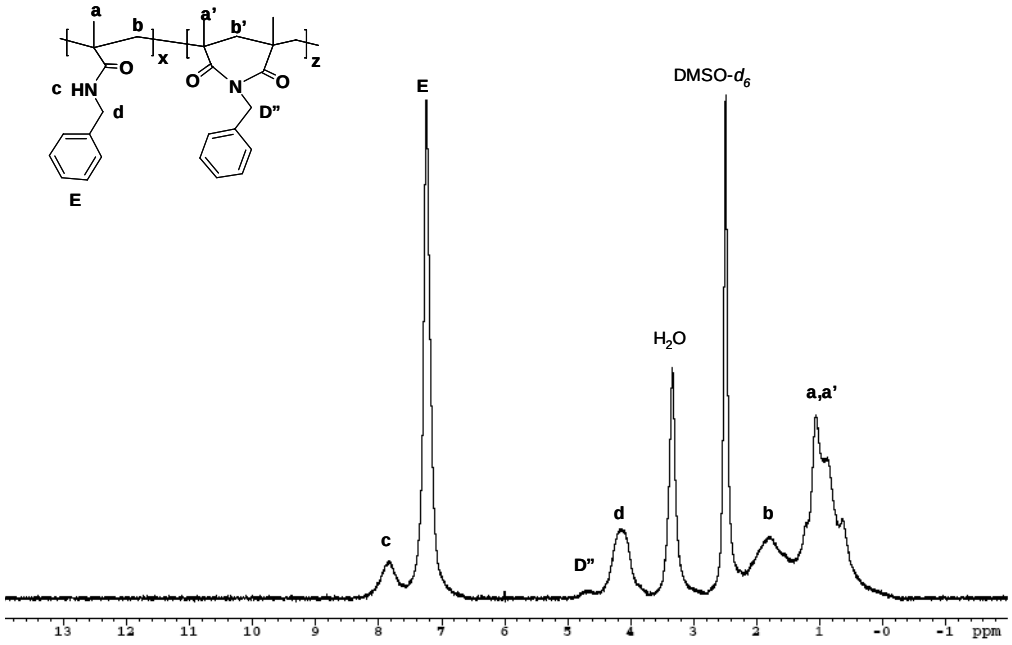

Figure 3-11. Representative ^{1}H NMR spectra of resultant functionalized polymer produced from the revised protocol - 5 equivalents benzylamine, 75 °C, 24 hrs, 4 hrs evacuation, 25mg poly(MAOS)/600µL DMSO - showing the absence of the ring-opened side product. Peaks labeled in capital letters were used for quantification via signal integration of respective pendant groups.

To address our initial goal of utilizing poly(MAOS) to synthesize molecularly diverse libraries, we extended the conjugation protocol to both single and binary

conjugations of other alkyl (e.g., butylamine, hexylamine) and water-solubilizing functional groups (e.g., histamine, 1-amino-2-propanol) (Table 3-1).

Table 3-1. Diverse functional groups conjugated to poly(MAOS).

Alkyl Functional Groups		
Name		**Structure**
butylamine		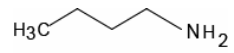
hexylamine		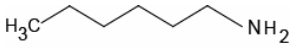
Water Solubilizing Functional Groups		
Name	**Abbreviation**	**Structure**
1-amino-2-propanol	1A2P	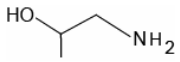
ethylenediamine [a]	1N	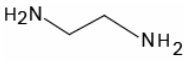
N-methylethylenediamine [a]	2N	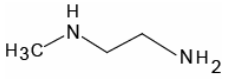
N,*N*-dimethylethylenediamine	3N	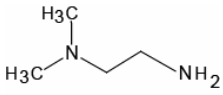
2-(aminoethyl)-trimethylammonium chloride - HCl	4N	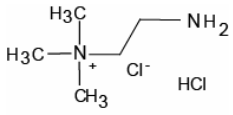
histamine		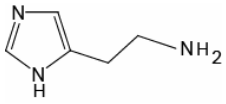

[a] derived from its *N*-Boc-protected precursor

No apparent side reaction conjugations resulted from butylamine and hexylamine functionalization presumably due to less steric hindrance relative to benzylamine functionalization. In the case of the water-solubilizing moieties, solvent

solubility appears to be the predominant factor affecting conjugation dynamics. 3N and histamine, both soluble in DMSO in their free base state, render poly(MAOS) notably less soluble in DMSO upon functionalization, which we believe results in an increased presence of glutarimide-bound conjugation relative to the alkyl functional group conjugations. We hypothesize that as conjugation proceeds, the decreasing solubility causes the semi-functionalized polymer precursor to assume a more tightly coiled and closed conformation. Consequently, accessibility of the primary amine to the activated esters becomes limited leaving any remaining esters to form *N*-substituted glutarimides with neighboring amides (Figure 3-12). [11]

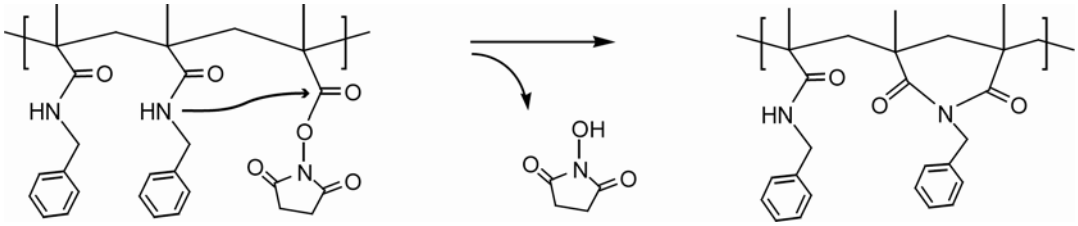

Figure 3-12. Proposed route for N-substituted glutarimide formation presumably between amide-bound conjugates and neighboring active esters.

To further support this hypothesis, we look to the 1A2P, 1N, and 2N conjugations. 1A2P, also miscible in DMSO in its primary amine reactant state, renders poly(MAOS) readily soluble in both water and DMSO upon conjugation. The proposed effect of the polymer coiling up upon conjugation would be expected not to occur to any appreciable degree which is supported by the absence of the glutarimide-indicating ^{1}H NMR peak. In the case of the 1N and 2N pendant groups, it is important to clarify that their pendant distributions shown in Figure 3-13 were quantified from polymers that were synthesized by functionalizing poly(MAOS) with their respective Boc-protected precursor and subsequently deprotected. Because 1N and 2N would

render poly(MAOS) relatively insoluble in DMSO, one might expect their conjugation profiles to liken that of 3N conjugation. However, their conjugation dynamics were dictated by their Boc-protected precursor which results in a readily DMSO-soluble functionalized polymer. Thus it is not surprising that their conjugation profiles are similar to those of other DMSO-soluble polymers, namely the alkyl functionalized polymers. Furthermore, direct conjugation of 2N (i.e., no Boc-protected precursor was used) resulted in a polymer whose NMR spectra yielded the expected desired and glutarimide-bound conjugates, presumably influenced by the hypothesized coiling up effect, in addition to other side reaction products, presumably between the 2° amine and activated esters.

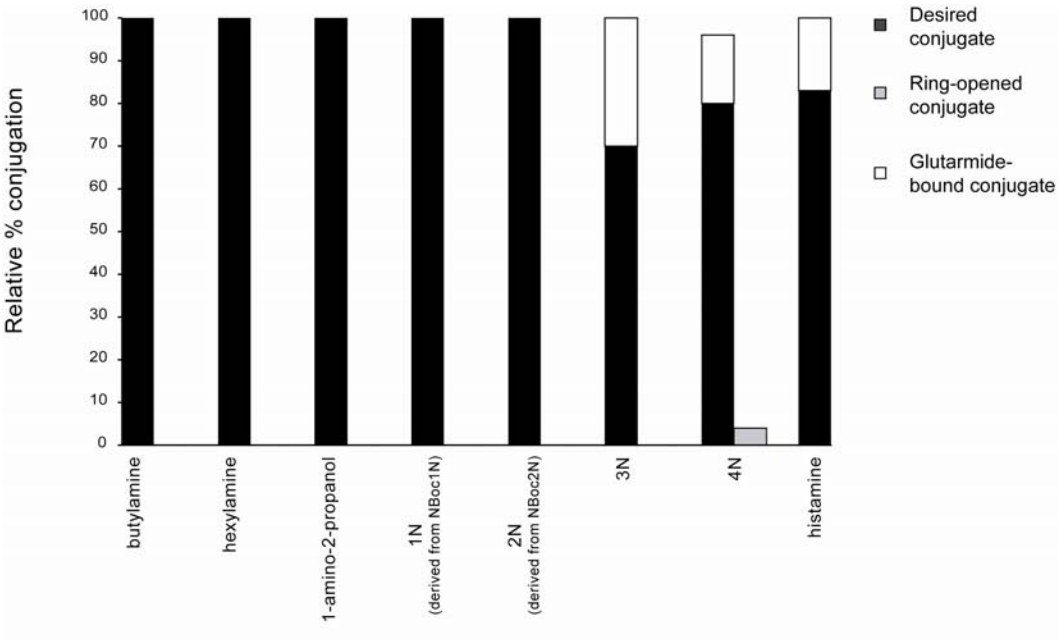

Figure 3-13. Conjugation profile of various NH_2-FGs to poly(MAOS). The revised protocol -5 equivalents NH_2-FG, 75 °C, 24 hrs, 4 hrs evacuation, 25mg poly(MAOS)/600μL DMSO- results in the absence of any labile ring-opened conjugates for a diverse set of functional groups with only a minimal amount (~4%) remaining for the 4N conjugation. 50K g/mol poly(MAOS) was used for all reactions.

In addition to the solubility effects of the functionalized polymer, the solubility of the nucleophilic reactant also appears to influence conjugation behavior. 4N, insoluble in DMSO in both its salt reactant state and upon conjugating to poly(MAOS) resulted in a small, but persistent amount of the ring-opened pendant group remaining on the functionalized polymer. Efforts to eliminate all ring-opened conjugates by varying temperature and time conditions were ineffective and resulted in a similar pendant distribution at all conditions (Figure 3-14). Nevertheless, the conjugation behavior of 4N provides evidence that the solubility of both the nucleophilic reactant and the functionalized polymer plays a role in conjugation behavior.

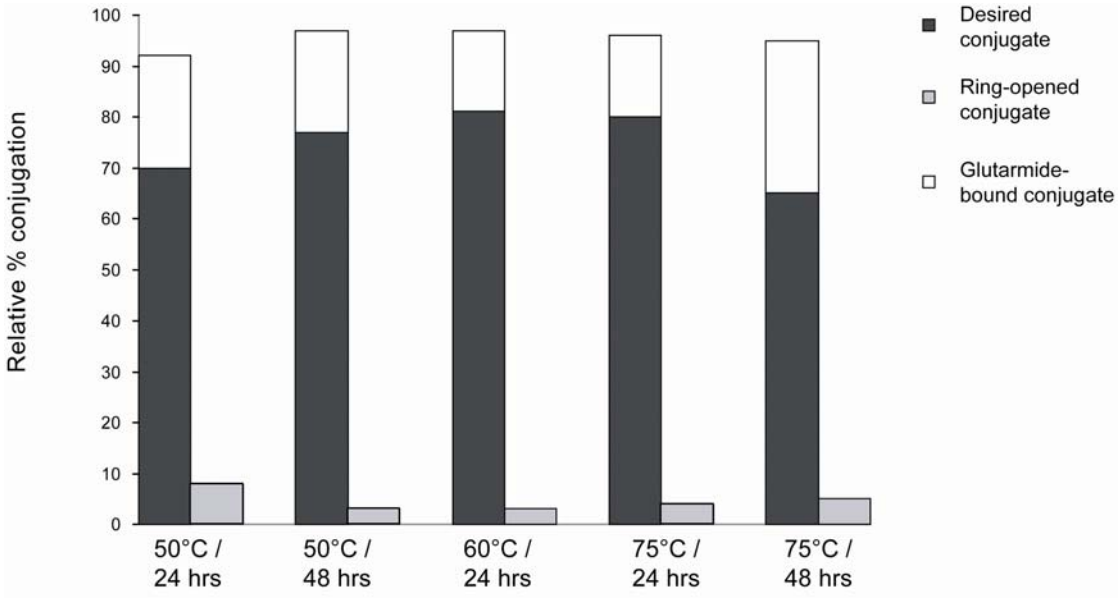

Figure 3-14. Conjugation profile of 2-(aminoethyl)-trimethylammonium chloride – HCl (4N) to poly(MAOS) under various time and temperature reaction conditions. A similar pendant distribution persists upon conjugating 4N to poly(MAOS). (5 equivalents 4N, 4 hrs evacuation, 25mg poly(MAOS)/600μL DMSO) 50K g/mol poly(MAOS) was used for all reactions.

Due to proton exchange between hydroxyl protons and deuterium in D_2O, ^1H NMR analysis was also performed for all water-soluble samples in DMSO-d_6. [16] This additional analysis was performed to ensure that premature hydrolysis of the activated ester to its carboxylic acid did not occur either during the conjugation reaction or isolation process (Figure 3-15). The ^1H NMR spectra of the functionalized polymers in DMSO-d_6 were evaluated for the presence of a hydroxyl peak.

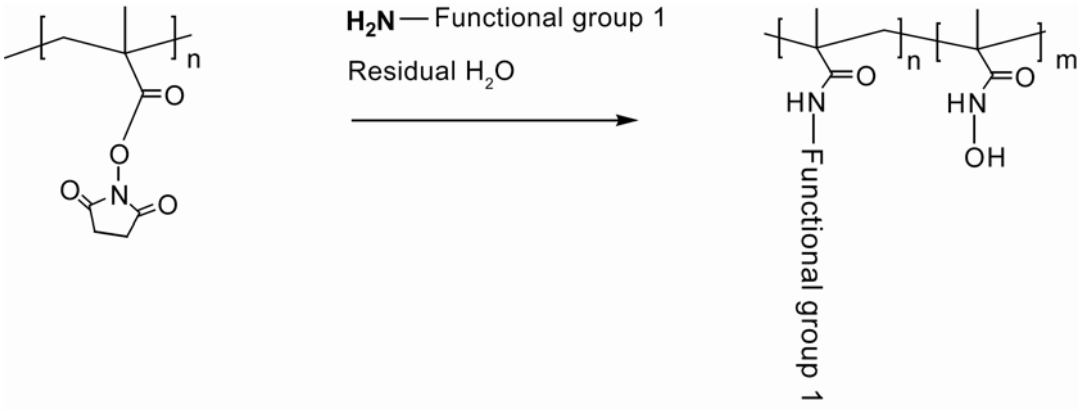

Figure 3-15. Potential hydrolysis of NHS-activated ester to methacrylic acid from residual water may occur during the conjugation or isolation process. Due to proton exchange between the hydroxyl proton of the carboxylic acid and deuterium in D_2O, NMR analysis was performed in DMSO-d_6 to ensure the absence of a hydroxyl peak.

Polymers functionalized with 4N and 1N (i.e., NBoc-1N deprotected to the 1N form) were insoluble in DMSO and prevented this additional evaluation. To illustrate the analysis, Figure 3-16a shows the ^1H NMR spectrum of a polymer functionalized with 1A2P that was used as-received from the manufacturer. Residual water in the 1A2P may have contributed to premature hydrolysis of the activated esters during conjugation resulting in the presence of a hydroxyl peak in the ^1H NMR spectrum (peak h in Figure 3-16a). Drying the 1A2P over 3Å molecular sieves resulted in a functionalized polymer with no apparent hydrolysis as shown in Figure 3-16b. This

analysis demonstrates the importance of using dried reagents with poly(MAOS) to ensure the desired products.

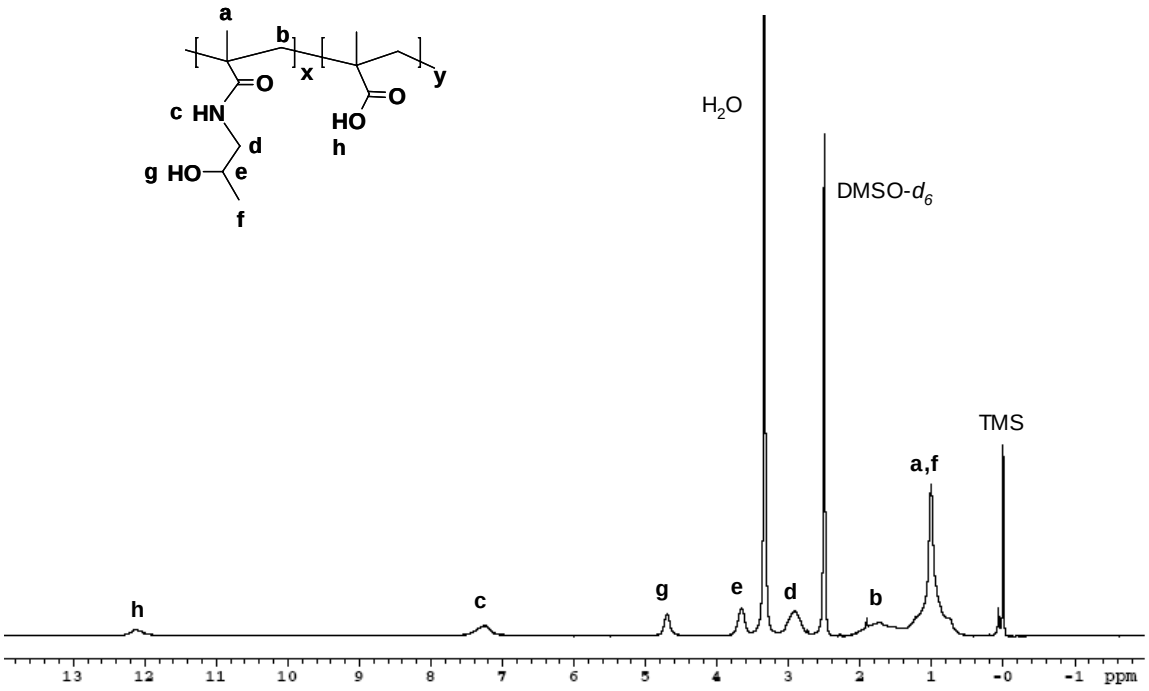

(a)

Figure 3-16. [1]H NMR spectra of poly(MAOS) functionalized with **a)** 1A2P as received and **b)** 1A2P dried over 3Å molecular sieves. Note the absence of the hydroxyl peak in (b) thus indicating that premature hydrolysis of the activated ester to its carboxylic acid did not occur. Both conjugations followed the revised protocol - 5 equivalents 1-amino-2-propanol, 75 °C, 24 hrs, 4 hrs evacuation, 25mg poly(MAOS)/600μL DMSO. 50K g/mol poly(MAOS) was used for all reactions.

Figure 3-16 (*continued*)

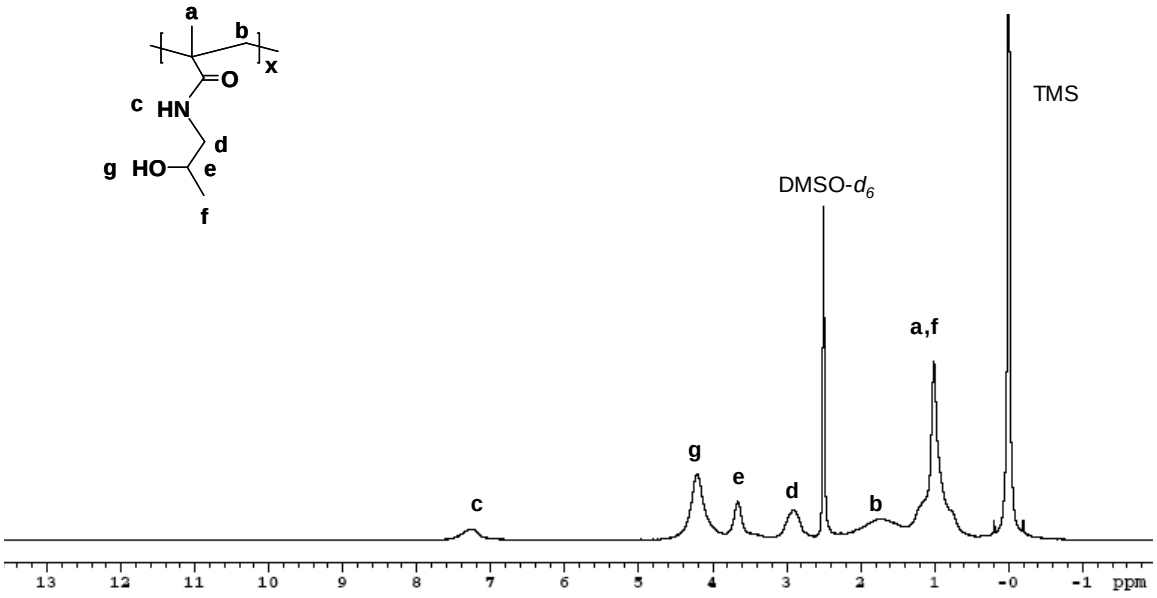

(b)

For functional groups with other nucleophilic atoms (e.g., 3° NH_2 on N,N-dimethylethylenediamine, imidazole on histamine), ^1H-^1H COSY was used to determine the presence of any additional side reactions. Figure 3-17 exemplifies how we used this technique to determine the side reaction products for the 3N-conjugated polymer. The peak at 4.0 ppm (peak d' in Figure 3-17) is shown to correlate with the 3.8 ppm peak (peak e in Figure 3-17) thus indicating the formation of side reaction z as opposed to side reaction z'.

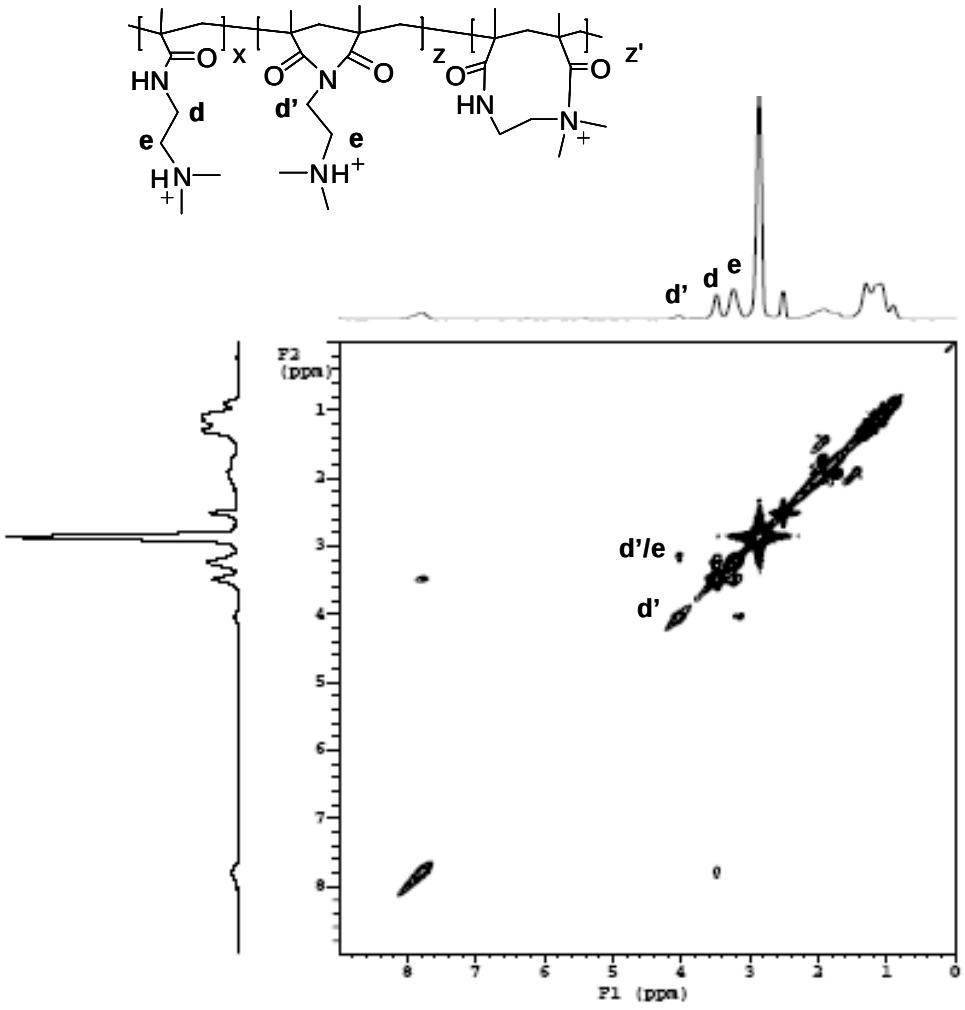

Figure 3-17. ^{1}H-^{1}H COSY of poly(MAOS) functionalized with N,N-dimethylethylenediamine (3N) following the revised protocol - 5 equivalents amine, 75 °C, 24 hrs, 4 hrs evacuation, 25mg poly(MAOS)/600µL DMSO. The correlation between the d' and e protons provide evidence that side product z is formed as opposed to z'.

Finally, we extended our protocol to binary conjugations using 1) benzylamine and 3N and 2) 1A2P and 3N as two independent model functional groups. Figure 3-18 shows the representative ^{1}H NMR spectra for both binary conjugations that were used to quantify the relative percent conjugations.

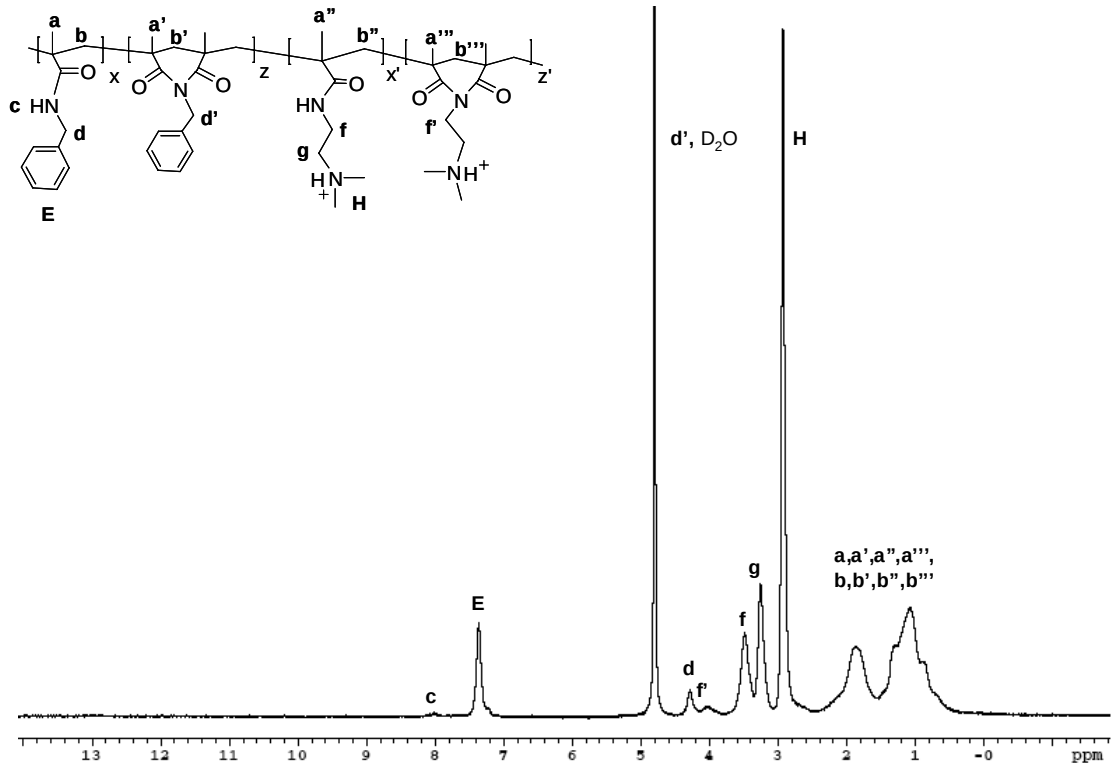

(a)

Figure 3-18. Representative ^{1}H NMR spectrum of poly(MAOS) functionalized with a binary mixture of a) 2.5 equivalents of N,N-dimethylethylenediamine (3N) and 2.5 equivalents of benzylamine and b) 2.5 equivalents of N,N-dimethylethylenediamine (3N) and 2.5 equivalents of 1-amino-2-propanol (1A2P). Both conjugations followed the revised protocol - 5 total equivalents of amine, 75 °C, 24 hrs, 4 hrs evacuation, 25mg poly(MAOS)/600μL DMSO. 50K g/mol poly(MAOS) was used for all reactions. Peaks labeled in capital letters were used for quantification via signal integration of respective pendant groups.

Figure 3-18 (*continued*)

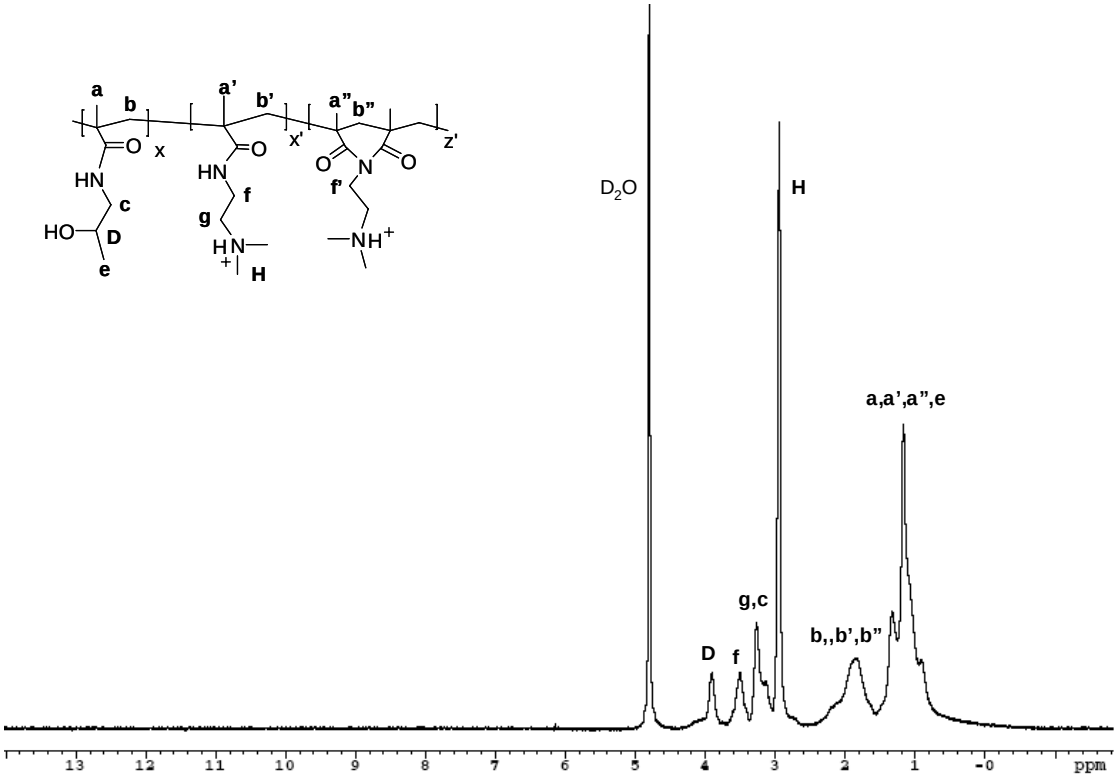

(b)

Figure 3-19 summarizes the conjugation profiles at various 3N equivalents for both binary conjugation experiments. The conjugation profile for the 3N/benzylamine system appears to follow a logarithmic trend compared to the linearly trending 3N/1A2P system. The difference in profiles is likely due to a dissimilarity in the degree of nucleophilicity between the conjugating pairs (i.e., 3N compared to benzylamine; 3N compared to 1A2P). [17] Further parametric studies, such as the effects of introducing each functional group at various times during the conjugation reaction, may be conducted to optimize the ligand distribution.

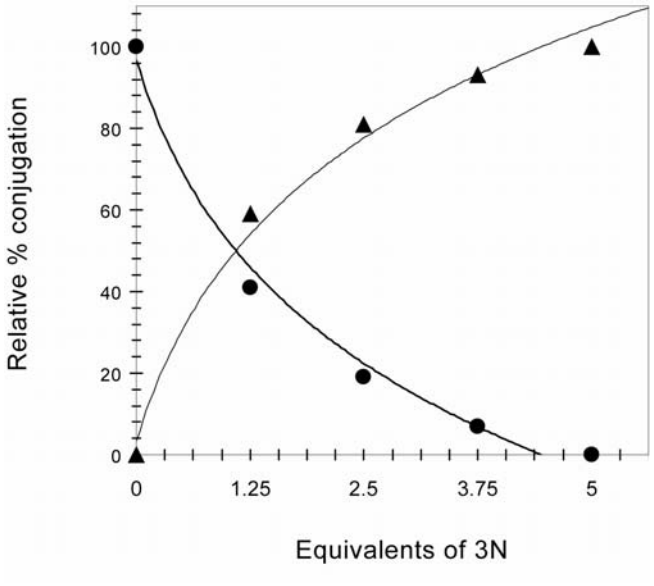

(a)

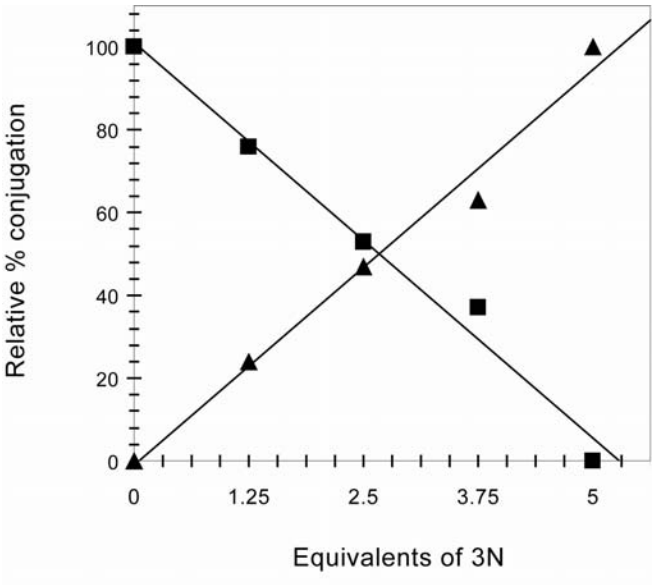

(b)

Figure 3-19. Conjugation profiles of a) N,N-dimethylethylenediamine (3N) (▲)/benzylamine (●) binary mixtures (logarithmic fit; $R^2 = 0.9893$) and b) 3N (▲) /1-amino-2-propanol (1A2P) (■) binary mixtures (linear fit; $R^2=0.9844$) at various feed equivalents of 3N. The conjugation profile of the 3N/1A2P mixtures resembles the theoretical conjugation and is likely due to a similar degree of nucleophilicity in contrast to the 3N/benzylamine conjugation profile.

In conclusion, we have established a protocol that overcomes the side reactions that are associated with the NHS-activated polymer precursor, poly(MAOS). The revised protocol entails conjugating poly(MAOS) in the presence of a five-mole excess of the primary amine-containing nucleophile for 24 hours at 75 °C at a reaction concentration of 25 mg poly(MAOS)/600μL DMSO. Using ^{1}H NMR and ^{1}H-^{1}H COSY analyses, we have quantified and characterized the resultant mono-functionalized polymer for a diverse range of functional groups. Moreover, we have also characterized the conjugation of two model binary systems: 1) N,N-dimethylethylenediamine (3N) and benzylamine and 2) N,N-dimethylethylenediamine (3N) and 1-amino-2-propanol (1A2P). Both systems were evaluated at various binary mixture compositions to demonstrate the compatibility of our protocol to conjugations comprising combinations of various functional groups.

An important and active area of research for which this work is applicable is the use of chemically and structurally diverse combinatorial libraries to develop polymeric biomaterials for drug and gene delivery systems. This area of research faces multiple challenges including: 1) a limited understanding of the biochemical and physical environment under which the materials must withstand thereby making rational design an extremely difficult task; and 2) resource constraints associated with synthesizing and evaluating a large number of diverse compounds efficiently.

Combinatorial strategies offer a systematic approach to designing libraries of polymer candidates that encompass a broad range of properties. Subsequent screening of each polymer enables the identification of both "hits" - specific polymers that possess desirable properties - and trends that demonstrate how an incrementally varied feature affects the measured output. [1] Hits are desired because they identify specific polymers that possess the desired biophysical and chemical properties (e.g., high drug/gene transfer efficiency, low cytotoxicity) as determined by screening assays.

Equally important are the trends that are observed between polymers that share an incrementally varied feature. These trends may provide information about the functional effects of a particular structural feature and potentially shed light on the underlying biochemical and physical environment and mechanisms that govern the system. Ultimately, the information gained from these libraries can point to ways to improve the design of drug and gene delivery systems.

The protocol that we have established offers a facile method to use poly(MAOS) precursor as the molecular backbone for each compound in a combinatorial library where chemical and structural properties can be easily imparted and modified by conjugating different functional groups at various ratios to the precursor. Coupled with high throughput methods, these libraries can be feasibly synthesized and evaluated efficiently and reliably, posing the potential for these promising research tools to significantly change the way new materials are discovered.

REFERENCES

[1] Brocchini, S., James, K., Tangpasuthadol, V., and Kohn, J. A combinatorial approach for polymer design. *J Am Chem Soc* **119**(19): 4553-4554 (1997).

[2] Brocchini, S., James, K., Tangpasuthadol, V., and Kohn, J. Structure-property correlations in a combinatorial library of degradable biomaterials. *J Biomed Mater Res* **42**(1): 66-75 (1998).

[3] Anderson, D.G., Levenberg, S., and Langer, R. Nanoliter-scale synthesis of arrayed biomaterials and application to human embryonic stem cells. *Nature Biotechnol* **22**(7): 863-866 (2004).

[4] Anderson, D.G., Peng, W.D., Akinc, A., Hossain, N., Kohn, A., Padera, R., Langer, R., and Sawicki, J.A. A polymer library approach to suicide gene therapy for cancer. *Proc Natl Acad Sci U S A* **101**(45): 16028-16033 (2004).

[5] Godwin, A., Hartenstein, M., Muller, A.H.E., and Brocchini, S. Narrow molecular weight distribution precursors for polymer-drug conjugates. *Angew Chem - Int Ed* **40**(3): 594-597 (2001).

[6] Lynn, D.M., Anderson, D.G., Putnam, D., and Langer, R. Accelerated discovery of synthetic transfection vectors: Parallel synthesis and screening of degradable polymer library. *J Am Chem Soc* **123**(33): 8155-8156 (2001).

[7] Monge, S. and Haddleton, D.M. Synthesis of precursors of poly(acryl amides) by copper mediated living radical polymerization in dmso. *Eur Polym J* **40**(1): 37-45 (2004).

[8] Pedone, E., Li, X.W., Koseva, N., Alpar, O., and Brocchini, S. An information rich biomedical polymer library. *J Mater Chem* **13**(11): 2825-2837 (2003).

[9] Rickerby, J., Prabhakar, R., Ali, M., Knowles, J., and Brocchini, S. Water-soluble polyacetals derived from diphenols. *J Mater Chem* **15**(18): 1849-1856 (2005).

[10] Hermanson, G., *Bioconjugate Techniques*. 1996, New York: Academic Press.

[11] Devenish, S.R.A., Hill, J.B., Blunt, J.W., Morris, J.C., and Munro, M.H.G. Dual side-reactions limit the utility of a key polymer therapeutic precursor. *Tetrahedron Lett* **47**(17): 2875-2878 (2006).

[12] Ferruti, P., Fere, A., and Bettelli, A. High polymers of acrylic and methacrylic esters of N-hydroxysuccinimide as polyacrylamide and polymethacrylamide precursors. *Polymer* **13**(10): 462-& (1972).

[13] Perrier, S., Armes, S.P., Wang, X.S., Malet, F., and Haddleton, D.M. Copper(i)-mediated radical polymerization of methacrylates in aqueous solution. *J Polym Sci, Part A: Polym Chem* **39**(10): 1696-1707 (2001).

[14] Morris, K.F. and Johnson, C.S. Diffusion-ordered 2-dimensional nuclear-magnetic-resonance spectroscopy. *J Am Chem Soc* **114**(8): 3139-3141 (1992).

[15] Viel, S., Capitani, D., Mannina, L., and Segre, A. Diffusion-ordered NMR spectroscopy: A versatile tool for the molecular weight determination of uncharged polysaccharides. *Biomacromolecules* **4**(6): 1843-1847 (2003).

[16] Macomber, R., *NMR spectroscopy: Basic princles and applications*. 1988, Florida: Harcourt Brace Jovanovich.

[17] Cline, G.W. and Hanna, S.B. The aminolysis of N-hydroxysuccinimide esters - a structure reactivity study. *J Am Chem Soc* **109**(10): 3087-3091 (1987).

CHAPTER 4

STRUCTURE-FUNCTION RELATIONSHIPS OF MOLECULAR WEIGHT, CATIONS, PH-SENSITIVE MOIETIES, AND HYDROPHOBIC RESIDUES DEDUCED FROM A COMBINATORIAL LIBRARY OF POLYMERIC GENE VECTORS

4.1. ABSTRACT

Three combinatorial libraries of polymeric vectors were evaluated in the present study to investigate the functional roles of molecular weight, cationic pendant groups, pH-sensitive moieties, and hydrophobic derivitization in polymer-mediated gene delivery. Four cationic and pH-sensitive moieties (primary amino, secondary amino, tertiary amino, and imidazole) and three hydrophobic residues (C4 butyl, C6 hexyl, and C8 octyl) were conjugated in single and serially-incremented binary combinations to a common polymer precursor of a single molecular weight and polydispersity index. Three molecular weights were evaluated herein – 10 kDa, 30 kDa, and 50kDa. Transfection levels comparable to branched-PEI (25 kDa) were achieved by several 30 kDa and 50 kDa formulations, most of which contained imidazole and primary amino groups. All but two of the ten highest transfecting polymers possessed IC_{50} values greater than the maximum concentration of free polymers exposed to cells (200 μg/mL). These high-transfecting polymers appeared to harness the superior charge neutralizing and size condensing capacity of primary amino groups while benefiting from the polyplex stabilizing role of imidazole groups. Contrary to the widely held belief that imidazole groups facilitate endo-lysosomal escape via their enhanced buffering capacity, imidazole groups appeared to enhance

transfection primarily through their ability to bind to DNA via non-electrostatically mediated interactions, which stabilized resultant polyplexes and ultimately resulted in more efficient delivery to cells. The results from this study have not only identified highly efficient polymeric formulations with superb toxicity profiles, but have also shed light on the functional roles that the investigated polymeric pendant groups play in the transfection process. Future studies will be critical to fully understand and clearly define the structure-function relationships that govern gene delivery. The reported polymeric system offers a simple and robust platform upon which such structure-function studies may be based in a move towards safer and more efficient polymeric vectors.

4.2. INTRODUCTION

Significant advances in molecular biology and genomic research have uncovered the genetic basis for a variety of diseases, and have given rise to the use of gene therapy as a possible mode of treatment. [1-4] Unfortunately, one of the primary obstacles preventing human gene therapy from becoming widely available is the lack of safe and efficient gene delivery systems.

A variety of vectors have been designed to overcome the known biological barriers that hinder safe and efficient delivery of exogenous genes. Most delivery systems developed to date fall under the general categories of viral, lipid-based, inorganic, and polymeric delivery systems. [5-8] However, safety concerns and inefficient delivery profiles have restricted the advancement of any one of these systems towards a broader clinical application. In particular, polymeric systems have fallen short in their delivery efficiency, despite the diverse strategies for improving polymer-mediated gene delivery that have been reported in the past two decades. [8]

Many of the polymeric systems currently in development are based on design concepts that have been reinforced by a number of reports. Such design concepts include the use of cationic moieties to complex with DNA; pH-sensitive functional groups to promote intracellular trafficking; derivitization with carbohydrates to enhance biocompatibility and facilitate both cellular and nuclear targeting; and hydrophobic functionalization to promote cellular uptake. [9-14] The wealth of information produced from these studies has reinforced the strategy of altering the chemical and structural characteristics of polymeric vectors to enhance and fine-tune their biophysical properties and transfection capacities. However, because many of these studies have been conducted under heterogeneous experimental conditions (e.g., the use of different polymeric backbones of different molecular weights and polydispersities, diverse synthetic techniques, various cell lines transfected, different transfection protocols, etc.), it is difficult to directly correlate how the chemical and structural attributes of polymeric vectors influence transfection efficiency based solely on analysis of the existing literature. In the absence of clearly defined structure-function relationships, the rational modification of polymer vector designs remains a challenge.

This study aims to determine the structure-function relationships that govern one class of polymer-mediated gene delivery by systematically altering molecular weight and side chain composition in a combinatorial fashion. To explore 1) the effects of different charge groups and 2) the hypothesized role of pH-sensitive moieties as buffering agents that facilitate intracellular trafficking and enhance transfection efficiency, we evaluated primary, secondary, tertiary amino, and imidazole groups. [9, 14-16] To understand whether the hydrophobic properties of linear hydrocarbon alkyl chains affect the transfection capacity of polymeric vectors, C4 butyl, C6 hexyl, and C8 octyl group were also investigated. The effect of each

functional group was systematically evaluated by forming single and binary combinations of all moieties at 75/25, 50/50, and 25/75 molar ratios to constitute a combinatorial library of polymeric vector candidates. Three such combinatorial libraries were synthesized, each representing a different molecular weight (10, 30, and 50 kDa) and comprising the same polymer formulations. Characterization of the polymeric vectors included *in vitro* transfection capacity, polyplex size, zeta potential, relative binding affinity, polyplex stability, buffering capacity, and cytotoxicity.

The results from this study have 1) revealed the structure-function relationships of different charge groups, pH-sensitive moieties, and hydrophobic residues; 2) identified several polymeric vectors with transfection capacities as high as branched PEI (25 kDa) with more favorable cytotoxicity profiles; and 3) established a robust system of polymers for future structure-function studies in a move towards safer and more efficient polymeric vector designs.

4.3. MATERIALS AND METHODS

4.3.1. Reagents

Cu(I)Br, Cu(II)Br_2, 2,2'-dipyridyl, *N,N,N´,N´´,N´´*-pentamethyldiethylenetriamine, ethyl 2-bromoisobutyrate, benzylamine, butylamine, hexylamine, octylamine, *N*-Boc-ethylenediamine, *N*-Boc-*N*-methylethylenediamine, *N,N*-dimethylethylenediamine, histamine, anhydrous DMSO, anhydrous DMF, anisole, heparin sodium salt (# H9399) were all purchased from Sigma-Aldrich (St. Louis, MO) and used without further purification. Dowex® Marathon® MSC hydrogen ion exchange resin was purchased from Sigma-Aldrich and dried *in vacuo* overnight before use. Cell culture reagents were purchased from Gibco® (Carlsbad, CA), pCMV-luc reporter gene

plasmid was purchased from Elim Biopharmaceuticals (Hayward, CA), and reporter gene assays were purchased from Promega (Madison, WI).

4.3.2. General procedure for the synthesis of polymer precursor, poly(methacryloxysuccimimide) (poly(MAOS))

The monomer, *N*-methacryloxysuccinimide was synthesized as previously reported. [17] The polymer precursor, poly(methacryloxysuccinimide), was synthesized with a slight modification to two previously reported methods. [18, 19] To obtain a precursor molecular weight of 10 kDa, the protocol reported by Shunmugam and Tew was adopted, whereas a modified version of the protocol by Godwin et al. was employed for synthesis of the precursor at 30 kDa and 50 kDa. Both protocols followed the same experimental set-up with the only difference being the reaction temperature, transition metal ligand, and solvent used. Reaction conditions are summarized in Table 4-1. Briefly, a 5 ml pear shaped flask with a flea magnetic stir bar was fitted with a rubber septum and flame dried while purging with N_2(g), then cooled to ambient temperature. Cu(I)Br, Cu(II)Br_2, and the ligand were added to the flask and resealed with the septum. Solvent that was purged with N_2(g) for ten minutes prior to use was injected into the flask and the contents were stirred under a nitrogen atmosphere for approximately ten minutes until dissolved. *N*-methacryloxysuccinimide was added to the flask and allowed to dissolve for another ten minutes. The initiator, ethyl-2-bromoisobutyrate, was directly injected through the septum into the flask with a Hamilton syringe and immersed into a thermostated oil bath. To stop the polymerization, the flask was quenched in an ice bath and the product was dissolved with anhydrous DMF at a 1:3.75 (w/w) ratio of monomer:DMF. Approximately 20 mg of Dowex® Marathon® MSC hydrogen ion exchange resin was

added to the redissolved solution and allowed to stir for approximately ten minutes. The ion exchange resin was added to remove any active copper catalysts remaining in the solution. [20] The final polymer was isolated as a white powder by precipitation into stirring acetone. The precipitated polymer was filtered through a fine-fritted Buchner funnel, washed three times with fresh acetone, and dried overnight *in vacuo*. ^{1}H NMR (DMSO-d_6) δ:1.44 (b,3H,CH_3), 2.41 (b,2H,CH_2), 2.78 (b,4H,CH_2CH_2).

Molecular weight and polydispersity index were determined by hydrolyzing poly(MAOS) to its sodium salt form. Upon dissolving poly(MAOS) in DMSO at a 1:8.8 (w/w) ratio of poly(MAOS):DMSO, a two-fold excess of 5M NaOH was added dropwise to the reaction and allowed to stir for 7 hours at room temperature. The cloudy solution was redissolved in filtered deionized water at a 1:80 (w/w) ratio of poly(MAOS):water and allowed to stir overnight at room temperature. The solution was then dialyzed against deionized water using Spectra/Por regenerated cellulose tubing (MWCO 3500 Da) for three days. The dialysate was subsequently lyophilized to give a white powder.

4.3.3. General procedure for amine conjugation

The seven pendant groups of interest, shown in Figure 4-1a, were conjugated to the poly(MAOS) precursor in single and binary combinations. Binary combinations of the pendant groups were evaluated at 25/75, 50/50, and 75/25 input molar ratios. The details of the mono- and bi-functionalized polymer syntheses have been previously reported by our group. [21]

4.3.4. Polymer characterization

4.3.4.1. *Molecular weight and chemical composition of polymer precursor*

The molecular weight and polydispersity index of each poly(MAOS) precursor were evaluated via gel permeation chromatography of the hydrolyzed sodium salt. The chemical composition of the polymer precursor was confirmed via ^{1}H NMR spectroscopy. The details of the characterization protocol for both methods are provided in our previous report. [21] Table 4-1 summarizes the molecular weight and polydispersity index values determined for each of the three precursors used in the present study.

4.3.4.2. *Chemical composition of bi-functionalized polymer*

To characterize the conjugation ratio of polymers that were bi-functionalized with two of the pendant groups in Figure 4-1a, a secondary set of polymer conjugates were first synthesized, according to our previously reported protocol, comprising each pendant group in Figure 4-1a co-functionalized with benzylamine at 25/75, 50/50, and 75/25 molar input ratios. [21] Owing to benzylamine's characteristic UV/Vis absorbance wavelength of 260 nm and ^{1}H NMR chemical shift of ~7.2 ppm, the benzylamine content of the secondary set of polymer conjugates could be quantified using both analytical methods. Indirectly, the conjugation efficiency of the co-functionalized pendant group could then be determined.

To quantify the benzylamine content via UV/Vis spectrophotometry, 5 mg of the polymer, co-functionalized with benzylamine and the amine of interest (1N, 2N, 3N, histamine (i.e., imidazole group), hexylamine), was dissolved in 6 mL of either methanol or tetrahydrofuran and vortexed until visibly dissolved. All polymers containing 1N, 2N, 3N, and histamine were soluble in methanol. Polymers co-

functionalized with hexylamine were soluble in tetrahydrofuran. Benzylamine content was quantified by aliquoting 1 mL of dissolved solution into a quartz cuvette and obtaining absorbance values at 260 nm on a Molecular Devices SpectraMax Plus[384] UV/Vis spectrophotometer. Absorbance values were corrected for background absorbance by subtracting the absorbance of the solvent measured on the same day as the samples. Poly(methacrylic acid) (MW~100 kDa purchased from Polysciences, Inc.) and poly(methyl methacrylate) (MW~120 kDa from Sigma Aldrich) were used as the negative controls for samples soluble in methanol and tetrahydrofuran, respectively.

To determine the conjugation ratio of benzylamine from the measured absorbance values of the benzylamine co-functionalized polymers, the benzylamine concentration that corresponded to different theoretical conjugation ratios of benzylamine was calculated according to the following equations:

$$MW_{bipoly,x} = \frac{x(MW_{benz}) + y(MW_y) + (x+y)(MW_{backbone})}{x} \qquad (4.1)$$

where $MW_{bipoly,x}$ is the molecular weight of a repeat unit containing x conjugation ratio of benzylamine in units of g/mol of benzylamine; x is the theoretical benzylamine conjugation ratio; MW_{benz} is the calculated molecular weight of conjugated benzylamine (106 g/mol); $y = 1\text{-}x$ is the theoretical conjugation ratio of the co-functionalized pendant group; MW_y is the calculated molecular weight of the conjugated co-functionalized pendant group; and $MW_{backbone}$ is the calculated molecular weight of a repeat unit of the polymeric backbone (69 g/mol).

$$C_{benz} = \frac{m}{v * MW_{bipoly,x}} \qquad (4.2)$$

where C_{benz} is the benzylamine concentration in units of mol/L that corresponds to the theoretical benzylamine conjugation ratio, x, of a UV/Vis polymer sample of weight, m (0.005 g), dissolved in volume, v (0.006 L), of solvent.

Absorbance values at 260 nm, A_{260}, corresponding to C_{benz} values were determined from a calibration curve generated from free base benzylamine dissolved in the same solvent as the bi-functionalized polymeric samples. A linear trendline fitted to the plot of x vs. A_{260} for each bi-functionalized pair was then used to convert the measured UV/Vis absorbance of bi-functionalized polymers to the conjugation ratio of benzylamine, X_{benz}.

The conjugation ratio of the pendant group, m, that was co-functionalized with benzylamine, $X_{exp,r,m}$, was then calculated by:

$$X_{\exp,r,m} = 1 - X_{benz} \qquad (4.3)$$

where X_{benz} is the conjugation ratio of benzylamine determined by either UV/Vis spectrophotometry, as described above, or ^{1}H NMR spectroscopy, as described in our previously reported protocol. [21] A conjugation efficiency value relative to benzylamine, $CE_{B,r,m}$, was then calculated according to the following equation:

$$CE_{B,r,m} = \frac{X_{\exp,r,m}}{r_m} \qquad (4.4)$$

where r is the input molar ratio (0.25, 0.50, 0.75) of pendant group m.

To calculate the coefficient efficiency of each pendant group relative to each other, the following equation was used:

$$CE_{m_1,m_2} = \frac{r_{m_1}}{r_{m_2}} * \frac{CE_{B,r,m_1}}{CE_{B,r,m_2}} \qquad (4.5)$$

The final conjugation ratio of polymers that were bi-functionalized with two pendant groups in Figure 4-1a at the molar input ratios of 25/75, 50/50, and 75/25 was calculated according to the following equation:

$$X_{calc,m_1} = \frac{CE_{m_1,m_2}}{(CE_{m_1,m_2} + CE_{m_2,m_1})} \qquad (4.6)$$

where $X_{calc,m1}$ is the calculated conjugation ratio of pendant group m_1 when co-functionalized with pendant group m_2. An example of the conjugation calculations determined by the UV/Vis spectrophotometry method is provided in the appendix at the end of the chapter.

4.3.5. Cell culture

The murine embryonic fibroblast NIH/3T3 cell line was purchased from the American Type Culture Collection (Manassas, VA). Cells were cultured in Dulbecco's Modified Eagle Medium (DMEM) supplemented with 10% v/v fetal calf serum, 100 units/mL penicillin, and 100 μg/mL streptomycin. Cells were grown at 37°C and 5% CO_2 to an approximately 70% confluent monolayer and passaged every 3-4 days.

4.3.6. Preparation of polymer-DNA complex (polyplex) transfection solutions and free polymer cytotoxicity solutions

For each unique polymer, five polymer:DNA (w:w) ratios were evaluated – 0.5:1, 1:1, 2.5:1, 5:1, and 10:1. First, 140 μL of polymer solution for each ratio was prepared by combining the appropriate volume of 1.5 mg/mL polymer stock solution with 10 mM HEPES buffer (pH 7.2) such that each 150 μL of polyplex transfection solution contained the intended amount of polymer required to condense 3 μg of plasmid. Polymer solutions were briefly vortexed before adding 140 μL of pCMV-luc stock solution (150 μg/mL pCMV-luc in 10mM HEPES buffer, pH 7.2) to each of the 140 μL of polymer solution. The polymer/DNA mixture was then vortexed for five seconds and incubated at room temperature for 15 minutes to allow for complex

formation. Serum-free OPTI-MEM I® medium (770 μL) was added to each polyplex solution and briefly vortexed to form the final polyplex transfection solution.

For the free polymer cytotoxicity solutions, 140 μL polymer solutions for each polymer:DNA ratio were prepared as previously described. Then, 140 μL of 10 mM HEPES buffer (pH 7.2) and 770 μL of OPTI-MEM I® medium were added to each solution and briefly vortexed to form the final free polymer cytotoxicity solution.

4.3.7. Plasmid DNA (pCMV-luc) transfection

NIH/3T3 cells were grown in clear and opaque, flat-bottomed tissue culture polystyrene 96-well plates (Costar, Corning, NY) at an initial density of 5,000 cells/well in 200 μL of phenol red-free, supplemented DMEM. Following 24 hours of incubation at 37°C and 5% CO_2, the growth medium was removed and replaced with 150 μL of polyplex transfection solution, which was prepared as described previously. Each 150 μL aliquot of transfection solution contained 3 μg of plasmid DNA. Cells were incubated with the polyplexes for 4 hours, after which the complex-containing medium was aspirated and replaced with 100 μL of phenol red-free, supplemented DMEM. Following 44 hours of additional incubation at 37°C and 5% CO_2, opaque plates were assayed for luciferase expression using the Bright-Glo™ Luciferase Assay (Promega, Madison, WI) and clear plates were assayed for total protein content using the BCA™ Protein Quantitation Assay (Pierce Biotechnology, Rockford, IL). All polymers were evaluated in triplicate. Transfection results are expressed as the ratio of relative light units to absorbance at 562 nm.

4.3.8. Bright-Glo™ luciferase assay

After a total incubation time of 48 hours from the time of polyplex solution addition, growth medium was aspirated and each well was rinsed with 200 μL of phosphate buffered saline (pH 7.4). In a Veritas™ Microplate Luminometer (Turner Biosystems, Sunnyvale, CA) 100 μL of Bright-Glo™ working solution, prepared according to the manufacturer's direction, was added to each well of the opaque 96-well plate. After two minutes of incubation at room temperature, luciferase expression was quantified as the relative light units measured in the luminometer.

4.3.9. BCA™ protein quantitation assay

After a total incubation time of 48 hours from the time of polyplex solution addition, growth medium was aspirated and each well was rinsed with 200 μL of phosphate buffered saline (pH 7.4). RIPA buffer (20 μL) (Pierce Biotechnology, Rockford, IL) was added to each well of the clear 96-well plate and incubated at room temperature for 10 minutes with gentle shaking. BCA™ working reagent (200 μL) (Pierce Biotechnology, Rockford, IL), prepared according to the manufacturer's directions, was then added to each well and gently shaken for 30 seconds at room temperature. Plates were incubated at 37°C and 5% CO_2 for one hour before being read at 562 nm on a Molecular Devices SpectraMax Plus^{384} UV/Vis spectrophotometer.

4.3.10. Relative binding affinity and polyplex stability assay

The relative degree of electrostatic binding between DNA and polymer in the absence and presence of a competing polyanion was measured using ethidium bromide (EtBr) (Fisher Scientific, Pittsburgh, PA) fluorescence quenching and recovery. [22-

24] Heparin sodium salt (4.38 mM) dissolved in 10mM HEPES buffer (pH 7.2) was used as the competing polyanion. [23] A free polymer solution (180 μL) for each polymer:DNA ratio was prepared by combining the appropriate volume of 1.5 mg/mL polymer stock solution with 10mM HEPES buffer (pH 7.2) such that each 50 μL aliquot resulted in the intended w:w ratio of polymer and pCMV-luc. A stock solution of EtBr/DNA was made by combining equal volumes of pCMV-luc (150 μg/mL pCMV-luc in 10mM HEPES buffer, pH 7.2) and EtBr (0.1095mM EtBr in 10mM HEPES buffer, pH 7.2) stock solutions, resulting in a 4:1 ratio of phosphate groups to EtBr monomer units. All fluorescence readings were obtained in a Molecular Devices SpectraMax GeminiXS at λ_{ex} = 535 nm and λ_{em} = 595nm (automatic calibration, 10 seconds of mixing prior to reading, and automatic sensitivity of PMT detector). All polymers were evaluated in triplicate.

First, 100 μL of EtBr/DNA solution was added to each well of a black polystyrene 96-well plate (Costar, Corning, NY) and the fluorescence was measured. An aliquot of 50 μL of free polymer solution was then added to each EtBr/DNA-containing well, gently shaken at room temperature on a microplate shaker for 15 minutes, and the fluorescence measured again. A 50 μL aliquot of 4.38 mM heparin was added to each well, gently shaken at room temperature on a microplate shaker for 4 hours, and the fluorescence measured for a final time. The relative binding affinity (*BA*) and relative binding strength (*BS*) were calculated from the following equations:

$$BA = \frac{F_{E/D} - F_{polymer}}{F_{E/D}} \qquad (4.7)$$

$$BS = \frac{F_{E/D} - F_{hep}}{F_{E/D} - F_{polymer}} \qquad (4.8)$$

where $F_{E/D}$ is the corrected fluorescence of EtBr/DNA in the absence of polymeric vector; $F_{polymer}$ is the corrected fluorescence of EtBr/DNA in the presence of polymeric vector; F_{hep} is the corrected fluorescence of EtBr/DNA in the presence of polymeric vector and heparin.

All fluorescence measurements were corrected by subtracting background fluorescence due to free EtBr and due to volume effects. Background values from free EtBr were obtained from triplicate wells, on each 96 well plate, containing EtBr and 10mM HEPES buffer for the first two fluorescence readings and EtBr, HEPES buffer, and heparin for the final fluorescence measurement. Background values due to volume effects were determined from triplicate wells, on each 96 well plate, containing EtBr/DNA and HEPES buffer in volumes equal to those added to the polymer samples.

4.3.11. Polyplex size and zeta potential measurement

A 140 μL solution of free polymer was prepared for each polymer:DNA ratio by combining the appropriate volume of 1.5 mg/mL polymer stock solution with 10 mM HEPES buffer (pH 7.2) such that the final 1.05 mL polyplex solution contained the intended w:w ratio of polymer and pCMV-luc. Polymer solutions were briefly vortexed before adding 140 μL of pCMV-luc stock solution (150 μg/mL pCMV-luc in 10mM HEPES buffer, pH 7.2) to each of the 140 μL of free polymer solution. The polymer:DNA mixture was vortexed for five seconds and incubated at room temperature for 15 minutes to allow for complex formation. Then, 770 μL of 10mM HEPES buffer (pH 7.2) was added to each polymer:DNA solution and briefly vortexed to form the final polyplex solution used in both sizing and zeta potential measurements.

Size and zeta potential characterizations were performed using the Nanosizer Nano ZS (Malvern Instruments). The refractive index and viscosity values of water were used as parameter inputs. Malvern Dispersion Technology Software was used for data acquisition and analysis, applying the general purpose algorithm for calculating size distributions and the Smoluchowski approximation for determining zeta potential.

4.3.12. Buffering capacity assay

Titration curves were generated for each polymer to assess their respective buffering capacities. First, 4 mg of polymer was dissolved in 10mL of 18.2MΩ distilled water. Using a TitraLab 856 automatic titrator (Radiometer Analytical, Lyon, France), the pH of the polymer-containing solution was adjusted to 11.5 with 1 M NaOH (25 seconds pH stabilization time before and after the addition of NaOH at a rate of 0.06 mL/min) and subsequently titrated with 1M HCl until the solution was stabilized at pH 2 (25 seconds pH stabilization time before and after the addition of HCl at a rate of 0.06 mL/min). Hydrogen ion concentrations were monitored with TitraMaster 85 software v.1.2.1. Using the OriginPro 8 software, titration curves were fitted to a Boltzmann sigmoidal curve, from which the slope at the inflection point was determined. The buffering capacity of each polymer is expressed as the absolute value of the reciprocal slope.

4.3.13. MTS cell viability assay

NIH/3T3 cells were grown and incubated with the free polymer solution, which was prepared as described previously, according to the protocol described for pCMV-luc transfection. The final free polymer concentrations evaluated were 10, 20,

50, 100, and 200 μg/mL, which corresponded to the polymer:DNA weight ratios of 0.5:1, 1:1, 2.5:1, 5:1, and 10:1, respectively. For cell viability measurements of branched PEI, the additional free polymer concentrations of 1-9 μg/mL in increments of 1 μg/mL were evaluated. After 48 hours of total incubation and rinsing with 200 μL of phosphate buffered saline (pH 7.4), 20 μL of CellTitre 96® AQ_{ueous} One Solution Cell Proliferation Assay (MTS) reagent (Promega, Madison, WI) was added to each well. Plates were incubated for an additional two hours at 37°C, after which the absorbance at 490 nm of each well was read in a Molecular Devices SpectraMax Plus^{384} UV/Vis spectrophotometer. All polymers were evaluated in triplicate. Using the OriginPro 8 software, data points were fitted to a Boltzmann sigmoidal curve. Cytotoxicity results are expressed as IC_{50} values and calculated as the concentration of free polymer, in micrograms per milliliter, at which the measured absorbance was one-half the absorbance measured at a polymer concentration of 0 μg/mL.

4.3.14. Statistical testing

Statistical testing between samples was performed via a two-sample t-test assuming unknown variances with an alpha level of 0.05.

4.4. RESULTS

4.4.1. Polymer synthesis and characterization

To isolate the effects of the various pendant groups on transfection and polyplex properties, pendant groups were conjugated to a polymer precursor, poly(MAOS), of a single molecular weight (MW) and polydispersity index (PDI), to form the functionalized polymeric vector. Three polymer libraries were synthesized,

each representing a different MW but comprising the same polymeric vector formulations. The MW and PDI of the three libraries are summarized in Table 4-1.

Table 4-1. Conditions and results for the synthesis of homopolymer precursor, poly(methacryloxysuccinimide)

Library	monomer : initiator : CuBr : ligand : $Cu(II)Br_2$ (molar ratio)	Reaction solvent (wt solvent:wt monomer)	Temperature (°C)	Reaction time (min)	M_p (kDa)	Polydispersity index
Low MW	50 : 1 : 1 : 2[a] : 0	anisole (200%)	90	20	10	1.22
Mid MW	50 : 1 : 1 : 2[b] : 1	anhydrous DMSO (150%)	100	10	29	1.26
High MW	200 : 1 : 1 : 2[b] : 1	anhydrous DMSO (125%)	100	15	49	1.25

[a] ligand = *N,N,N′,N″,N‴*-pentamethyldiethylenetriamine
[b] ligand = 2,2'-dipyridyl

The pendant groups investigated in this study are shown in Figure 4-1a and the general reaction scheme for the synthesis of the mono- and bi-functionalized polymers is shown in Figure 4-1b. Pendant groups were conjugated in single and binary combinations to poly(MAOS) to form the functionalized polymeric vector. Within the binary combinations, the following input molar ratios were evaluated – 25/75, 50/50, and 75/25. Seventy unique formulations may be generated from the single and serially-incremented binary combinations. However, solubility issues associated with polymers co-functionalized with the hydrophobic alkyl groups limited the total number of water-soluble polymers to 38 unique formulations within the combinatorial library. Detailed characterization of the mono-functionalized polymer conjugates are reported elsewhere. [21] The conjugation profiles of bi-functionalized polymers are shown in Figure 4-2 and illustrate the nearly quantitative conjugation efficiencies at the three molar input ratios for all bi-conjugated pairs.

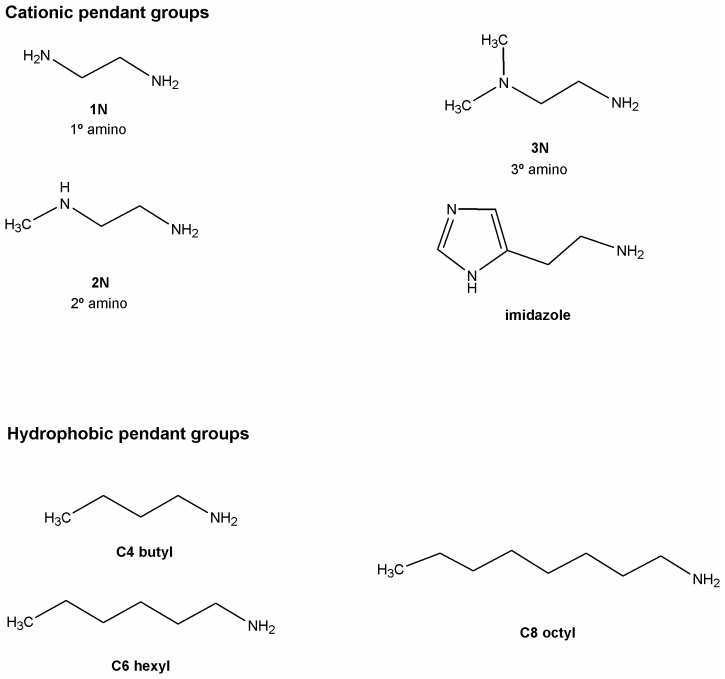

(a)

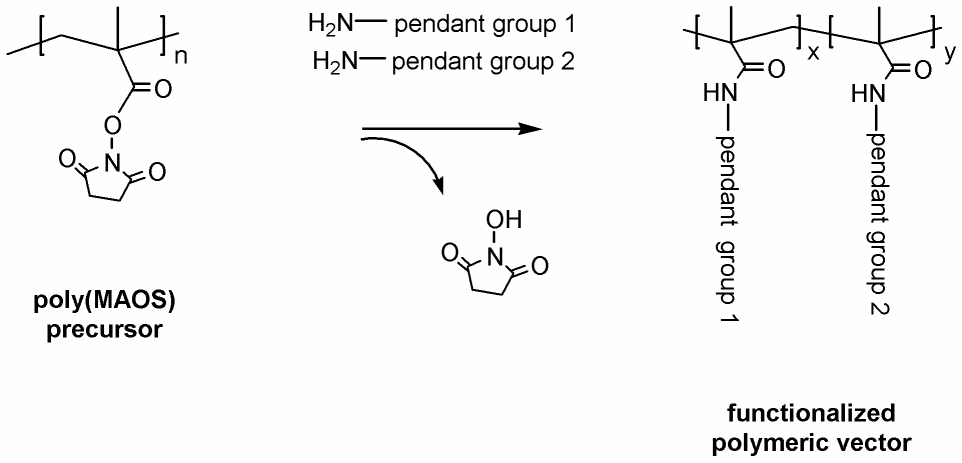

(b)

Figure 4-1. a) Cationic, pH-sensitive, and hydrophobic pendant groups **b)** General synthetic scheme for functionalizing pendant groups to the poly(methacryloxysuccimide) (poly(MAOS)) precursor to form mono- and bi-functionalized polymeric vectors

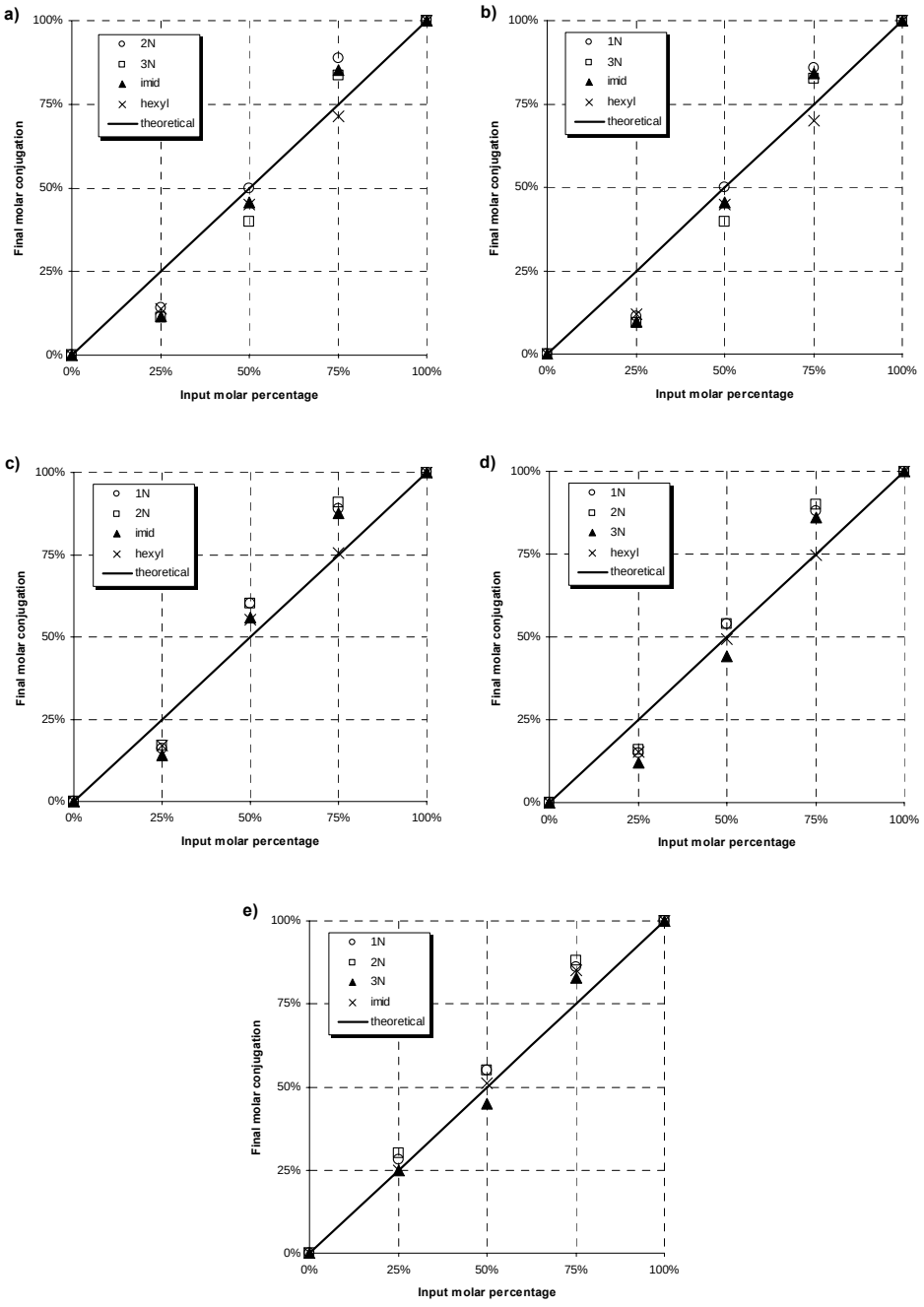

Figure 4-2. Conjugation profiles of polymers bi-functionalized with **a)** 1N **b)** 2N **c)** 3N **d)** imidazole and **e)** C6 hexyl and the pendant group indicated. The co-functionalization profiles for C4 and C8 were estimated by the C6 conjugation profile shown in (e). The results presented are based on the ^{1}H NMR characterization method and correspond to the profiles quantified via UV/Vis spectrophotometry (data not shown).

4.4.2. Trends in transfection and biophysical properties

For organizational purposes, all transfection and biophysical characterization results are divided into two sub-populations of polymers and referred to hereafter as the cationic polymers and the alkylated polymers. The cationic polymers comprise all mono- and bi-functionalized polymer formulations containing only cationic pendant groups. The alkylated polymers comprise formulations that contain an alkyl group. To conveniently identify the effects of alkylation, data from the four mono-functionalized cationic polymers are also included with the results for the alkylated polymers.

4.4.2.1. *Trends in transfection as a function of polymer pendant group*

An exhaustive screen of the 30 kDa MW library of polymers revealed several interesting trends in transfection as a function of the pendant groups conjugated to the polymeric vector. Amongst the cationic polymers, those co-functionalized with up to 50% imidazole or at least 50% 1N mediated the greatest levels of transfection at a polymer:DNA weight ratio of at least 5:1 (labeled with †), while polymers containing 2N and 3N mediated only moderate levels of transfection at their best (Figure 4-3a).

Figure 4-3b shows the transfection profiles of the alkylated polymers arranged as a function of hydrocarbon chain length and as a function of the degree of alkyl conjugation. In general, conjugating alkyl groups to cationic polymers did not result in any outstanding benefits towards transfection. Transfection profiles of the alkylated polymers did not appear to trend in any specific manner with respect to either hydrocarbon chain length or degree of conjugation, with one exception. As alkyl chain length increased for alkylated polymers co-functionalized with 3N, transfection efficiency also appeared to increase. Of the alkylated polymers the

25%Octyl/75%3N formulation mediated the greatest level of transfection at a polymer:DNA weight ratio of 10:1, although still one order of magnitude less than the highest transfecting cationic formulation. In addition, polymers co-functionalized with C6 and 1N or 2N mediated a relatively high degree of transfection compared to their C4 and C8 counterparts (labeled with *).

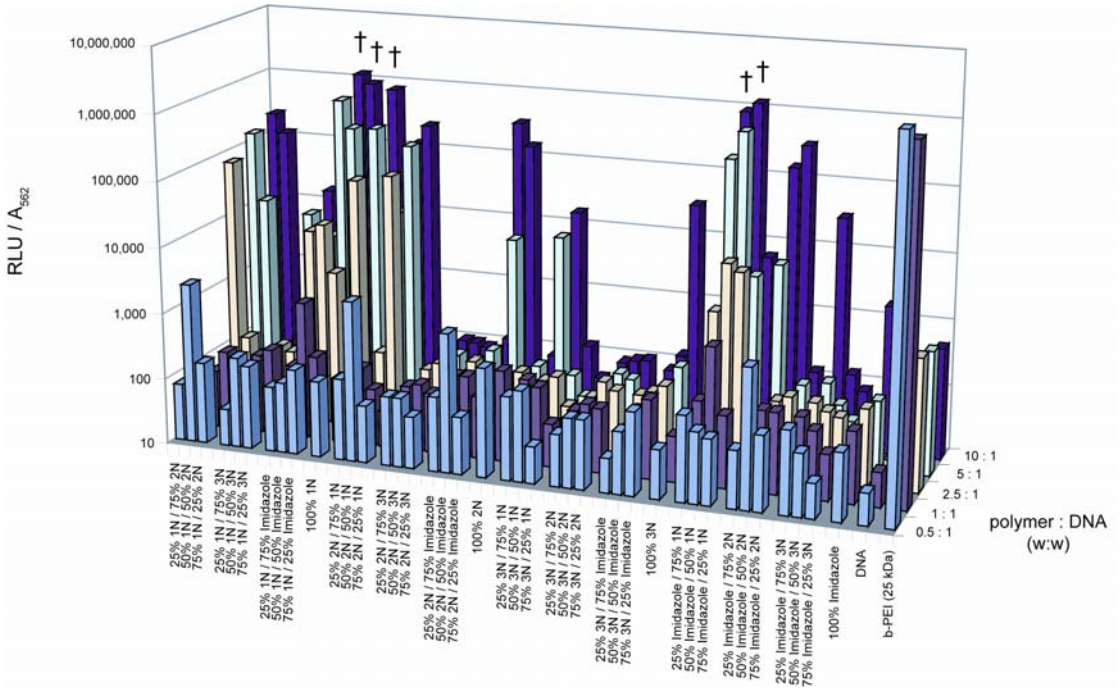

(a)

Figure 4-3. Transfection profile of NIH/3T3 cells with **a)** cationic polymers and **b)** alkylated polymers. The molecular weight of all polymers is 30 kDa. Transfection efficiency is expressed as the relative light units (RLU) measured from luciferase reporter protein expression normalized to the absorbance measured at 562 nm. Each polymer was evaluated at five polymer:DNA weight ratios – 0.5:1, 1:1, 2.5:1, 5:1, and 10:1. Samples labeled with a dagger (†) represent polymer formulations with the highest transfection capacities. Samples labeled with an asterisk (*) represent C6-containing formulations that mediated relatively high levels of transfection compared to their C4 and C8 counterparts.

Figure 4-3 (*continued*)

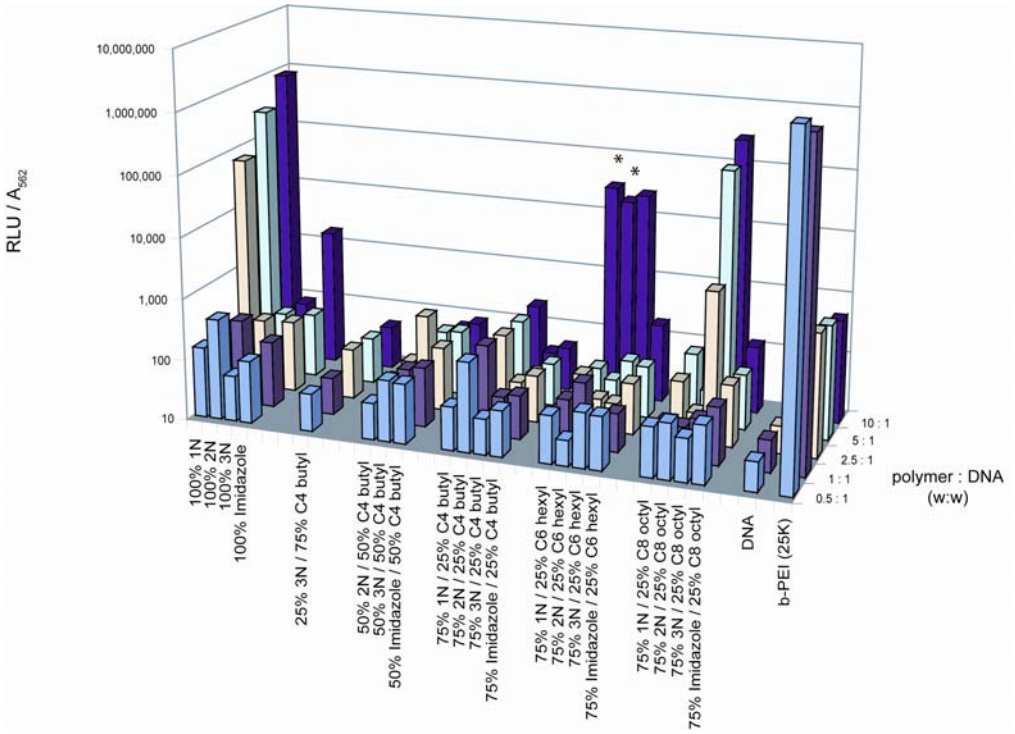

(b)

4.4.2.2. *Trends in biophysical properties as a function of polymer pendant group*

To understand how physicochemical changes to the polymeric vectors may give rise to the observed transfection trends, we evaluated various biophysical properties of resultant polyplexes as a function of the pendant groups conjugated to the polymer. For reasons provided below, the following polyplex and free polymer properties were investigated- relative binding affinity, polyplex stability, net surface charge, and effective diameter of polyplexes; and buffering capacity and cytotoxicity of free polymers.

4.4.2.2.1 Relative binding affinity and polyplex stability

One of the principal design criteria for polymeric delivery systems is the ability to bind with DNA and protect it from enzymatic degradation. [25-27] Furthermore, this binding interaction must be sufficiently stable to withstand competitive interactions from anionic species, such as extracellular and intracellular proteins, cytosolic RNA, or nuclear DNA, that can displace the bound DNA and result in its premature release. [28, 29] To assess the binding affinity of polymer to DNA and the stability of resultant polyplexes, we employed the EtBr fluorescence quenching and recovery assay. [9, 22, 23] The EtBr assay makes use of the increase in fluorescence intensity of the EtBr dye when it intercalates into DNA. Upon addition of a polycation and its subsequent complexation with DNA, EtBr is expelled from DNA, resulting in the reduction of fluorescence intensity. The relative binding affinity between polymer vector and DNA may be quantified by the magnitude to which fluorescence is quenched. To further quantify the strength of the binding affinity, recovery of the quenched fluorescence may be measured by subsequent addition of a polyanion, which serves to represent the competitive anionic environment encountered by polyplexes during transfection. Addition of the polyanion competes for binding with the polymeric vector and displaces DNA. EtBr/DNA interaction may then resume, resulting in the recovery of the fluorescence intensity. A ten-fold molar excess of the competing polyanion heparin, relative to DNA was employed in the polyplex stability studies to ensure that heparin competed with DNA and bound not only with uncomplexed free polymer that may be present in solution. [22]

Overall inspection of the relative binding affinities of the cationic polymers (Figure 4-4a) shows that 1N-containing polymers generally possessed the greatest binding affinities. Quantitative analysis of polymers at the 5:1 and 10:1 polymer:DNA

ratios revealed that 1N-containing polymers had approximately 10% greater binding affinities over 2N- and imidazole-containing polymers and 25% greater affinities over 3N-containing polymers. Imidazole-containing polymers possessed comparable binding affinities to 2N-containing polymers and roughly 15% greater binding affinities over 3N-containing polymers.

To summarize the effects of alkylation on the relative binding affinity, Figure 4-4b plots the percent change in binding levels of alkylated polymers relative to their respective mono-functionalized cationic polymer. The effects of alkyl co-functionalization appeared to be specific to the cationic co-functionalized partner as well as to the polymer:DNA weight ratio. In particular, when compared to mono-functionalized polymers of 1N or 2N, alkyl groups reduced the levels of binding by approximately 30% at weight ratios of 10:1, regardless of the hydrocarbon chain length of the alkyl group. In contrast, alkylation of imidazole-containing polymers generally reduced binding to a degree that was proportional to chain length; however, at a 10:1 polymer:DNA ratio, the trend was reversed with binding reduced more so with shorter chained alkyl groups. Of particular interest was the increase in relative binding affinities due to alkylation of 3N-containing polymers. However, as the butyl content increased from 25% to 75% conjugation, the effects were reversed and binding affinity was reduced relative to the 100% 3N polymer.

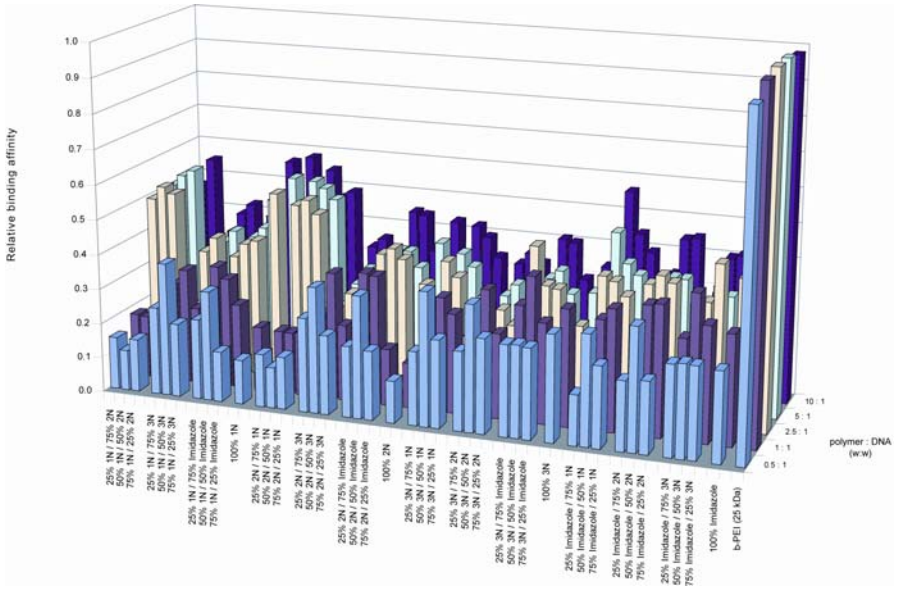

(a)

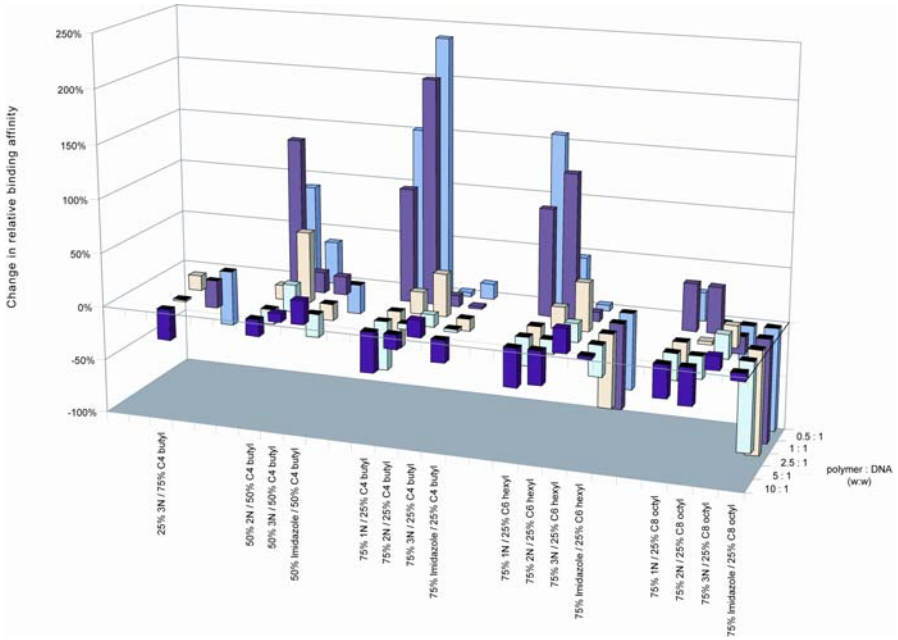

(b)

Figure 4-4. Relative binding affinities of **a)** cationic polymers and **b)** alkylated polymers. Alkylation effects on binding affinity are summarized as the percentage change in binding affinity relative to the mono-functionalized cationic polymer. Results for the alkylated polymers are shown in reverse order of the polymer:DNA weight ratios for clarity. Binding affinities were measured with the ethidium bromide fluorescence quenching assay. Each polymer was evaluated at five polymer:DNA weight ratios – 0.5:1, 1:1, 2.5:1, 5:1, and 10:1.

The relative strengths of polyplex binding for the cationic polymers, which estimate the stability of resultant polyplexes, are shown in Figure 4-5a. In general, imidazole-containing polymers formed more stable polyplexes that were more resistant to dissociation compared to polymers that contained only 1N, 2N, and 3N at nearly all polymer:DNA weight ratios. In particular, at polymer:DNA ratios of 5:1 and 10:1, imidazole-based polyplexes were on average 140% more resistant to dissociation than 1N-based polyplexes. Compared to 2N- and 3N-based polyplexes, enhanced resistance was approximately 75% and 50%, respectively.

The effects of alkylation on polyplex stability are summarized similarly to the binding affinities of alkylated polymers where the percent change in dissociation relative to the mono-functionalized polymer is plotted (Figure 4-5b). In general, alkylation reduced the degree to which DNA dissociated from 1N-, 2N-, and 3N-containing polymers, thus indicating an enhancement in binding strength. This enhancement did not appear to follow any consistent trends as a function of hydrocarbon chain length or degree of conjugation. In the case of the 75%1N/25%C8 formulation, the binding strength was increased by nearly 75% at a polymer:DNA ratio of 5:1. In contrast, alkylation decreased the strength of the binding interactions between DNA and polymers co-functionalized with imidazole groups.

Figure 4-5. Polyplex stability is shown as **a)** the relative binding strength for the cationic polymers and **b)** summarized for the alkylated polymers as the percentage change in polyplex dissociation relative to the mono-functionalized cationic polymer. Positive values represent an increase in dissociation, or decrease in binding strength, due to alkylation and vice versa for negative values. Results for the alkylated polymers are shown in reverse order of the polymer:DNA weight ratios for clarity. Polyplex stability was evaluated with the ethidium bromide fluorescence recovery assay performed immediately subsequent to the relative binding affinity quenching assay. Each polymer was evaluated at five polymer:DNA weight ratios – 0.5:1, 1:1, 2.5:1, 5:1, and 10:1.

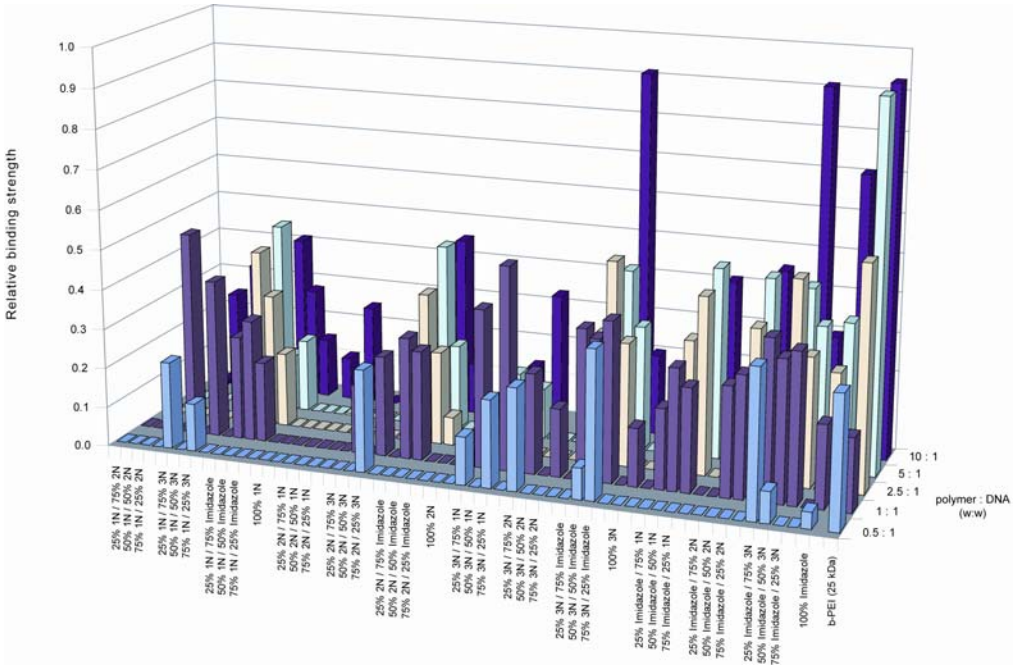
Relative binding strength
1.0
0.9
0.8
0.7
0.6
0.5
0.4
0.3
0.2
0.1
0.0
10 : 1
5 : 1
2.5 : 1
1 : 1
0.5 : 1
polymer : DNA (w:w)
25% 1N / 75% 2N
50% 1N / 50% 2N
75% 1N / 25% 2N
25% 1N / 75% 3N
50% 1N / 50% 3N
75% 1N / 25% 3N
25% 1N / 75% Imidazole
50% 1N / 50% Imidazole
75% 1N / 25% Imidazole
100% 1N
25% 2N / 75% 1N
50% 2N / 50% 1N
75% 2N / 25% 1N
25% 2N / 75% 3N
50% 2N / 50% 3N
75% 2N / 25% 3N
25% 2N / 75% Imidazole
50% 2N / 50% Imidazole
75% 2N / 25% Imidazole
100% 2N
25% 3N / 75% 1N
50% 3N / 50% 1N
75% 3N / 25% 1N
25% 3N / 75% 2N
50% 3N / 50% 2N
75% 3N / 25% 2N
25% 3N / 75% Imidazole
50% 3N / 50% Imidazole
75% 3N / 25% Imidazole
100% 3N
25% Imidazole / 75% 1N
50% Imidazole / 50% 1N
75% Imidazole / 25% 1N
25% Imidazole / 75% 2N
50% Imidazole / 50% 2N
75% Imidazole / 25% 2N
25% Imidazole / 75% 3N
50% Imidazole / 50% 3N
75% Imidazole / 25% 3N
100% Imidazole
b-PEI (25 kDa)

(a)

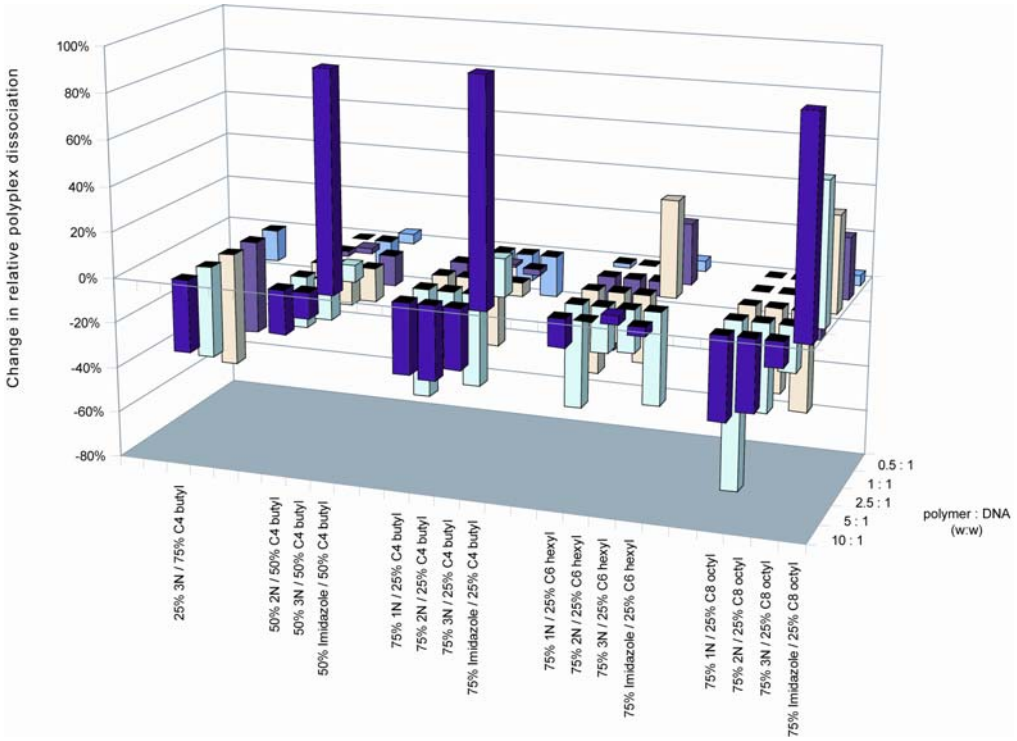
Change in relative polyplex dissociation
100%
80%
60%
40%
20%
0%
-20%
-40%
-60%
-80%
0.5 : 1
1 : 1
2.5 : 1
5 : 1
10 : 1
polymer : DNA (w:w)
25% 3N / 75% C4 butyl
50% 2N / 50% C4 butyl
50% 3N / 50% C4 butyl
50% Imidazole / 50% C4 butyl
75% 1N / 25% C4 butyl
75% 2N / 25% C4 butyl
75% 3N / 25% C4 butyl
75% Imidazole / 25% C4 butyl
75% 1N / 25% C6 hexyl
75% 2N / 25% C6 hexyl
75% 3N / 25% C6 hexyl
75% Imidazole / 25% C6 hexyl
75% 1N / 25% C8 octyl
75% 2N / 25% C8 octyl
75% 3N / 25% C8 octyl
75% Imidazole / 25% C8 octyl

(b)

4.4.2.2.2 Zeta potential and size

In addition to protecting DNA from enzymatic degradation, polymer/DNA complexation also acts to neutralize the negatively charged phosphate backbone of DNA and condense its bulky structure to appropriate length scales for cellular internalization. [30] It is generally accepted that a neutral to slightly electropositive surface charge favors transfection, presumably through non-specific interactions with membrane-associated, anionic proteoglycans. [27, 31] Additionally, an effective polyplex diameter of 200 nm or less is typically desired to promote uptake via endocytic pathways. [30] Based on the zeta potential profiles of both cationic and alkylated libraries shown in Figures 4-6a and 6b, the charge neutralizing capacities of the cations decrease in the order of 1N > 2N ~ 3N > imidazole. This relative order of charge neutralizing capacity is illustrated in the alkylated library where alkylated polymers co-functionalized with 1N produced polyplexes with a more positive zeta potential than 3N, which produced polyplexes with a slightly higher zeta potential than 2N. In contrast to the greater charge neutralizing power of 3N over 2N seen amongst the alkylated polymers, polymers within the cationic library suggested otherwise. Comparison of the mono-functionalized 2N and 3N polymers revealed that 100% 2N polymers had approximately +4 mV higher zeta potentials than 100% 3N polymers at comparable polymer: DNA ratios; while comparison of 1N/2N formulations and 1N/3N formulations showed comparable zeta potentials. Imidazole, on the other hand, possessed clearly less charge neutralizing ability compared to 1N, 2N, and 3N. All alkylated imidazole-containing polymers were unable to charge neutralize DNA. The weak charge neutralizing capacity of imidazole was further supported by the zeta potential profiles of the cationic polymers seen in Figure 4-6a where the polymer:DNA ratio required to produce a positive zeta potential was at least 5:1 compared to the 2.5:1 ratio required by non-imidazole containing polymers.

Moreover, polymers containing 100% imidazole formed polyplexes that were barely neutralized (+1.3mV) at the highest polymer:DNA ratio (10:1).

Alkyl co-functionalization resulted in a markedly lower charge neutralizing power observed amongst alkylated polymers compared to their respective mono-functionalized polymers. In general, the charge neutralizing power of alkylated polymers appeared to decrease with decreasing chain length. That is, polymers alkylated with 25% C8 resulted in polyplexes with a zeta potential more positive than those produced from 25% C6 polymers, which were more positive than those from 25% C4 polymers. However, as alkyl content increased beyond 25% functionalization, charge neutralization was not achieved with any of the cationic co-functionalization partners (Figure 4-6b).

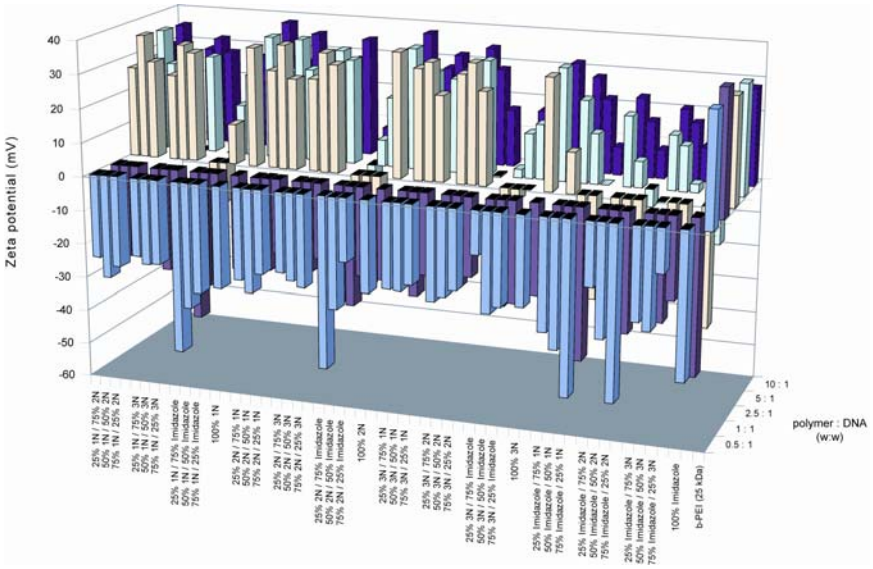

(a)

Figure 4-6. Surface charge measurements of polyplexes formed by **a)** cationic polymers and **b)** alkylated polymers. Each polymer was evaluated at five polymer:DNA weight ratios – 0.5:1, 1:1, 2.5:1, 5:1, and 10:1.

Figure 4-6 (*continued*)

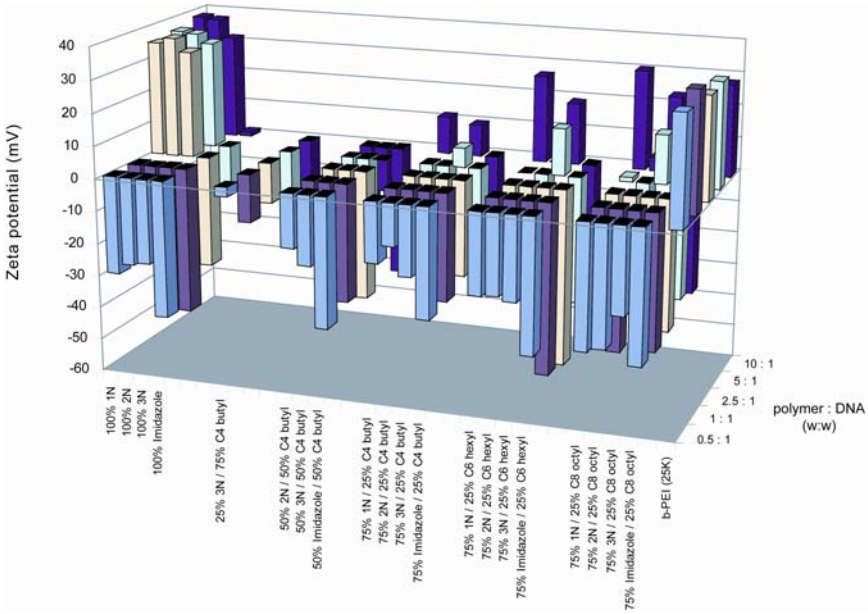

(b)

Similar to the trends in charge neutralizing power as a function of the cationic group, the relative size condensing capacity decreased in the order of 1N > 3N > 2N> imidazole (data not shown). Specifically, polyplexes formed by cationic and alkylated polymers containing 1N, 3N, and 2N were generally less than 200, 250, 300 nm in size, respectively. Polyplexes larger than these respective size limits were typically polymers that were co-functionalized with either alkyl or imidazole groups.

4.4.2.2.3 Buffering capacity

If cellular entry is gained by endocytosis, polyplexes are sequestered within membrane-bound vesicles and shuttled along intracellular routes including the endo-lysosomal pathway. Release from these vesicles is paramount for avoiding enzymatic

degradation within the lysosomal compartment. [32] One strategy for avoiding lysosomal degradation is by incorporating pH-sensitive moieties into polymeric vector designs to act as buffering agents within endosomes. It has been hypothesized that the buffering effect induces vesicle swelling, rupture, and finally release of the polyplexes into the cytosol. [33, 34] In this study, we have evaluated the buffering capacity of each polymer in its free uncomplexed state via acid-base titration.

The buffering capacities for the cationic and alkylated polymers are shown in Figures 4-7a and 7b. In general, the polymers with the greatest buffering capacity were those functionalized with 100% imidazole and 100% 3N. However, upon co-functionalizing with another cationic group, the buffering capacities of resultant polymers were diminished. In some cases, buffering capacities were reduced to levels below that of the two mono-functionalized polymers containing 100% of each cation of the conjugation pair. For comparison, the buffering capacities of b-PEI and water are shown in the buffering capacity plots. The buffering capacity of b-PEI was clearly greater than any of the polymers in the library.

Amongst the alkylated polymers, alkylation reduced the buffering capacity compared to the respective mono-functionalized polymers, with the exception of 2N-containing polymers, which remained relatively unaffected by alkylation. With the imidazole containing polymers, buffering capacity generally decreased with increasing alkyl chain length; whereas the reduction in buffering capacity of 1N- and 3N-containing polymers appeared to be independent of chain length and remained constant at all degrees of alkyl conjugation.

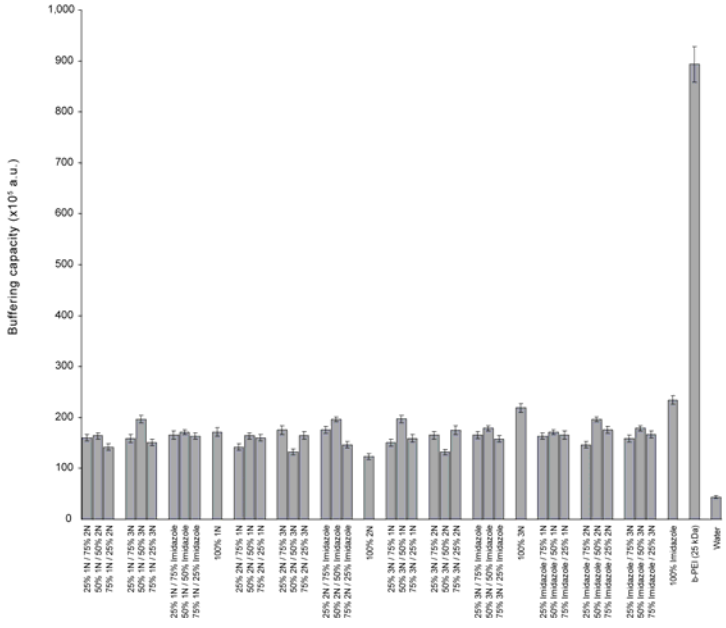

(a)

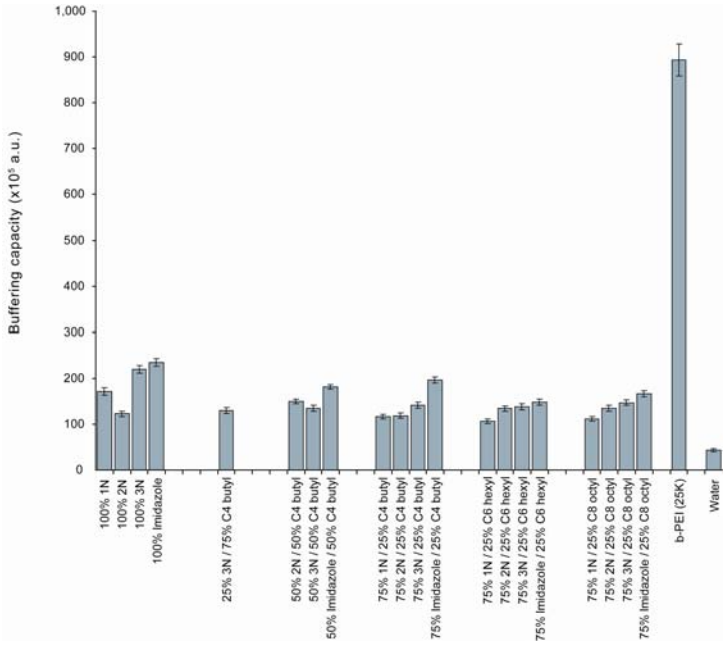

(b)

Figure 4-7. Buffering capacity of free, uncomplexed **a)** cationic polymers and **b)** alkylated polymers. The buffering capacity was evaluated via acid-base titration. Titration curves were fitted to a Boltzmann sigmoidal curve, from which the slope at the inflection point was determined. Buffering capacities are expressed as the absolute value of the reciprocal slope. Error bars represent the standard error propagated from data fitted to the sigmoidal curve.

4.4.2.2.4 Cytotoxicity

One of the biggest challenges facing synthetic delivery systems, second to subtherapeutic transfection efficiencies, is cytotoxicity. For gene delivery to be successful, the cells receiving the therapeutic genes must remain viable to sustain the expression of the prescribed proteins. Therefore, an important design consideration is the cytotoxic effect of both the polyplex and the free polymer, derived from any uncomplexed vector remaining after polyplex formation or upon intracellular release of the DNA. [35, 36]

The *in vitro* cytotoxicity of each polymer was assessed by the MTS cell viability assay following the same protocol as the transfection assay but measuring metabolic activity at the conclusion of the assay rather than reporter gene expression. Cytotoxicity was quantified as the concentration of free polymer at which the metabolic activity of cells, as determined by the measured UV/Vis absorbance associated with the MTS cell viability assay, was one-half the metabolic activity of cells that were treated with free polymer solutions containing 0 μg/mL of polymer. All polymers were evaluated in their free, uncomplexed form at the polymer concentrations that corresponded with the five polymer:DNA weight ratios evaluated in the transfection assay. Since the cytotoxic effects of polymeric vectors are typically greater in their free form compared to their complexed state, the cell viability measurements reported herein represent a conservative cytotoxicity estimate of each polymeric vector. [9, 37]

All cationic and alkylated polymers in the library possessed IC_{50} values greater than 200 μg/mL, with only a single exception (data not shown). The 100% 1N polymer formulation possessed an IC_{50} value of approximately 50 μg/mL. For comparison, the IC_{50} value of b-PEI was approximately 5 μg/mL.

4.4.2.3. *Characteristics of high transfecting polymers*

Shown in Figure 4-8 are the aggregated transfection levels as a function of the biophysical properties of the polyplex or the free polymer. In general, the greatest levels of transfection were achieved by polyplexes with at least a +10 mV zeta potential and less than 220 nm in size. Also characteristic of high transfecting formulations was the ability to quench at least 40% of the EtBr/DNA fluorescence and maintain at least 10% and at most 30% of the quenched fluorescence in the presence of competing polyanions. Based on the trends shown in Figures 4-8e and 4-8f, there appears to be little correlation between transfection levels and either the buffering capacity or the cytotoxicity of polymers.

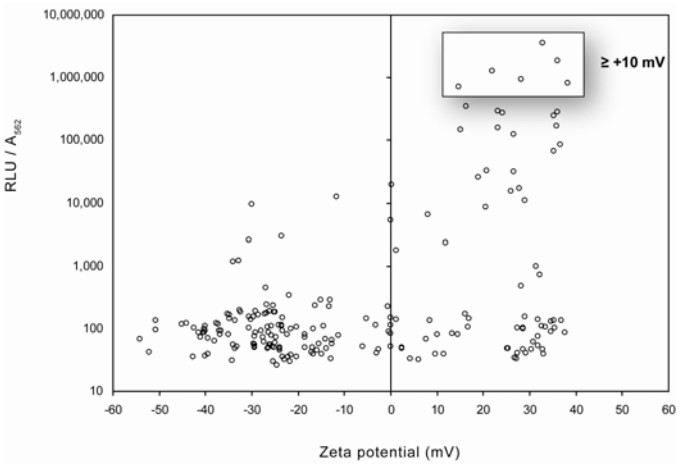

(a)

Figure 4-8. Aggregated trends in transfection as a function of **a)** polyplex surface charge, **b)** effective diameter of polyplexes, **c)** relative binding affinity, **d)** relative binding strength, **e)** buffering capacity, and **f)** cytotoxicity. In general, high levels of transfection correlated with polyplexes that carried at least a +10 mV surface charge and were less than 220 nm in size. Also correlative of high transfecting polymers were those with ≥ 10% binding affinity and binding strengths ranging between 10-30%. No salient correlations were observed with buffering capacity and cytotoxicity. The samples with IC_{50} = 5 ug/mL represent b-PEI and those with IC_{50} = 50 ug/mL represent 100% 1N.

Figure 4-8 (*continued*)

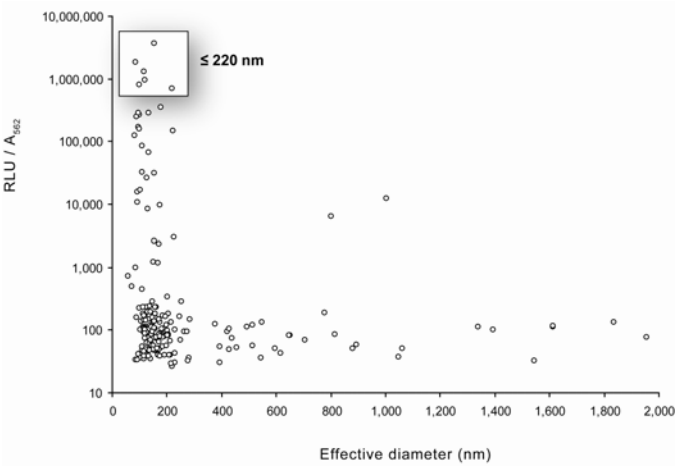

(b)

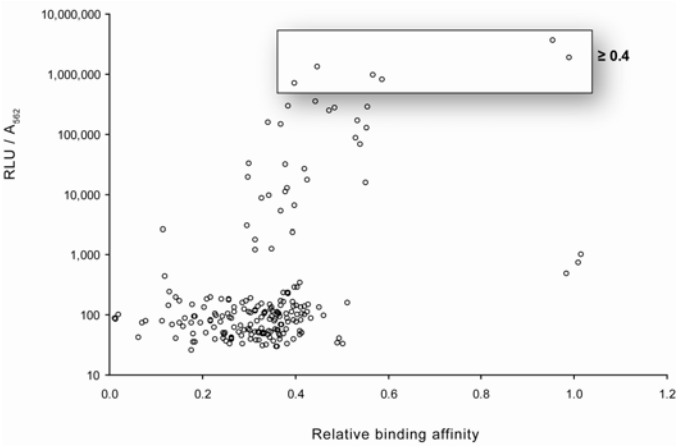

(c)

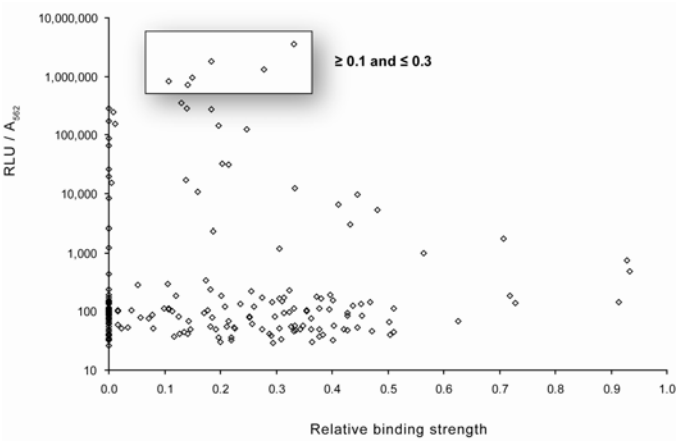

(d)

Figure 4-8 (*continued*)

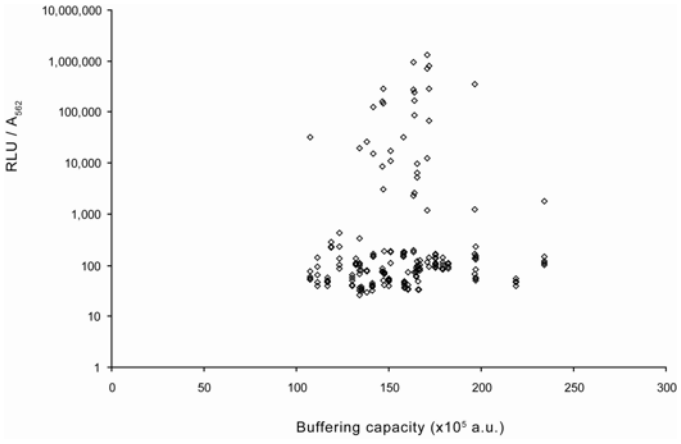

(e)

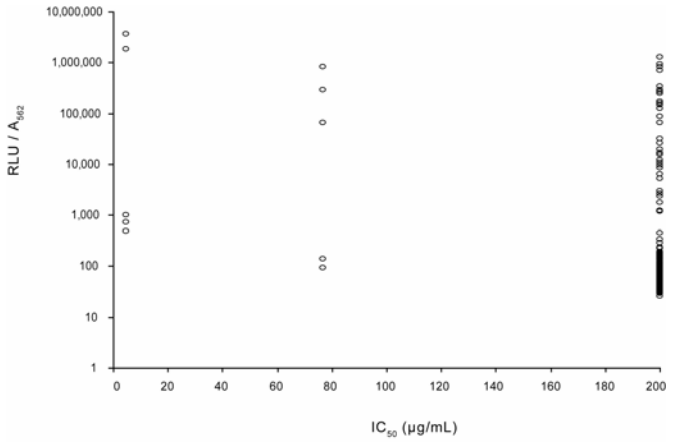

(f)

4.4.3. Effects of MW on transfection trends

Numerous reports have shown MW to be a critical structural attribute that can greatly influence the transfection capacity and biophysical properties of polymeric delivery systems. In general, high MW (≥ 25 kDa) polymers are typically associated with enhanced transfection efficiency and higher levels of cytotoxicity; while low MW

polymers (≤ 2 kDa) typically result in lower levels of transfection and are less cytotoxic. [38-41]

To investigate the effects of MW on this system of polymers, two additional libraries were synthesized and screened - one at 10 kDa and the other at 50 kDa, each comprising the same polymer formulations as the previously described 30 kDa library. The transfection profiles of cationic polymers at all three MWs are shown in Figure 4-9a.

In general, the trends in transfection within the 10 kDa and 50 kDa libraries remained fairly consistent with those observed in the 30 kDa library. That is, polymers containing up to 50% imidazole or at least 50% 1N afforded the greatest levels of transfection and polymers co-functionalized with either 2N or 3N mediated only moderate levels of transfection. Although the trends remained the same, the levels of transfection appeared to increase with increasing MW. Overall inspection of Figure 4-9a shows that the 50 kDa polymer library is populated with a greater number of high performing polymers that mediated high levels of transfection at a lower polymer:DNA ratio compared to the 30 kDa polymer library. Within the 10 kDa polymer library, the highest transfecting polymers mediated an order of magnitude less transfection compared to the highest performing polymers identified in the 30 kDa and 50 kDa libraries.

MW did not have as marked of an effect on the alkylated polymers as it did with the cationic polymers. (Figure 4-9b) Although the trends generally remained the same - polymers co-functionalized with C6 and either 1N, 2N, or 3N resulted in moderate degrees of transfection; and the 25%OCtyl/75%3N formulation mediated the greatest level of transfection of the alkylated polymers, though still less than the highest transfecting cationic polymers – they were not enhanced or diminished as a result of MW effects.

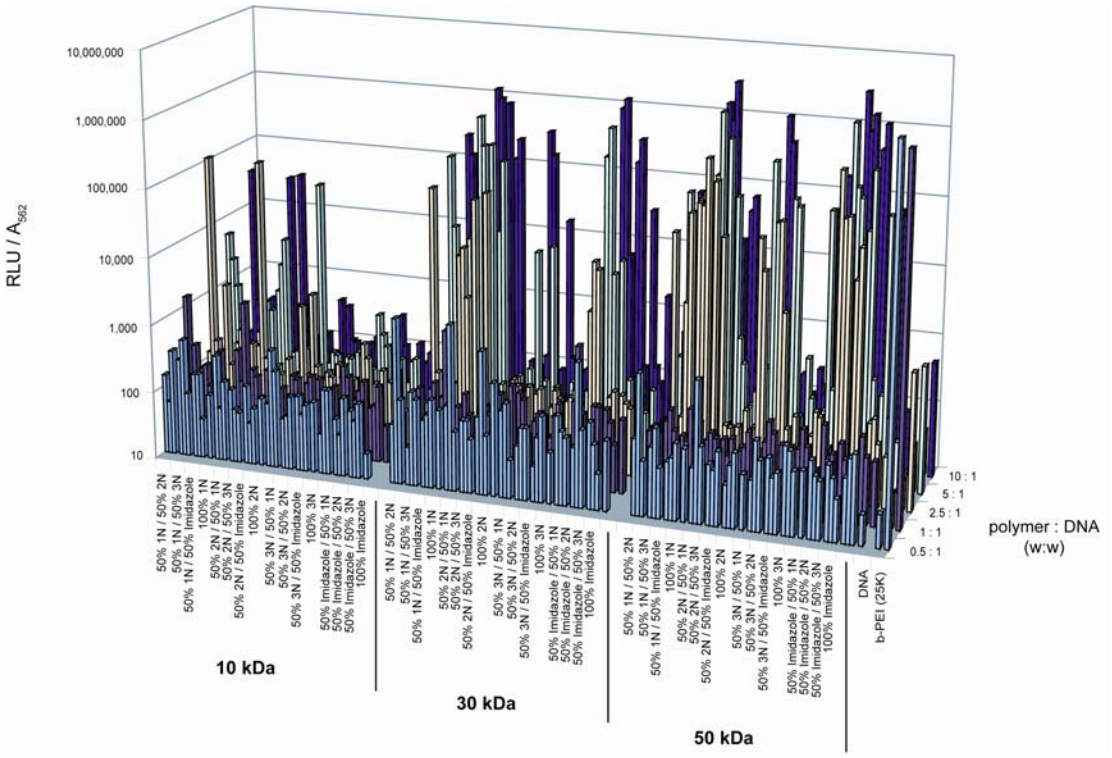

(a)

Figure 4-9. Effects of molecular weight on the transfection profile of NIH/3T3 cells with **a)** cationic polymers and **b)** alkylated polymers. Molecular weights of 10, 30, and 50 kDa were evaluated. The three molecular weight libraries had comparable polydispersity indices of 1.2-1.3. Transfection efficiency is expressed as the relative light units (RLU) measured from luciferase reporter protein expression normalized to the absorbance measured at 562 nm. Each polymer was evaluated at five polymer:DNA weight ratios – 0.5:1, 1:1, 2.5:1, 5:1, and 10:1. For clarity, not all formulations are labeled on the x-axis.

Figure 4-9 (*continued*)

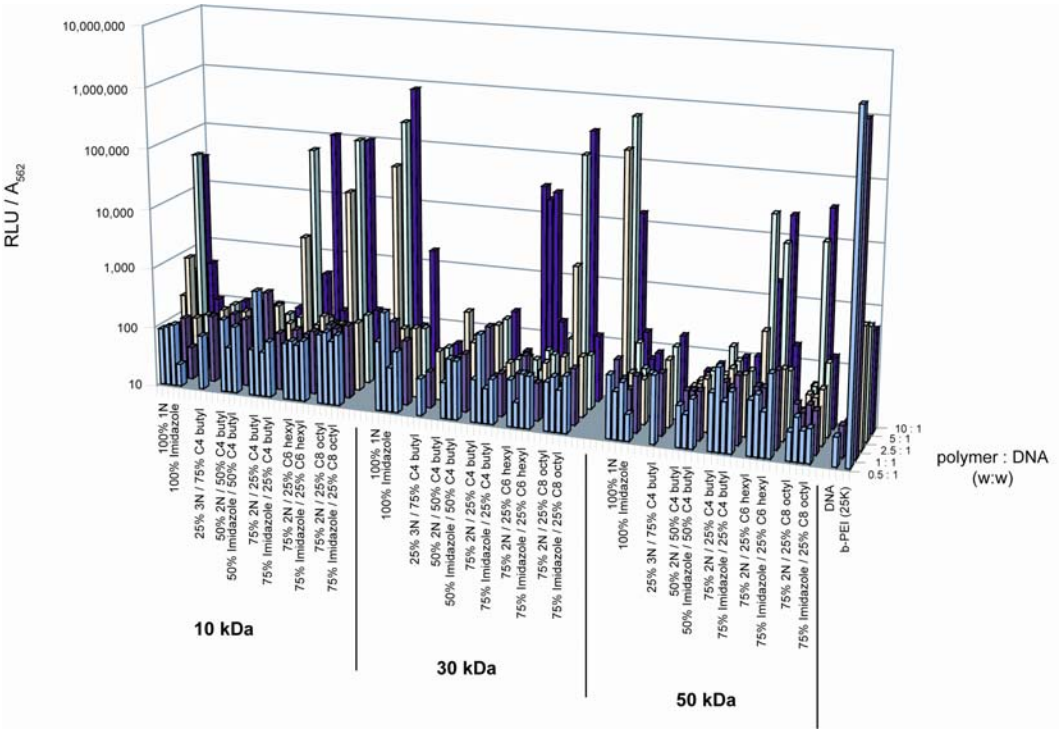

(b)

Figure 4-10 shows the highest transfecting 30 kDa and 50 kDa polymers plotted alongside their 50 kDa and 30 kDa counterparts, respectively. The highest transfecting polymers (labeled with †) mediated statistically comparable levels of transfection to b-PEI (25 kDa) at its optimal weight ratio with DNA (0.5:1). Labeled with an asterisk (*) are the formulations for which an increase in MW from 30 kDa to 50 kDa resulted in statistically higher levels of transfection.

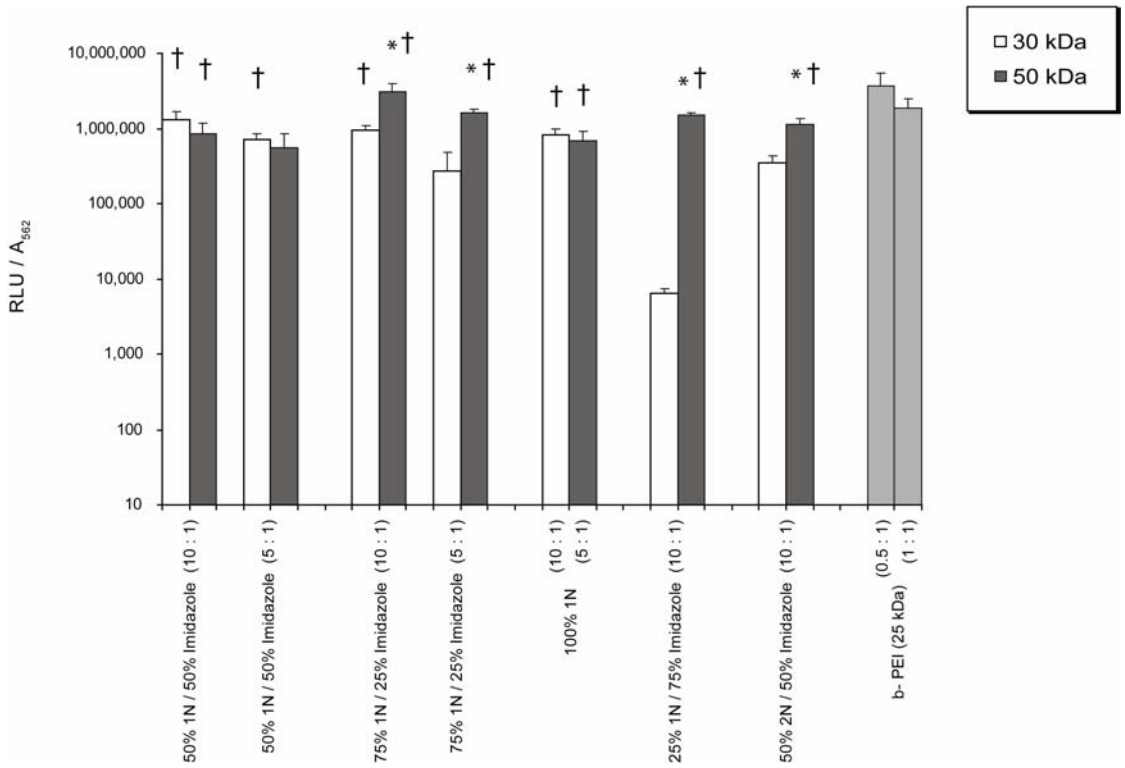

Figure 4-10. Transfection profiles of 30 kDa and 50 kDa polymers that mediated statistically comparable levels of transfection to b-PEI (25 kDa) at its optimal weight ratio with DNA (0.5:1) (labeled with a dagger (†)). Labeled with an asterisk (*) are the 50 kDa formulations that mediated statistically higher levels of transfection compared to their 30 kDa counterparts. The biophysical properties corresponding to each formulation are detailed in Table 4-2.

Table 4-2. Biophysical properties of high transfecting 30 kDa and 50 kDa polymers compared with branched PEI (25 kDa).

Polymer formulation [a]	Molecular Weight	polymer : DNA (w:w)	Size (nm)	Zeta potential (mV)	Relative binding affinity	Relative binding strength	Buffering capacity ($x10^5$ a.u.)	IC_{50} (μg/mL)
50% 1N / 50% Imidazole	30 kDa	10 : 1	118 ± 1.0	21 ± 0.15	0.45 ± 0.005	0.28 ± 0.001	171 ± 4.7	> 200
	50 kDa		114 ± 0.6	21 ± 0.65	0.48 ± 0.012	0.12 ± 0.002	149 ± 7.5	> 200
50% 1N / 50% Imidazole	30 kDa	5 : 1	219 ± 2.3	14 ± 0.31	0.4 ± 0.004	0.14 ± 0.001	171 ± 4.7	> 200
	50 kDa		256 ± 11.5	13.2 ± 0.40	0.4 ± 0.008	0.17 ± 0.002	149 ± 7.5	> 200
75% 1N / 25% Imidazole	30 kDa	10 : 1	119 ± 2.9	28 ± 0.81	0.57 ± 0.022	0.15 ± 0.003	164 ± 6.2	> 200
	50 kDa		107 ± 0.1	33 ± 0.85	0.42 ± 0.016	0.48 ± 0.005	184 ± 7.9	> 200
75% 1N / 25% Imidazole	30 kDa	5 : 1	98 ± 1.1	24 ± 0.55	0.48 ± 0.016	0.18 ± 0.003	164 ± 6.2	> 200
	50 kDa		140 ± 7.5	30 ± 1.15	0.44 ± 0.016	0.41 ± 0.004	184 ± 7.9	> 200
100% 1N	30 kDa	10 : 1	99 ± 2.5	38 ± 0.35	0.59 ± 0.009	0.11 ± 0.001	172 ± 8.2	76.6 ± 1.0
	50 kDa	5 : 1	87 ± 0.5	26 ± 0.32	0.56 ± 0.015	0.25 ± 0.001	202 ± 8.0	48.9 ± 0.3
25% 1N / 75% Imidazole	30 kDa	10 : 1	802 ± 18.8	8.1 ± 0.27	0.40 ± 0.006	0.41 ± 0.002	166 ± 7.7	> 200
	50 kDa		397 ± 31.2	10 ± 0.59	0.37 ± 0.014	0.49 ± 0.009	124 ± 6.6	> 200
50% 2N / 50% Imidazole	30 kDa	10 : 1	179 ± 1.0	16 ± 0.26	0.45 ± 0.005	0.13 ± 0.001	197 ± 4.5	> 200
	50 kDa		99 ± 1.9	16 ± 1.08	0.40 ± 0.011	0.43 ± 0.005	171 ± 7.7	> 200
b-PEI 25 kDa		0.5 : 1	152 ± 6.7	33 ± 0.56	0.95 ± 0.169	0.33 ± 0.014	893 ± 34.7	4.83 ± 0.17
b-PEI 25 kDa		1 : 1	84 ± 1.8	36 ± 0.87	0.99 ± 1.10	0.18 ± 0.745	893 ± 34.7	

[a] Formulations in bold achieved statistically higher levels of transfection than their 30 kDa counterparts

4.4.4. Effects of MW on biophysical trends

Biophysical characterization of the high-transfecting polymers, identified in Figure 4-10, uncovered some interesting trends, particularly amongst the formulations for which transfection efficiencies were enhanced due to an increase in MW. (Table 4-2). In general, higher transfection efficiencies afforded by a higher MW corresponded with polyplexes with slightly greater zeta potentials and reduced effective diameters, although polyplexes as large as 400 nm were still able to mediate high levels of transfection. Interestingly, MW appeared to have little effect on the relative binding affinity, yet significantly affected the stability of polyplexes, with over a three-fold increase in the relative binding strengths afforded by some 50 kDa polymers compared to equivalent 30 kDa formulations. Higher transfection efficiencies did not appear to correlate with buffering capacities nor coincide with any salient compromises in cell viability.

To further examine whether the trends in biophysical properties observed amongst the high performing 50 kDa polymers were representative of the rest of the 50 kDa library, the relative binding affinities, relative binding strengths, and cytotoxicity profiles were characterized for the entire 50 kDa library. Molecular weight appeared to have little appreciable effect on the relative binding affinity of cationic and alkylated polymers, unaffecting both the trends and magnitude of binding affinities (data not shown).

In contrast, MW appeared to have a more pronounced effect on the stability of polyplexes and their ability to resist dissociation by competing anionic species. These MW effects, however, seemed to affect the cationic polymers only. To summarize the general effects of MW on polyplex stability, Figure 4-11 shows the aggregated binding strengths of all 1N-, 2N-, 3N-, and imidzole-containing formulations, at the

5:1 and 10:1 weight ratios, amongst the cationic polymers. Based on the upward trend of binding strengths as the MW of cationic polymers increased, high MW polymers appeared to form polyplexes that were more stable and resistant to dissociation. In contrast, no salient trends as a function of MW were observed amongst the alkylated polymers (data not shown).

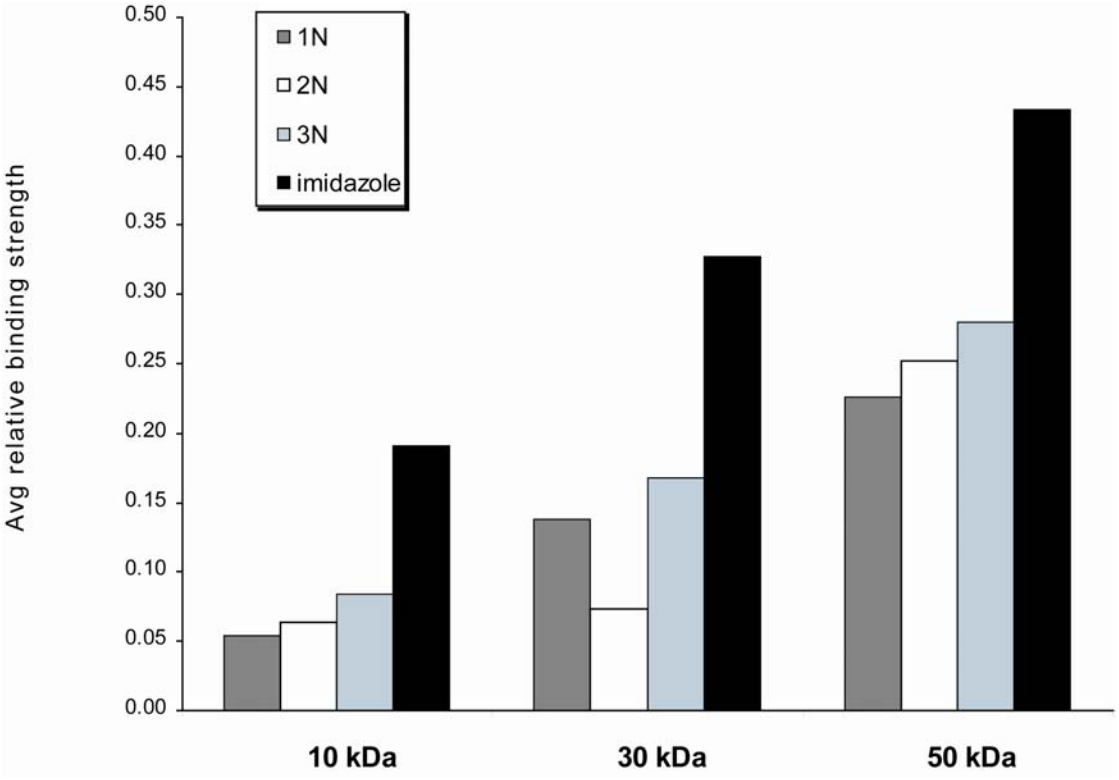

Figure 4-11. Effects of molecular weight on the binding strengths of cationic polymers. The binding strengths of 1N-, 2N-, 3N-, and imidazole-containing polymers were averaged together to summarize the general trend in binding strength as a function of molecular weight. Averages for each group of polymers were based on polyplexes formed at the polymer:DNA weight ratios of 5:1 and 10:1.

The cytotoxic effects of the free polymers increased slightly with increasing MW. Figure 4-12 shows a decrease in IC_{50} values of three formulations as MW

increases from 10 kDa to 50 kDa. All other formulations maintained IC_{50} values greater than 200 μg/mL (data not shown).

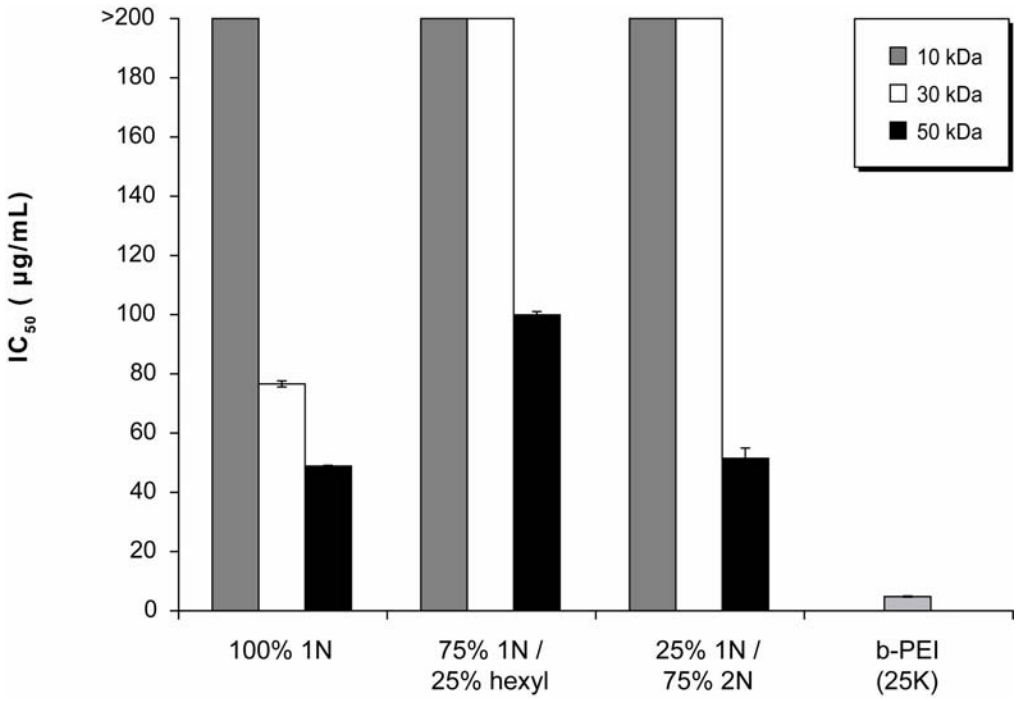

Figure 4-12. Effects of molecular weight on the cytotoxicity of polymeric vectors. The *in vitro* cytotoxicity of each polymer was assessed by the MTS cell viability assay at the free polymer concentrations - 10, 20, 50, 100, and 200 μg/mL, which corresponded to the following polymer:DNA weight ratios evaluated in the transfection assay - 0.5:1, 1:1, 2.5:1, 5:1, and 10:1, respectively. Cytotoxicity results are expressed as IC_{50} values and calculated as the concentration of free polymer at which the measured absorbance (MTS cell viability assay) was one-half the absorbance measured at a polymer concentration of 0 μg/mL.

4.5. DISCUSSION

The results in this study have revealed several important correlations with regard to the chemical attributes of polymeric vectors that favor transfection. In particular, polymers containing ≥ 50% 1N or ≤ 50% imidazole groups mediated the greatest levels of transfection. Based on the biophysical trends observed as a function

of the chemical changes made to the polymeric vector, the functional role of 1N appeared to be based on its superior ability to efficiently complex with DNA. Figure 4-4a shows the relatively high binding affinities of 1N-containing polymers, which resulted in polyplexes that were less than 220 nm in size and carried a net positive zeta potential (Figure 4-6a).

The transfection enhancing activity of imidazole also appeared to stem from its function as a DNA-complexing agent. However, in contrast to 1N, its mode of interaction with DNA seemed to include non-electrostatic interactions, which may have explained its enhanced ability to prevent polyplexes from dissociating in the presence of competing polyanions and prematurely releasing DNA. Imidazole's non-electrostatically mediated condensing property has been reported previously by others and is supported here by several lines of evidence. [9, 24, 42] First, Figure 4-6a shows that imidazole-containing polymers have a weaker ability to charge neutralize DNA relative to polymers containing 1N, 2N, or 3N. In principle, the zeta potential of polyplexes should be closely related to the binding affinity of cationic polymers since the electrostatic interaction between cation and anionic DNA is the condensation mode for which cations are employed in polymeric vector designs. Cationic polymers that induce polyplexes with a more positive zeta potential presumably bind to DNA more tightly. [43] Thus, one might expect the binding affinity of the cationic pendant groups to trend in the same order as that determined for charge neutralizing power (i.e., 1N>2N~3N>imidazole). Figure 4-4a, however, suggests that imidazole-containing polymers possessed comparable levels of binding to 2N-containing polymers and in fact, 15% greater binding levels than 3N-containing polymers. The enhanced binding, yet inferior charge neutralizing and size condensing capacity of imidazole, compared to both 2N and 3N, suggest an additional, non-electrostatic mode of binding mediated by imidazole groups.

A second line of evidence for the non-ionic binding interactions of imidazole with DNA is provided by the results from the polyplex stability studies shown in Figure 4-5a. In this study, the stability of polyplex binding, or the binding strength, was evaluated by the degree to which polyplexes were dissociated upon exposure to an excess of a competing polyanion. The use of an ionic species to effect polyplex dissociation assumes that any interaction that is of an electrostatic nature or weaker, between the polymer and DNA, will be disrupted by the competing electrostatics. The results from the stability studies revealed that imidazole-containing polymers dissociated less compared to 1N-, 2N-, and 3N-containing polymers, suggesting that 1) the strength of the binding interactions between DNA and imidazole-containing polymers was greater than that between DNA and 1N-, 2N-,and 3N-containing polymers; and/or 2) binding interactions between imidazole and DNA may be mediated by non-electrostatic forces, which stabilized polyplexes and resulted in more efficient delivery to cells.

Imidazole has also been employed in numerous vector designs for their buffering capacity, which purportedly enables them to mediate endo-lysosomal escape.[9, 15, 16] Indeed, Figure 4-7a shows that amongst the mono-functionalized cationic polymers, imidazole had the greatest buffering capacity. Upon co-functionalization with 1N, however, the buffering contributions by imidazole groups appeared to be masked as suggested by the diminished buffering levels of imidazole/1N co-functionalized polymers. Therefore, it is unclear whether the high transfection levels achieved by 1N/imidazole co-functionalized polymers are attributable to any endo-lysosomal escape functionality that the imidazole groups may have contributed.

Collectively, the results from the polyplex stability studies showed that all of the polymers possessed a mechanism by which DNA may be released, an event that is

believed to be necessary in order for efficient gene expression to occur. [29, 44] However, the ability to release DNA must also be balanced with the capacity to prevent premature dissociation into non-productive or enzymatically degradative environments. [45] Indeed, Figure 4-8d shows that high levels of transfection are associated with an optimal range of polymer binding strengths, outside of which transfection efficiency is diminished. Based on the binding affinity, dissociation, and transfection results, polymers co-functionalized with imidazole groups were able to afford appropriate levels of binding and subsequent release. Additionally, the fact that high levels of transfection were mediated mostly by imidazole-containing polymers, despite their similar buffering capacities to low-transfecting polymers, suggests that imidazole's primary transfection- enhancing effect in this system of polymers may not be its purported buffering capacity. Rather, it may lie in its ability to effectively interact with DNA to form stable polyplexes that were able to withstand competing anionic forces without dissociating. Further evaluation of the intracellular trafficking mechanisms, cellular localization, and transport dynamics will be needed to correlate with the stability results observed here in order to fully resolve the spatial and temporal details of DNA dissociation from imidazole-based polymers. The information obtained from these studies could have important implications on the strategic use of imidazole groups in polymer vector design.

The highest transfecting polymers identified in the 50 kDa library also included imidazole and 1N co-functionalized together. Figure 4-10 shows the transfection levels of the highest-transfecting polymers identified in both the 30 kDa and 50 kDa libraries, with their respective biophysical properties summarized in Table 4-2. Although a MW increase did not necessarily enhance the transfection levels of all the high-performing polymers identified in the 30 kDa library (e.g., 50%1N/50% imidazole at 10:1 polymer:DNA ratio), a couple of trends emerged that were common

amongst polymers that did mediate statistically higher levels of transfection as a result of a higher MW. For the most part, polyplexes formed by the high-transfecting 50 kDa polymers carried a greater zeta potential, were smaller in size, and dissociated less readily in the presence of competing polyanions, compared to their 30 kDa counterparts.

Interestingly, the chemical and structural features shared by high performing polymers in this study stand in direct contrast to previous reports from our group that showed improved transfection profiles with lower MW and increasing imidazole conjugation, upwards of 85%, to a polylysine backbone. [9, 16] A likely explanation for the disparate trends may be attributed to the different polymer backbone employed in each study. Whereas the previous two studies employed a polylysine backbone to which imidazole groups were attached, the present study utilized a methyl methacrylate backbone to which pendant groups were conjugated. Although the pendant groups evaluated in each of the three reports are similar, they are not identical, highlighting the dramatic effects that seemingly subtle structural and chemical modifications may have on the transfection capacity of polymeric vectors.[46-48]

Also observed in this study were the trends associated with the 2N, 3N, C4, C6, and C8 pendant groups. In general, polymers containing these pendant groups did not mediate high levels of transfection; however, the correlations between their biophysical characterizations and transfection profiles have provided important insights into their respective functional roles in transfection.

Like imidazole groups, 3N has been proposed to offer enhanced buffering capabilities to facilitate endo-lysosomal escape. [49] The buffering capacity results in Figure 4-7a show that at certain conjugation ratios, 3N increased the buffering capacity of polymers when co-functionalized with 1N and 2N, compared to 100% 1N

and 100% 2N polymers, respectively. However, the added capacity did not translate to enhancements in transfection efficiency. In light of other reports that have also questioned the endo-lysosomal disrupting ability of 3N-containing polymers, further studies will be needed to clarify the buffering role of the 3N moiety in gene delivery. [50]

Similar to 1N, 2N and 3N functioned primarily as cationic centers that electrostatically interacted with DNA to bind, condense, and neutralize its charge, though to a lesser degree than 1N. (Figure 4-4a, Figure 4-6a) When co-functionalized with 1N, 2N and 3N appeared to function as charge moderators, forming polyplexes with less positive zeta potentials compared to 100% 1N polymers. In contrast, when co-functionalized with less cationic groups, (e.g., imidazole and alkyl groups), 2N and 3N facilitated DNA complexation through their relatively greater charge capacity. However, based on the collective results of all biophysical properties evaluated in the present work, there appeared to be little other transfection-enhancing ability offered by 2N and 3N and their use merely as cationic centers did not appear to be advantageous, at least in this system of polymers.

Hydrophobic residues have been shown to enhance transfection presumably through favorable interactions with membrane components that result in cellular uptake. [43, 51] To investigate the effects of hydrophobic derivitization on transfection and the biophysical properties of resultant polyplexes, we evaluated both the effect of hydrocarbon chain length and degree of alkyl conjugation using the C4 butyl, C6 hexyl, and C8 octyl hydrophobic alkyl groups. Based on the binding affinity and polyplex stability trends observed amongst the alkylated polymers (Figure 4-4b, Figure 4-5b), hydrophobic moieties appeared to function primarily in altering the dynamics of polyplex formation. Particularly noteworthy was the reduced ability for DNA to dissociate from alkylated polymers that were co-functionalized with either

1N, 2N, or 3N, compared to their respective mono-functionalized cationic polymers. This result was surprising since the trends in Figure 4-6b show that alkylation tended to reduce the charge neutralizing capacity of cationic polymers. The reduction in charge neutralization might imply a weaker interaction between alkylated polymers and DNA and thus an increased tendency for dissociating in the presence of competing polyanions. However, the observed decrease in dissociation suggests that alkylation may induce a hydrophobically-driven conformational rearrangement of the polymer perhaps during polyplex formation. That is, to achieve a more thermodynamically-favorable conformation, hydrophobic residues may drive the polyplex to assume a conformation that collapses down on the DNA thereby preventing it from dissociating readily, even in the presence of a ten-fold excess of a competing polyanion. In contrast to the benefits that a reduced ability for polyplex dissociation appeared to have for imidazole-based polyplexes, this characteristic seemed to be detrimental for alkylated polymers. Since the dissociation properties for alkylated polymers did not appear to change with MW (data not shown), it was difficult to verify whether the inability for the polyplex to unravel explains the poor transfection profiles of the alkylated polymers. In light of other reports that have conjectured similar clustering effects of hydophobically-derivitized polymeric vectors and their subsequent effect on transfection, it is clear that hydrophobic derivitization of polymers may be a strategy for enhancing transfection. [10, 43] However, further investigation will be needed to fully understand the underlying mechanisms by which hydrophobic moieties can augment the transfection process before they can be strategically incorporated into polymeric gene delivery systems.

Despite the relatively unfavorable biophysical properties of polyplexes formed by alkylated polymers, there were a few formulations that resulted in moderate levels of transfection. Specifically, polymers co-functionalized with 25% C6 and either 1N

or 2N mediated moderate levels of transfection. This result was rather unexpected considering formulations of 25% C4 and 25% C8 resulted in negligible transfection. In the case of 25% alkylation with 75% 3N, moderate levels of transfection were realized with C6 and further enhanced as the alkyl chain length increased to C8. Taken together, these results suggest that an optimal degree of hydrophobicity may be beneficial towards transfection, and deviations from that optimum may be deleterious. Similar observations have been reported by others and serve to reinforce the critical, yet poorly understood, hydrophobic/hydrophilic balance that must be considered in polymeric vector design. [10, 43] Analysis of the biophysical properties of the moderately transfecting alkylated polyplexes did not reveal any obvious incongruities that might explain the disparate transfection profiles.

An important general attribute worth noting is the favorable cytotoxicity profiles of the polymers examined in this study, even those with a MW of 50 kDa. Of the 114 total polymers evaluated, only four formulations possessed IC_{50} values less than the maximum concentration of free polymers exposed to cells (200 μg/mL). (Figure 4-12) Amongst the ten highest-transfecting formulations identified in the present study, only two possessed IC_{50} values less than 200 μg/mL. (Table 4-2) For comparison, the IC_{50} value of b-PEI was approximately 5 μg/mL. Considering that the majority of polymers within the three MW libraries exhibited relatively good cell viability, it is likely that cytotoxicity was not a predominant factor in explaining the transfection differential observed between the three libraries of polymers. More importantly, in light of the cytotoxic effects of b-PEI and many PEI-based vector designs, these favorable cytotoxicity profiles further reinforce the utility of the polymeric system reported herein as a viable, alternative platform for future studies of various polymeric chemical and structural features and their functional roles in gene delivery.

In conclusion, we have demonstrated the utility of combinatorial strategies for systematically evaluating the functional role of cationic, pH-sensitive, and hydrophobic pendant groups in the transfection process. In addition to reporting the polymeric chemical and structural features that most favor transfection and their purported mechanisms, this work introduces a simple and robust polymeric platform upon which future structure-function studies may be based. By standardizing the polymeric structures and synthetic protocols, the structure-function relationships that govern polymer-mediated gene delivery may be more clearly defined, potentially leading to safer and more efficient polymeric delivery systems.

APPENDIX

Conversion of measured UV/Vis absorbance (at 260 nm) of polymers co-functionalized with benzylamine to conjugation ratio

Example:

Bi-functionalized polymer with 25% benzylamine and 75% 3N (A_{260}=0.346)

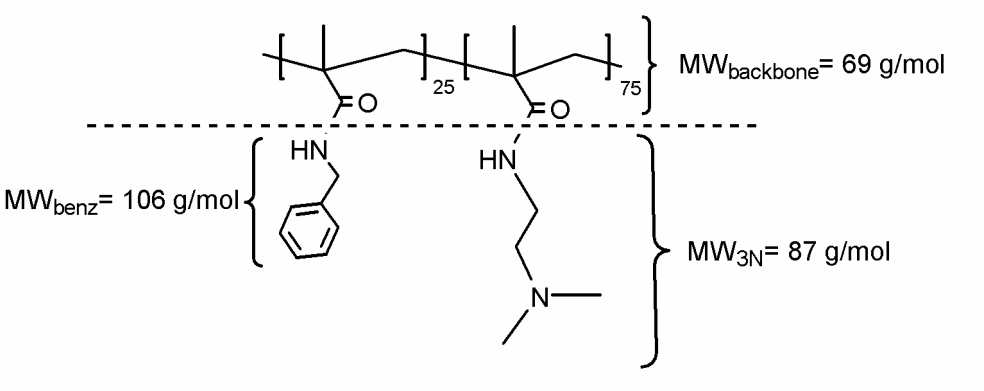

Bi-functionalized polymer with 75% benzylamine and 25% imidazole (A_{260}=0.842)

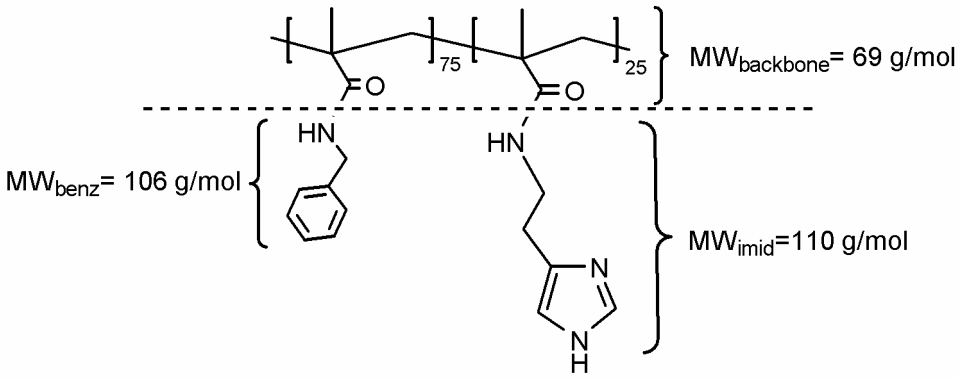

To determine the benzylamine concentration that corresponds to different theoretical conjugation ratios of benzylamine, the following equations were used:

$$MW_{bipoly,x} = \frac{x(MW_{benz}) + y(MW_y) + (x+y)(MW_{backbone})}{x} \qquad (4.1)$$

where $MW_{bipoly,x}$ is the molecular weight of a repeat unit containing x conjugation ratio of benzylamine in units of g/mol of benzylamine; x is the theoretical benzylamine conjugation ratio; MW_{benz} is the calculated molecular weight of conjugated benzylamine (106 g/mol); $y = 1 - x$ is the theoretical conjugation ratio of the co-functionalized pendant group; MW_y is the calculated molecular weight of the conjugated co-functionalized pendant group; and $MW_{backbone}$ is the calculated molecular weight of a repeat unit of the polymeric backbone (69 g/mol).

$$C_{benz} = \frac{m}{v * MW_{bipoly,x}} \qquad (4.2)$$

where C_{benz} is the benzylamine concentration in units of mol/L that corresponds to the theoretical benzylamine conjugation ratio, x, of a UV/Vis polymer sample of weight, m (0.005 g), dissolved in volume, v (0.006 L), of solvent. Absorbance values at 260 nm, A_{260}, corresponding to C_{benz} values were determined from a calibration curve generated from free base benzylamine dissolved in the same solvent as the bi-functionalized polymeric samples.

		benzylamine/3N co-functionalization			benzylamine/imidazole co-functionalization		
x	y	$MW_{bipoly,x}$ (g/mol benzylamine)	C_{benz} (mol/L)	A_{260} [a]	$MW_{bipoly,x}$ (g/mol benzylamine)	C_{benz} (mol/L)	A_{260} [a]
1.0	0.0	175	0.0048	0.849	175	0.0048	0.849
0.9	0.1	192	0.0043	0.774	195	0.0043	0.764
0.8	0.2	214	0.0039	0.697	220	0.0038	0.679
0.7	0.3	242	0.0034	0.618	252	0.0033	0.594
0.6	0.4	279	0.0030	0.537	294	0.0028	0.510
0.5	0.5	331	0.0025	0.455	354	0.0024	0.426
0.4	0.6	409	0.0020	0.370	444	0.0019	0.343
0.3	0.7	539	0.0015	0.284	593	0.0014	0.259
0.2	0.8	799	0.0010	0.196	891	0.0009	0.177
0.1	0.9	1579	0.0005	0.105	1786	0.0005	0.094

[a] The absorbance values were determined from a calibration curve generated from free base benzylamine dissolved in 0.1N HCl at concentrations ranging from 0.1mM - 5 mM. The linear fit trendline used in this example is $A_{260} = 175.69 * C_{benz} + 0.0124$.

A linear trendline fitted to the plot of x vs. A_{260} for each bi-functionalized pair was then used to convert the measured absorbance of bi-functionalized polymers to the conjugation ratio of benzylamine, X_{benz}.

A_{260} for benzylamine/3N polymer = 0.346 corresponds to X_{benz} = 32% benzylamine conjugation

A_{260} for benzylamine/imidazole polymer = 0.842 corresponds to X_{benz} = 71% benzylamine conjugation

The conjugation ratios of 3N and imidazole were calculated by:

$$X_{\exp,r,m} = 1 - X_{benz} \qquad (4.3)$$

$X_{exp,\ 0.75,3N}$ = 68% conjugation of 3N

$X_{exp,\ 0.25,imid}$ = 29% conjugation of imidazole

A conjugation efficiency value relative to benzylamine, $CE_{B,r,m}$, was then calculated according to the following equation:

$$CE_{B,r,m} = \frac{X_{\exp,r,m}}{r_m} \qquad (4.4)$$

where r is the input molar ratio (0.25, 0.50, 0.75) of pendant group m.

$CE_{B,\ 0.75,3N}$ = 0.68/0.75 =0.91

$CE_{B,\ 0.25,imid}$ = 0.29/0.25 =1.16

To calculate the coefficient efficiency of each pendant group relative to each other, the following equation was used:

$$CE_{m_1,m_2} = \frac{r_{m_1}}{r_{m_2}} * \frac{CE_{B,r,m_1}}{CE_{B,r,m_2}} \qquad (4.5)$$

For 25% input molar percentage (r=0.25) of imidazole:

$$\mathbf{CE_{imid,3N} = (0.25/0.75) * (1.16/0.91) = 0.42}$$

For 75% input molar percentage (r=0.75) of 3N:

$$\mathbf{CE_{3N,imid} = (0.75/0.25) * (0.91/1.16) = 2.35}$$

To calculate the conjugation ratio of a polymer bi-functionalized with 75%3N and 25% imidazole, the following equation was used:

$$X_{calc,m_1} = \frac{CE_{m_1,m_2}}{(CE_{m_1,m_2} + CE_{m_2,m_1})} \qquad (4.6)$$

where $X_{calc,m1}$ is the calculated conjugation ratio of pendant group, *m1*, when co-functionalized with pendant group, *m2*.

$$\mathbf{X_{calc,3N} = 0.42 / (0.42+ 2.35) = 15\%}$$

$$\mathbf{X_{calc,imid} = 2.35 / (0.42+ 2.35) = 85\%}$$

REFERENCES

[1] Burton, E., Glorioso, J., and Fink, D. Gene therapy progress and prospects: Parkinson's disease. *Gene Ther.* **10**(20): 1721-1727 (2003).

[2] Factor, P. Gene therapy for acute diseases. *Mol. Ther.* **4**(6): 515-524 (2001).

[3] Pawliuk, R., Westerman, K., Fabry, M., Payen, E., Tighe, R., Bouhassira, E., Acharya, S., Ellis, J., London, I., Eaves, C., Humphries, R., Beuzard, Y., Nagel, R., and Leboulch, P. Correction of sickle cell disease in transgenic mouse models by gene therapy. *Science* **294**(5550): 2368-2371 (2001).

[4] Von Laer, D., Hasselmann, S., and Hasselmann, K. Gene therapy for HIV infection: what does it need to make it work? *J Gene Med* **8**(6): 658-667 (2006).

[5] Coura, R. and Nardi, N. A role for adeno-associated viral vectors in gene therapy. *Genet Mol Biol* **31**(1): 1-11 (2008).

[6] Flotte, T. Gene therapy: The first two decades and the current state-of-the-art. *J Cell Physiol* **213**(2): 301-305 (2007).

[7] Xu, Z., Zeng, Q., Lu, G., and Yu, A. Inorganic nanoparticles as carriers for efficient cellular delivery. *Chem. Eng. Sci.* **61**(3): 1027-1040 (2006).

[8] Wong, S., Pelet, J., and Putnam, D. Polymer systems for gene delivery-past, present, and future. *Prog. Polym. Sci.* **32**(8-9): 799-837 (2007).

[9] Chen, D., Majors, B., Zelikin, A., and Putnam, D. Structure-function relationships of gene delivery vectors in a limited polycation library. *J Control Release* **103**(1): 273-283 (2005).

[10] Doody, A., Korley, J., Dang, K., Zawaneh, P., and Putnam, D. Characterizing the structure/function parameter space of hydrocarbon-conjugated branched polyethylenimine for DNA delivery in vitro. *J Control Release* **116**(2): 227-237 (2006).

[11] Hartmann, L., Haefele, S., Peschka-Suess, R., Antonietti, M., and Borner, H. Tailor-made poly(amidoamine)s for controlled complexation and condensation of DNA. *Chemistry-A European Journal* **14**(7): 2025-2033 (2008).

[12] Masuda, T., Akita, H., Nishio, T., Niikura, K., Kogure, K., Ijiro, K., and Harashima, H. Development of lipid particles targeted via sugar-lipid conjugates as novel nuclear gene delivery system. *Biomaterials* **29**(6): 709-723 (2008).

[13] Neu, M., Fischer, D., and Kissel, T. Recent advances in rational gene transfer vector design based on poly(ethylene imine) and its derivatives. *J Gene Med* **7**(8): 992-1009 (2005).

[14] Wang, J., Gao, S., Zhang, P., Wang, S., Mao, M., and Leong, K. Polyphosphoramidate gene carriers: effect of charge group on gene transfer efficiency. *Gene Ther* **11**(12): 1001-1010 (2004).

[15] Midoux, P. and Monsigny, M. Efficient gene transfer by histidylated polylysine pDNA complexes. *Bioconjug Chem* **10**(3): 406-411 (1999).

[16] Putnam, D., Gentry, C., Pack, D., and Langer, R. Polymer-based gene delivery with low cytotoxicity by a unique balance of side-chain termini. *Proc Natl Acad Sci U S A* **98**(3): 1200-+ (2001).

[17] Ferruti, P., Fere, A., and Bettelli, A. High polymers of acrylic and methacrylic esters of N-hydroxysuccinimide as polyacrylamide and polymethacrylamide precursors. *Polymer* **13**(10): 462-& (1972).

[18] Godwin, A., Hartenstein, M., Muller, A., and Brocchini, S. Narrow molecular weight distribution precursors for polymer-drug conjugates. *Angewandte Chemie - International Edition* **40**(3): 594-597 (2001).

[19] Shunmugam, R. and Tew, G. Efficient route to well-characterized homo, block, and statistical polymers containing terpyridine in the side chain. *J. Polym. Sci., Part A: Polym. Chem.* **43**(23): 5831-5843 (2005).

[20] Matyjaszewski, K., Pintauer, T., and Gaynor, S. Removal of copper-based catalyst in atom transfer radical polymerization using ion exchange resins. *Macromolecules* **33**(4): 1476-1478 (2000).

[21] Wong, S. and Putnam, D. Overcoming limiting side reactions associated with an NHS-activated precursor of polymethacrylamide-based polymers. *Bioconjug Chem* **18**(3): 970-982 (2007).

[22] Danielsen, S., Maurstad, G., and Stokke, B. DNA-polycation complexation and polyplex stability in the presence of competing polyanions. *Biopolymers* **77**(2): 86-97 (2005).

[23] Danielsen, S., Strand, S., Davies, C., and Stokke, B. Glycosaminoglycan destabilization of DNA-chitosan polyplexes for gene delivery depends on chitosan chain length and GAG properties. *Biochimicha et Biophysica Acta - General Subjects* **1721**(1-3): 44-54 (2005).

[24] Zelikin, A., Trukhanova, E., Putnam, D., Izumrudov, V., and Litmanovich, A. Competitive reactions in solutions of poly-L-histidine, calf thymus DNA, and synthetic polyanions: Determining the binding constants of polyelectrolytes. *J Am Chem Soc* **125**(45): 13693-13699 (2003).

[25] Abdelhady, H., Allen, S., Davies, M., Roberts, C., Tendler, S., and Williams, P. Direct real-time molecular scale visualisation of the degradation of condensed DNA complexes exposed to DNase I. *Nucleic Acids Research* **31**(14): 4001-4005 (2003).

[26] Lechardeur, D., Sohn, K., Haardt, M., Joshi, P., Monck, M., Graham, R., Beatty, B., Squire, J., O'brodovich, H., and Lukacs, G. Metabolic instability of plasmid DNA in the cytosol: a potential barrier to gene transfer. *Gene Ther* **6**(4): 482-497 (1999).

[27] Schaffer, D. and Lauffenburger, D. Optimization of cell surface binding enhances efficiency and specificity of molecular conjugate gene delivery. *J Biol Chem* **273**(43): 28004-28009 (1998).

[28] Huth, S., Hoffmann, F., Von Gersdorff, K., Laner, A., Reinhardt, D., Rosenecker, J., and Rudolph, C. Interaction of polyamine gene vectors with RNA leads to the dissociation of plasmid DNA-carrier complexes. *J Gene Med* **8**(12): 1416-1424 (2006).

[29] Schaffer, D., Fidelman, N., Dan, N., and Lauffenburger, D. Vector unpacking as a potential barrier for receptor-mediated polyplex gene delivery. *Biotechnol Bioeng* **67**(5): 598-606 (2000).

[30] Putnam, D. Polymers for gene delivery across length scales. *Nat Mater* **5**(6): 439-451 (2006).

[31] Mislick, K. and Baldeschwieler, J. Evidence for the role of proteoglycans in cation-mediated gene transfer. *Proc Natl Acad Sci U S A* **93**(22): 12349-12354 (1996).

[32] Medina-Kauwe, L., Xie, J., and Hamm-Alvarez, S. Intracellular trafficking of nonviral vectors. *Gene Ther* **12**(24): 1734-1751 (2005).

[33] Akinc, A., Thomas, M., Klibanov, A., and Langer, R. Exploring polyethylenimine-mediated DNA transfection and the proton sponge hypothesis. *J Gene Med* **7**(5): 657-663 (2005).

[34] Boussif, O., Lezoualch, F., Zanta, M., Mergny, M., Scherman, D., Demeneix, B., and Behr, J. A versatile vector for gene and oligonucleotide transfer into cells in culture and *in-vivo* - polyethylenimine. *Proc Natl Acad Sci U S A* **92**(16): 7297-7301 (1995).

[35] Boeckle, S., Von Gersdorff, K., Van Der Piepen, S., Culmsee, C., Wagner, E., and Ogris, M. Purification of polyethylenimine polyplexes highlights the role of free polycations in gene transfer. *J Gene Med* **6**(10): 1102-1111 (2004).

[36] Godbey, W., Ku, K., Hirasaki, G., and Mikos, A. Improved packing of poly(ethylenimine)/DNA complexes increases transfection efficiency. *Gene Ther* **6**(8): 1380-1388 (1999).

[37] Kunath, K., Von Harpe, A., Fischer, D., and Kissel, T. Galactose-PEI-DNA complexes for targeted gene delivery: degree of substitution affects complex size and transfection efficiency. *J Control Release* **88**(1): 159-172 (2003).

[38] Godbey, W., Wu, K., and Mikos, A. Size matters: Molecular weight affects the efficiency of poly(ethylenimine) as a gene delivery vehicle. *J Biomed Mater Res* **45**(3): 268-275 (1999).

[39] Plank, C., Mechtler, K., Szoka, F., and Wagner, E. Activation of the complement system by synthetic DNA complexes: A potential barrier for intravenous gene delivery. *Hum Gene Ther* **7**(12): 1437-1446 (1996).

[40] Plank, C., Zatloukal, K., Cotten, M., Mechtler, K., and Wagner, E. Gene-transfer into hepatocytes using asialoglycoprotein receptor mediated endocytosis of DNA complexed with an artificial tetra-antennary galactose ligand. *Bioconjug Chem* **3**(6): 533-539 (1992).

[41] Wolfert, M., Dash, P., Nazarova, O., Oupicky, D., Seymour, L., Smart, S., Strohalm, J., and Ulbrich, K. Polyelectrolyte vectors for gene delivery: Influence of cationic polymer on biophysical properties of complexes formed with DNA. *Bioconjug Chem* **10**(6): 993-1004 (1999).

[42] Dervan, P. and Edelson, B. Recognition of the DNA minor groove by pyrrole-imidazole polyamides. *Curr Opin Struct Biol* **13**(3): 284-299 (2003).

[43] Thomas, M. and Klibanov, A. Enhancing polyethylenimine's delivery of plasmid DNA into mammalian cells. *Proc Natl Acad Sci U S A* **99**(23): 14640-14645 (2002).

[44] Honore, I., Grosse, S., Frison, N., Favatier, F., Monsigny, M., and Fajac, I. Transcription of plasmid DNA: Influence of plasmid DNA/polyethylenimine complex formation. *J Control Release* **107**(3): 537-546 (2005).

[45] Burke, R. and Pun, S. Extracellular barriers to in Vivo PEI and PEGylated PEI polyplex-mediated gene delivery to the liver. *Bioconjug Chem* **19**(3): 693-704 (2008).

[46] Eldred, S.E., Pancost, M.R., Otte, K.M., Rozema, D., Stahl, S.S., and Gellman, S.H. Effects of side chain configuration and backbone spacing on the gene delivery properties of lysine-derived cationic polymers. *Bioconjug Chem* **16**(3): 694-699 (2005).

[47] Liu, Y.M. and Reineke, T.M. Hydroxyl stereochemistry and amine number within poly(glycoamidoamine)s affect intracellular DNA delivery. *J Am Chem Soc* **127**(9): 3004-3015 (2005).

[48] Zugates, G.T., Tedford, N.C., Zumbuehl, A., Jhunjhunwala, S., Kang, C.S., Griffith, L.G., Lauffenburger, D.A., Langer, R., and Anderson, D.G. Gene delivery properties of end-modified polyo(beta-amino ester)s. *Bioconjug Chem* **18**(6): 1887-1896 (2007).

[49] Van De Wetering, P., Moret, E., Schuurmans-Nieuwenbroek, N., Van Steenbergen, M., and Hennink, W. Structure-activity relationships of water-soluble cationic methacrylate/methacrylamide polymers for nonviral gene delivery. *Bioconjug Chem* **10**(4): 589-597 (1999).

[50] Jones, R., Poniris, M., and Wilson, M. (P)DMAEMA is internalised by endocytosis but does not physically disrupt endosomes. *J Control Release* **96**(3): 379-391 (2004).

[51] Takigawa, D. and Tirrell, D. Disruption of phospholipid packing by branched poly(ethylenimine) derivatives. *Macromolecules* **18**(3): 338-342 (1985).

CHAPTER 5

EFFECTS OF THE POLYDISPERSITY INDEX OF POLYMERIC VECTORS ON GENE DELIVERY

5.1. ABSTRACT

The molecular weight distribution, or polydispersity index (PDI), of polymeric vectors has been implicated as an important parameter for gene delivery. Yet, direct investigation of the functional role that PDI may have on the transfection capacity of polymeric gene delivery systems has been scarce in the literature. In this report, we examined the effects of the PDI on the *in vitro* transfection efficiency and biophysical properties of one class of polymeric vectors. Two polymer libraries, both with identically-formulated polymeric vector candidates, were evaluated - 1) a low PDI library comprising polymers with PDI=1.3 and 2) a high PDI library comprising polymers with PDI =2.0. The results from this study showed that polymers with a high PDI, in general, mediated higher levels of transfection compared to equivalent polymers with a low PDI. The effects of PDI on transfection were found to be molecular weight (MW)-specific. Polymers with a MW = 30 kDa and PDI = 2.0 by and large possessed greater transfection efficiencies than equivalent polymers with PDI=1.3. In contrast, PDI effects on 50 kDa polymers were more formulation-specific with high PDI polymers affording greater levels of transfection in some cases while offering a negligible difference in others. Particularly interesting were three high PDI polymers that mediated transfection levels three-fold greater than branched PEI (25 kDa), while maintaining superior cell viability profiles. Biophysical characterization revealed that high PDI polymers may provide greater polyplex stability than their low PDI counterparts, which may prevent premature polyplex dissociation and enhance

cellular delivery. Collectively, these results show that the molecular weight distribution of polymeric vectors can significantly influence their biophysical properties and enhance transfection efficiency and is an important structural attribute that should be considered in the design of polymeric gene delivery systems.

5.2. INTRODUCTION

The development of polymer-based gene delivery systems has been an active and important area of research for over two decades. [1, 2] Numerous studies investigating the functional roles that various chemical and structural polymeric features play in the gene transfer process have emerged. Such structure-function studies have revealed the significance and strategic opportunities that these polymeric attributes may provide toward enhancing the transfection capacity of polymeric gene vectors. Surprisingly, there has been little research to investigate the effects of an important characteristic of synthetic polymers – the molecular weight distribution, or polydispersity index (PDI). [3]

Conventional wisdom suggests that monodisperse polymers offer more uniform and well defined biophysical properties, which presumably translate to better transfection capacities. [4] Indeed, several studies have suggested the importance of PDI on gene delivery by investigating polymers with comparable PDIs while varying other polymeric attributes such as molecular weight, polymer backbone formulation, and side chain composition. [5-7] However, studies that investigate comparable polymeric vectors with different PDIs have been scarcely reported in the existing literature. [8]

As a step toward a more critical analysis of the effects of PDI on polymer-mediated transfection, we have evaluated two libraries of polymeric vectors, each

comprising identically-formulated polymers, but with different PDIs. Polymers with a PDI of 1.3 were synthesized to represent the low PDI library and polymers with a PDI of 2.0 represented the high PDI library. Characterization of the polymeric vectors included *in vitro* transfection capacity, polyplex size, zeta potential, relative binding affinity, polyplex stability, buffering capacity, and cytotoxicity.

The results from this study showed that polymers with a high PDI, in general, mediated higher levels of transfection compared to equivalent polymers with a low PDI. Three high PDI formulations were identified to possess transfection capacities superior to branched PEI (25 kDa), while maintaining more favorable cell viability profiles. Biophysical characterization revealed that high PDI polymers may provide greater polyplex stability than their low PDI counterparts, which may prevent premature polyplex dissociation and enhance cellular delivery. The results from this study show that the molecular weight distribution of polymeric vectors can significantly influence their biophysical properties and enhance transfection efficiency and is an important structural attribute that should be considered in the design of polymeric gene delivery systems.

5.3. MATERIALS AND METHODS

5.3.1. Reagents

All chemicals were purchased from Sigma-Aldrich without further purification unless otherwise specified. Cell culture reagents were purchased from Gibco® (Carlsbad, CA), pCMV-luc reporter gene plasmid was purchased from Elim Biopharmaceuticals (Hayward, CA), and reporter gene assays were purchased from Promega (Madison, WI).

5.3.2. General procedure for the synthesis and characterization of homopolymer precursor, poly(methacryloxysuccimimide) (poly(MAOS))

The monomer, *N*-methacryloxysuccinimide was synthesized as previously reported. [9] Details of the synthetic protocol for the polymer precursor, poly(MAOS), with a polydispersity index of 1.3 have been previously reported by our group. [10] In brief, a 5 ml pear shaped flask with a flea magnetic stir bar was fitted with a rubber septum and flame dried while purging with N_2(g), then cooled to ambient temperature. Cu(I)Br, Cu(II)Br_2, and the ligand were added to the flask and resealed with the septum. Solvent that was purged with N_2(g) for ten minutes prior to use was injected into the flask and the contents were stirred under a nitrogen atmosphere for approximately ten minutes until dissolved. *N*-methacryloxysuccinimide was added to the flask and allowed to dissolve for another ten minutes. The initiator, ethyl-2-bromoisobutyrate, was directly injected through the septum into the flask with a Hamilton syringe and immersed into a thermostated oil bath. To stop the polymerization, the flask was quenched in an ice bath and the product was dissolved with anhydrous DMF at a 1:3.75 (w/w) ratio of monomer:DMF. Approximately 20 mg of Dowex® Marathon® MSC hydrogen ion exchange resin was added to the redissolved solution and allowed to stir for approximately ten minutes. The ion exchange resin was added to remove any active copper catalysts remaining in the solution. [11] The final polymer was isolated as a white powder by precipitation into stirring acetone. The precipitated polymer was filtered through a fine-fritted Buchner funnel, washed three times with fresh acetone, and dried overnight *in vacuo*. Reaction conditions for the synthesis of the low PDI polymer precursors are summarized in Table 5-1.

Polymer precursors with a polydispersity index of 2.0 were synthesized with a slight modification to a previously reported method. [12] The initiator used to

synthesize the high PDI precursors, azobisisobutyronitrile (AIBN), was recrystallized in methanol prior to use. For polymer precursor synthesis, a 10 mL round bottom flask with a flea magnetic stir bar was fitted with a rubber septum and flame dried while purging with N_2(g), then cooled to ambient temperature. *N*-methacryloxysuccinimide and AIBN were added to the flask and resealed with the rubber septum. The reaction solvent, acetone, was purged with N_2(g) for ten minutes before injecting with a Hamilton syringe through the septum into the reaction flask. The contents were stirred under a nitrogen atmosphere for approximately ten minutes until dissolved. The reaction flask was then immersed into a thermostated oil bath for 24 hours during which polymer precipitated out of solution. To stop the polymerization, the flask was quenched in an ice bath. The precipitated polymer was filtered through a fine-fritted Buchner funnel, washed three times with fresh acetone, and dried overnight *in vacuo*. Reaction conditions for the synthesis of the high PDI polymer precursors are summarized in Table 5-1.

Molecular weight and polydispersity index were determined by hydrolyzing poly(MAOS) to its sodium salt form. Upon dissolving poly(MAOS) in DMSO at a 1:8.8 (w/w) ratio of poly(MAOS):DMSO, a two-fold excess of 5M NaOH was added dropwise to the reaction and allowed to stir for 7 hours at room temperature. The cloudy solution was redissolved in filtered deionized water at a 1:80 (w/w) ratio of poly(MAOS):water and allowed to stir overnight at room temperature. The solution was then dialyzed against deionized water using Spectra/Por regenerated cellulose tubing (MWCO 3500 Da) for three days. The dialysate was subsequently lyophilized to give a white powder.

The molecular weight and polydispersity index of each poly(MAOS) precursor were evaluated via gel permeation chromatography of the hydrolyzed sodium salt. The chemical composition of the polymer precursor was confirmed via ^{1}H NMR

spectroscopy. The details of the characterization protocol for both methods are provided in our previous report. [13] Table 5-1 summarizes the molecular weight and polydispersity index values determined for each of the polymer precursors used in the present study.

Table 5-1. Conditions and results for the synthesis of homopolymer precursor, poly(methacryloxysuccinimide)

I) Low polydispersity library - synthesis via atom transfer radical polymerization (Ref. 10)

	monomer : ethyl 2-bromoisobutyrate : CuBr : 2,2'-dipyridyl : Cu(II)Br_2 (molar ratio)	Reaction solvent (wt solvent:wt monomer)	Temperature (°C)	Reaction time	Mp (kDa)	Polydispersity index
1	50 : 1 : 1 : 2 : 1	anhydrous DMSO (150%)	100	10 mins	29	1.26
2	200 : 1 : 1 : 2 : 1	anhydrous DMSO (125%)	100	15 mins	49	1.25

II) High polydispersity library - synthesis via free radical polymerization

	monomer : azobisisobutyronitrile (wt : wt)	Reaction solvent (wt solvent:wt monomer)	Temperature (°C)	Reaction time	Mp (kDa)	Polydispersity index
1	4.5 : 1	acetone (700%)	50	24 hrs	34	1.95
2	18 : 1	acetone (700%)	50	24 hrs	49	1.97

5.3.3. General procedure for the synthesis and characterization of functionalized polymers

The details of the mono- and bi-functionalized polymer syntheses have been previously reported by our group. [13] Briefly, a 5 ml pear shaped flask with flea magnetic stir bar was fitted with a rubber septum and flame dried while purging with N_2(g) until cooled to ambient temperature. Poly(MAOS) was added to the flask and dissolved with deoxygenated anhydrous DMSO at a 1:26.4 (w/w) ratio of poly(MAOS):DMSO. Upon dissolution of the contents, 5 equivalents of the NH_2-containing functional group was dropwise added via a Hamilton syringe and immersed in a 75 °C thermostated oil bath. For the binary conjugations, the first NH_2-containing

functional group was dropwise added via a Hamilton syringe followed immediately by dropwise addition of the second NH_2-containing functional group via a separate Hamilton syringe. After 24 hours, the septum was replaced with a punctured piece of Parafilm and placed *in vacuo* for 4 hours to remove excess solvent. The final product was isolated via dropwise addition into stirring acetone and filtered through a fine fritted Buchner funnel and washed twice with acetone, twice with diethyl ether, and dried overnight *in vacuo*. *N*-Boc-protected functionalized polymers were isolated via dropwise addition into diethyl ether. The gummy precipitate was redissolved in methylene chloride and reprecipitated into diethyl ether to give a white flaky powder. The powder was filtered through a fine fritted Buchner funnel and immediately deprotected with 20 equivalents of neat trifluoroacetic acid for 8 minutes. The final product was isolated via dropwise addition into stirring diethyl ether and filtered through a fine fritted Buchner funnel. All functionalized polymers were redissolved in and dialyzed against 0.1N HCl in Spectra/Por regenerated cellulose tubing (MWCO 3500 Da) for 4 days. The dialysate was subsequently lyophilized to give a flaky solid.

Conjugation profiles of the functionalized polymers were characterized by UV/Vis spectrophotometry and ^{1}H NMR spectroscopy. The details and results of the characterization protocol for both methods are provided in our previous report. [10]

5.3.4. Cell culture

The murine embryonic fibroblast NIH/3T3 cell line was purchased from the American Type Culture Collection (Manassas, VA). Cells were cultured in Dulbecco's Modified Eagle Medium (DMEM) supplemented with 10% v/v fetal calf serum, 100 units/mL penicillin, and 100 μg/mL streptomycin. Cells were grown at

37°C and 5% CO_2 to an approximately 70% confluent monolayer and passaged every 3-4 days.

5.3.5. Preparation of polymer-DNA complex (polyplex) transfection solutions and free polymer cytotoxicity solutions

For each unique polymer, five polymer:DNA (w:w) ratios were evaluated – 0.5:1, 1:1, 2.5:1, 5:1, and 10:1. First, 140 μL of polymer solution for each ratio was prepared by combining the appropriate volume of 1.5 mg/mL polymer stock solution with 10 mM HEPES buffer (pH 7.2) such that each 150 μL of polyplex transfection solution contained the intended amount of polymer required to condense 3 μg of plasmid. Polymer solutions were briefly vortexed before adding 140 μL of pCMV-luc stock solution (150 μg/mL pCMV-luc in 10mM HEPES buffer, pH 7.2) to each of the 140 μL of polymer solution. The polymer/DNA mixture was then vortexed for five seconds and incubated at room temperature for 15 minutes to allow for complex formation. Serum-free OPTI-MEM I® medium (770 μL) was added to each polyplex solution and briefly vortexed to form the final polyplex transfection solution.

For the free polymer cytotoxicity solutions, 140 μL polymer solutions for each polymer:DNA ratio were prepared as previously described. Then, 140 μL of 10 mM HEPES buffer (pH 7.2) and 770 μL of OPTI-MEM I® medium were added to each solution and briefly vortexed to form the final free polymer cytotoxicity solution.

5.3.6. Plasmid DNA (pCMV-luc) transfection

NIH/3T3 cells were grown in clear and opaque, flat-bottomed tissue culture polystyrene 96-well plates (Costar, Corning, NY) at an initial density of 5,000 cells/well in 200 μL of phenol red-free, supplemented DMEM. Following 24 hours of

incubation at 37°C and 5% CO_2, the growth medium was removed and replaced with 150 μL of polyplex transfection solution, which was prepared as described previously. Each 150 μL aliquot of transfection solution contained 3 μg of plasmid DNA. Cells were incubated with the polyplexes for 4 hours, after which the complex-containing medium was aspirated and replaced with 100 μL of phenol red-free, supplemented DMEM. Following 44 hours of additional incubation at 37°C and 5% CO_2, opaque plates were assayed for luciferase expression using the Bright-Glo™ Luciferase Assay (Promega, Madison, WI) and clear plates were assayed for total protein content using the BCA™ Protein Quantitation Assay (Pierce Biotechnology, Rockford, IL). All polymers were evaluated in triplicate. Transfection results are expressed as the ratio of relative light units to absorbance at 562 nm.

5.3.7. Bright-Glo™ luciferase assay

After a total incubation time of 48 hours from the time of polyplex solution addition, growth medium was aspirated and each well was rinsed with 200 μL of phosphate buffered saline (pH 7.4). In a Veritas™ Microplate Luminometer (Turner Biosystems, Sunnyvale, CA) 100 μL of Bright-Glo™ working solution, prepared according to the manufacturer's direction, was added to each well of the opaque 96-well plate. After two minutes of incubation at room temperature, luciferase expression was quantified as the relative light units measured in the luminometer.

5.3.8. BCA™ protein quantitation assay

After a total incubation time of 48 hours from the time of polyplex solution addition, growth medium was aspirated and each well was rinsed with 200 μL of phosphate buffered saline (pH 7.4). RIPA buffer (20 μL) (Pierce Biotechnology,

Rockford, IL) was added to each well of the clear 96-well plate and incubated at room temperature for 10 minutes with gentle shaking. BCA™ working reagent (200 μL) (Pierce Biotechnology, Rockford, IL), prepared according to the manufacturer's directions, was then added to each well and gently shaken for 30 seconds at room temperature. Plates were incubated at 37°C and 5% CO_2 for one hour before being read at 562 nm on a Molecular Devices SpectraMax Plus^{384} UV/Vis spectrophotometer.

5.3.9. Relative binding affinity and polyplex stability assay

The relative degree of electrostatic binding between DNA and polymer in the absence and presence of a competing polyanion was measured using ethidium bromide (EtBr) (Fisher Scientific, Pittsburgh, PA) fluorescence quenching and recovery. [14-16] Heparin sodium salt (4.38 mM) dissolved in 10mM HEPES buffer (pH 7.2) was used as the competing polyanion. [15] A free polymer solution (180 μL) for each polymer:DNA ratio was prepared by combining the appropriate volume of 1.5 mg/mL polymer stock solution with 10mM HEPES buffer (pH 7.2) such that each 50 μL aliquot resulted in the intended w:w ratio of polymer and pCMV-luc. A stock solution of EtBr/DNA was made by combining equal volumes of pCMV-luc (150 μg/mL pCMV-luc in 10mM HEPES buffer, pH 7.2) and EtBr (0.1095mM EtBr in 10mM HEPES buffer, pH 7.2) stock solutions, resulting in a 4:1 ratio of phosphate groups to EtBr monomer units. All fluorescence readings were obtained in a Molecular Devices SpectraMax GeminiXS at λ_{ex} = 535 nm and λ_{em} = 595nm (automatic calibration, 10 seconds of mixing prior to reading, and automatic sensitivity of PMT detector). All polymers were evaluated in triplicate.

First, 100 μL of EtBr/DNA solution was added to each well of a black polystyrene 96-well plate (Costar, Corning, NY) and the fluorescence was measured. An aliquot of 50 μL of free polymer solution was then added to each EtBr/DNA-containing well, gently shaken at room temperature on a microplate shaker for 15 minutes, and the fluorescence measured again. A 50 μL aliquot of 4.38 mM heparin was added to each well, gently shaken at room temperature on a microplate shaker for 4 hours, and the fluorescence measured for a final time. The relative binding affinity (BA) and relative binding strength (BS) were calculated from the following equations:

$$BA = \frac{F_{E/D} - F_{polymer}}{F_{E/D}} \qquad (5.1)$$

$$BS = \frac{F_{E/D} - F_{hep}}{F_{E/D} - F_{polymer}} \qquad (5.2)$$

where $F_{E/D}$ is the corrected fluorescence of EtBr/DNA in the absence of polymeric vector; $F_{polymer}$ is the corrected fluorescence of EtBr/DNA in the presence of polymeric vector; F_{hep} is the corrected fluorescence of EtBr/DNA in the presence of polymeric vector and heparin.

All fluorescence measurements were corrected by subtracting background fluorescence due to free EtBr and due to volume effects. Background values from free EtBr were obtained from triplicate wells, on each 96 well plate, containing EtBr and 10mM HEPES buffer for the first two fluorescence readings and EtBr, HEPES buffer, and heparin for the final fluorescence measurement. Background values due to volume effects were determined from triplicate wells, on each 96 well plate,

containing EtBr/DNA and HEPES buffer in volumes equal to those added to the polymer samples.

5.3.10. Polyplex size and zeta potential measurement

A 140 μL solution of free polymer was prepared for each polymer:DNA ratio by combining the appropriate volume of 1.5 mg/mL polymer stock solution with 10 mM HEPES buffer (pH 7.2) such that the final 1.05 mL polyplex solution contained the intended w:w ratio of polymer and pCMV-luc. Polymer solutions were briefly vortexed before adding 140 μL of pCMV-luc stock solution (150 μg/mL pCMV-luc in 10mM HEPES buffer, pH 7.2) to each of the 140 μL of free polymer solution. The polymer:DNA mixture was vortexed for five seconds and incubated at room temperature for 15 minutes to allow for complex formation. Then, 770 μL of 10mM HEPES buffer (pH 7.2) was added to each polymer:DNA solution and briefly vortexed to form the final polyplex solution used in both sizing and zeta potential measurements.

Size and zeta potential characterizations were performed using the Nanosizer Nano ZS (Malvern Instruments). The refractive index and viscosity values of water were used as parameter inputs. Malvern Dispersion Technology Software was used for data acquisition and analysis, applying the general purpose algorithm for calculating size distributions and the Smoluchowski approximation for determining zeta potential.

5.3.11. Buffering capacity assay

Titration curves were generated for each polymer to assess their respective buffering capacities. First, 4 mg of polymer was dissolved in 10mL of 18.2MΩ

distilled water. Using a TitraLab 856 automatic titrator (Radiometer Analytical, Lyon, France), the pH of the polymer-containing solution was adjusted to 11.5 with 1 M NaOH (25 seconds pH stabilization time before and after the addition of NaOH at a rate of 0.06 mL/min) and subsequently titrated with 1M HCl until the solution was stabilized at pH 2 (25 seconds pH stabilization time before and after the addition of HCl at a rate of 0.06 mL/min). Hydrogen ion concentrations were monitored with TitraMaster 85 software v.1.2.1. Using the OriginPro 8 software, titration curves were fitted to a Boltzmann sigmoidal curve, from which the slope at the inflection point was determined. The buffering capacity of each polymer is expressed as the absolute value of the reciprocal slope.

5.3.12. MTS cell viability assay

NIH/3T3 cells were grown and incubated with the free polymer solution, which was prepared as described previously, according to the protocol described for pCMV-luc transfection. The final free polymer concentrations evaluated were 10, 20, 50, 100, and 200 μg/mL, which corresponded to the polymer:DNA weight ratios of 0.5:1, 1:1, 2.5:1, 5:1, and 10:1, respectively. For cell viability measurements of branched PEI, the additional free polymer concentrations of 1-9 μg/mL in increments of 1 μg/mL were evaluated. After 48 hours of total incubation and rinsing with 200 μL of phosphate buffered saline (pH 7.4), 20 μL of CellTitre 96® AQ_{ueous} One Solution Cell Proliferation Assay (MTS) reagent (Promega, Madison, WI) was added to each well. Plates were incubated for an additional two hours at 37°C, after which the absorbance at 490 nm of each well was read in a Molecular Devices SpectraMax Plus^{384} UV/Vis spectrophotometer. All polymers were evaluated in triplicate. Using the OriginPro 8 software, data points were fitted to a Boltzmann sigmoidal curve.

Cytotoxicity results are expressed as IC_{50} values and calculated as the concentration of free polymer, in micrograms per milliliter, at which the measured absorbance was one-half the absorbance measured at a polymer concentration of 0 μg/mL.

5.4. RESULTS AND DISCUSSION

Two libraries of polymeric vectors were evaluated to investigate the effects of the polydispersity index (PDI) on the transfection capacity of polymer-based gene delivery systems. Each library represented polymers that shared a common PDI – 1.3 or 2.0 - and comprised the same set of vector formulations. The polymeric vectors that constituted each PDI library were synthesized according to the synthetic scheme shown in Figure 5-1a, where one or two of the functional groups shown in Figure 5-1b were conjugated to the homopolymer precursor, poly(methacryloxysuccinimide). [13] The formulations of the functionalized polymeric vectors were chosen based on a previous study that identified such formulations to possess moderate to high transfection capacities. [10] For the present study, high levels of transfection were defined as having within the same order of magnitude or greater levels of transfection as 25 kDa branched PEI (b-PEI).

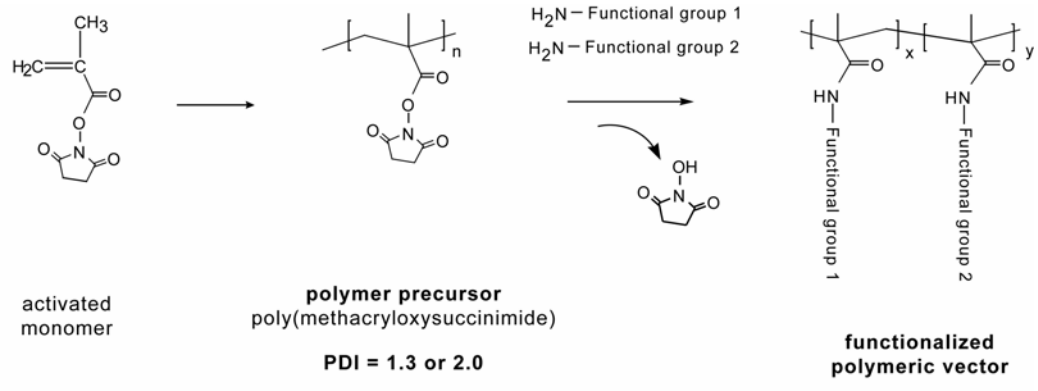

(a)

Figure 5-1. **a)** General synthetic scheme for polymer vectors. One or two NH_2-containing functional groups were conjugated to the homopolymer precursor, poly(methacryloxysuccimide), to form the mono- and bi-functionalized polymeric vectors. **b)** Functional groups conjugated to the polymer precursor

Figure 5-1 (*continued*)

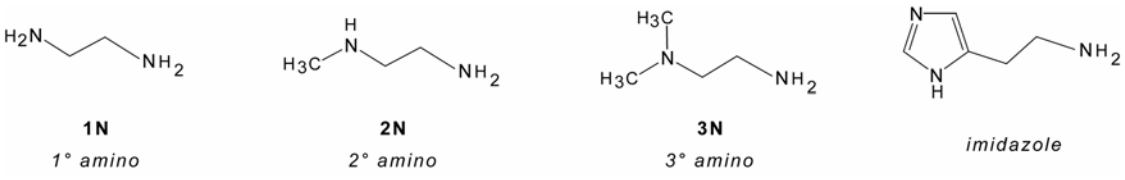

(b)

All polymers were assessed for their utility as gene delivery vectors by an *in vitro* luciferase reporter gene transfection assay on NIH/3T3 cells. [10] Figure 5-2 shows the transfection profiles of the low PDI and high PDI libraries. In general, polymers with a high PDI mediated moderately higher levels of transfection than polymers with a low PDI. An interesting observation was the MW-specific effects of PDI on transfection capacity. That is, amongst the 30 kDa polymers, those with a high PDI mediated greater levels of transfection compared to their low PDI counterparts. Whereas amongst the 50 kDa polymers, PDI effects were less consistent - some high PDI formulations possessed enhanced transfection capacities over their low PDI counterparts, while other formulations possessed diminished capacities or offered a negligible difference.

Closer examination of the highest performing polymers (i.e., polymers that mediated transfection efficiencies within an order of magnitude or greater than b-PEI) revealed several high PDI formulations that resulted in significant enhancements in transfection compared to both b-PEI and their low PDI counterparts. Figure 5-3 identifies the five high PDI formulations that resulted in statistically greater transfection efficiencies compared to their low PDI equivalents (labeled with *) and the three formulations that mediated transfection levels superior to b-PEI, with up to a three-fold improvement (labeled with †).

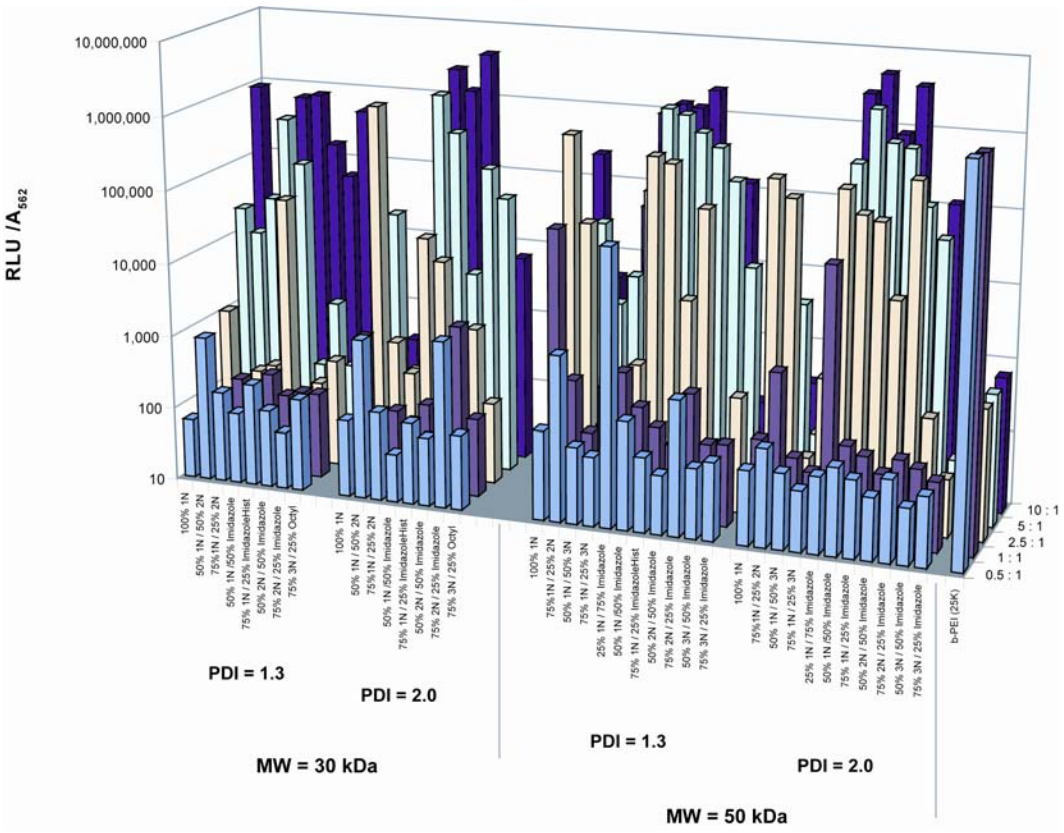

Figure 5-2. Transfection efficiencies of all polymers within the low polydispersity and high polydispersity (PDI) libraries. Transfection efficiencies are expressed as the measured relative light unit (RLU) of luciferase expression normalized to the UV/Vis absorbance at 562nm (BCA™ protein quantitation assay). Polymers were evaluated at the following polymer:DNA weight ratios – 0.5:1, 1:1, 2.5:1, 5:1, and 10:1. Polymers with PDI=1.3 represented the low PDI library and those with PDI=2.0 represented the high PDI library. All samples were performed in triplicate. Standard errors for samples with RLU/A_{562} ≥100,000 were typically within 30% of the average value (data not shown).

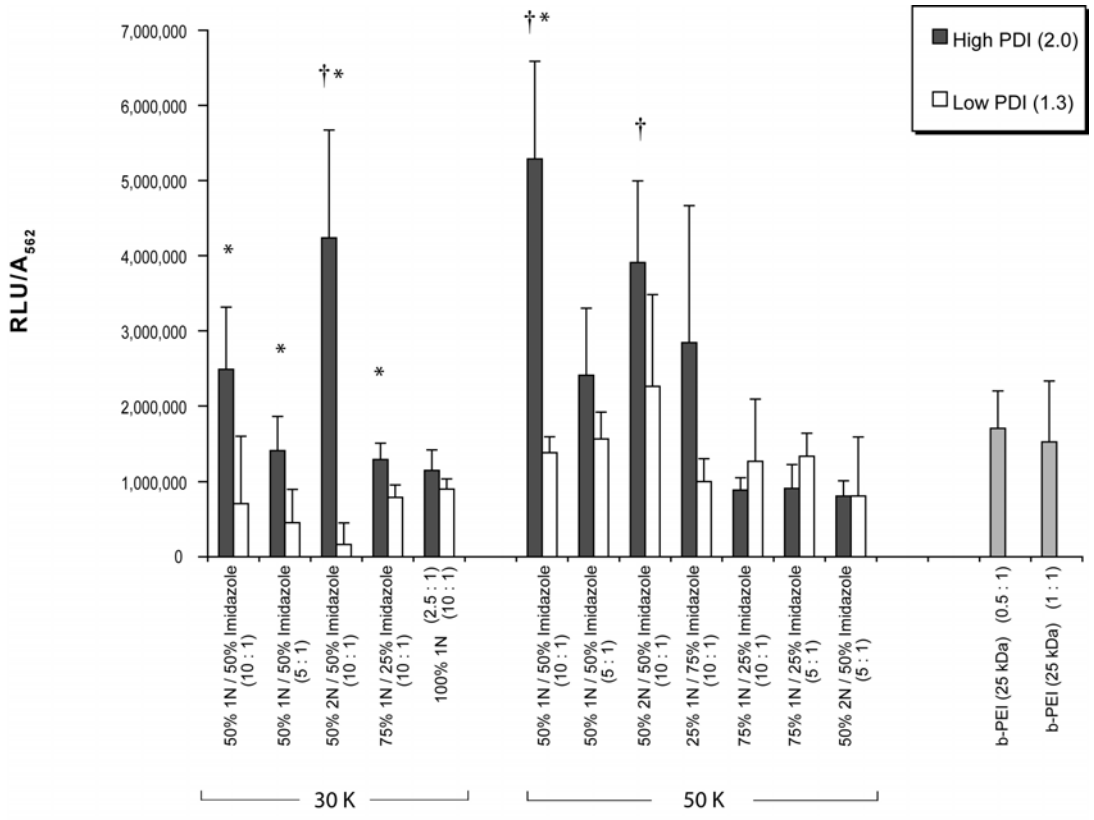

Figure 5-3. Transfection efficiencies of high-performing polymers at their optimal polymer:DNA weight ratios identified within the low and high polydispersity libraries. Transfection efficiencies are expressed as the measured relative light unit (RLU) of luciferase expression normalized to the UV/Vis absorbance at 562nm (BCA^{TM} protein quantitation assay). Asterisks (*) denote statistical significance between the low and high PDI polymers of the same molecular weight and formulation. Daggers (†) represent statistical significance compared to branched-PEI at a polymer:DNA weight ratio of 0.5:1. Statistical testing between samples was performed via a two-sample t-test assuming unknown variances with an alpha level of 0.05. Samples were performed in triplicate and error bars represent +/- one standard deviation.

To understand the transfection-enhancing effects of PDI, the biophysical properties of each polyplex were characterized to ascertain differences that might explain the divergent transfection profiles. The biophysical properties investigated in this study have been shown in previous reports to be important for the transfection efficiency of polymeric vectors. [2, 17-22] These properties include- the relative binding affinity, polyplex stability, net surface charge, and effective diameters of polyplexes; and the buffering capacity and cytotoxicity of free polymers.

Polymers with a high PDI, in general, had comparable buffering capacities and formed polyplexes that carried comparable zeta potentials as polymers with a low PDI (data not shown). Although the relative binding affinity between polymeric vector and DNA was observed to be different between equivalent polymers of different PDIs, the difference did not appear to trend with transfection in any correlative manner and was therefore considered unlikely to be a predominant factor in explaining the PDI effects on transfection (data not shown). The cytotoxicity levels and the size of resultant polyplexes formed by the high PDI polymers were generally greater than those of the low PDI polymers (data not shown). However, upon examining the cytotoxicity profiles of the highest transfecting polymers, most maintained superb cell viability as evidenced in Figure 5-4a, which shows that most of the high performing formulations were associated with an IC_{50} value greater than the maximum free polymer concentration exposed to cells (200 μg/mL). For comparison, the IC_{50} value of b-PEI was calculated to be approximately 4.8 μg/mL. Furthermore, in contrast to the general trend that high PDI polymers produced polyplexes with greater effective diameters, most of the high performing polyplexes were less than 200 nm in size (Figure 5-4b).

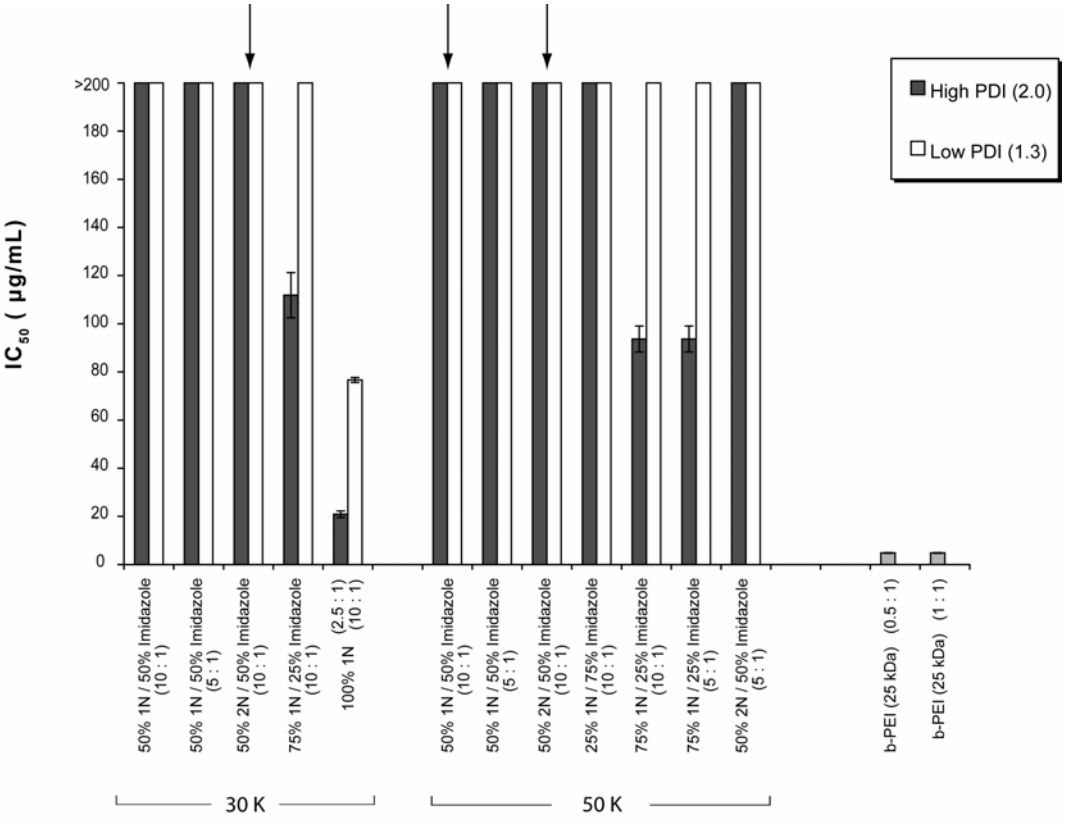

(a)

Figure 5-4 a) Cytotoxicity profiles of high-transfecting polymers. The *in vitro* cytotoxicity of each polymer was assessed by the MTS cell viability assay at the free polymer concentrations - 10, 20, 50, 100, and 200 µg/mL, which corresponded to the following polymer:DNA weight ratios evaluated in the transfection assay - 0.5:1, 1:1, 2.5:1, 5:1, and 10:1, respectively. Cytotoxicity results are expressed as IC_{50} values and calculated as the concentration of free polymer at which the measured absorbance (MTS cell viability assay) was one-half the absorbance measured at a polymer concentration of 0 µg/mL. **b)** Size of high-transfecting polyplexes. The polyplex size was measured using dynamic light scattering. Arrows indicate formulations that achieved transfection efficiencies superior to branched PEI. Cytotoxicity and sizing samples were performed in triplicate and error bars represent +/- one standard deviation. Polymers with an IC_{50} >200 µg/mL did not induce a decrease in absorbance by one-half at all free polymer concentrations evaluated. Thus, exact IC_{50} values for such samples and corresponding error bars are not shown.

Figure 5-4 (*continued*)

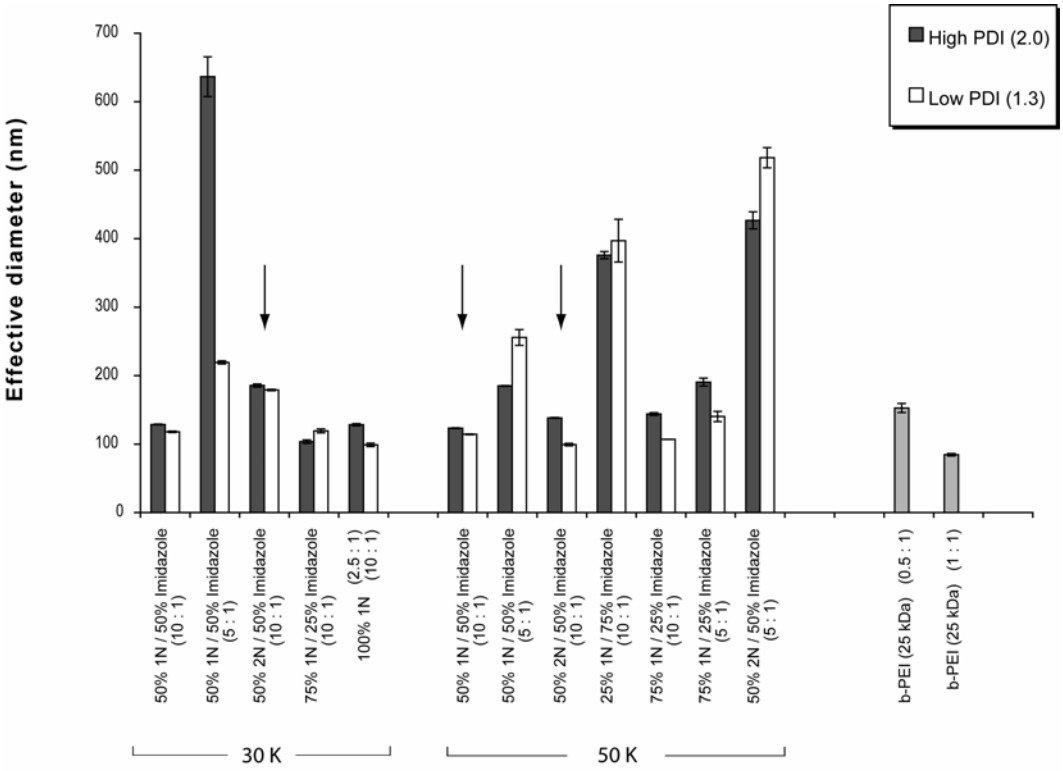

(b)

Of the biophysical properties evaluated in this study, the PDI of polymers had the most pronounced effect on the stability of resultant polyplexes. Similar to the MW-specific effects of PDI observed in transfection efficiency, the effect on polyplex stability also differed between the 30 kDa and 50 kDa polymers. Figure 5-5 shows the change in relative binding strengths between high PDI polymers and their low PDI counterparts, for all vector formulations, at the representative polymer:DNA weight ratio of 10:1.

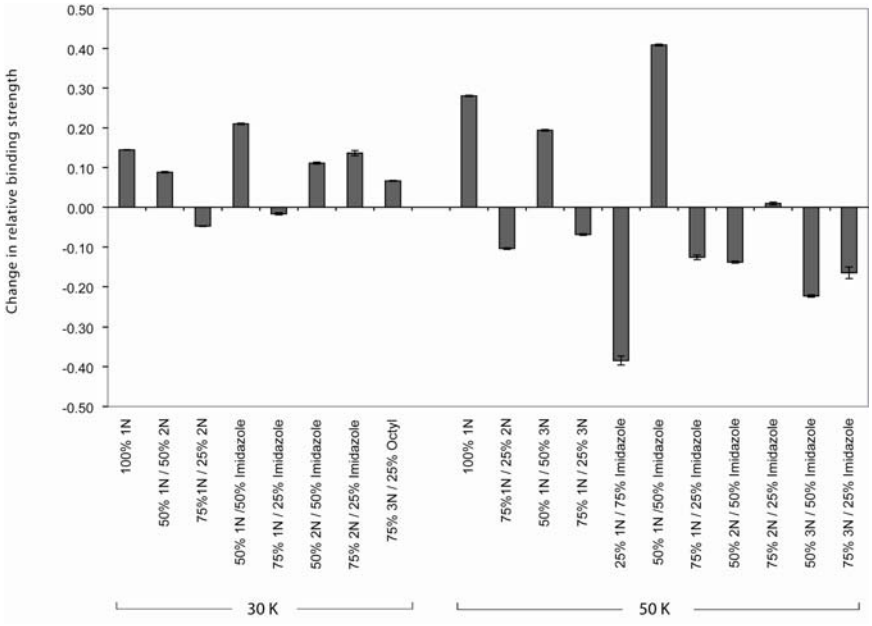

Figure 5-5. Change in relative binding strength between high polydispersity polymers and their low polydispersity (PDI) counterparts for all vector formulations. Shown are the results for each polymer at a polymer:DNA weight ratio of 10:1 as they are representative of the results obtained at the 5:1 and 2.5:1 weight ratios. Positive values represent higher binding strengths of high PDI polymers compared to their low PDI equivalents. Error bars represent the standard error associated with the calculated difference in average relative binding strengths between equivalent formulations at the low and high PDI values.

With few exceptions, high PDI polymers with a molecular weight of 30 kDa generally afforded more stable polyplexes than their low PDI/30 kDa equivalents. However, this general trend was reversed for the 50 kDa set of polymers - those with a high PDI produced polyplexes that were less stable and dissociated more readily in the presence of competing polyanions.

Interestingly, closer examination of the high PDI formulations that outperformed their low PDI counterparts (i.e., formulations labeled with an asterisk in Figure 5-3) revealed an anomaly to this trend (Figure 5-6). The single 50kDa/high PDI formulation that mediated a statistically greater level of transfection than its low PDI counterpart had over 330% greater binding strength. This result suggests that a

higher PDI may enhance the transfection capacity of polymeric vectors by producing more stable polyplexes that are more resistant to dissociating in the presence of competing polyanions, compared to equivalent polymeric vectors with a lower PDI.

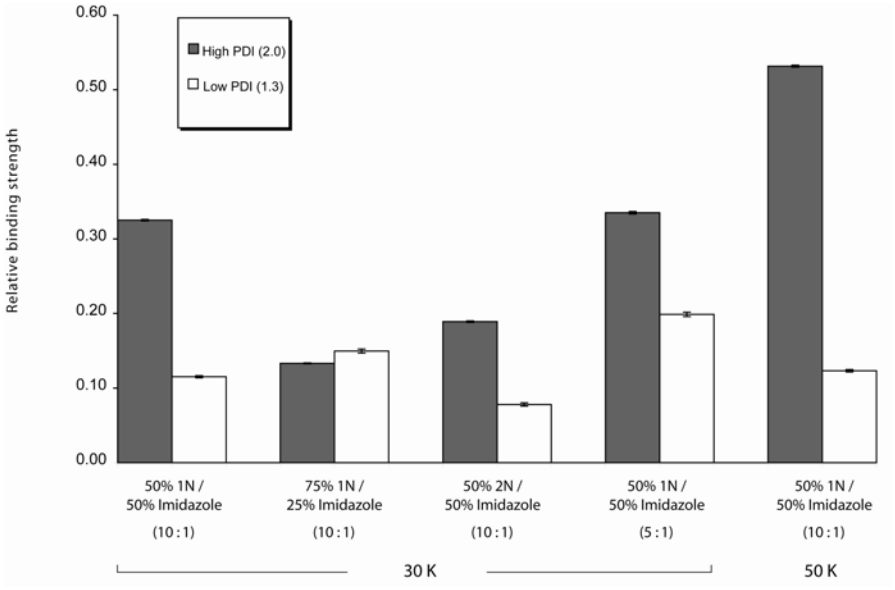

Figure 5-6. Relative binding strengths of formulations that achieved statistically greater levels of transfection than their low PDI counterparts. With only one exception, formulations with a high PDI had greater binding strengths than their respective low PDI formulation.

The underlying molecular mechanisms that govern the different binding stabilities observed between the low and high PDI polymers are not clearly understood. Possible insight may be afforded, however, by the interpolyelectrolyte exchange and substitution theory postulated and extensively investigated by Kabanov and coworkers. [23-26] Based on synthetic model polyions, they showed that in a polyelectrolyte system comprising a polycation and two polyanionic species, the polycation exists in dynamic electrostatic equilibrium with the polyanions, each of which exchange and substitute with the other, competing for interaction with the

polycation. [24] That is, polycation A electrostatically binds with polyanion B to form complex A/B. Polyanion B, meanwhile, undergoes electrostatic exchange with polyanion C to form complex A/C. The equilibrium that arises is the exchange between polyanions B and C to form complexes A/B and A/C, respectively.

Extending this investigation to polymeric gene delivery systems and employing DNA as one of the polyanions, they showed a similar exchange and substitution reaction between a polycationic vector and a synthetic polyanion, which represented competing biological polyanions that the polycation/DNA complex may encounter during the DNA delivery process. [24, 25] Moreover, they provided evidence that the molecular weight of the polycation may affect the dynamics of the equilibrium and consequently the degree to which the polycationic vector could protect the DNA cargo from enzymatic degradation within extra- and intracellular spaces and prevent its premature release before arriving at the cell nucleus.

Applying this theory to the present study, the polyplex transfection solution may be considered as a system of independent polycation chains ranging in MWs. In accordance with the MW dependence of the exchange and substitution reactions, the collective binding behavior of the polyplex solution will therefore be dictated by the range of the polycation MWs and the dynamic interplay between each polycation chain and DNA in the presence of a competing polyanion. Further, if we compare two polyplex solutions, each composed of polymers with different PDIs, but otherwise identical in composition and experimental conditions, then it follows that polymers with a higher PDI will offer a broader range of polyplex binding behavior compared to their lower PDI counterparts.

Based on the relative binding strengths of the high-transfecting polymers identified amongst the present system of polymers (Figure 5-6), it appeared that a broader range of binding behavior provided by certain high PDI formulations

enhanced the overall polyplex binding strength, which ultimately led to higher levels of transfection. These results agree well with those observed by Koping-Hoggard et al. in that both studies show a PDI-dependent effect on the transfection capacity and polyplex stability of polymeric vectors. [8]

The effect that a higher PDI appeared to have toward increasing polyplex stability also resembles the observations from a previous report that showed a similar effect of higher molecular weights on polyplex stability. [10] In both studies, enhanced transfection efficiencies were achieved by changes in a structural attribute of the polymeric vector that resulted in increased polyplex stability. Together, these results underscore the importance of polyplex stability and the requirement for polymeric vectors to prevent premature dissociation for enhanced cellular delivery. [27]

In conclusion, the results reported herein demonstrate that the molecular weight distribution of polymeric vectors can greatly influence their biophysical properties and transfection capacities. Contrary to the widely held assumption that polymers with near unity PDI values may result in greater transfection efficiencies, the polymers investigated in the present study with a PDI of 2.0 generally mediated higher levels of transfection than equivalent polymers with a PDI of 1.3. Moreover, three formulations, all with a PDI of 2.0, were identified in this study to achieve transfection levels that exceeded the popular polymeric vector, b-PEI. Biophysical characterization revealed that high PDI polymers may provide greater polyplex stability than equivalent polymers with a lower PDI, which may prevent premature polyplex dissociation and enhance cellular delivery. Thus, the molecular weight distribution of polymers is an important consideration in both the design of polymer-based gene delivery systems as well as the interpretation of transfection results that originate from polymers with disparate polydispersity indices.

REFERENCES

[1] Wong, S., Pelet, J., and Putnam, D. Polymer systems for gene delivery-past, present, and future. *Prog. Polym. Sci.* **32**(8-9): 799-837 (2007).

[2] Putnam, D. Polymers for gene delivery across length scales. *Nat. Mater.* **5**(6): 439-451 (2006).

[3] Gilbert, R.G. Molecular-weight distributions in free-radical polymerizations - their cause and cure. *Trends in Polymer Science* **3**(7): 222-226 (1995).

[4] Hunter, A.C. Molecular hurdles in polyfectin design and mechanistic background to polycation induced cytotoxicity. *Adv. Drug Delivery Rev.* **58**(14): 1523-1531 (2006).

[5] De Wolf, H., De Raad, M., Snel, C., Van Steenbergen, M., Fens, M., Storm, G., and Hennink, W. Biodegradable poly(2-dimethylamino ethylamino)phosphazene for in vivo gene delivery to tumor cells. Effect of polymer molecular weight. *Pharm. Res.* **24**(8): 1572-1580 (2007).

[6] Lee, C., Liu, Y., and Reineke, T. General structure-activity relationship for poly(glycoamidoamine)s: The effect of amine density on cytotoxicity and DNA delivery efficiency. *Bioconjug. Chem.* **19**(2): 428-440 (2008).

[7] Wang, J., Gao, S., Zhang, P., Wang, S., Mao, M., and Leong, K. Polyphosphoramidate gene carriers: effect of charge group on gene transfer efficiency. *Gene Ther.* **11**(12): 1001-1010 (2004).

[8] Koping-Hoggard, M., Varum, K., Issa, M., Danielsen, S., Christensen, B., Stokke, B., and Artursson, P. Improved chitosan-mediated gene delivery based on easily dissociated chitosan polyplexes of highly defined chitosan oligomers. *Gene Ther.* **11**(19): 1441-1452 (2004).

[9] Ferruti, P., Fere, A., and Bettelli, A. High polymers of acrylic and methacrylic esters of N-hydroxysuccinimide as polyacrylamide and polymethacrylamide precursors. *Polymer* **13**(10): 462-& (1972).

[10] Wong, S., Sood, N., and Putnam, D. Structure-function relationships of molecular weight, cations, pH-sensitive moeties, and hydrophobic residues deduced from a combinatorial library of polymeric gene vectors. *(in preparation)*:

[11] Matyjaszewski, K., Pintauer, T., and Gaynor, S. Removal of copper-based catalyst in atom transfer radical polymerization using ion exchange resins. *Macromolecules* **33**(4): 1476-1478 (2000).

[12] Nan, A., Croft, S.L., Yardley, V., and Ghandehari, H. Targetable water-soluble polymer-drug conjugates for the treatment of visceral leishmaniasis. *J. Control. Release* **94**(1): 115-127 (2004).

[13] Wong, S. and Putnam, D. Overcoming limiting side reactions associated with an NHS-activated precursor of polymethacrylamide-based polymers. *Bioconjug. Chem.* **18**(3): 970-982 (2007).

[14] Danielsen, S., Maurstad, G., and Stokke, B. DNA-polycation complexation and polyplex stability in the presence of competing polyanions. *Biopolymers* **77**(2): 86-97 (2005).

[15] Danielsen, S., Strand, S., Davies, C., and Stokke, B. Glycosaminoglycan destabilization of DNA-chitosan polyplexes for gene delivery depends on chitosan chain length and GAG properties. *BBA-GEN SUBJECTS* **1721**(1-3): 44-54 (2005).

[16] Zelikin, A., Trukhanova, E., Putnam, D., Izumrudov, V., and Litmanovich, A. Competitive reactions in solutions of poly-L-histidine, calf thymus DNA, and synthetic polyanions: Determining the binding constants of polyelectrolytes. *J. Am. Chem. Soc.* **125**(45): 13693-13699 (2003).

[17] Boeckle, S., Von Gersdorff, K., Van Der Piepen, S., Culmsee, C., Wagner, E., and Ogris, M. Purification of polyethylenimine polyplexes highlights the role of free polycations in gene transfer. *J. Gene Med.* **6**(10): 1102-1111 (2004).

[18] Abdelhady, H., Allen, S., Davies, M., Roberts, C., Tendler, S., and Williams, P. Direct real-time molecular scale visualisation of the degradation of condensed DNA complexes exposed to DNase I. *Nucleic Acids Res.* **31**(14): 4001-4005 (2003).

[19] Lechardeur, D., Sohn, K., Haardt, M., Joshi, P., Monck, M., Graham, R., Beatty, B., Squire, J., O'brodovich, H., and Lukacs, G. Metabolic instability of plasmid DNA in the cytosol: a potential barrier to gene transfer. *Gene Ther.* **6**(4): 482-497 (1999).

[20] Schaffer, D. and Lauffenburger, D. Optimization of cell surface binding enhances efficiency and specificity of molecular conjugate gene delivery. *J. Biol. Chem.* **273**(43): 28004-28009 (1998).

[21] Medina-Kauwe, L., Xie, J., and Hamm-Alvarez, S. Intracellular trafficking of nonviral vectors. *Gene Ther* **12**(24): 1734-1751 (2005).

[22] Godbey, W., Ku, K., Hirasaki, G., and Mikos, A. Improved packing of poly(ethylenimine)/DNA complexes increases transfection efficiency. *Gene Ther.* **6**(8): 1380-1388 (1999).

[23] Bakeev, K., Izumrudov, V., Kuchanov, S., Zezin, A., and Kabanov, V. Kinetics and mechanism of interpolyelectrolyte exchange and addition-reactions. *Macromolecules* **25**(17): 4249-4254 (1992).

[24] Izumrudov, V., Kargov, S., Zhiryakova, M., Zezin, A., and Kabanov, V. Competitive reactions in solutions of DNA and water-soluble interpolyelectrolyte complexes. *Biopolymers* **35**(5): 523-531 (1995).

[25] Kabanov, A. and Kabanov, V. DNA complexes with polycations for the delivery of genetic material into cells. *Bioconjug. Chem.* **6**(1): 7-20 (1995).

[26] Kabanov, A. and Kabanov, V. Interpolyelectrolyte and block ionomer complexes for gene delivery: Physicochemical aspects. *Adv. Drug Delivery Rev.* **30**(1-3): 49-60 (1998).

[27] Burke, R. and Pun, S. Extracellular barriers to in Vivo PEI and PEGylated PEI polyplex-mediated gene delivery to the liver. *Bioconjug. Chem.* **19**(3): 693-704 (2008).

CHAPTER 6

A SIMPLE AND ECONOMICAL HIGH – THROUGHPUT EQUILIBRIUM DIALYSIS SYSTEM

6.1. ABSTRACT

As high-throughput strategies become increasingly employed by a broader and more diverse research community, simple yet reliable technology will be critical to fully realize the benefits that high-throughput strategies can offer. In this report, we describe a robust 96-well equilibrium dialysis system designed to purify high molecular weight product from a mixture of low molecular byproducts in solution. The proposed high-throughput dialysis system offers important enhancements over both recently reported and commercially available systems in its easy integration with in-line automated high-throughput technology (e.g., robotic liquid and solid handling systems, 96-well plate readers), resistance to acidic environments, minimal creation of waste, and simple assembly. Moreover, the dialysis apparatus can be economically constructed from commercially available materials and easily fabricated in a standard machine shop. The validation protocol and detailed drawings presented herein can be readily modified and applied to other high-throughput platforms such as 6-, 24-, and 384-well microtiter plates.

6.2. INTRODUCTION

High-throughput technology (HTT) has transformed a broad and diverse range of research areas from DNA sequencing to compound synthesis to reaction protocol optimization. The small molecule pharmaceutical industry is perhaps one of the most

salient examples of this transformation. With the introduction of automated dispensing systems, thousands of compounds can be synthesized simultaneously in multiwell microtiter plates, replacing the arduous task of synthesizing individual compounds in separate reaction flasks. Coupling this technology with high throughput analytical equipment, the pace at which viable drug candidates can be identified and optimized has greatly accelerated [1].

Given the potential benefits of HTT for small molecule drug development, the extension of these strategies to a polymeric biomaterials application may seem natural considering both areas of research share similar organic synthesis processes. As such, we and others have adopted high-throughput strategies to facilitate the creation of polymer libraries for use in various biomedical research [2-4]. In particular, we have adopted HTT to facilitate the synthesis, purification, characterization, and screening of a combinatorial library of polymeric biomaterials. Each step is amenable to high-throughput processing within 96-well microtiter plates, with the exception of polymer purification from within the individual reaction wells. In smaller scale experiments where the number of polymers to purify is modest and each polymer solution is on the milliliter scale or greater, traditional equilibrium dialysis is a reliable and commonly used method for purifying a high molecular weight (MW) product. However, in high-throughput experiments on the microliter scale, transferring individual reaction batches into separate dialysis tubes can quickly become unmanageable and inefficient.

Several high-throughput equilibrium dialysis systems were recently reported in the literature or are currently available commercially [5, 6]. Some were specifically designed to purify a desired high MW product from reaction batches, while others were designed for use in protein binding assays, but could likely be adapted for a purification application. All of the systems, however, are either cumbersome to assemble, require access to specialized equipment (e.g., centrifuge), involve costly

investment in start-up equipment, or require dialysis from a custom-made multiwell plate to and from which samples would need to be transferred.

In this report we describe a robust high-throughput equilibrium dialysis apparatus aimed at addressing the aforementioned limitations associated with the reported and commercially available systems. The dialysis system reported herein was designed to purify a high molecular weight polymer from a reaction mixture comprising a two-fold excess of a low MW molecule that represents reaction byproducts, reagents, and other contaminants. Moreover, the dialysis apparatus can be economically constructed from commercially available materials and easily fabricated in an average machine shop. Attributes of the reported system include 1) compatibility with automated liquid handling systems, 2) resistance to acidic environments, 3) minimal creation of waste, 4) ease of assembly, 5) the obviation of specialized equipment, and 6) ready integration with in line high-throughput data acquisition technology (e.g., 96-well plate reader).

6.3. MATERIALS AND METHODS

Figures 6-1a and 6-1b show an assembled and exploded illustration of the dialysis apparatus with the source of all materials summarized in Table 6-1. Detailed drawings are provided in the appendix at the end of the chapter.

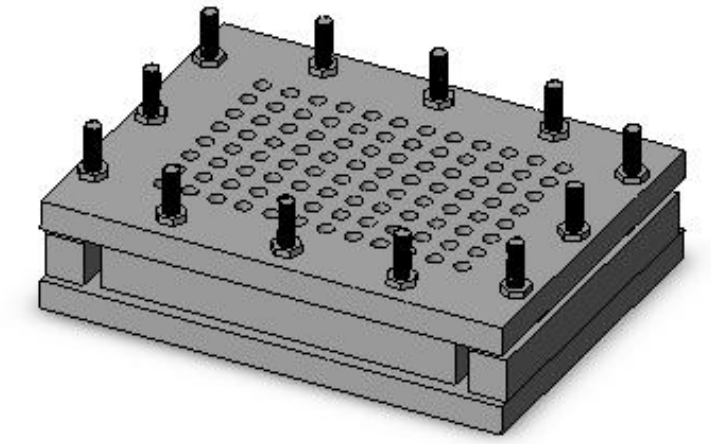

(a)

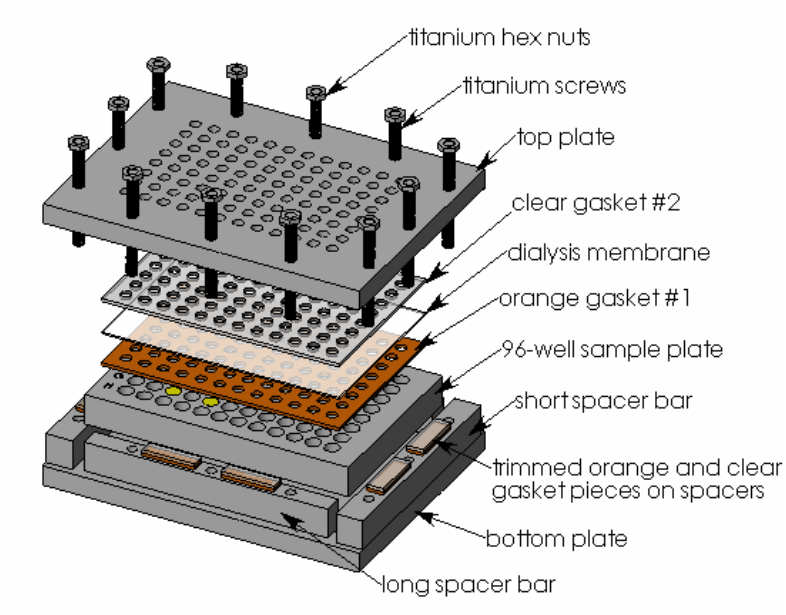

(b)

Figure 6-1. High throughput equilibrium dialysis system **a)** Assembled view of dialysis apparatus **b)** Exploded view of dialysis apparatus including 96-well microtiter sample plate **c)** Well assignment of tartrazine and dextran-rhodamine for dialysis experiments (yellow). All other wells contained an equivalent volume of 0.1N HCl

Figure 6-1 (*continued*)

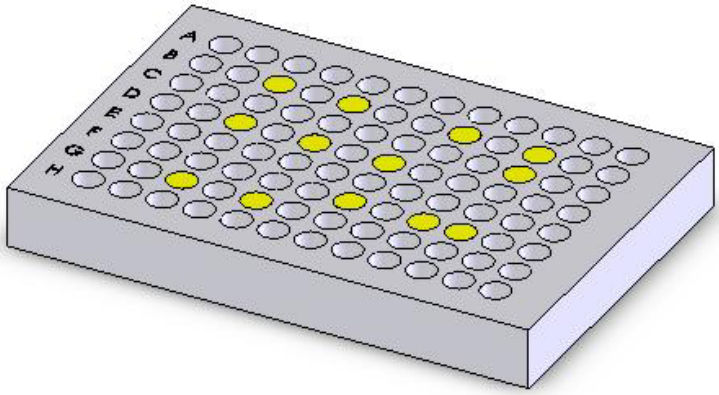

(c)

Table 6-1. Materials for equilibrium dialysis system

Material	Manufacturer	Catalog No.
Regenerated Cellulose Dialysis Membrane (flat sheet) MWCO=3.5K Da	Spectra/Por (Rancho Dominguez, CA)	132723
Regenerated Cellulose Dialysis Membrane (flat sheet) MWCO=6-8K Da		132677
Clear gasket (silicone rubber)	McMaster-Carr (Elmhurst, IL)	86915K16
Orange gasket (silicone rubber)		8608K51
Polycarbonate sheet (12"x12"x 3/8")		8574K31
Polycarbonate sheet (12"x12"x 1/4")		8574K28
Polycarbonate bar (48"x1"x1/2")		1749K14
96 Well Assay Microplate (Flat Bottom; Polystyrene; Clear)	Matrix Technologies (Hudson, NY)	4915
Titanium Hex Nut (10-32)	Small Parts, Inc. (Miramar, FL)	HNTT-1032
Titanium Threaded Rod (10-32)		TRTT-1032

6.3.1. Samples

Dextran-rhodamine (D/R) was purchased from Molecular Probes, Inc. (#D-1824, Eugene, OR) and tartrazine from Sigma-Aldrich (#86310, St. Louis, MO). D/R (10K g/mol, 1:1 mol ratio of rhodamine:dextran) and tartrazine (534 g/mol) were used as model compounds in this study to represent the high MW retentate and low MW dialysate, respectively, dissolved and dialyzed against 0.1N HCl. All tartrazine and D/R calibration standards were made via serial dilutions from a 0.1mM and 0.12mM stock solution, respectively. Solutions with final concentrations of either 50μM tartrazine only or 25μM D/R and 50μM tartrazine were made in scintillation vials, from which 200μL aliquots were taken and added to their assigned wells of the 96-well assay plate as shown in Figure 6-1c. Sample well positions were assigned as shown to monitor for cross contamination between wells during dialysis.

6.3.2. Dialysis system assembly

The 96-well assay plate was set on the bottom plate of the dialysis apparatus as guided by the spacer. Orange gasket #1 was placed over the assay plate, carefully aligning the gasket holes over each well. A pre-soaked, trimmed dialysis membrane (soaked in 0.1N HCl for at least 30 minutes) was placed over gasket #1 and gently smoothened out with a gloved finger to remove any air pockets. According to the manufacturer's instruction, pre-soaking the membrane in an acidic medium is critical for neutralizing the cellulose membrane. Failure in doing so may result in a negatively charged membrane that can electrostatically interact with ionic retentate and/or dialysate molecules and prevent dialysis. Clear gasket #2 was placed over the dialysis membrane, carefully aligning the gasket holes over each well of the assay plate. Trimmed pieces of orange and clear gaskets were laid on the spacer bars before sliding

the top plate through the screws. (See Figure 6-1b) Hex nuts were tightened over the top plate with a wrench beginning with the lengths of the plate before fastening the widths of the plate to ensure a leveled, secured top plate.

6.3.3. Dialysis

The assembled dialysis system was flipped over and forcefully shaken in one downward motion such that the solution in each well was resting on the dialysis membrane. Carefully rotating the apparatus by ninety degrees so that the dialyzing front was perpendicular to the liquid surface, the system was slowly lowered into the dialysis bath. A plastic container with a 9" x 6" base and 5" height filled with approximately 4 liters of 0.1N HCl served as the dialysis bath. The water in front of the top plate was manually agitated to relieve any air bubbles that may have become trapped in the holes of the top plate. Upon removing all visible air bubbles, the apparatus was flipped over so that the dialyzing front faced the bottom of the water bath. The apparatus was propped up in the water bath with 20mL scintillation vials, while remaining completely submerged, to allow for unobstructed stirring of a magnetic stir bar set underneath the apparatus. The stirring speed was set to approximately 200rpm. For experiments with D/R, the water bath was covered with aluminum foil. The apparatus was removed from the bath and the assembly taken apart for UV/Vis spectrophotometry analysis at the designated time points, then reassembled using a fresh, pre-soaked dialysis membrane.

6.3.4. UV/Vis spectrophotometry and data analysis

Absorbance values for tartrazine were read at 430nm and D/R at 550nm on a Molecular Devices SpectraMax Plus^{384} (pathlength check on; water blank cuvette).

Absorbance values at 700nm were taken as a negative control. Wells with abnormally high absorbance values at all three wavelengths due to dust were not included in the tartrazine and D/R average calculations. Tartrazine and D/R values were corrected for background absorbance by subtracting the absorbance of 200μL of 0.1N HCl (background absorbance = .038 at 430nm, .036 at 550nm, and .035 at 700nm). Tartrazine absorbance values were additionally corrected for absorbance contributions at 430nm due to D/R. All tartrazine and D/R concentrations at 430nm and 550 nm were quantified against their respective calibration curves. Average tartrazine and D/R concentrations reported are averages of all sample wells (n=13) for one dialysis run taken at the designated time point.

6.4. RESULTS AND DISCUSSION

6.4.1. Time study of equilibrium dialysis of low MW compound through a 3.5K MWCO and 6-8K MWCO membrane

To characterize the time course of dialysis from the reported apparatus, dialysis of 50μM of tartrazine through a 3.5K MWCO and a 6-8K MWCO membrane was quantified daily. Experiments consisted of tartrazine dialysis from wells containing no high MW polymer. Based on the dialysis profiles, shown in Figure 6-2, of three independent experiments at each MWCO, there is little disparity between tartrazine dialysis through a 3.5K and 6-8K MWCO membrane. However, in one of the three 6-8K experiments, a relatively large standard deviation was observed at t=38 hours (arrow in Figure 6-2). Upon removing the apparatus to obtain the time point reading, it was discovered that an air bubble was present in a well of the top plate that corresponded to a tartrazine well in the 96-well assay plate. The bubble prevented dialysis from the well resulting in the relatively large standard deviation. Removing

the air bubble for the remainder of the experiment resumed dialysis. The results highlight the importance of expelling all air bubbles before commencing dialysis. Nevertheless, in both experimental setups, tartrazine was dialyzed to less than 10% of the initial concentration after 60 hours and less than 1% after 130 hours.

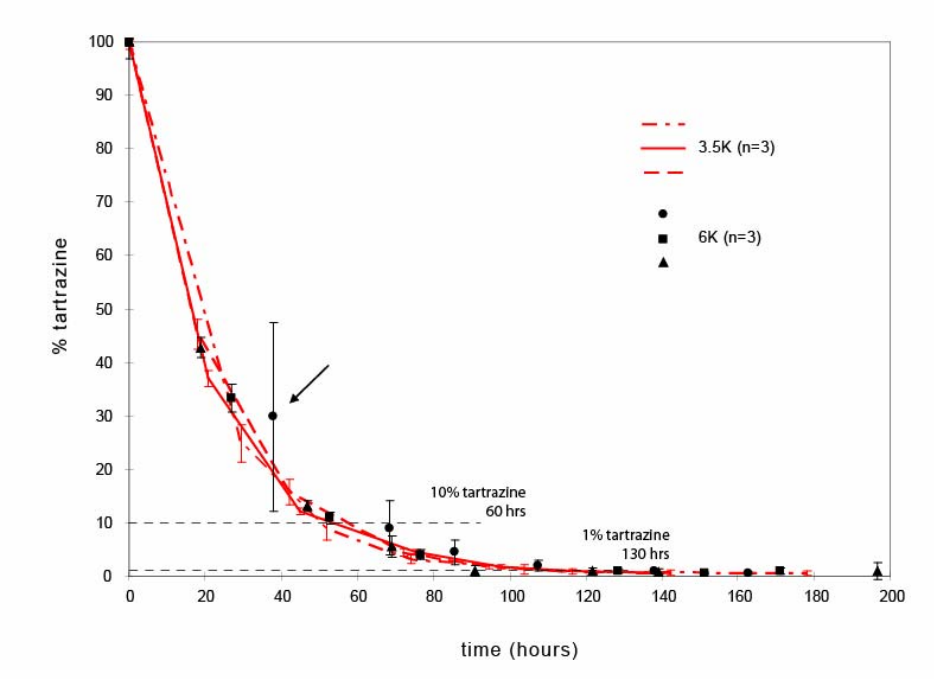

Figure 6-2. Dialysis profiles of tartrazine from wells initially containing 50μM tartrazine in 0.1N HCl. Tartrazine dialyzed to less than 10% after approximately 60 hours and less than 1% after approximately 130 hours. Arrow marks the time point at which dialysis was delayed due to an air bubble trapped in one well of the top plate. Upon removing the air bubble, dialysis resumed. Red lines represent dialysis through a 3.5K MWCO dialysis membrane; shapes represent dialysis through a 6-8K MWCO membrane. Tartrazine concentrations reported are averages of all sample wells (n=13) for one dialysis run taken at the designated time point. Error bars represent ± one standard deviation

6.4.2. Effects of high MW polymer on equilibrium dialysis of low MW compound

In the presence of a high MW species, dialysis of a low MW molecule may be retarded due to accumulation of the high MW species at the membrane surface, which may prevent the low MW molecule from freely permeating through. Alternatively, if both the high and low MW species possess aromatic functional groups, pi-pi orbital stacking interactions may also affect dialysis. To determine the potential effects on dialysis of such situations, the time course for the dialysis of 50μM of tartrazine through a 3.5K and 6-8K MWCO membrane from wells containing 25μM D/R (MW=10,000 g/mol) was quantified. Similar to the initial experiments of dialyzing tartrazine in the absence of a high MW polymer, there is little disparity between dialyzing through a 3.5K and a 6-8K MWCO membrane (data not shown). However, tartrazine dialysis appeared to be slightly retarded in the presence of D/R with dialysis to less than 10% of the initial concentration occurring after 75 hours and to less than 1% after 160 hours (Figure 6-3). The precise cause for this is not fully understood although it is likely to be attributed to one or both of the previously mentioned factors.

The presence of D/R was also monitored throughout dialysis to confirm that it was not leaking out either during dialysis or while obtaining the time point readings. The D/R profiles shown in Figure 6-3 confirm that D/R was indeed present throughout dialysis at its initial concentration.

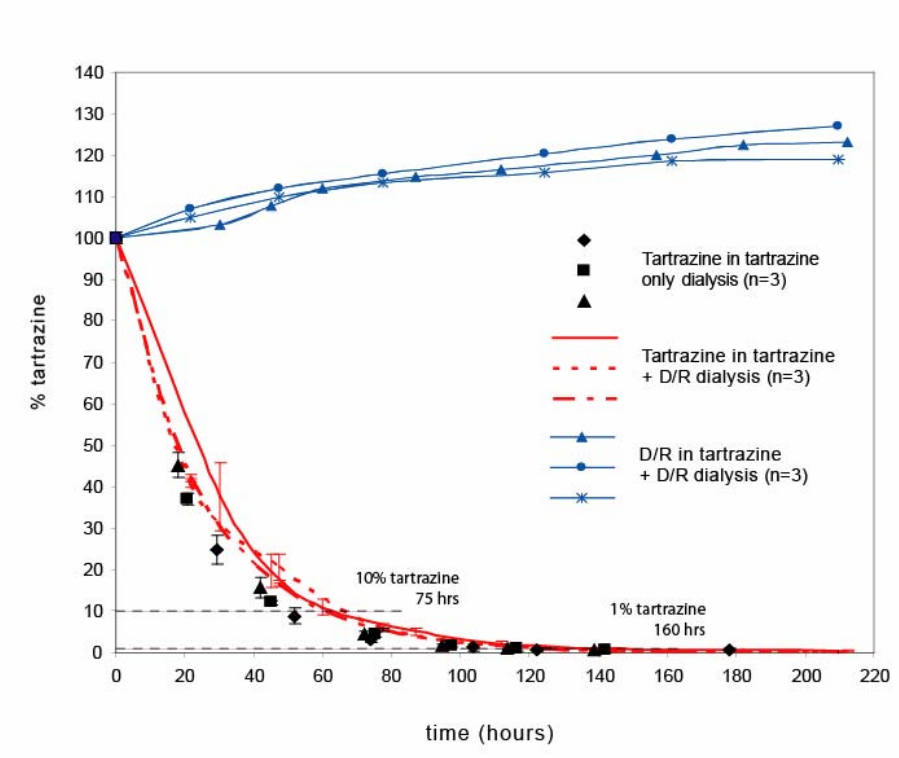

Figure 6-3. Dialysis profiles of tartrazine from wells initially containing 25μM dextran-rhodamine (10K g/mol, 1:1 mol ratio of rhodamine:dextran) and 50μM tartrazine in 0.1N HCl. Dialysis of tartrazine was slightly retarded in the presence of dextran-rhodamine (D/R) with dialysis to less than 10% occurring after approximately 75 hours and less than 1% after approximately 160 hours. D/R profiles were also monitored to confirm that leakage did not occur throughout dialysis. Shapes represent tartrazine profiles in tartrazine only dialyses; red lines represent tartrazine profiles in tartrazine + D/R dialyses; blue lines represent D/R profiles in tartrazine + D/R dialyses. Tartrazine and D/R concentrations reported are averages of all sample wells (n=13) for one dialysis run taken at the designated time point. Error bars represent ± one standard deviation

6.4.3. Effects of membrane replacement and evaluation of leak resistance throughout dialysis

To confirm that replacing a fresh dialysis membrane between each UV/Vis absorbance time point reading in the daily experiments did not alter the time course for tartrazine dialysis, the presence of tartrazine was also quantified after 160 and 220 hours of uninterrupted dialysis, for the tartrazine only and tartrazine plus D/R experiments, respectively. The commercially available Harvard Apparatus DispoDialyzer with a 2K and a 5K MWCO membrane were also evaluated for comparison. The results shown in Table 6-2 confirm that after the prescribed time course, tartrazine had indeed dialyzed out of their respective wells to less than 1% as expected. Further, the presence of D/R at 100% of its initial concentration after the dialysis time course indicates no apparent leakage of the high MW molecule from their respective wells. In contrast, D/R appears to have leaked out of the wells of the Harvard Apparatus system with a 5K MWCO membrane, a limitation also experienced by others even in a neutral pH dialyzing medium [7].

Table 6-2. Comparison of percent tartrazine remaining after 160 hours and 220 hours of uninterrupted dialysis

	Tartrazine Only dialysis (160 hrs)	**Tartrazine + Dextran-Rhodamine dialysis (220 hrs)**	
Reported dialysis system	% Tartrazine	% Tartrazine	% Dextran-Rhodamine
3.5K MWCO	**0.53%**	**0.58%**	**112.18%**
Std Err	0.003%	0.028%	0.095%
6-8K MWCO	**1.62%**	**0.63%**	**105.53%**
Std Err	0.008%	0.015%	0.097%
Harvard Apparatus dialysis system	% Tartrazine	% Tartrazine	% Dextran-Rhodamine
2K MWCO	**<.01%**	**<.01%**	**100.70%**
Std Err	0.002%	0.006%	0.226%
5K MWCO	**0.69%**	**<.01%**	**64.00%**
Std Err	0.132%	0.012%	0.330%

In all of the dialysis experiments, the presence of cross contamination of tartrazine and/or D/R into neighboring wells was monitored by observing increases in absorbance at 430nm and 550nm, respectively, within wells that originally contained the 0.1N HCl dialyzing media. No such increase was observed, thereby confirming an acid-resistant and leak-free seal that prevented cross contamination between wells.

6.4.4. Comparison of additional factors with commercially available dialysis systems

In addition to dialysis performance, important factors to also consider are the costs per sample plate, range of MWCO membranes available, easy integration with in-line high-throughput data acquisition systems (e.g., microtiter plate reader), minimal creation of waste, and ease of assembling the apparatus. These factors served as additional design criteria for the proposed dialysis system and are compared in Table 6-3 with several commercially available systems including those that were designed for protein binding assays, but could likely be adapted for equilibrium dialysis.

A striking distinction between the reported dialysis system and all other systems compared in Table 6-3 is the use of a standard 96-well microtiter plate as the sample plate from which dialysis occurs. This feature was designed to facilitate seamless integration into a continuous process workflow that may include standard multiwell dispensing systems for sample preparation before dialysis as well as high-throughput data acquisition systems after dialysis. Additionally, use of a microtiter sample assay plate can potentially reduce the amount of waste generated, especially if the microtiter plate can be reused for multiple dialyses, compared to other dialysis systems where the sample plate and dialysis membrane are manufactured as one conjoined unit.

Table 6-3. Comparison between reported dialysis system and several commercially available systems

Type	Description	Start up cost	Cost per 96 samples	Notes
Equilibrium dialysis system	**Spectra/Por®** 96 well microdialyzer *(#132326)*	$1,379		- Available in 3.5K, 6-8K, 12-14K MWCO membranes - Samples must be transferred for high-throughput data acquisition (e.g., microtire plate reader) - Reusable sample plate - Minimal assembly required
	custom made 96 well plate *(#132330)*	$224		
	dialysis sheets (MWCO=3.5K) *(#132723)*		$8	
	dialysis sheets (MWCO=6-8K) *(#132677)*		$3	
	Harvard Apparatus 96-Well DispoDIALYZER *			- Available in 1K, 2K, 5K, 10K, 25K MWCO membranes - Samples must be transferred for high-throughput data acquisition (e.g., microtire plate reader) - New sample plate required for each dialysis - No assembly required
	MWCO =2K *(#740901)*		$317	
	MWCO =5K *(#740902)*		$317	
	Novagen/EMD Biosciences D-Tube96™ Dialyzer *(#71712-2)*		$354	- Available in 6-8K and 12-14K MWCO membranes - Samples must be transferred for high-throughput data acquisition (e.g., microtire plate reader) - New dialysis tubes per sample required for each dialysis
Ultrafiltration	**Millipore** MultiScreen Filter Plate with Ultracel-10 Membrane *(#MAUF01010)*		$6	- Centrifuge equipped with a 96-well plate rotor required - Available in 10K MWCO membrane only - Samples must be transferred for high-throughput data acquisition (e.g., microtire plate reader) - New sample plate required for each dialysis - No assembly required
	standard 96-well receiver plate		$2	
	centrifuge			
Plasma protein binding systems	**Pierce®** Biotech Rapid Equilibrium Dialysis (RED) Device			- Available in 8K MWCO membrane only - Samples must be transferred for high-throughput data acquisition (e.g., microtire plate reader) - Reusable sample plate - Minimal assembly required
	reusable Base Plate *(#89811)*	$320		
	RED Device Inserts *(#89809)*		$700	
	HTDialysis, LLC 96 - well Micro Equilibrium Dialysis block- Complete Set *(#1006)* **	$2,995		- Available in 3.5K, 6-8K, 10K, 12-14K, 25K, 50K MWCO membranes - Samples must be transferred for high-throughput data acquisition (e.g., microtire plate reader) - Reusable sample plate - Assembly of dialysis apparatus can be cumbersome
	dialysis strips (MWCO=3.5K) *(#1135)*		$35	
	dialysis strips (MWCO=6-8K) *(#1103)*		$30	
Reported dialysis system	Polycarbonate housing, titanium screws and hex nuts, gaskets	$153		- Available in 3.5K, 6-8K, 12-14K MWCO membranes - Compatible with standard 96 well plate (re-usability optional) - Minimal assembly required
	96-well plate		$2	
	dialysis sheets (MWCO=3.5K)		$8	
	dialysis sheets (MWCO=6-8K)		$3	

* Design similar to the one reported by Banker, et al. (5)

** Design similar to the one reported by Kariv, et al. (6)

An additional enhancement of the reported dialysis system is its economical construction compared with the other systems presented in Table 6-3. The Spectra/Por® 96-well microdialyzer, the most similar in design to our apparatus, is costlier by ten-fold. While products such as the MilliPore MultiScreen Filter Plate offer an affordable ultrafiltration system, only a 10K MWCO membrane is currently available and dialysis requires a centrifuge equipped with 96-well plate rotors.

6.5. CONCLUSIONS

As more areas of research embrace the advantages of high-throughput strategies, simple yet reliable technology will be critical to fully realize the benefits that such strategies can offer. The reported dialysis system offers researchers an improved high-throughput approach to purifying high MW product from solutions comprising a mixture of low MW by-products and reagents. Constructed from materials that are commercially available, the apparatus can be affordably and easily fabricated in a standard machine shop. The proposed system also provides important enhancements over both recently reported and commercially available systems. In particular, the system is 1) readily integrated with in-line automated high-throughput technology (e.g., robotic liquid and solid handling systems, 96-well plate readers), 2) resistant to acidic environments, 3) creates minimal waste, and 4) easy to assemble.

More importantly, the dialysis apparatus and the validation approach described herein for a 96-well assay platform provides a readily transferable template upon which other multi-well assay platforms can be produced. With all other components of the dialysis apparatus interchangeable, simply modifying the dimensions of the top plate and the gasket sheets can enable high-throughput dialysis on a 6-, 24-, and 384-well plate platform.

APPENDIX

Drawings of apparatus components

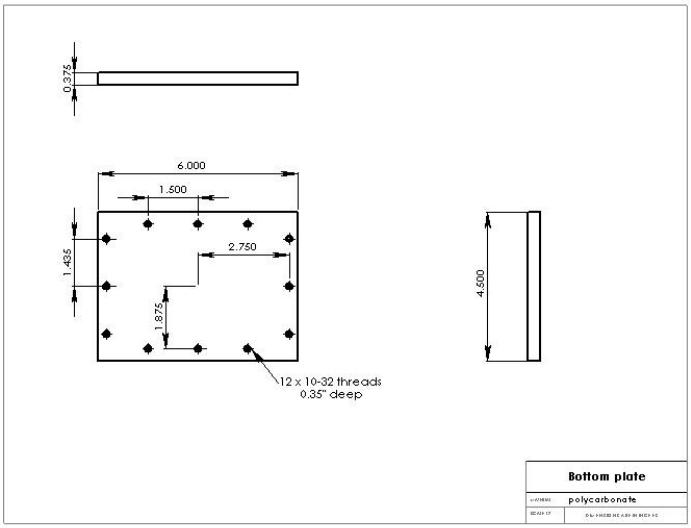

Drawing of bottom plate

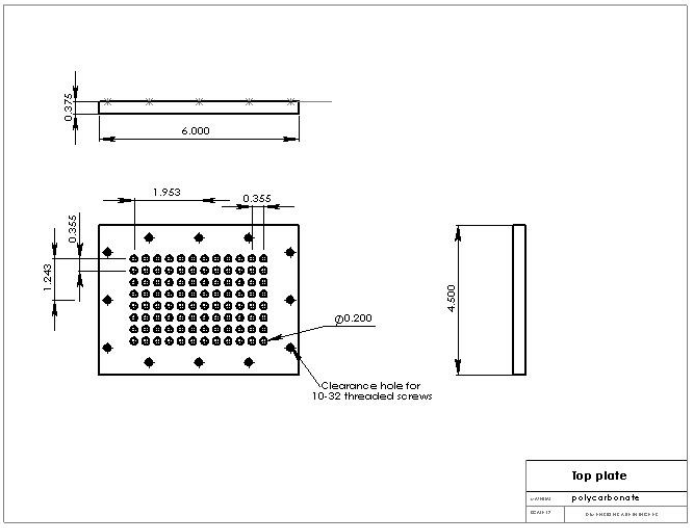

Drawing of top plate

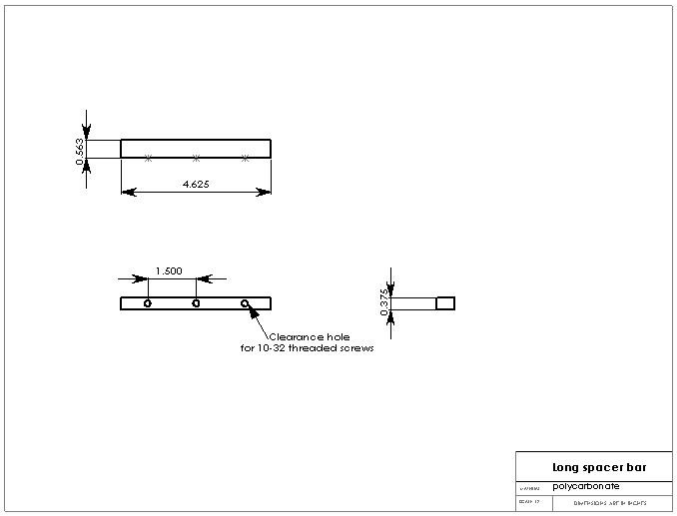

Drawing of long spacer bar

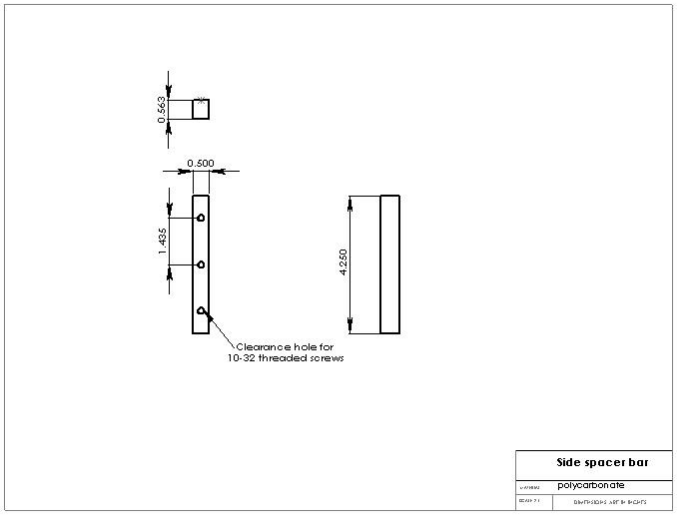

Drawing of side spacer bar

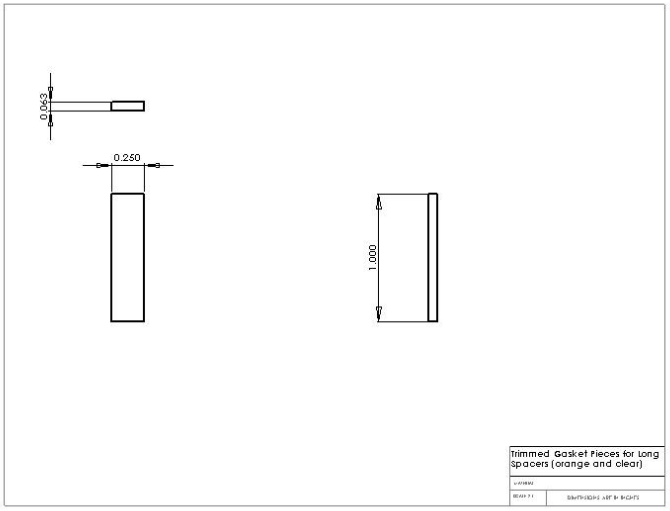

Drawing of trimmed gasket pieces for long spacer bar

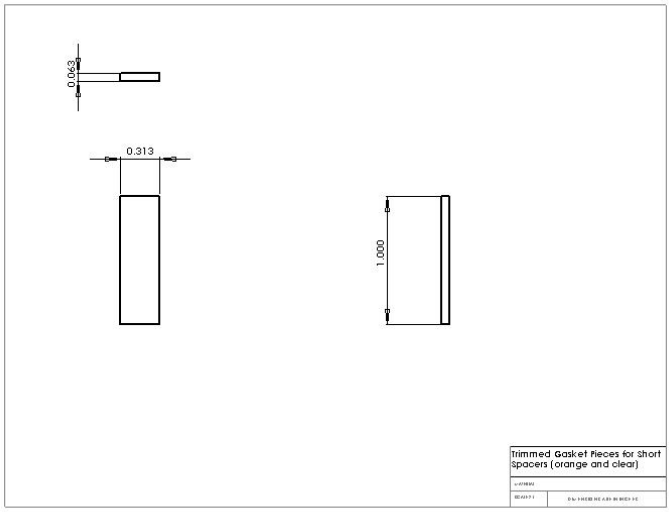

Drawing of trimmed gasket pieces for short spacer bar

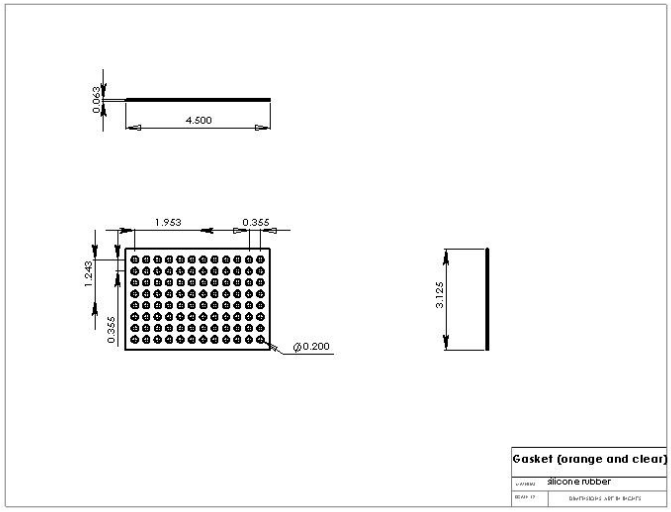

Drawing of 96-well gasket

REFERENCES

[1] Rubin, A.E., Tummala, S., Both, D.A., Wang, C.C., and Delaney, E.J. Emerging technologies supporting chemical process r&d and their increasing impact on productivity in the pharmaceutical industry. *Chem. Rev.* **106**(7): 2794-2810 (2006).

[2] Anderson, D.G., Lynn, D.M., and Langer, R. Semi-automated synthesis and screening of a large library of degradable cationic polymers for gene delivery. *Angew. Chem. Int. Edit.* **42**(27): 3153-3158 (2003).

[3] Brocchini, S., James, K., Tangpasuthadol, V., and Kohn, J. A combinatorial approach for polymer design. *J. Am. Chem. Soc.* **119**(19): 4553-4554 (1997).

[4] Lynn, D.M., Anderson, D.G., Putnam, D., and Langer, R. Accelerated discovery of synthetic transfection vectors: Parallel synthesis and screening of degradable polymer library. *J. Am. Chem. Soc.* **123**(33): 8155-8156 (2001).

[5] Banker, M.J., Clark, T.H., and Williams, J.A. Development and validation of a 96-well equilibrium dialysis apparatus for measuring plasma protein binding. *J. Pharm. Sci.* **92**(5): 967-974 (2003).

[6] Kariv, I., Cao, H., and Oldenburg, K.R. Development of a high throughput equilibrium dialysis method. *J. Pharm. Sci.* **90**(5): 580-587 (2001).

[7] www.piercenet.com/Objects/View.cfm?type=ProductFamily&ID=CF207C7A-34DA-4A16-BA83-5BB2F5D8F6AC

CHAPTER 7

A STOCHASTIC MONTE CARLO APPROACH TO COMBINATORIAL LIBRARY DESIGN

7.1. ABSTRACT

The exhaustive screening of large combinatorial libraries continues to be resource-limited, thus underscoring the need for strategies to representatively sample these vast libraries. In this study, stochastic Metropolis and parallel tempering Monte Carlo algorithms were implemented *in silico* to sample a 5,008 buffer formulation library to locate optimal refolding conditions of a model protein. In contrast to single-pass random sampling, Monte Carlo sampling occurs through a round-by-round iterative process. In each progressive round, formulations undergo a proposed change according to an assigned step increment scheme. The proposed formulations are accepted with probability $\exp(\beta\Delta E)$, where ΔE is the difference in refolding yield between the original and proposed formulations and β is an empirically determined parameter that controls the randomness of the sampling. The results show that Metropolis and parallel tempering Monte Carlo sampling protocols locate formulations of higher protein refolding yield more frequently than random sampling. The average refolding yields of formulations constructed by Metropolis Monte Carlo in a 1,000-formulation library increased in a manner dependent on the β parameter and the step increment scheme.

Following each Monte Carlo simulation, the molecular diversity of formulations was quantified within a low-dimensional descriptor space as parameterized by the surface tension, critical micelle concentration, and solubility of

formulation excipients. The diversity of formulations in the final sampling rounds constructed by the Monte Carlo methods was either maintained or enhanced relative to the initial randomly-generated formulation rounds. The striking results observed in this study were obtained through simple parameterization of a combinatorial library, absent any *a priori* information of how individual excipients influence the complex phenomena that underlie protein refolding. This hybrid experimental-computational study demonstrates that stochastic Monte Carlo algorithms offer a dramatic improvement over the random sampling of combinatorial libraries that may be too arduous to exhaustively search otherwise.

7.2. INTRODUCTION

The formulation of molecular chaperones in protein refolding buffers is critical for the recovery of active proteins for applications in structural genomics, proteomics, and biopharmaceuticals. Given that refolding conditions for proteins are highly specific, combinatorial approaches have been employed to formulate buffers for optimal protein refolding. [1-5] Combinatorial strategies involve creating combinations of a prescribed set of components and screening the assembled products for desired attributes. [6] Challenges emerge as the number of components increases, leading to a rapid escalation in the number of possible combinations in the final combinatorial library. Despite the development of high-throughput screening strategies, the degree to which vast combinatorial libraries may be exhaustively investigated continues to be limited by space, time, and financial resources. Therefore, methods or alternative approaches that reduce the number of samples per screen, while maintaining integrity of results, are desired.

Random sampling of a combinatorial library is arguably the simplest alternative to screening each individual constituent of the library. This approach, however, is unsystematic and unreliable because it ignores any *a priori* knowledge or chemical intuition. Although random sampling does not preclude the identification of constituents with optimal characteristics, or "figures of merit", per se, it is unlikely to give consistently dependable results.

Stochastic Monte Carlo (MC) methods have been previously proposed as potential alternatives to the random sampling of large combinatorial libraries. [7] Chemical intuition and *a priori* knowledge can be inherently incorporated into these MC approaches, thereby increasing the probability of identifying higher figure of merit constituents relative to random sampling.

In combinatorial screening experiments, however, a maximal figure of merit may be only one of several desired attributes. For instance, in medicinal chemistry, discovering compounds that exhibit high potency against a target is clearly valuable. Yet, if subsequent analyses reveal such compounds to possess adverse toxicological effects, they may be rendered non-viable for further development. For this reason, a "molecularly diverse" collection of lead compounds that each possess the desired figure of merit, but are also sufficiently dissimilar in chemical or structural characteristics, may be desirable to increase the probability of identifying compounds that are successful through multiple levels of safety and efficacy screens.

The previous study that used MC methods to locate compounds with high figures of merit also showed that molecular diversity was maintained at sufficient levels. [7] However, this study relied on libraries produced solely through *in silico* simulations rather than through experimentally acquired *ex silico* approaches.

The present study first examines the refolding of a denatured model protein to its functional conformation in each of 5,008 combinatorially-assembled buffer

formulations. This library represents an exhaustive collection of formulations containing combinations of one, two, or three synthetic molecular chaperones (i.e., excipients) per formulation. With this exhaustive data set in hand, the utility of two MC sampling approaches, namely Metropolis MC and parallel tempering MC, was explored to locate optimal protein refolding buffer formulations as an alternative to exhaustive screening and random sampling. The results of this hybrid experimental-computational study are consistent with previously established studies that utilized only virtual libraries and provide further validation that Monte Carlo methods offer a more systematic and efficient approach toward determining high figure of merit (refolding yield) formulations compared to random sampling without compromising molecular diversity.

7.3. MATERIALS & METHODS

7.3.1. Protein refolding combinatorial data set

A total of 5,008 unique formulation conditions for lysozyme refolding, representing an exhaustive screen of combinations of one, two, or three excipients per formulation, was generated and used as the reference data set for all sampling simulations. Refolding solutions were formulated from 32 possible excipients, comprising 16 chemical species of two concentrations each (Table 7-1). Individual formulations were constrained to not contain duplicate chemical species.

Table 7-1. Summary of excipients, concentrations, and associated descriptors

Excipient Number	Concentration (mg/mL)	Excipient	Descriptor	Descriptor Metric	Reference
1	0.293	Methylcellulose	Solubility	-5.0	[8]
2	2.93			-4.9	
3	0.029	Polyethylene Glycol (M_w 3500)	Solubility	-5.0	[9]
4	0.293			-5.0	
5	0.293	Dextran	Solubility	-5.0	[10]
6	2.93			-4.9	
7	29.3	Glycerin	Surface Tension	1.1	[10]
8	58.6			1.1	
9	29.3	Sorbitol	Surface Tension	-3.3	[10]
10	58.6			-5.0	
11	10.26	Cyclodextrin	Solubility	-5.0	[11]
12	20.51			-4.9	
13	0.029	Polysorbate 80	CMC	-0.4	[12]
14	0.293			-0.3	
15	0.029	Polysorbate 20	CMC	-5.0	[12]
16	0.293			-0.3	
17	5.43	CHAPS	CMC	1.0	[12]
18	10.81			5.0	
19	0.19	Triton X-100	CMC	-0.3	[12]
20	1.9			0.9	
21	12.31	Urea	Solubility	-2.4	[13]
22	46.88			5.0	
23	24.64	Guanidinium chloride	Solubility	-1.1	[14]
24	55.96			4.0	
25	6.3	Lithium Chloride	Surface Tension	1.8	[10]
26	24.91			4.3	
27	8.56	Sodium Chloride	Surface Tension	2.9	[10]
28	34.22			5.0	
29	4.16	Sodium Sulfate	Surface Tension	1.3	[10]
30	32.91			3.4	
31	12.77	L-arginine	Solubility	-4.8	[13]
32	38.3			-4.4	

Lysozyme refolding yields were quantified following a previously reported protocol. [15] Hen egg white lysozyme (Sigma) was dissolved at 40 mg/mL in denaturing buffer (8M guanidinium chloride, 16 mM dithiolthreitol, 1 mM EDTA, 50 mM Tris-HCl, pH 8.0). Protein concentration was verified by ultraviolet absorbance at 280 nm. [16] Refolding solutions were generated in tissue culture treated 96-well polystyrene plates from stock solutions dispensed into the plates using a Tecan RSP150 liquid handling system. The total volume of each refolding solution was 180 μL. Protein refolding was initiated by rapid addition of 20 μL of the denatured lysozyme solution followed by immediate aspirating and dispensing to prevent protein aggregation. The 96-well plates were then sealed and incubated at room temperature for 48 hours. Refolding was quenched by addition of 0.5 M iodoacetic acid (20 μL). Lysozyme samples were diluted 1:100 in 50 mM Tris-HCl (pH 8.0), and the activity for each sample was quantified by measuring the rate of optical density change of a *M. luteus* cell wall suspension. Assays were performed in triplicate, and the refolding yield was quantified relative to native lysozyme activity.

7.3.2. Random library construction

For library construction *in silico*, each excipient in Table 7-1 was randomly assigned a unique integer value, and formulations were thus represented as a sequence of three integers. For example, a formulation composed of 2.93 mg/mL methylcellulose, 5.43 mg/mL CHAPS, and 12.31 mg/mL urea was represented as (2, 17, 21). Formulations with less than three excipients were assigned with zero values where appropriate. Formulations were constructed by random assembly from the 32 possible stock excipients, where each excipient had equal probability of being in a formulation. The lysozyme refolding yield corresponding to the constructed

formulation was obtained from the protein refolding combinatorial data set described above.

7.3.3. Metropolis Monte Carlo library construction

In contrast to libraries generated by single-pass random construction, formulation libraries constructed by Metropolis MC simulation proceeded in an iterative manner. For illustrative purposes, a 1,000-formulation library generated from 50 rounds of 20 formulations each is described here. A starting set of 20 formulations was assembled by random construction as described above. In each subsequent round n ($n>1$), one excipient, x, in each of the 20 formulations was selected at random with equal probability to undergo a proposed move to a new excipient, x'. The integer value by which x was changed to x' was determined by the increment size, k, and the increment scheme, namely a fixed step scheme or a fluctuating step scheme. For a given step increment, k, excipients in the fixed step simulations were allowed to move to new excipient $x' = x + k$ or $x' = x - k$ with equal probability, while for fluctuating step simulations, excipients were permitted to move within the range $(x - k) \leq x' \leq (x + k)$, where the probability of moving to a specific excipient within this range was $(1/2k)$. Simulations were performed for $1 \leq k \leq 16$. Periodic boundary conditions were applied to the excipient table such that for $x + k > 32$, then $x' = x + k - 32$ or for $x - k < 1$, then $x' = x - k + 32$.

The lysozyme refolding yield corresponding to the newly proposed formulation was obtained from the refolding data set. The move to the new formulation configuration was accepted with the following Metropolis acceptance probability:

$$P_{acc}\,(\text{current}\rightarrow\text{proposed}) = \min\left(1, \exp\left[\beta\,(E_{proposed} - E_{current})\right]\right) \qquad (7\text{-}1)$$

where E represents the protein refolding yield, and β represents a constant-value control parameter reflecting a propensity to accept trial moves that would result in a decrease in the protein refolding yield.

For proposed moves that were accepted according to equation 7-1, the new formulation configuration was assigned to round *n+1*; otherwise, the formulation in round *n+1* remained the same configuration as in round *n*. New formulations resulting from proposed moves in round *n*, regardless of whether they were accepted to round *n+1*, are referred to as "accessed" formulations throughout this text. A schematic representation of the Metropolis MC library construction method is illustrated in Figure 7-1.

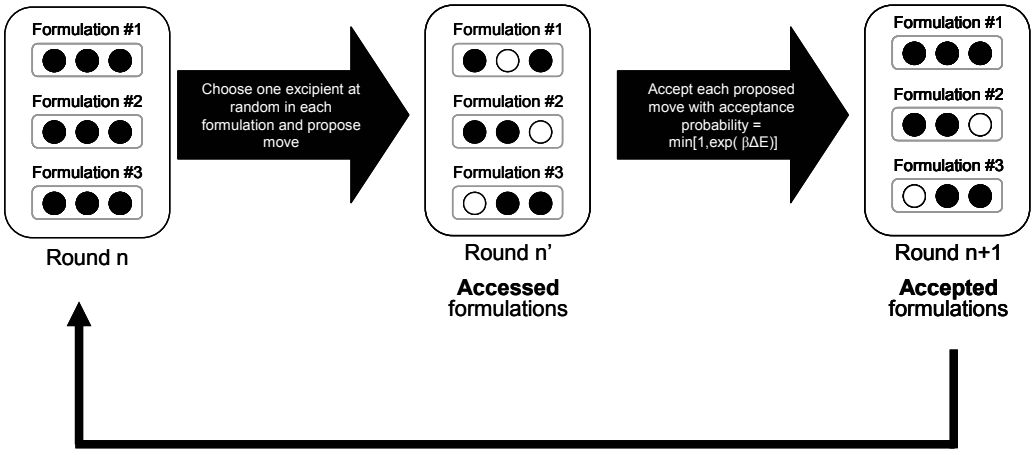

Figure 7-1. Schematic diagram of the Metropolis Monte Carlo algorithm. Each formulation consists of three individual excipients, as represented by the black circles. For a given round *n*, one excipient in each formulation in the round is chosen at random to undergo a change to a new excipient, as represented by the white circle. The resulting set of proposed formulations, termed accessed formulations, comprises round *n'*. The proposed formulations are then accepted or rejected by the Metropolis acceptance criterion, which determines the makeup of the accepted formulations for round *n+1*.

For Metropolis MC simulations, the initial round was comprised of *m* randomly constructed formulations; with each successive round of MC moves, the algorithm accepted the proposed moves according to the specific acceptance probability. After a finite number of rounds, *p*, the total number of formulations sampled was (*m x p*). Libraries of 1,000 total formulations were assembled through 20x50 or 10x100 sampling experiments.

7.3.4. Parallel Tempering Monte Carlo library construction

For parallel tempering MC library construction, three Metropolis systems of five formulations each were simultaneously simulated for 66 rounds. The three simultaneous Metropolis systems were each performed at different, but constant, β. Initial formulations within each of the systems were generated by random construction. Within an individual system, one excipient for every formulation was selected to undergo a proposed move. The excipient undergoing the move was selected at random, and the proposed move from excipient *x* to *x'* was subject to either the fixed step or fluctuating step schemes as described previously. The move to the new excipient was accepted according to the Metropolis acceptance probability, equation 7-1. Once all formulations within the new round were constructed for the three Metropolis systems, two of the three parallel systems, randomly chosen, were allowed to swap their current set of formulation configurations. The probability for one of the three systems in the simulation to be chosen to participate in a swapping move was 2/3. The acceptance rule for the parallel tempering exchange was:

$$P_{acc}\,(\text{current} \rightarrow \text{proposed}) = \min\,[1, \exp(\Delta\beta\Delta\bar{E})] \qquad (7\text{-}2)$$

where $\Delta\bar{E}$ is the difference in the average refolding yield of the five formulations in each system, and $\Delta\beta$ is the difference in β between the two systems undergoing exchange. A diagram of the parallel tempering configuration exchange is shown in Figure 7-2. Libraries of 990 total formulations were assembled in 15x66 sampling experiments.

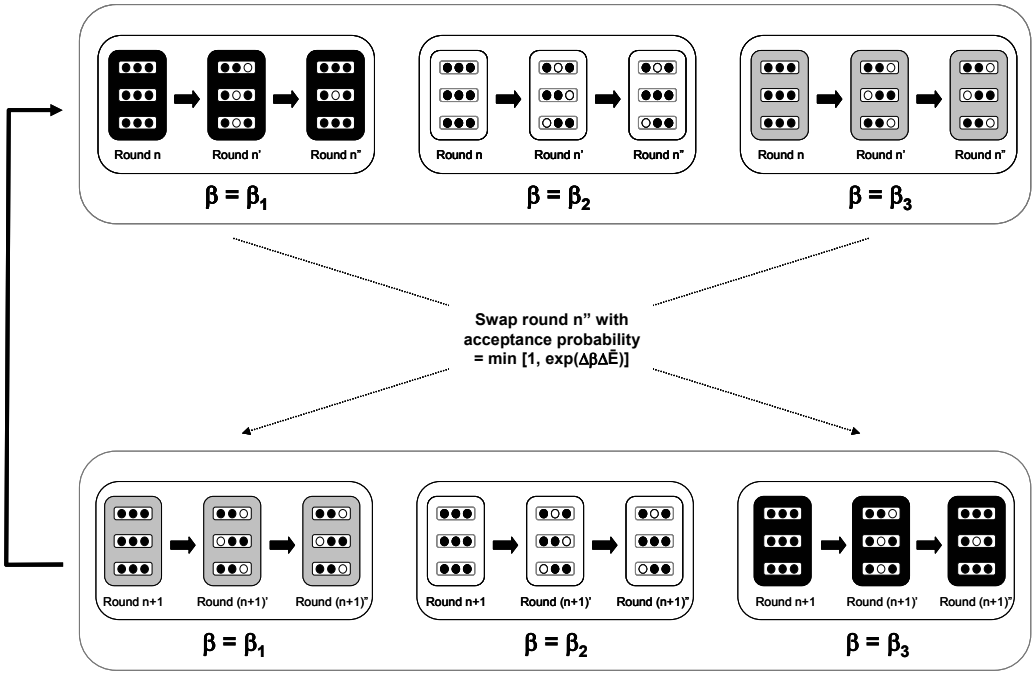

Figure 7-2. Schematic diagram of the parallel tempering Monte Carlo configuration exchange. Three parallel systems, represented in white, grey, and black, are depicted. Formulations within each of the parallel systems first undergo Metropolis Monte Carlo moves as illustrated in Figure 7-1. Following each round of Metropolis Monte Carlo, two of the three parallel systems participate in a conditional configuration swap.

7.3.5. Data analysis and statistical significance testing

Formulation libraries generated by the Metropolis and parallel tempering MC sampling algorithms, as described previously, were compared with equally-sized libraries generated by random construction. The key difference was that random

formulations were sampled in a single pass, while the MC libraries were constructed in an iterative round-over-round fashion. Regardless of the library construction method, the total number of formulations remained constant among comparison groups. Simulated libraries were generated in Fortran and performed in triplicate for each condition. Significance testing between samples was performed via the Student's t-test assuming unknown variances ($p<0.05$ was considered significant).

7.3.6. Molecular diversity

Given a set of formulations, a quantitative measure of diversity, D, was defined to be:

$$D^2 = \frac{1}{N}\sum_{k=1}^{N}\left[\sum_{j=1}^{3}\left(d_{ij} - \langle d_i \rangle\right)^2\right] \qquad (7\text{-}3)$$

where i, j, and k correspond to indices designating the descriptor, the excipient, and the formulations, respectively, and N is the number of formulations. [7] Diversity values were calculated for each of three independent libraries for each simulation condition and compared with values obtained from random library construction.

To maintain a manageable yet useful number of descriptors for this work, a low-dimensional descriptor space was established to quantify the diversity of formulations within each library. Excipients were sorted into one of three distinct descriptor categories: the critical micelle concentration (CMC), surface tension, and solubility in water. Cooperative effects among different descriptor categories were not taken into account in the diversity measurements.

In general, surfactant excipients were assigned to the CMC descriptor, polyols and salts were assigned to the surface tension descriptor, and hydrophilic solubilizing agents were assigned to the solubility descriptor. To account for the effects of

excipient concentration in the surface tension and solubility descriptor metrics, the magnitude of the metric was made proportional to the appropriate physical characteristic multiplied by the concentration. For scaling purposes, and to ensure that each descriptor had an equal weight in the determination of molecular diversity, the descriptor metrics were scaled to values between -5 and 5. A summary of each excipient and its corresponding descriptor value is provided in Table 7-1.

For CMC descriptors, to account for differences between micelle and uni-molecular binding, surfactant excipients were scaled according to the difference between experimental concentrations and the respective published CMC (i.e., ΔCMC = experimental concentration – CMC). To capture the step-like change in binding behavior at the CMC, an additional margin of 10 units was introduced in the descriptor scaling. In instances where the experimental surfactant concentration was below the CMC, the descriptor value assigned in that case was (ΔCMC – 5); similarly, in instances where the concentration was above the CMC, the descriptor value was (ΔCMC + 5). The resulting value was subsequently rescaled to range from -5 to 5, to remain consistent with the convention established for the surface tension and solubility descriptors.

To illustrate the concept of molecular diversity, Figure 7-3 shows two collections of formulations within the three dimensional descriptor space whose axes are defined as the critical micelle concentration, surface tension, and solubility. An individual formulation is represented by a single point within the descriptor space and its position is specified by the magnitude of each excipient's respective descriptor. The diversity of a collection of formulations is then quantified to be the Euclidean distance as defined by equation 7-3. Formulations represented by the black spheres are considered collectively more diverse than those represented by the white spheres.

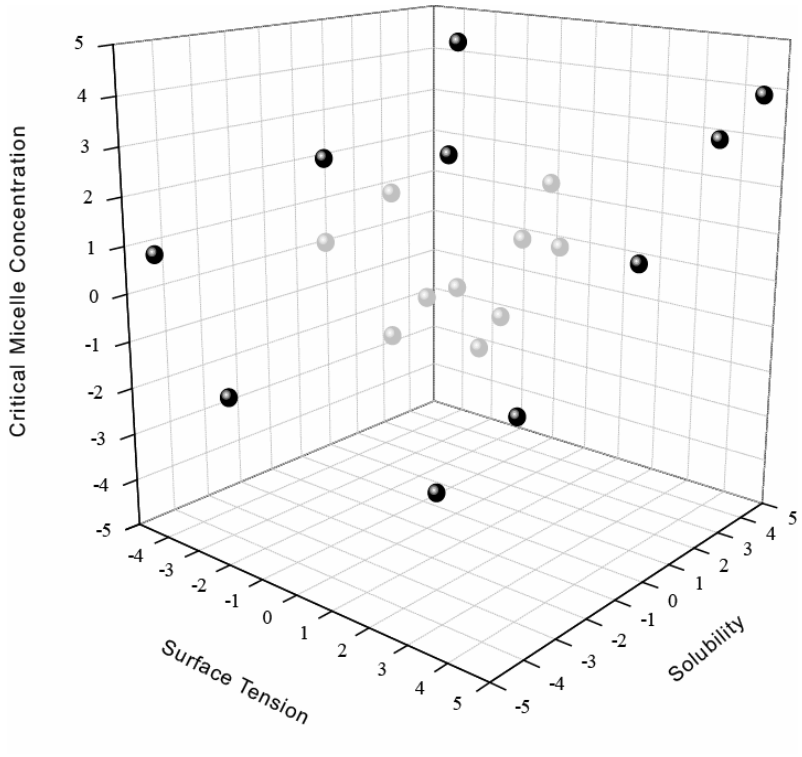

Figure 7-3. Schematic illustration of the three dimensional diversity space whose axes are defined as the critical micelle concentration, surface tension, and solubility. Formulations represented by the black spheres are more broadly distributed within diversity space compared to the white spheres and are thus considered more molecularly diverse.

7.4. RESULTS

7.4.1. Simulation conditions and parameters

Formulation libraries were constructed by Metropolis MC simulation with both fixed and fluctuating step schemes to monitor the behavior of the change in refolding yield as a function of β, step increment size, and step increment scheme. Libraries of 1,000 formulations each were constructed for $1 \leq \beta \leq 100$, in 20x50 and 10x100 experiments (data not shown). For each value of β, simulations were performed under

the fixed and fluctuating step increment schemes for $1 \leq k \leq 16$. The optimal β and step increment parameter pair for each simulation was determined to be that which resulted in the largest change in refolding yield between the initial and final sampling rounds. Libraries constructed using these optimal parameter pairs were selected for further investigation. These parameter pairs are listed in Table 7-2.

Table 7-2. Simulation conditions and parameters

Metropolis Monte Carlo		
Formulations x Rounds	20 x 50	10 x 100
Fixed Step	β = 19 k = 12	β = 15 k = 13
Fluctuating Step	β = 100 k = 13	β = 85 k = 15

Parallel Tempering Monte Carlo	
Formulations x Rounds	15 x 66
Fixed Step k = 13	$\beta_1 = 15$, $\beta_2 = 46$, $\beta_3 = 89$
Fluctuating Step k = 15	$\beta_1 = 22$, $\beta_2 = 66$, $\beta_3 = 85$

Parallel tempering MC simulations consisted of three simultaneous Metropolis systems of five formulations each, with each Metropolis system proceeding at a different constant β. These parallel tempering simulations were performed, using both the fixed and fluctuating step increment schemes, for 66 rounds of 15 formulations each, resulting in 990 total formulations. To determine the β parameters for use with

the three simultaneous Metropolis systems in parallel tempering, a single system within the simulation was held fixed at the optimal β and step increment parameter pair as determined in the 10x100 Metropolis simulations described above. The step increment *k* was kept constant across the three simultaneous systems. The β values for the two remaining systems were selected to achieve a swapping rate between neighboring systems of approximately 20% (data not shown). [17] The parameters for the parallel tempering simulations are also summarized in Table 7-2.

7.4.2. Effects of β and number of rounds on refolding yield

To determine the effects of the β parameter on the change in refolding yield of formulations between the initial and final sampling rounds, simulations were conducted at all integer β values of 1-100 as the step increment value, *k*, was held constant at the pre-determined optimum values summarized in Table 7-2. For each step increment scheme, 20x50 and 10x100 libraries were constructed.

Figure 7-4a shows similar trends in the change in refolding yield for both the 10x100- and 20x50-constructed libraries generated from the fixed step scheme. An initial steep increase in refolding yield is observed for $\beta < 13$, beyond which the yield reaches a maximal level, and then trends subtly downward at increasing values of β. The rate at which proposed formulations resulting in lower refolding yields are accepted is plotted alongside the corresponding β value in Figure 7-4a. In general, the acceptance rate decays as β increases. The acceptance rate corresponding to the maximal improvement in refolding yield is approximately 8% for both 10x100 and 20x50 sampling experiments. In contrast, simulations performed under the fluctuating step scheme resulted in the average change in refolding yield reaching an asymptotic limit beyond $\beta = 15$ as shown in Figure 7-4b. Further, the acceptance rate

corresponding to the maximal change in refolding yield appeared more stringent in the fluctuating step simulations than in the fixed step simulations. For both the 10x100- and 20x50-library constructions, the acceptance rate was approximately 1% at $\beta > 15$.

In general, there appears to be no appreciable effect on the change in refolding yield due to the number of rounds at all values of β, as suggested by the comparison between the 20x50 and 10x100 plots within each step increment scheme.

7.4.3. Effects of step increment size and number of rounds on refolding yield

To control the sampling movement about the formulation parameter space, moves from excipient *x* to *x'* were restricted by the step increment size, *k*, within either the fixed or fluctuating step increment scheme. The effects of the step increment size on the change in refolding yield of formulations between the initial and final sampling rounds were evaluated via simulations conducted at $1 \leq k \leq 16$ for each step increment scheme as β was held constant at the values summarized in Table 7-2. For each step increment scheme, 20x50 and 10x100 libraries were constructed.

In the fixed step scheme simulations, no salient trends were observed between the step size and the number of rounds on the average refolding yield (Figure 7-4c). The fluctuating step scheme simulations, on the other hand, revealed a steep initial approach toward an asymptotic limit as step increment size increased (Figure 7-4d), similar to the trend observed with β as shown in Figure 7-4b. For both fixed and fluctuating step schemes, the 20x50 and 10x100 sampling experiments behaved comparably.

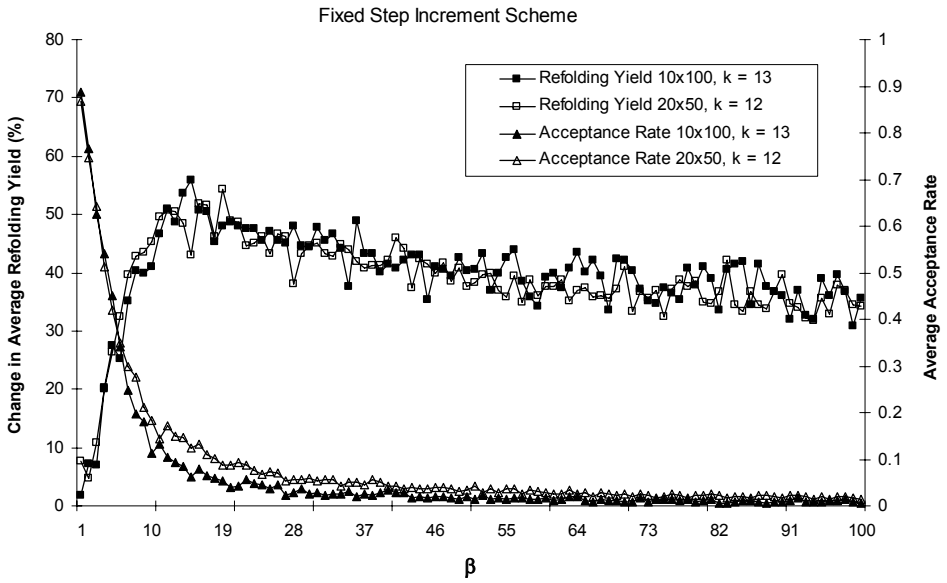

(a)

Figure 7-4. Difference in average protein refolding yield between the initial and final formulation rounds for 1,000-formulation Metropolis Monte Carlo sampling experiments. Simulations were conducted in triplicate for each set of parameters. **a)** Acceptance rates and change in average protein refolding yield as a function of β for Metropolis Monte Carlo sampling with a fixed step increment scheme. The step increment was held constant at 13 and 12 for 10x100 and 20x50 simulations, respectively. The change in average refolding yield reaches a maximum at an optimal value of β corresponding to an acceptance rate of approximately 8%, beyond which the change in refolding yield decreases. **b)** Acceptance rate and change in average protein refolding yield as a function of β for Metropolis Monte Carlo sampling with a fluctuating step increment scheme. The step increment limit remained constant at 15 and 13 for the 10x100 and 20x50 simulations, respectively. The change in refolding yield reaches a maximal level at a critical threshold value of β corresponding to an approximate acceptance rate of 1%, above which there is no additional improvement in the refolding yield. **c)** Difference in protein refolding yield as a function of the step increment size for fixed step increment simulations at constant β of 15 and 19 for 10x100 and 20x50 simulations, respectively. **d)** Difference in protein refolding yield as a function of the step increment size for fluctuating step increment simulations at constant β of 85 and 100 for 10x100 and 20x50 simulations, respectively.

Figure 7-4 (*continued*)

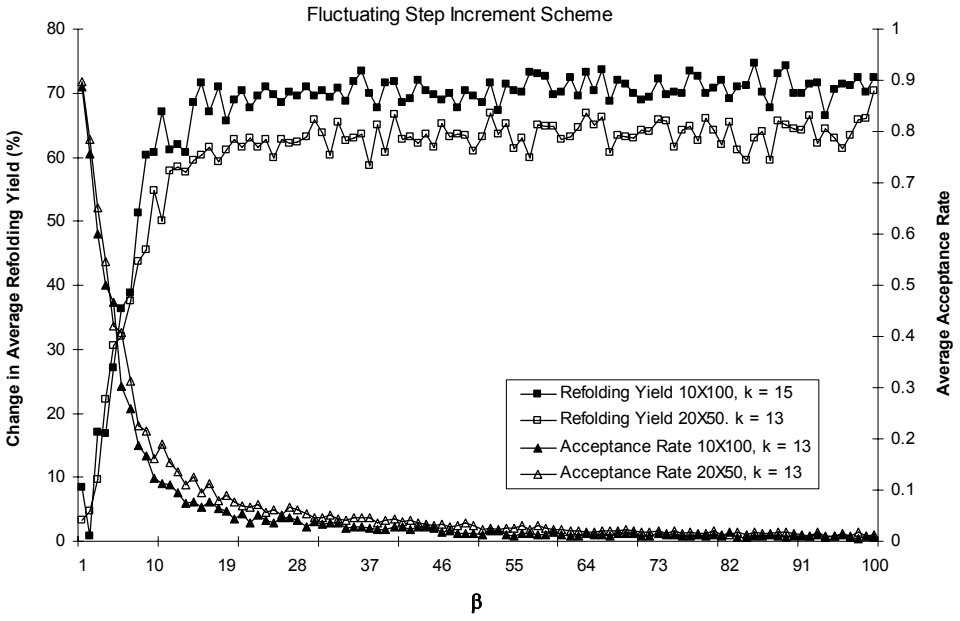

(b)

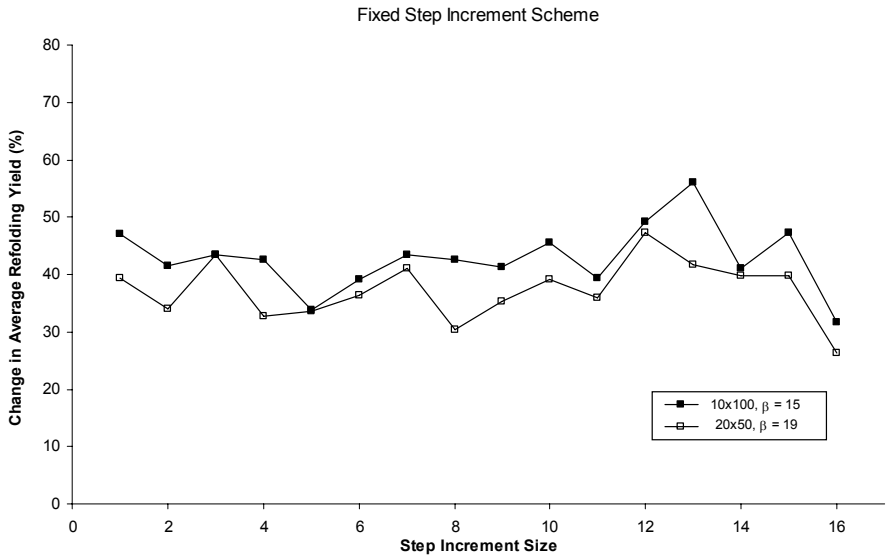

(c)

Figure 7-4 (*continued*)

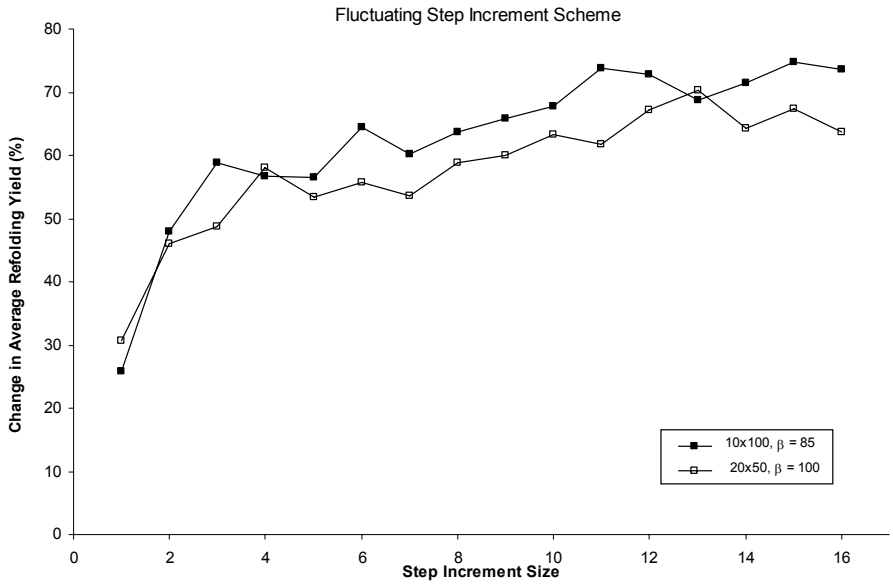

(d)

7.4.4. Effects of sampling schemes on *accessibility* to formulations with high refolding yields.

Figures 7-5a and 7-5b are histograms of formulations accessed by random, Metropolis, and parallel tempering sampling protocols. With regard to the MC methods, accessed formulations refer to all proposed formulations during library construction, regardless of whether the move was accepted or rejected by the Metropolis criterion. The 1,000-formulation Metropolis MC libraries were generated by 20x50 or 10x100 simulations, while 990-formulation parallel tempering libraries were constructed by 15x66 experiments. For both Metropolis and parallel tempering MC simulations conducted under the fixed step increment scheme, formulations with higher refolding yields were accessed more frequently than with random sampling, as

shown by the rightward shift in the formulation distributions, with no apparent dependence on the number of sampling rounds employed.

The distributions of accessed formulations under fluctuating step increment Metropolis and parallel tempering simulations show a similar behavior to the fixed step simulations, in that formulations with higher refolding yields are accessed more frequently than with random sampling. However, the increased frequency appears to occur to a greater extent than the fixed step scheme protocols.

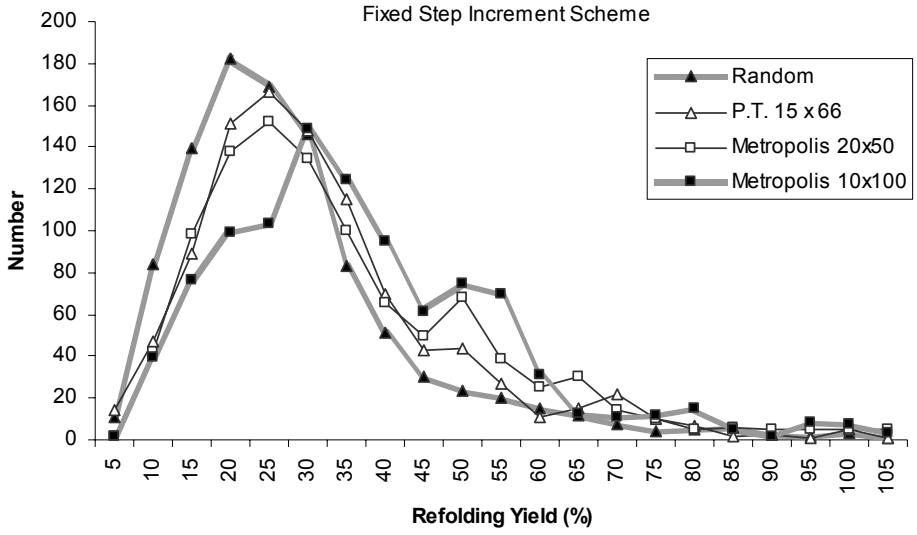

(a)

Figure 7-5. Distribution of formulations accessed by Metropolis and parallel tempering (PT) Monte Carlo sampling at their respective optimized parameter pairs under **a)** fixed step increment schemes and **b)** fluctuating step increment schemes. The data are from 1,000 formulation libraries for Metropolis Monte Carlo and 990-formulation libraries for parallel tempering. The shifts in the histograms indicate that Metropolis Monte Carlo and parallel tempering sampling methods access high refolding yield formulations more frequently than random sampling.

Figure 7-5 (*continued*)

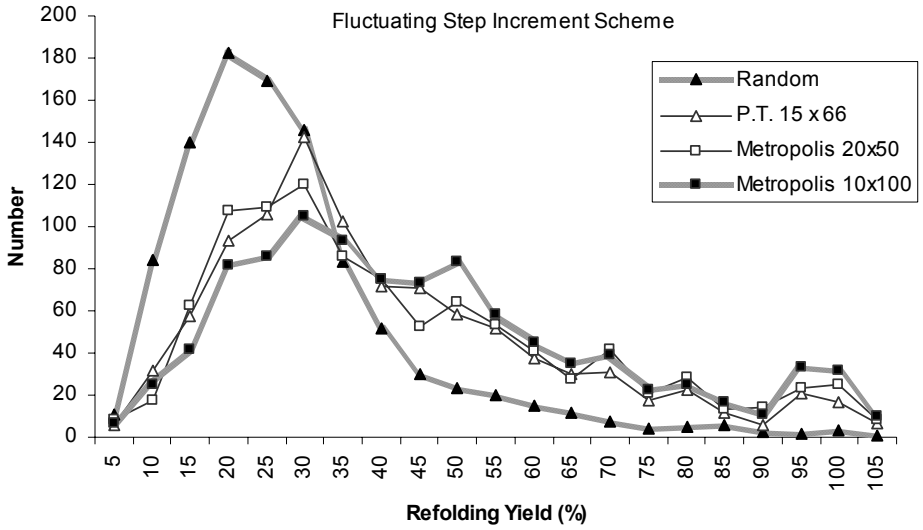

(b)

7.4.5. Effects of sampling schemes on *acceptance* of formulations with high refolding yields

Figure 7-6 shows the average refolding yields of unique formulations resulting from proposed moves that were accepted by the Metropolis criterion. Here, the term "unique" is used to describe non-repeating formulations when multiple copies of the same formulation appear in a sampling library. In general, there is a propensity for higher refolding yield formulations to remain in the library and propagate throughout the rounds, thereby biasing the arithmetic average of a particular MC formulation library. To account for this situation, only contributions from unique, non-repeating formulations were recognized.

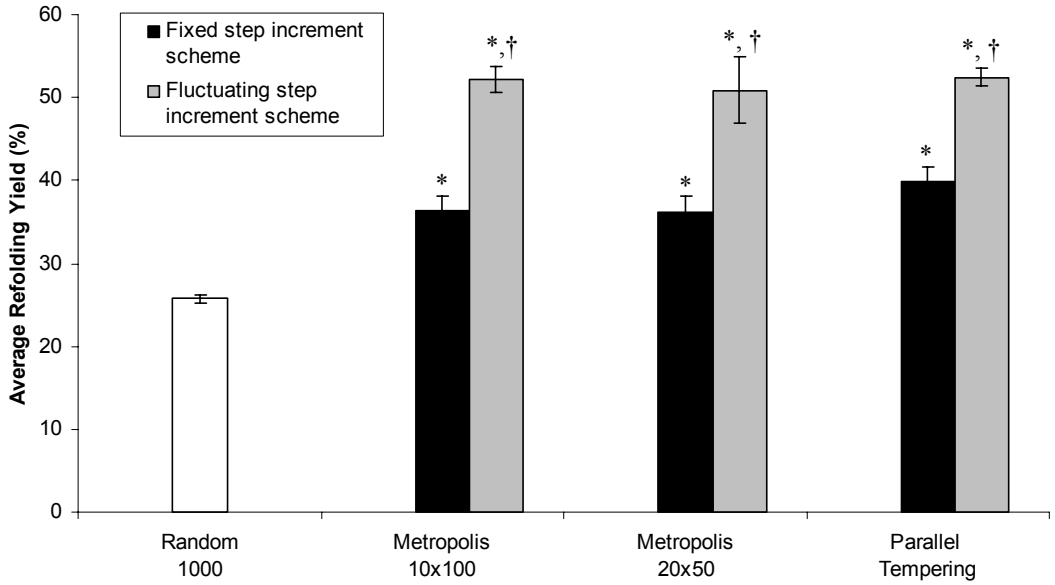

Figure 7-6. Comparison of average refolding yields of unique, accepted formulations for random, Metropolis Monte Carlo, and parallel tempering Monte Carlo sampling. In all cases, Metropolis and parallel tempering Monte Carlo sampling methods with either fixed or fluctuating step increment schemes result in increases in the average refolding yield of formulations relative to random sampling. In addition, the average refolding yields of formulations constructed with fluctuating step increment schemes are higher than formulations constructed by corresponding simulations using fixed step increment schemes. Data for random and Metropolis Monte Carlo libraries are based on 1,000 formulations; parallel tempering libraries contain 990 formulations. Simulations were performed in triplicate, and error bars represent +/- one standard deviation. Asterisks (*) denote statistical significance ($p < 0.05$) compared to random sampling, and daggers (†) denote statistical significance ($p < 0.05$) between fixed and fluctuating step schemes within libraries constructed with the same number of formulations per round.

All Metropolis and parallel tempering MC sampling methods generated formulations with greater refolding yields compared to those obtained from random sampling. For both Metropolis and parallel tempering MC, the fluctuating step scheme produced libraries with statistically greater refolding yields compared to its fixed step scheme counterpart. For instance, a 10x100 Metropolis library employing the fluctuating step scheme resulted in formulations with a larger aggregated refolding

yield average than a 10x100 Metropolis library that employed the fixed step scheme. In both fluctuating and fixed step scheme Metropolis simulations, the number of formulation rounds had no significant effect on the average refolding yield.

7.4.6. Molecular diversity.

Molecular diversity values were calculated for formulations in the initial and final rounds (containing 10, 15, or 20 formulations each) of 1,000-formulation libraries constructed by Metropolis and parallel tempering MC algorithms with fixed and fluctuating step schemes (Figure 7-7). As indicated previously, initial formulation rounds were randomly generated, and thus the diversity of the initial round was deemed an appropriate baseline reference. All libraries generated by Metropolis and parallel tempering sampling approaches resulted in no significant change in the molecular diversity between formulations in the initial (random) round and formulations in the final sampling round.

The molecular diversity was also determined for the ten highest yield formulations within each formulation library, as these high-performing formulations are likely candidates for subsequent screening. Figure 7-8 shows that, in all cases, the diversity of the ten highest yield formulations generated by MC sampling were comparable to those generated by random sampling. When compared to the exhaustive screen of the complete 5,008-formulation library, two MC sampling methods resulted in sustained levels of diversity among the ten highest yield formulations – the10x100 Metropolis fluctuating step scheme and the parallel tempering fluctuating step scheme.

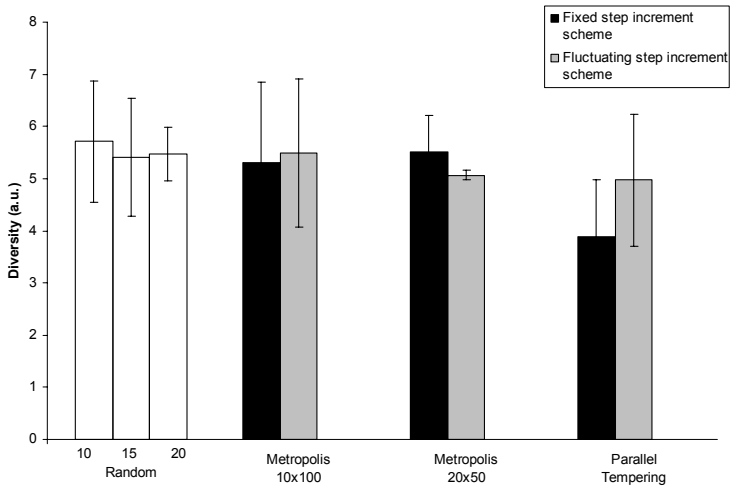

Figure 7-7. Comparison of molecular diversity of formulations of the initial (random) and final rounds of Metropolis Monte Carlo sampling for 1,000-formulation experiments (10x100 and 20x50) and parallel tempering Monte Carlo sampling for 990-formulation experiments. Three separate initial rounds generated from random construction, containing 10, 15, or 20 formulations each, are plotted alongside the simulation data for comparison. In all cases, the level of molecular diversity is maintained from the initial to the final round of formulations. Simulations were performed in triplicate, error bars represent +/- standard deviation.

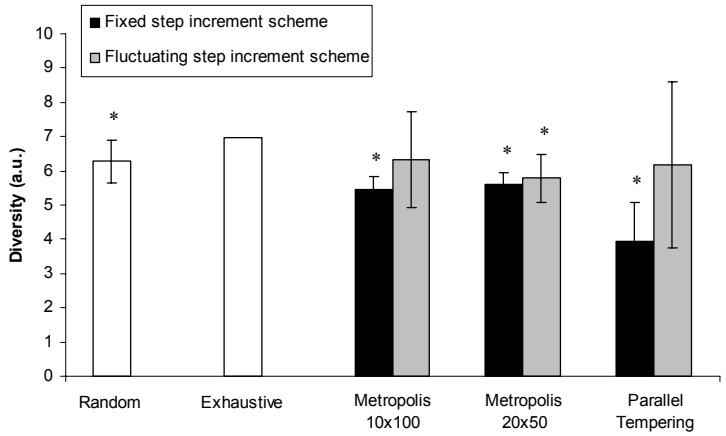

Figure 7-8. Molecular diversity comparison of the ten highest refolding yield formulations within each of the exhaustive, random, Metropolis Monte Carlo, and parallel tempering Monte Carlo libraries. Compared to the exhaustive screen, the molecular diversity was maintained for the 10x100 Metropolis fluctuating step scheme and the parallel tempering fluctuating step scheme simulations. Relative to random sampling, all sampling methods resulted in no significant change in molecular diversity. Simulations were conducted in triplicate. The asterisks (*) denote statistical significance ($p < 0.05$) compared with formulations derived from the exhaustive screen.

7.5. DISCUSSION

Protein expression and folding is important for a range of applications in structural genomics, proteomics, and biopharmaceuticals. Prokaryotes such as *E. coli* are often used to express high quantities of foreign proteins, however the aggregation of misfolded proteins into inclusion bodies reduces the recovery yield and complicates the purification process. To recover functional proteins from inclusion bodies, the proteins are first solubilized in a denatured form using concentrated chaotropic agents (primarily urea or guanidinium chloride). The denaturing agents are then replaced with a refolding buffer whose composition will dictate the yield of functional protein recovery. The formulation of these refolding buffers is notoriously fastidious, so a universal refolding buffer is not available and protein recovery yields from inclusion bodies are typically low.

To improve recovery yields, a number of high-throughput approaches have been described where the refolding buffers are formulated in a combinatorial fashion, thereby allowing for a large number of refolding conditions to be simultaneously evaluated with the hope of identifying formulations of suitable compositions. [1-5] The current high-throughput refolding literature presents data for tens or hundreds of different refolding conditions whereas a full combinatorial analysis of refolding conditions requires upwards of thousands of samples. This numerical challenge is not restricted to protein refolding but is pervasive in combinatorial experimentation in general. Given the large number of samples necessary to fully map a meaningful refolding parameter space, there is a great need for alternative strategies to exhaustive screening.

Two stochastic Monte Carlo sampling approaches, Metropolis and parallel tempering, have emerged as viable alternatives to both exhaustive screening and random sampling of combinatorial libraries. [7] Although the traditional roots of the

MC sampling method began with molecular simulations of thermonuclear reactions, it quickly became a general optimization algorithm in a variety of diverse applications. [18, 19] One of the earlier extensions of the method was developed by Metropolis et al. to determine the equilibrium properties of systems comprised of individual particles interacting in a two-dimensional space. [20] Such properties were calculated based on a series of simulated particle displacements and their corresponding changes in energy. Displacements that resulted in a reduction of the calculated energy of the system reflected a thermodynamically consistent event, and were therefore allowed. In contrast, displacements that resulted in an increase in the energy were allowed conditionally based on a probability that was biased by the Boltzmann factor, exp(-E/kT). Simulated adjustments in the spatial positioning of individual particles and the calculation of a corresponding change in energy create, in essence, the traversal along an energy landscape that exists in configuration space. Since particle configurations resulting in an increase in energy were only allowed occasionally, whereas those resulting in a reduction in energy were always allowed, the simulation was designed to trend toward the lowest free energy state of the system without becoming trapped in local minima.

Parallel tempering is an extension of the Metropolis MC method that is shown to be particularly adept at traversing rugged energy landscapes. [21-23] The parallel tempering scheme simulates replicas of systems, with each system at a different constant β, where β replaces 1/kT in the Boltzmann factor. Systems at lower β sample the configuration space more comprehensively, while systems at higher β tend to sample the space more locally. Parallel tempering MC facilitates improved sampling by allowing the configurations of one system at, say, β_1 to exchange with the configurations of another system at, say, β_2 (Figure 7-2). Thus, a system at lower β

which undergoes configuration exchange with a system at higher β theoretically allows for representative sampling of many local regions of the configuration space.

There are clear analogies between sampling particle configuration space for a free energy minimum and searching composition space for formulations with a maximum figure of merit. [7] In both instances, MC is used to optimize a particular attribute of the system, the only difference being a sign change in the exponential factor of the acceptance probability (i.e., $\exp(-\beta\Delta E)$ versus $\exp(\beta\Delta E)$).

It is also important to recognize, however, distinctions with regard to the concept of step size used in conventional molecular simulations and the concept of step size employed here in the formulation parameter space. In the former application, particle physics and statistical thermodynamics enable the energy landscape to be a function of the physical particle configurations, and a step change in particle configuration represents the physical displacement between atoms. In the latter application, on the other hand, excipients are unable to be organized in a chemically and physically relevant manner due to the absence of any information regarding how multiple excipients together affect the complex interactions governing protein refolding. Given this limitation, excipients were arbitrarily assigned to unique integer values and the step size is not directly related to a physical or chemical distance.

This work is an experimental validation of two MC approaches, Metropolis and parallel tempering, toward identifying high protein refolding buffer formulations with greater efficiency than exhaustive screening and random sampling. A key advantage to MC library construction lies in its iterative approach to creating formulations compared to random library construction, which occurs in a single pass without incorporating any *a priori* knowledge gleaned from previous formulation cycles. This iterative approach to sampling formulations, where one excipient in each formulation of a given round is conditionally incremented according to a specified

step scheme, is how the formulation parameter space is sampled and the figure of merit landscape is traversed. Thus, the degree to which the Metropolis MC algorithms may improve sampling efficiency is greatly dependent on the factors that determine the probability and increment by which excipients are changed from one round to the next. In this study, the modeling parameters β, step increment size, and step increment scheme were examined to determine their effects on the sampling efficiency.

Figures 7-4a and 7-4b show that the change in refolding yield from the initial to the final formulation round generally increases with increasing β. The figure of merit enhancement as a function of β resembles a parabolic behavior under the fixed step scheme and resembles an asymptotic behavior under the fluctuating step scheme. For both 20x50 and 10x100 libraries constructed under the fixed step scheme, the change in refolding yield reaches a maximal level at some optimal value of β corresponding to an acceptance rate of approximately 8%, beyond which the change in refolding yield decreases. In contrast, for libraries constructed with the fluctuating step scheme, the change in refolding yield reaches a maximal level at a critical threshold value of β corresponding to an acceptance rate of approximately 1%, above which there is no additional improvement in refolding yield. For both step schemes, the initial increase in the change in refolding yield as β increases is consistent with the Metropolis acceptance criterion: at higher values of β, moves to formulations of lower refolding yields are accepted with less frequency and formulations with higher refolding yields tend to survive the repeated sampling; lower values of β result in accepting moves less discriminately and tend to mimic random sampling.

The observed contrast between the two step schemes with regard to the behavior in the figure of merit enhancement as a function of β may be attributed to differences in the step schemes' ability to access formulations within the parameter

space. Moves proposed under the fixed step scheme are only able to access formulations that fall a constant step-distance away from the original formulation, while moves proposed with the fluctuating step scheme simulations may access all formulations within a step-distance perimeter. Sampling the parameter space under fixed step increment conditions are, therefore, more tightly restricted than sampling under the fluctuating step increment. In the fixed step scheme, restrictions on formulation accessibility are combined with the more stringent acceptance criteria imposed by higher values of β to cause formulations to eventually become trapped in local maxima over repeated rounds of sampling, thus leading to a reduction in the change in figure of merit beyond the optimal value of β. Fluctuating step scheme sampling prevents the reduction in the figure of merit at higher β that might otherwise occur because formulations can escape local maxima over rounds of repeated sampling, despite high β, due to increased access to proposed formulations. This situation of escaping local maxima likens the purported goals of parallel tempering sampling where β values are swapped between parallel systems to improve the thoroughness of the sampling in order to escape local maxima.

Another important factor to consider in MC-based simulations is the step size at which proposed moves are incremented. In molecular simulations, if the step size is too small, all moves tend to be accepted; if the step size is too large, moves tend to be frequently rejected. [24] Strategies have been developed to adjust the step size to optimize the performance of molecular simulations. In the same vein, similar efforts were taken in this study to examine the effects of step increment sizes on the sampling efficiency.

Figures 7-4c and 7-4d chart the change in refolding yield at all possible step increment sizes ($1 \leq k \leq 16$) while β was held constant. No trends beyond stochastic fluctuations are readily apparent for the fixed step scheme, as expected, since the

formulation parameter space was not parameterized with any meaningful physicochemical distance in mind. Interestingly, for the fluctuating step scheme, the average change in refolding yield increases steeply at step increments less than four and maintains the maximal change in refolding yield at larger step increments. This initial upward trend may be related to the sampling thoroughness afforded at differing values of k operating within the fluctuating step scheme, similar to the effects described previously with β. The observed sub-maximal enhancement in refolding yields at low values of k may be due to sampling within a more local region, thus increasing the possibility of becoming trapped in local maxima. The improved performance at larger step increments may be because higher values of k allow for a mixture of both large and small traversals across the refolding yield landscape.

Given the arbitrary organization of the formulation parameter space, it is unclear whether the dependence of the figure of merit on step size seen with the fluctuating step scheme is an inherent attribute to the sampling scheme, or rather an unintended result due to stochastic fluctuation. To further explore the combined effects of the step increment scheme and step size on sampling efficiency, formulations may need to be organized within a more structured physicochemical parameter space. Possibilities toward this effort include defining the distance along the landscape in binary terms, where changes in excipient concentration represent "short" distances and changes in chemical species represent "long" distances. Alternatively, the distance may also be defined in proportion to the number of chemical species changed with each proposed move such that changing three excipients represents a relatively "long" distance when compared with changing only one of the three excipients in a particular formulation.

In both the β and step increment studies (Figures 7-4a – 7-4d), increasing the number of sampling rounds by two-fold while keeping the library size constant did not

result in any meaningful increase in the average change in protein refolding yields. This is surprising since each of ten formulations undergoes 100 proposed moves in the 10x100 sampling experiments, while each of 20 formulations undergoes only half the number of proposed moves. Chen and Deem have previously observed a significant effect of the number of sampling rounds on figure of merit, however the figure of merit enhancement was realized with a 10-fold increase in the number of sampling rounds. [7] A more comprehensive evaluation on the effects of the number of rounds may require experiments with larger data sets that allow for more sampling rounds.

Based on a series of precursory simulations where 10x100 and 20x50 libraries were constructed at $1 \leq \beta \leq 100$ and $1 \leq k \leq 16$, the parameter pairs that resulted in the largest change in refolding yield between the initial and final rounds for each simulation condition were determined and are summarized in Table 7-2. These optimal parameter pairs were subsequently used to evaluate the performance of the various MC sampling algorithms relative to random sampling. Figures 7-5a and 7-5b suggest that Metropolis and parallel tempering MC methods, under both fixed and fluctuating step increment schemes, afford greater access to high refolding yield formulations than with random sampling, as indicated by the shifts in the distribution of accessed formulations toward higher refolding yields. In the fixed step increment simulations, this shift is more subtle with little discernible difference in the distribution of accessed formulations beyond 80% refolding yield among the Metropolis and parallel tempering sampling approaches compared to random sampling. Under fluctuating step increment moves, the trend toward higher refolding yields is particularly evident for formulations with refolding yield $\geq 90\%$.

In practice, the appeal of using MC sampling methods lies not only in the formulations accessed, but by those actually accepted by the Metropolis criterion to subsequent sampling rounds. Figure 7-6 shows the refolding yield data of accepted,

unique formulations in aggregate. The results demonstrate that MC sampling methods generate formulations with greater refolding yields, on average, than those obtained by random sampling. Moreover, Metropolis and parallel tempering simulations adopting the fluctuating step scheme with optimized parameters generate the greatest enhancements in refolding yield compared to those employing a fixed step scheme with optimized parameters. Note that the observed enhancements in refolding yields as generated by the sampling schemes are not attributable to top performing formulations that remain in the library and propagate throughout the rounds as a result of high values of β. Rather, the average refolding yields reported reflect the yields of only unique, non-repeating formulations.

Although the results suggest MC algorithms to be capable of locating formulations with high protein refolding yields more efficiently than by random sampling, refolding yield may not be the only figure of merit to consider. Subsequent screening (e.g., toxicology, stability, manufacturability) of these formulations are often necessary to fully evaluate their safety and efficacy profiles. One means of estimating how successful a collection of formulations will be in subsequent screens is by assessing the degree of similarity or dissimilarity (e.g., structurally, chemically, or conformationally) among individual formulations within a collection. The utility of quantifying this degree of similarity, often referred to as the molecular diversity, is based on the assumption that similar formulations share similar activity, while dissimilar formulations share dissimilar activity. [25] If a set of formulations with high protein refolding capabilities can be efficiently assembled, for instance via MC sampling algorithms, and is deemed to be molecularly diverse, then it is likely that at least some of the formulations within the collection will pass subsequent analyses that do not rely on refolding as the exclusive figure of merit.

Borrowing from a strategy typically used in small-molecule drug discovery applications, the diversity of the refolding formulations was quantified within a framework defined by three components: diversity metrics, diversity space, and diversity sampling. [26] Diversity metrics are used to translate the physicochemical characteristics of a set of compounds into a geometrical distance in order to quantify its diversity within some predefined chemical or structural space. Diversity space is a relevant chemical and structural space within which the diversity of a set of compounds is assessed. The boundaries and units of measure within this parameter space are defined by "molecular descriptors" that are used to numerically represent each compound within the diversity space. Diversity sampling refers to algorithms developed to identify a maximally diverse and representative subset of compounds from a typically much larger compound collection. Although algorithms specifically designed to maximize molecular diversity have been presented in the literature, the MC schemes employed in this study do not explicitly consider diversity optimization as part of the sampling procedure. [27] Table 7-3 summarizes the specific diversity components that were chosen to analyze the molecular diversity of the MC- and randomly-generated formulation libraries.

Table 7-3. Parameters Adopted for Molecular Diversity Analysis

	Specific Parameters
Diversity Metric	Euclidean distance-based method [7]
Diversity Space	Molecular Descriptors: 1) Surface tension 2) CMC 3) Solubility

There are no universally accepted set of molecular descriptors and those that are selected to parameterize the diversity space are often very application specific. [28] A collection of over 1800 different descriptors and their respective definitions have been compiled, demonstrating the vast assortment of descriptors that have been proposed for various applications in the past and more significantly, the absence of an absolute set of descriptors to quantify molecular diversity. [29] Additionally, the number of descriptors needed to uniquely describe each compound in a complex and large combinatorial library can easily become very large and unruly.

To maintain a manageable yet useful number of descriptors for the present work, three molecular descriptors - surface tension, critical micelle concentration (CMC), and solubility - were chosen to characterize the formulations within each library. Although each excipient may conceivably be allocated to more than one molecular descriptor category, only one descriptor was assigned to each excipient based upon what is believed to be the single predominant physical characteristic contributing to the protein refolding process. Cooperative effects between excipients were not accounted for in the diversity measurements.

The positive refolding effect of preferential hydration on denatured proteins is a widely accepted mechanism for protein stabilization and has been well documented in the literature. [30] Excipients that induce this phenomenon do so, by modifying the surface tension of water and consequently the interaction at the water-protein interface. Polyol and salt excipients were categorized within the surface tension descriptor to account for this important contribution to protein refolding. Refolding can also be facilitated with surfactants within the refolding buffer due to their amphiphilic nature that can bind to exposed hydrophobic regions of folding intermediates, thereby suppressing aggregation and maintaining protein solubility within the solvent. [30, 31] This binding interaction is dependent on the concentration

of the surfactant within the bulk solvent, although it is unclear whether detergents provide optimal protein refolding assistance at concentrations above or below the CMC. The literature suggests that the extent of binding, and thus the folding effects of detergent on the protein, exhibits a step-like change in binding behavior at the CMC. [30, 32] As such, the specific molecular descriptor value for surfactant excipients were assigned accordingly to capture this marked change in binding behavior at the CMC. (See Materials and Methods). Hydrogen bonding and hydrophobic effects play critical roles in stabilizing the three-dimensional conformation of folded proteins. [30] To capture these effects, solubility in water was chosen as a relative indicator of the hydrophilic or hydrophobic nature of selected excipients.

It is important to acknowledge that diversity is meaningful only with respect to the specified molecular descriptors, since every given set of descriptors generates a unique descriptor space within which the formulations are distributed. Moreover, the molecular diversity value alone is meaningless; its significance is limited to comparison with another set of formulations whose diversity is quantified with the same set of descriptors. Figure 7-3 illustrates a comparison between two collections of formulations. The collection represented by the black spheres is more broadly distributed within diversity space compared to the white spheres and are thus considered more molecularly diverse.

Based on the diversity analysis shown in Figure 7-7, all simulation schemes maintained a statistically comparable level of diversity amongst the formulations in the final sampling round when compared with the initial formulations generated by random sampling. These diversity results, in conjunction with the results shown in Figures 7-5 and 7-6, highlight the capacity of MC schemes to locate more formulations with high refolding yields, compared to random sampling, without compromising molecular diversity. What may be of more practical interest is the

diversity of a set of high-performing formulations as they are the likely candidates for subsequent screening (Figure 7-8). Compared to the ten highest-yielding formulations generated by random sampling, all MC sampling methods arrived at formulations whose molecular diversity measurements were statistically comparable in diversity. When compared with the top performing formulations derived from the exhaustive screen, libraries generated by two out of the six MC sampling conditions resulted in formulations with statistically comparable levels of diversity. Despite the reduction in molecular diversity observed for the other four sampling conditions, MC simulations often located at least four of the ten highest refolding yield formulations from the exhaustive screen while only requiring the sampling of 20% of the total number of samples (data not shown). This illustrates the potential compromise in molecular diversity and figure of merit that may exist between sampling only a fraction of a combinatorial library over exhaustively screening each constituent.

Two distinct situations are envisioned for experimenters who wish to implement these MC algorithms for sampling combinatorial libraries: first in instances where the figure of merit must be computationally estimated with an appropriate quantitative model, and second in instances where the figure of merit must be evaluated experimentally with each iterative round of library construction.

In the situation where the figure of merit is to be computationally estimated, appropriate metrics that can capture the characteristics of each library constituent's influence on the figure of merit need to be developed. The molecular descriptors used in the diversity analysis here are examples of such metrics. These metrics are then used as input variables in a quantitative model, which can predict the figure of merit of each library constituent. A similar concept has been demonstrated to predict protein adsorption on biomaterials in a combinatorial polymer library. [33-35]

When a quantitative model or a comprehensive data set is unavailable, the figure of merit for each library constituent may be evaluated experimentally with each iterative round of library construction. A sufficient starting set of samples, round 1, must first be obtained by random sampling from the parameter space. These samples must then be quantitatively evaluated for a figure of merit. The MC moves may then commence, resulting in a set of proposed new samples, collectively denoted as round 1', each of which must be synthesized and once again evaluated for the figure of merit. Once the figures of merit for both the original configuration and its corresponding proposed configuration have been evaluated, the appropriate acceptance probability criterion is applied. If the proposed move is accepted, the new sample in round 1' advances to round 2. Otherwise, the original sample from round 1 remains in round 2. The proposed moves and the subsequent synthesis and evaluation then proceed in this order in a loop wise fashion. At the conclusion of the sampling experiments, the total number of samples to be generated has not decreased compared to a randomly sampled library of equal size. Rather, the total number of samples is the same, but those with high figures of merit may be identified with greater efficiency using this proposed combination of traditional experimental methods coupled to computational decision-making algorithms.

7.6. CONCLUSIONS

In light of the imposing technical and financial challenges associated with high-throughput synthesis and screening, much attention has been directed at developing alternative strategies to efficiently and effectively cover the chemical parameter space without having to rely on exhaustive screening. Using an experimentally-acquired, exhaustive data set of protein refolding yields for a

combinatorial library of lysozyme refolding buffer formulations, this study illustrates that both Metropolis and parallel tempering MC algorithms can effectively sample the formulation parameter space, thereby affording access to high yielding formulations and ultimately a more efficient way to locate top performing formulations when compared to random sampling.

The results demonstrate that the change in average refolding yields is dependent upon the step increment scheme and the value of the Metropolis β parameter and the step increment size operating within the scheme. These tunable parameters are critical to the MC sampling schemes and afford experimenters the flexibility to tailor the use of such approaches in an application-specific manner. In addition to the protein refolding yield figure of merit, the effects of the sampling schemes on molecular diversity have been considered. Molecular diversity, as parameterized by surface tension, critical micelle concentration, and solubility, does not appear to diminish as formulations are sampled throughout the Metropolis or parallel tempering MC rounds compared with formulations generated by random sampling.

The results presented herein compellingly illustrate the versatility of MC methods in sampling combinatorial libraries. More highly resolved landscapes, by way of physiochemical parameterization, plus the availability of larger data sets may further illuminate the full range of capabilities of Monte Carlo-based strategies for applications beyond traditional molecular simulations.

REFERENCES

[1] Wang, T., John, S., Archuleta, S., and Jonsson, C.B. Rapid, high-throughput purification of hiv-1 integrase using microtiter plate technology. *Protein Expr. Purif.* **33**(2): 232-237 (2004).

[2] Voziyan, P., Johnston, M., Chao, A., Bomhoff, G., and Fisher, M. Designing a high throughput refolding array using a combination of the groel chaperonin and osmolytes. *J. Struct. Funct. Genomics* **6**(2-3): 183-188 (2005).

[3] Vincentelli, R., Canaan, S., Campanacci, V., Valencia, C., Maurin, D., Frassinetti, F., Scappucini-Calvo, L., Bourne, Y., Cambillau, C., and Bignon, C. High-throughput automated refolding screening of inclusion bodies. *Protein Sci.* **13**(10): 2782-2792 (2004).

[4] Lin, L., Seehra, J., and Stahl, M.L. High-throughput identification of refolding conditions for lxr beta without a functional assay. *Protein Expr. Purif.* **47**(2): 355-366 (2006).

[5] Cowieson, N.P., Wensley, B., Listwan, P., Hume, D.A., Kobe, B., and Martin, J.L. An automatable screen for the rapid identification of proteins amenable to refolding. *Proteomics* **6**(6): 1750-1757 (2006).

[6] Geysen, H.M., Schoenen, F., Wagner, D., and Wagner, R. Combinatorial compound libraries for drug discovery: An ongoing challenge. *Nat. Rev. Drug Discovery* **2**(3): 222-230 (2003).

[7] Chen, L.G. and Deem, M.W. Monte carlo methods for small molecule high-throughput experimentation. *J. Chem. Inf. Comput. Sci.* **41**(4): 950-957 (2001).

[8] Ott, E., *Cellulose and cellulose derivatives*. 1943, New York: Interscience Publishers. 1176.

[9] Larsson, C., Widell, S., and Kjellbom, P. Preparation of high-purity plasma-membranes. *Methods Enzymol.* **148**: 558-568 (1987).

[10] Weast, R.C., Astle, M.J., and Beyer, W.H., *Chemical rubber company handbook of chemistry and physics*. 1988, Boca Raton: CRC Press.

[11] Connors, K.A. The stability of cyclodextrin complexes in solution. *Chemical Reviews* **97**(5): 1325-1357 (1997).

[12] Helenius, A., D.R., M., Fries, E., and Tanford, C. Properties of detergents. *Methods Enzymol.* **56**: 734-749 (1979).

[13] www.sigmaaldrich.com

[14] Macdonald, R.J., Swift, G.H., Przybyla, A.E., and Chirgwin, J.M. Isolation of rna using guanidinium salts. *Methods Enzymol.* **152**: 219-227 (1987).

[15] Hevehan, D.L. and Clark, E.D. Oxidative renaturation of lysozyme at high concentrations. *Biotechnol. Bioeng.* **54**(3): 221-230 (1997).

[16] Wetlaufer, D.B., Johnson, E.R., and Clauss, L.M., *Lysozyme*, ed. E.F. Osserman, R.E. Canfield, and S. Beychok. 1974, New York: Academic.

[17] Rathore, N., Chopra, M., and De Pablo, J.J. Optimal allocation of replicas in parallel tempering simulations. *J. Chem. Phys.* **122**(2): - (2005).

[18] Frenkel, D. and Smit, B., *Understanding molecular simulation: From algorithms to applications*. 2002, San Diego: Academic Press. 638.

[19] Metropolis, N. The beginning of the monte carlo method. *Los Alamos Science Special Issue*: 125-130 (1987).

[20] Metropolis, N., Rosenbluth, A.W., Rosenbluth, M.N., Teller, A.H., and Teller, E. Equation of state calculations by fast computing machines. *J. Chem. Phys.* **21**(6): 1087-1092 (1953).

[21] Earl, D.J. and Deem, M.W. Parallel tempering: Theory, applications, and new perspectives. *Phys. Chem. Chem. Phys.* **7**(23): 3910-3916 (2005).

[22] Geyer, C.J. *Markov chain monte carlo maximum likelihood*. in *Computing Science and Statistics: Proceedings of the 23rd Symposium on the Interface. American Statistical Association*. 1991. New York.

[23] Swendsen, R.H. and Wang, J.S. Replica monte-carlo simulation of spin-glasses. *Phys. Rev. Lett.* **57**(21): 2607-2609 (1986).

[24] Miller, M.A., Amon, L.M., and Reinhardt, W.P. Should one adjust the maximum step size in a metropolis monte carlo simulation? *Chem. Phys. Lett.* **331**(2-4): 278-284 (2000).

[25] Gorse, A.D. Diversity in medicinal chemistry space. *Curr. Top. Med. Chem.* **6**(1): 3-18 (2006).

[26] Agrafiotis, D.K., Lobanov, V., Rassokhin, D., and Izrailev, S., *The measurement of molecular diversity*, in *Virtual screening for bioactive molecules*, H.J. Bohn and G. Schneider, Editors. 2000, Wiley-VCH: Weinheim, Germany. p. 265-300.

[27] Agrafiotis, D.K. Stochastic algorithms for maximizing molecular diversity. *J. Chem. Inf. Comput. Sci.* **37**(5): 841-851 (1997).

[28] Glen, R.C. and Adams, S.E. Similarity metrics and descriptor spaces - which combinations to choose? *QSAR Comb. Sci.* **25**(12): 1133-1142 (2006).

[29] Todeschini, R. and Consonni, V., *Handbook of molecular descriptors*. 2000, Weinheim, Germany: Wiley-VCH. 667.

[30] Wang, W. Instability, stabilization, and formulation of liquid protein pharmaceuticals. *Int. J. Pharm.* **185**(2): 129-188 (1999).

[31] Clark, E.D., Schwarz, E., and Rudolph, R. Inhibition of aggregation side reactions during in vitro protein folding. *Amyloid, Prions, and Other Protein Aggregates* **309**: 217-236 (1999).

[32] Ruckenstein, E. and Nagarajan, R. Critical micelle concentration - transition point for micellar size distribution. *J. Phys. Chem.* **79**(24): 2622-2626 (1975).

[33] Smith, J.R., Kholodovych, V., Knight, D., Kohn, J., and Welsh, W.J. Predicting fibrinogen adsorption to polymeric surfaces in silico: A combined method approach. *Polymer* **46**(12): 4296-4306 (2005).

[34] Smith, J.R., Knight, D., Kohn, J., Rasheed, K., Weber, N., Kholodovych, V., and Welsh, W.J. Using surrogate modeling in the prediction of fibrinogen adsorption onto polymer surfaces. *J. Chem. Inf. Comput. Sci.* **44**(3): 1088-1097 (2004).

[35] Smith, J.R., Seyda, A., Weber, N., Knight, D., Abramson, S., and Kohn, J. Integration of combinatorial synthesis, rapid screening, and computational modeling in biomaterials development. *Macromol. Rapid Commun.* **25**(1): 127-140 (2004).